

STUDIES ON OXIMIDINE II – TOTAL SYNTHESIS BY AN UNPRECEDENTED
REDUCTIVE COUPLING

BY

© 2009

Christopher M. Schneider

Submitted to the graduate degree program in Medicinal Chemistry
and the Graduate Faculty of the University of Kansas
in partial fulfillment of the requirements for the degree of
Doctor of Philosophy.

Dissertation Committee:

Chair

Date Defended: _____

The Dissertation Committee for Christopher M. Schneider certifies that this is the approved version of the following dissertation:

STUDIES ON OXIMIDINE II – TOTAL SYNTHESIS BY AN UNPRECEDENTED
REDUCTIVE COUPLING

Dissertation Committee:

Chair

Date Approved: _____

Abstract:

Studies on Oximidine II – Total Synthesis by an Unprecedented Reductive Coupling

Christopher Schneider

University of Kansas, 2009

Chapter 1 – Total Synthesis and Analog Development of Oximidine II

The benzolactone enamide natural products are identified by three structural characteristics: a salicylate arene, a 12- or 15-membered macrolactone, and an enamide side chain. These natural products exert their biological activity by inhibiting the vacuolar-(H⁺)-ATPase (V-ATPase) enzyme.

The benzolactone enamide oximidine II has been synthesized twice previously with only moderate yields realized for the key macrocyclization step. Following a previous Georg group strategy, we envisioned performing the ring-closure using a Castro-Stephens reaction. While optimizing this copper-mediated macrocyclization, we discovered an unprecedented copper-mediated reductive coupling reaction.

The enamide side chain of these natural products is postulated to be critical for biological activity. To probe the importance of this acid-sensitive moiety, we synthesized an allylic amide homolog of oximidine II and tested both oximidine II and this analog in melanoma cancer cells.

Chapter 2 – The Search for New Antibiotics – New Inhibitors of the MurA Enzyme

The bacterial enzyme UDP-*N*-acetylglucosamine enolpyruvyl transferase (MurA) catalyzes the first committed step of cell wall biosynthesis. Using high-throughput screening, 5 scaffolds were identified with MurA inhibitory activity. Analog development of the pyrrole-benzoic acid scaffold failed to generate compounds with improved potency. We then turned to structure-based drug design to investigate new MurA inhibitors. Using computer-modeling software, low molecular weight molecules were docked into various MurA crystal structures. Evaluation of these docking studies revealed 4 small molecules as potential leads for further optimization.

Chapter 3 – Synthesis and Initial Biological Evaluation of 2,3,7,8-Tetrachlorophenothiazine

Dioxins are environmental pollutants that cause a range of biological effects in a dose-dependent manner. The exact mechanism of action for dioxins is not fully understood. 2,3,7,8-Tetrachlorophenothiazine (TCPT) was designed to probe potential mechanisms of action and biological effects of dioxin analogs. Utilization of Buchwald-Hartwig coupling methodology produced TCPT in 37% yield. Preliminary biological testing of TCPT has shown favorable pharmacokinetic properties.

Acknowledgements

First and foremost, I praise Jesus Christ for blessing me with the talent and drive to succeed in life and graduate school.

To my advisor, Dr. Gunda Georg, I owe much gratitude. She has provided the resources, motivation, and creative freedom needed to be successful in exploring a variety of ideas on a variety of interdisciplinary projects. Her leadership has been a great example to follow.

I would like to thank all the members of the Medicinal Chemistry program at KU for their mentoring and teaching. They set high standards that make the department one of the best in the nation. In particular, I would like to thank Dr. Jeff Aubé for his guidance during my literature seminar and on career matters, and for serving on my dissertation committee. Dr. Apurba Dutta has been gracious with his time, serving on both my oral and dissertation committees and for always taking time to answer any questions I have had. I acknowledge Dr. Lester Mitscher for his professional words of wisdom and for serving on my oral committee.

I would like to thank Dr. Jon Tunge in the KU Chemistry department for his exceptional classroom teaching, for serving on my oral and dissertation committees, and for writing important letters of recommendation.

I also owe Dr. Robert Carlson in the Chemistry department at KU thanks for being a part of both my oral and dissertation committees and for being instrumental in expanding my knowledge of chemistry.

I would also like to thank the Medicinal Chemistry department at the University of Minnesota for accepting me into their community.

I have been fortunate to work on many collaborative projects during my career. These collaborations, with Dr. Kristian Fried working under Dr. Karl Rozman at KUMC and with the group of Dr. Ernst Schönbrunn, have given me an appreciation for the biological side of medicinal chemistry. Dr. Gerry Lushington at the KU Molecular Graphics and Modeling Laboratory was generous with his time and patience when providing guidance during the MurA modeling studies. I am also grateful for Dr. Harry Tian at the UM HTS facility for performing cytotoxicity assays and Dr. Douglass Powell and Dr. Victor Day at KU for performing X-ray crystallography.

My success in graduate school is greatly attributed to two individuals. Dr. Jared Spletstoser has always been there to school me on a variety of topics including chemistry, music, and dog training. Dr. Oliver Hutt demonstrated the importance of attention to detail in the lab and what leadership qualities were needed to succeed in science. Their examples have helped me be a better mentor for younger students in the Georg group.

Without Wayne Gu, graduate school would have been much different. His light-heartedness made frustrating days in the lab enjoyable and he was always there to share chemistry ideas, swap funny stories, or to work out. Matt Leighty has been a lot of fun to watch ND–Michigan football games with and helpful while preparing this dissertation. Without Tim Ribelin as a classmate, the first few years of grad

school would have been much less enjoyable. I'd also like to thank Andy Knickerbocker, Amy, Brandon, Bryant, Haibo, Jack, Karen, Kriangsak, and Micah for making being part of the Georg group an unforgettable experience.

My family has been outrageously supportive and loving, specifically my parents Mark and Colleen and Mike and Brenda. While they may not have always understood what my projects were about or understood my attempts to relate chemistry to baking or any other everyday happening, they were always the first to say "good job" or "we're very proud of you". Without the hard work ethic they instilled in me, I would not have been successful in graduate school.

Finally, I am a lucky man to have such a supportive wife. Graduate school would have been more difficult without Jenna's continual love and encouragement.

*This dissertation is dedicated to my wife, Jenna,
and my parents Mike and Brenda and Mark and Colleen
for their love and encouragement*

Table of Contents

List of Figures	11
List of Tables	14
List of Compounds	15
List of Abbreviations	21

Chapter 1

Total Synthesis and Analog Development of Oximidine II

1.1	Introduction to Benzolactone Enamides	24
1.2	Biological Significance of V-ATPases	28
1.3	V-ATPase Inhibitors – Investigation of Benzolactone Enamides	34
1.4	Previous Synthetic Studies of the Oximidines	58
1.5	Total Synthesis of Oximidine II	83
1.6	Synthesis and Biological Activity of Oximidine II Analogs	118
1.7	Copper-mediated Reductive Ring-closure Mechanistic Investigation	130
1.8	Conclusions	137

Chapter 2

The Search for New Antibiotics – New Inhibitors of the MurA Enzyme

2.1	Background	138
2.2	Generation of HTS-Inspired Library	147
2.3	Structure-Based / Fragment-Based Drug Design Approach	160
2.4	Conclusions	168

Chapter 3

Synthesis and Initial Biological Evaluation of 2,3,7,8-Tetrachlorophenothiazine

3.1	Background	170
3.2	TCPT Synthesis	173
3.3	Initial Biological Evaluation of TCPT	180
3.4	Conclusions	184

Chapter 4

Experimental Data

4.1	Materials and Methods	185
4.2	Biological Procedures	186
4.3	Experimental Procedures	190
	4.3.1 Chapter 1	190
	4.3.2 Chapter 2	249
	4.3.3 Chapter 3	260
4.4	References	279

List of Figures

Figure 1. Members of benzolactone enamide natural product family	25
Figure 2. Structure of V-ATPase	30
Figure 3. V-ATPase catalytic cycle	32
Figure 4. Reported V-ATPase inhibitors	39
Figure 5. Proposed mechanism of inhibition by the enamide side chain	41
Figure 6. Lobatamide benzophenone photoaffinity compound	48
Figure 7. Cruentaren A and B	51
Figure 8. Predicted enamide <i>in vivo</i> hydrolysis and allylic amide stability	58
Figure 9. Methods of enamide side chain installation	63
Figure 10. Oximidine II retrosynthesis by Porco and Shen	64
Figure 11. Oximidine II retrosynthesis by Georg group	69
Figure 12. Oximidine II retrosynthesis by Molander and Dehmel	75
Figure 13. Second-generation retrosynthesis by Molander and Dehmel	78
Figure 14. Our second-generation oximidine II retrosynthesis	86
Figure 15. Sharpless's mnemonic device for asymmetric induction	89
Figure 16. Crystal structure of desired acetal 124	90
Figure 17. Castro-Stephens macrocyclization followed by C8-C9 olefin inversion	104
Figure 18. Retrosynthesis for allylic amide homolog	119
Figure 19. IC ₅₀ graphs for oximidine II, tested against SK-Mel-5 and SK-Mel-28 melanoma cells	128

Figure 20. IC ₅₀ graphs for allylic amide analog, tested against SK-Mel-5 and SK-Mel-28 melanoma cells	129
Figure 21. Possible reductive cyclization mechanisms	131
Figure 22. Potential deuterium-proton exchange pathway	133
Figure 23. Proposed mechanism for copper-mediated reductive cyclization	136
Figure 24. Examples of antibiotic therapeutics	139
Figure 25. Dimer of peptidoglycan layer	141
Figure 26. Crosslinking of peptidoglycan layer	141
Figure 27. MurA in open state	143
Figure 28. MurA with UNAG bound	144
Figure 29. MurA-catalyzed conversion of UNAG to EP-UNAG	145
Figure 30. Inhibitors of the enolpyruvyl transferase enzyme family	146
Figure 31. Recently reported MurA inhibitors	149
Figure 32. Unusual mechanism for cnicin binding	149
Figure 33. MurA HTS hits	150
Figure 34. HTS compounds from lead series 1	151
Figure 35. Pyrrole-benzoic acid synthetic strategies	153
Figure 36. Relative MurA inhibitory activity for synthesized analogs	159
Figure 37. Initial IC ₅₀ determined for compound 265 vs. 226	160
Figure 38. MurA docking results	166
Figure 39. Structure of ANS	167

Figure 40. Virtual screen hits 267-270 and analog 271 tested for MurA inhibition	168
Figure 41. Structures of TCDD, chlorpromazine, and TCPT	170
Figure 42. Synthetic strategies for phenothiazine synthesis	175
Figure 43. Crystal structure of TCPT	180
Figure 44. <i>In vitro</i> EROD activity of TCDD and TCPT	181
Figure 44. Serum profile of TCPT in rats after i.v. administration	183
Figure 45. Serum profile of TCPT in guinea pigs after i.v. administration	183

List of Tables

Table 1. Salicylilalamide enamide analogs and biological activity	44
Table 2. Salicylilalamide core analogs and biological activity	45
Table 3. Lobatamide analogs and biological activity	47
Table 4. Apicularen A analogs and biological activity	50
Table 5. Cruentaren A analogs and biological activity	54
Table 6. Biological activity of oximidines and oximidine III analogs	56
Table 7. Calculations of relative macrocycle stabilities	72
Table 8. Optimization of Peterson olefination	97
Table 9. Castro-Stephens macrocyclization optimization	102
Table 10. Castro-Stephens optimization with model system 144	105
Table 11. Optimization of reductive macrocyclization	112
Table 12. Investigation of phenol protecting group on reductive macrocyclization	113
Table 13. Optimization of pyrrole-benzoic acid formation	155
Table 14. Pyrrole benzoic acid analogs	157
Table 15. Optimization of reaction parameters for TCPT formation	179

List of Compounds

Oximidine II (14).	229
(2 <i>Z</i> ,4 <i>E</i>)-4-(Methoxyimino)but-2-enamide (54).	229
2,2-Dimethyl-4-oxo-4 <i>H</i> -benzo[<i>d</i>][1,3]dioxin-5-yl Trifluoromethane-sulfonate (63).	191
(3 <i>S</i> ,4 <i>S</i> ,5 <i>Z</i> ,7 <i>Z</i> ,9 <i>E</i>)-4,14-Bis(<i>tert</i> -butyldimethylsilyloxy)-3-((<i>Z</i>)-3-iodoallyl)-3,4-dihydro-1 <i>H</i> -benzo[<i>c</i>][1]oxacyclododecin-1-one (67).	227
5-(<i>E</i>)-5-(2-Iodovinyl)-2,2-dimethyl-4 <i>H</i> -benzo[<i>d</i>][1,3]dioxin-4-one (108).	193
(5 <i>S</i> ,6 <i>S</i>)-5-((<i>Z</i>)-But-1-en-3-ynyl)-11,11-dimethyl-10,10-diphenyl-2,4,9-trioxa-10-siladodecan-6-ol (109).	210
Prop-1-yne-1,3-diylbis(triisopropylsilane) (110).	110
(2 <i>R</i> ,3 <i>S</i>)-5-(<i>tert</i> -Butyldiphenylsilyloxy)-3-(4-methoxybenzyloxy)-2-(methoxymethoxy)pentanal (111).	206
(2 <i>R</i> ,3 <i>S</i>)-Ethyl 5-(<i>tert</i> -Butyldiphenylsilyloxy)-2,3-dihydroxypentanoate (112).	200
(<i>E</i>)-2,2-Dimethyl-5-(2-(trimethylsilyl)vinyl)-4 <i>H</i> -benzo[<i>d</i>][1,3]dioxin-4-one (115).	192
Hydroxy-2,2-dimethyl-4 <i>H</i> -benzo[<i>d</i>][1,3]dioxin-4-one (116).	190
3-(<i>tert</i> -Butyldiphenylsilyloxy)propan-1-ol (119).	194
3-(<i>tert</i> -Butyldiphenylsilyloxy)propanal (120).	194
(<i>E</i>)-Ethyl 5-(<i>tert</i> -Butyldiphenylsilyloxy)pent-2-enoate (121).	195
(<i>E</i>)-5-(<i>tert</i> -Butyldiphenylsilyloxy)pent-2-en-1-ol (122).	196
(2 <i>S</i> ,3 <i>S</i>)-5-(<i>tert</i> -Butyldiphenylsilyloxy)pentane-1,2,3-triol (123).	196

(2 <i>R</i> ,4 <i>S</i> ,5 <i>S</i>)-4-(2-(<i>tert</i> -Butyldiphenylsilyloxy)ethyl)-2-(4-methoxyphenyl)-1,3-dioxan-5-ol (124).	198
<i>tert</i> -Butyl-(2-((2 <i>R</i> ,4 <i>S</i> ,5 <i>S</i>)-5-(methoxymethoxy)-2-(4-methoxyphenyl)-1,3-dioxan-4-yl)ethoxy)diphenylsilane (127).	199
(2 <i>S</i> ,3 <i>S</i>)-5-(<i>tert</i> -Butyldiphenylsilyloxy)-3-(4-methoxybenzyloxy)-2-(methoxymethoxy)pentan-1-ol (128).	205
(2 <i>R</i> ,4 <i>R</i> ,5 <i>S</i>)-Ethyl 5-(2-(<i>tert</i> -Butyldiphenylsilyloxy)ethyl)-2-(4-methoxyphenyl)-1,3-dioxolane-4-carboxylate (129).	201
(2 <i>S</i> ,3 <i>S</i>)-5-(<i>tert</i> -Butyldiphenylsilyloxy)-3-(4-methoxybenzyloxy)pentane-1,2-diol (130).	202
(2 <i>S</i> ,3 <i>S</i>)-5-(<i>tert</i> -Butyldiphenylsilyloxy)-2-hydroxy-3-(4-methoxybenzyloxy)pentyl Ethanoate (131).	203
(2 <i>S</i> ,3 <i>S</i>)-5-(<i>tert</i> -Butyldiphenylsilyloxy)-3-(4-methoxybenzyloxy)-2-(methoxymethoxy)pentyl Ethanoate (132).	204
(5 <i>S</i> ,6 <i>S</i>)-6-(4-Methoxybenzyloxy)-11,11-dimethyl-10,10-diphenyl-5-((<i>Z</i>)-4-(triisopropylsilyl)but-1-en-3-ynyl)-2,4,9-trioxa-10-siladodecane (133).	208
(5 <i>S</i> ,6 <i>S</i>)-5-((<i>Z</i>)-But-1-en-3-ynyl)-6-(4-methoxybenzyloxy)-11,11-dimethyl-10,10-diphenyl-2,4,9-trioxa-10-siladodecane (135).	209
(5 <i>S</i> ,6 <i>S</i>)-5-((<i>Z</i>)-But-1-en-3-ynyl)-11,11-dimethyl-10,10-diphenyl-2,4,9-trioxa-10-siladodecan-6-yl 2-((<i>E</i>)-2-Iodovinyl)-6-methoxybenzoate (136).	211

(3 <i>S</i> ,4 <i>S</i> ,5 <i>Z</i> ,9 <i>Z</i>)-3-(2-(<i>tert</i> -Butyldiphenylsilyloxy)ethyl)-14-methoxy-4-(methoxy-methoxy)-3,4-dihydro-1-oxabenzocyclododeca-5,9-dien-7-ynone (139).	212
(3 <i>S</i> ,4 <i>S</i> ,5 <i>Z</i> ,7 <i>Z</i> ,9 <i>E</i>)-3-(2-(<i>tert</i> -Butyldiphenylsilyloxy)ethyl)-14-methoxy-4-(methoxymethoxy)-3,4-dihydro-1 <i>H</i> -benzo[<i>c</i>][1]oxacyclododecin-1-one (140).	213
(<i>Z</i>)- <i>tert</i> -Butyldiphenyl(6-(triisopropylsilyl)hex-3-en-5-ynyl)oxy)silane (141).	231
(<i>Z</i>)-6-(Triisopropylsilyl)hex-3-en-5-yn-1-ol (142).	232
(<i>Z</i>)-6-(Triisopropylsilyl)hex-3-en-5-ynyl 2-((<i>E</i>)-2-iodovinyl)-6-methoxybenzoate (143).	232
(<i>Z</i>)-Hex-3-en-5-ynyl 2-((<i>E</i>)-2-Iodovinyl)-6-methoxybenzoate (144).	234
(5 <i>Z</i> ,9 <i>Z</i>)-14-Methoxy-3,4-dihydro-1-oxabenzocyclododeca-5,9-dien-7-ynone (145).	235
(5 <i>Z</i> ,9 <i>E</i>)-14-Methoxy-3,4-dihydro-1-oxabenzocyclododeca-5,9-dien-7-ynone (146).	236
(5 <i>S</i> ,6 <i>S</i>)-5-((<i>Z</i>)-But-1-en-3-ynyl)-11,11-dimethyl-10,10-diphenyl-2,4,9-trioxa-10-siladodecan-6-yl 2-(<i>tert</i> -butyldiphenylsilyloxy)-6-((<i>E</i>)-2-iodovinyl)benzoate (150).	215
(5 <i>S</i> ,6 <i>S</i>)-5-((<i>Z</i>)-But-1-en-3-ynyl)-11,11-dimethyl-10,10-diphenyl-2,4,9-trioxa-10-siladodecan-6-yl 2-(<i>tert</i> -butyldimethylsilyloxy)-6-((<i>E</i>)-2-iodovinyl)benzoate (151).	216

trioxa-10-siladodecan-6-yl 2-(Ethanoyloxy)-6-((<i>E</i>)-2-iodovinyl)benzoate (152) .	218
(5 <i>S</i> ,6 <i>S</i>)-5-((<i>Z</i>)-But-1-en-3-ynyl)-11,11-dimethyl-10,10-diphenyl-2,4,9- trioxa-10-siladodecan-6-yl 2-Hydroxy-6-((<i>E</i>)-2-iodovinyl)benzoate (153) .	219
(3 <i>S</i> ,4 <i>S</i> ,5 <i>Z</i> ,7 <i>Z</i> ,9 <i>E</i>)-3-(2-(<i>tert</i> -Butyldiphenylsilyloxy)ethyl)-14-hydroxy-4- (methoxymethoxy)-3,4-dihydro-1 <i>H</i> -benzo[<i>c</i>][1]oxacyclododecin-1-one (154) .	220
(<i>E</i>)-Hex-5-ynyl 2-(2-Iodovinyl)-6-methoxybenzoate (156) .	236
(7 <i>Z</i> ,9 <i>E</i>)-14-Methoxy-3,4,5,6-tetrahydro-1 <i>H</i> -benzo[<i>c</i>][1]oxacyclododecin-1- one (157) .	237
(3 <i>S</i> ,4 <i>S</i> ,5 <i>Z</i> ,7 <i>Z</i> ,9 <i>E</i>)-3-(2-Hydroxyethyl)-14-methoxy-4-(methoxymethoxy)- 3,4-dihydro-1 <i>H</i> -benzo[<i>c</i>][1]oxacyclododecin-1-one (159) .	222
2-((3 <i>S</i> ,4 <i>S</i> ,5 <i>Z</i> ,7 <i>Z</i> ,9 <i>E</i>)-14-Methoxy-4-(methoxymethoxy)-1-oxo-3,4- dihydro-1 <i>H</i> -benzo[<i>c</i>][1]oxacyclododecin-3-yl)ethanal (160) .	223
(3 <i>S</i> ,4 <i>S</i> ,5 <i>Z</i> ,7 <i>Z</i> ,9 <i>E</i>)-3-((<i>Z</i>)-3-Iodoallyl)-14-methoxy-4-(methoxymethoxy)- 3,4-dihydro-1 <i>H</i> -benzo[<i>c</i>][1]oxacyclododecin-1-one (161) .	224
(3 <i>S</i> ,4 <i>S</i> ,5 <i>Z</i> ,7 <i>Z</i> ,9 <i>E</i>)-4,14-Dihydroxy-3-((<i>Z</i>)-3-iodoallyl)-3,4-dihydro-1 <i>H</i> - benzo[<i>c</i>][1]oxacyclododecin-1-one (162) .	226
(3 <i>S</i> ,4 <i>S</i> ,5 <i>Z</i> ,7 <i>Z</i> ,9 <i>E</i>)-4-Hydroxy-3-((<i>Z</i>)-3-iodoallyl)-14-methoxy-3,4- dihydro-1 <i>H</i> -benzo[<i>c</i>][1]oxacyclododecin-1-one (163) .	225
5-Hydroxy-1 <i>H</i> -pyrrol-2(5 <i>H</i>)-one (164) .	228

(2Z)-N-((Z)-4-((3S,4S,5Z,7Z,9E)-4,14-Dihydroxy-1-oxo-3,4-dihydro-1H-benzo[<i>c</i>][1]oxacyclododecin-3-yl)but-2-enyl)-4-(methoxyimino)but-2-enamide (165).	245
(3S,4S,5Z,7Z,9E)-4,14-Bis(<i>tert</i> -butyldimethylsilyloxy)-3-((Z)-4-hydroxybut-2-enyl)-3,4-dihydro-1H-benzo[<i>c</i>][1]oxacyclododecin-1-one (166).	240
(Z)-Methyl 4-((3S,4S,5Z,7Z,9E)-4,14-Bis(<i>tert</i> -butyldimethylsilyloxy)-1-oxo-3,4-dihydro-1H-benzo[<i>c</i>][1]oxacyclododecin-3-yl)but-2-enoate (170).	238
1-((Z)-4-((3S,4S,5Z,7Z,9E)-4,14-Bis(<i>tert</i> -butyldimethylsilyloxy)-1-oxo-3,4-dihydro-1H-benzo[<i>c</i>][1]oxacyclododecin-3-yl)but-2-enyl)-1H-pyrrole-2,5-dione (175).	241
1-((Z)-4-((3S,4S,5Z,7Z,9E)-4,14-Bis(<i>tert</i> -butyldimethylsilyloxy)-1-oxo-3,4-dihydro-1H-benzo[<i>c</i>][1]oxacyclododecin-3-yl)but-2-enyl)-5-hydroxy-1H-pyrrol-2(5H)-one (178).	242
(2Z)-N-((Z)-4-((3S,4S,5Z,7Z,9E)-4,14-Bis(<i>tert</i> -butyldimethylsilyloxy)-1-oxo-3,4-dihydro-1H-benzo[<i>c</i>][1]oxacyclododecin-3-yl)but-2-enyl)-4-(methoxyimino)but-2-enamide (179).	243
(Z)-Methyl 4-((3S,4S,5Z,7Z,9E)-4,14-Dihydroxy-1-oxo-3,4-dihydro-1H-benzo[<i>c</i>][1]oxacyclododecin-3-yl)but-2-enoate (180).	246
(3S,4S,5Z,7Z,9E)-4,14-Dihydroxy-3-((Z)-4-hydroxybut-2-enyl)-3,4-dihydro-1H-benzo[<i>c</i>][1]oxacyclododecin-1-one (181).	247

1-((<i>Z</i>)-4-((3 <i>S</i> ,4 <i>S</i> ,5 <i>Z</i> ,7 <i>Z</i> ,9 <i>E</i>)-4,14-Dihydroxy-1-oxo-3,4-dihydro-1 <i>H</i> -benzo[<i>c</i>][1]oxacyclododecin-3-yl)but-2-enyl)-5-hydroxy-1 <i>H</i> -pyrrol-2-(5 <i>H</i>)-one (183).	248
1-(4-Chloro-3-nitrophenyl)-1 <i>H</i> -pyrrole (238).	253
Methyl 2-Chloro-5-(1 <i>H</i> -pyrrol-1-yl)benzoate (239).	258
2-Chloro- <i>N,N</i> -dimethyl-5-(1 <i>H</i> -pyrrol-1-yl)benzamide (240).	259
2-Chloro-3-(1 <i>H</i> -pyrrol-1-yl)benzoic acid (242).	249
2-Chloro-4-(2,5-dimethyl-1 <i>H</i> -pyrrol-1-yl)benzoic acid (245).	250
3-Hydroxy-4-(1 <i>H</i> -pyrrol-1-yl)benzoic acid (247).	250
2-Hydroxy-4-(1 <i>H</i> -pyrrol-1-yl)benzoic acid (249).	251
2-Chloro-4-(1 <i>H</i> -pyrrol-1-yl)benzoic acid (251).	252
3-Nitro-4-(1 <i>H</i> -pyrrol-1-yl)benzoic acid (253).	253
4-(1 <i>H</i> -Pyrrol-1-yl)phenol (256).	254
2-(3-(1 <i>H</i> -Pyrrol-1-yl)phenyl)acetic acid (258).	255
2-Chloro-5-(Pyrrolidin-1-yl)benzoic acid (261).	256
2-Chloro-5-(2,5-dioxopyrrolidin-1-yl)benzoic acid (263).	256
2-Chloro-5-(2,5-dioxo-2,5-dihydro-1 <i>H</i> -pyrrol-1-yl)benzoic acid (265).	257
2,3,7,8-Tetrachloro-10 <i>H</i> -phenothiazine (274).	261
(4,5-Dichloro-2-nitrophenyl)(2,4,5-trichlorophenyl)sulfane (277).	260
4,5-Dichloro-2-(2,4,5-trichlorophenylthio)aniline (278).	260

List of Abbreviations

AcCl – acetyl chloride

AD - asymmetric dihydroxylation

atm – atmosphere

br – broad

CuTC – copper thiophene carboxylate

d – doublet

DEAD – diethyl azodicarboxylate

DDQ – 2,3-dichloro-4,5-dicyano-1,4-benzoquinone

DIBAL – diisobutylaluminum hydride

DIPEA – *N,N*-diisopropylethylamine

DMA – *N,N*-dimethylacetamide

DMF – *N,N*-dimethylformamide

er – enantiomeric ratio

EDCI - *N*-(3-dimethylaminopropyl)-*N'*-ethylcarbodiimide hydrochloride

ESI – electrospray ionization

EtOAc – ethyl acetate

Et₂O – diethyl ether

g - gram

g – relative centrifugal force

h – hour

HCl – hydrochloric acid

HF – hydrofluoric acid

HMPA - hexamethylphosphoramide

HPLC – high pressure liquid chromatography

HWE – Horner-Wadsworth-Emmons

Hz – Hertz

ⁱPr – isopropyl

IR – infrared

KO^tBu – potassium *tert*-butoxide

LG – leaving group

LRMS – low resolution mass spectrometry

m – multiplet

Me – methyl

MeCN – acetonitrile

MeOH – methanol

mg – milligram

MHz – megahertz

min – minute

μL – microliter

mL – milliliter

mmol – millimole

MOM – methoxymethyl

NA – not available

NaHMDS – sodium bis(trimethylsilyl)amide

NaO^tBu – sodium *tert*-butoxide

NCI – National Cancer Institute

ⁿBuLi – lithium-1-butanide

NMR – nuclear magnetic resonance

PMB – *p*-methoxybenzyl

PPTS – pyridinium *p*-toluenesulfonate

PS-TSNH₂ – polystyrenyl sulfonyl hydrazine

Py. – pyridine

q – quartet

qu – quintet

s – singlet

se – sextet

t – triplet

TBAF – *n*-tetrabutylammonium fluoride

^tBuLi – lithium-2-methyl-2-propanide

^tBuOH – 2-methyl-2-propanol

THF – tetrahydrofuran

TLC – thin layer chromatography

TMSCH₂N₂ – (trimethylsilyl)diazomethane

UPLC-MS – ultra-high pressure liquid chromatography-mass spectrometry

V-ATPase – vacuolar-(H⁺)-adenosine triphosphatase

Chapter 1

Total Synthesis and Analog Development of Oximidine II

1.1 Introduction to Benzolactone Enamides

Natural products are great resources for pharmaceutical lead development.^{1,2} These molecules possess certain advantages when compared to molecules typically found in high-throughput screening (HTS) collections. Natural products contain diverse structural complexity and inherent chirality that may favor binding to certain enzymes or protein interfaces. Depending upon the specific biochemical role of the molecule inside the engineering organism, the molecule may be expected to cross cell membranes. Whether this process occurs by active or passive transport, this inherent permeability quality gives natural products another advantage over synthesized molecules with respect to cellular uptake. Natural products may or may not follow Lipinski's rules for oral absorption.³ Regardless, they possess many attractive features that prompt their continued investigation for new therapeutic development.

The benzolactone enamides are a family of recently identified natural products with potent biological activity. These molecules, displayed in Figure 1, have three characteristic structural features – a salicylate moiety, a macrolactone, and an enamide side chain. There are currently five families in this natural product class: (–)-salicylihalamide A (**1**) and B (**2**), CJ-12,950 (**3**) and CJ-13,357 (**4**), lobatamides A-F (**5-10**), apicularen A (**11**) and B (**12**), and oximidines I-III (**13-15**). The lobatamide

molecules contain 15-membered macrolactones, while the other members contain 12-membered macrolactones.⁴

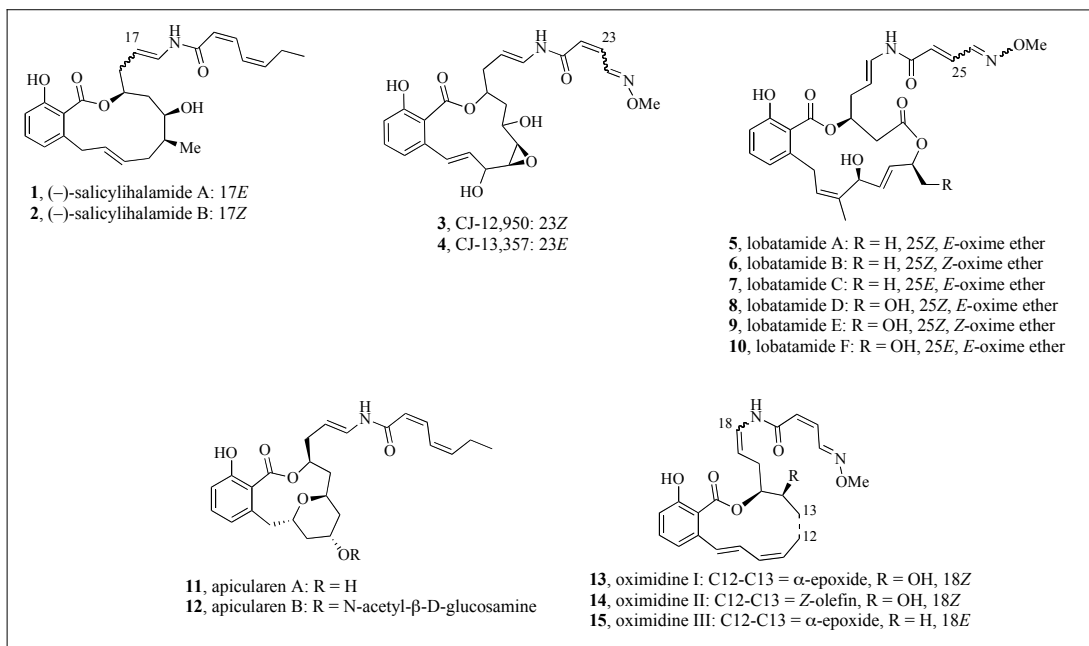


Figure 1. Members of benzolactone enamide natural product family

Salicylihalamides A and B were discovered from a cytotoxicity assay of the crude extract of the *Haliclona* sponges in 1997 by Boyd and coworkers at the National Cancer Institute (NCI).^{5,6} Testing of these compounds in the NCI 60-cell cancer assay revealed a selective cytotoxicity profile at that time unmatched in the NCI database, suggestive of a new mechanism of action. Salicylihalamide A (**1**) was shown to be most cytotoxic against melanoma cancer types and displayed an overall mean GI₅₀ of 15 nM with a sensitivity range of 1000 across the panel of cell lines.

While screening secondary metabolites of the zygomycete *Mortierella verticillata* for expression of the low density lipoprotein (LDL) receptor gene,

researchers from Pfizer discovered the CJ compounds, CJ-12,950 (**3**) and CJ-13,357 (**4**).⁷ Increasing the production of LDL receptors leads to an increase in the cellular uptake of circulating LDL, thus decreasing the potential of freely circulating cholesterol to deposit on blood vessel walls.⁸ LDL, the “bad cholesterol”, is a contributing factor to a variety of diseases including atherosclerosis and coronary heart disease. Compounds **3** and **4**, however, did not affect cholesterol synthesis, tubulin polymerization, or lysosomal pH.

The Boyd group isolated lobatamides A and B (**5** and **6**) in 1997⁹ and lobatamides C-F (**7-10**) in 1998¹⁰ from tunicate *Aplidium* species of the southwest Pacific Ocean. Following Boyd’s discovery in 1997, Suzumura *et al.* isolated YM-75518 from the fermentation broth of *Pseudomonas* sp. Q38009.¹¹ Later, this molecule was reassigned as lobatamide A. The isolation of the molecule from two different species suggests that its biosynthesis may occur in related microorganisms living in the parent species or that the molecule is present in their diet. Testing of compounds **5-8** in the NCI 60-cell human cancer assay revealed a differential cytotoxicity profile similar to salicylhalimide A¹⁰ as determined by a COMPARE analysis.¹² The COMPARE analysis is an algorithm used to compare results from the NCI-60 cell assay between compounds to determine if the compounds share a similar mechanism of action. Lobatamide A and salicylhalamide A were most active against melanoma and leukemia cancer types.

Apicularen A (**11**) and its *N*-acetyl-glucosamine glycoside apicularen B (**12**) were isolated in 1998 from myxobacteria of the *Chondromyces* genus by Kunze *et*

*al.*¹³ Interestingly, apicularen A was potently cytotoxic and displayed single digit nM IC₅₀ values across 9 different cell lines but displayed no antibiotic activity, while apicularen B was modestly antibiotic and 1000-fold less cytotoxic than apicularen A. The biosynthesis of apicularen A was investigated through ¹³C-acetate feeding experiments.¹⁴ Based on incorporation of the carbon isotope, biosynthesis of apicularen was proposed to occur through a modular polyketide synthase containing a nonribosomal peptide synthetase.

Hayakawa and coworkers isolated the highly unsaturated benzolactone enamides oximidines I-III (**13-15**) from *Pseudomonas* strains.¹⁵⁻¹⁷ These molecules demonstrated selective cytotoxicity towards rat 3Y1 fibroblasts mutated with the *src* oncogene,¹⁸ *ras* oncogene,¹⁹ or adenovirus E1A²⁰ compared to normal rat 3Y1 fibroblasts. Oximidines II and III, containing only one oxygen bonded to carbons 12, 13, or 14, were generally at least twice as active as the doubly-oxygenated oximidine I in these assays.

In 2001, the Boyd laboratories at the NCI identified the cellular target for the benzolactone enamides.²¹ Screening oximidine II in the 60-cell panel gave a differential selectivity profile matching the previous salicylhalimide A and lobatamide A screening results, suggesting that these molecules share a similar mechanism of action. Apicularen A was subsequently shown to share an identical screening profile.^{14,22} Database analyses from the 60-cell assay matched reactivity profiles to the known vacuolar-(H⁺)-adenosine triphosphatase (V-ATPase) inhibitors bafilomycin A₁ (**16**, Figure 4)²³⁻²⁵ and concanamycin A (**17**, Figure 4).²⁶⁻²⁸ A

COMPARE analysis¹² correlated the results between the benzolactone enamides and these V-ATPase inhibitors.²¹ Testing of the benzolactone enamides in various V-ATPase assays confirmed their biological target. Interestingly, this family of natural products inhibits only mammalian types of this eukaryotic enzyme. Subsequent biological assessment of salicylihalamide A and lobatamide A showed they too were selective for rat mutated 3Y1 fibroblasts similar to oximidines I-III. Additional biological information regarding the CJ compounds has not been reported beyond the initial isolation publication.

1.2 Biological Significance of V-ATPases

The eukaryotic transport protein V-ATPase (Figure 2) is responsible for pH homeostasis in various intracellular organelles, such as the Golgi apparatus, endosomes²⁹ and lysosomes.^{30,31} This pH control results in the regulation of cellular processes such as the degradation of proteins and other molecules, receptor-mediated endocytosis, and coupled transport of various small molecules. V-ATPases have also been found on the plasma membrane of certain cells.³² These enzymes play crucial roles in renal acidification (renal intercalated cells in kidneys),³³ bone resorption and degradation (osteoclasts),³⁴ control of cytoplasmic pH (macrophages)³¹ and sperm maturation (clear cells in vas deferens and epididymus).³⁵

V-ATPases are ATP-dependent proton pumps and use energy released by ATP hydrolysis to shuttle protons from external sources into the organelle or cell.^{30,31} They are comprised of two domains, a membrane-bound V_0 domain and an

extramembranal V_1 domain (Figure 2). These domains can dissociate and re-associate under certain conditions, but the underlying mechanisms of these processes are not completely understood. The domains are formed by a number of subunits that serve specific enzymatic functions. V_0 consists of 6 subunits: a, c, c', c'', d and e, of which only a, c, c'', d and e are found in mammalian cells. Subunit a contains an arginine residue that is critical for proton influx. Subunits c and c'' contain glutamate residues buried deep within these channel-shaped subunits that are responsible for harboring the proton to be transported across the membrane. The exact stoichiometry of these subunits remains to be deduced, but most evidence supports a total of six c and c'' subunits and one a, d, and e subunit per enzyme as shown in Figure 2. V_1 consists of eight subunits, A-H. Subunits A and B serve as the ATP binding sites. These two subunits are present in a higher stoichiometry than the other subunits, similar to the subunits of V_0 . The other subunits of V_1 function either to rigidify the enzyme complex or to connect the two domains.

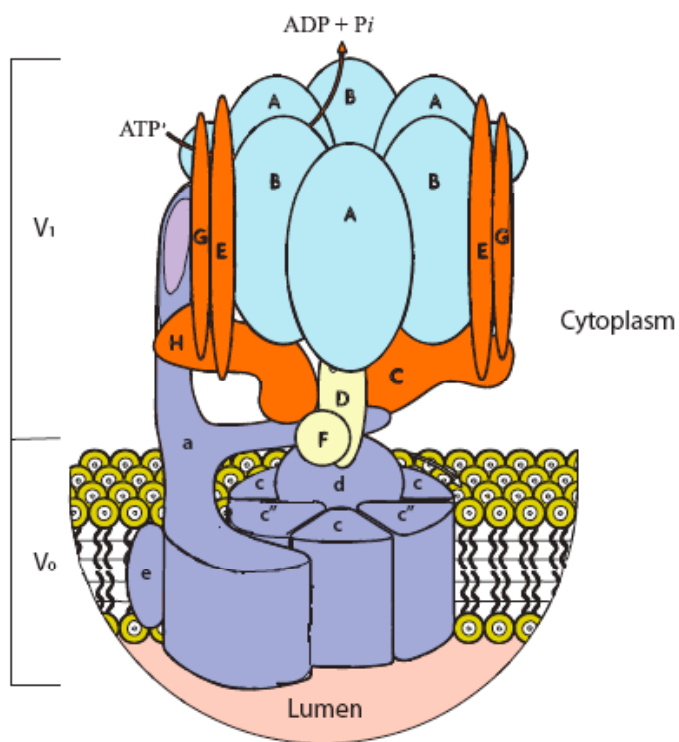


Figure 2. Structure of V-ATPase³¹

There are three known types of ATPases – P-ATPases, F-ATPases, and V-ATPases.³⁶ These enzymes transport ions through ATP-dependent processes. P-ATPases use ATP hydrolysis to fuel the transport of cations, such as Na^+ , K^+ or Ca^{2+} , across membranes and are widely distributed throughout the body. F-ATPases and V-ATPases are structurally similar and transport protons across different membranes. They differ in location and how ATP is involved in the enzymatic activity. F-ATPases are found mostly in the mitochondria and are partly responsible for synthesizing ATP in the cell, hence the classification as an ATP-synthase. V-ATPases are found elsewhere in the cell and hydrolyze ATP to ADP as part of its catalytic mechanism.

The V-ATPase proton pumps operate via a rotary mechanism as shown in Figure 3.³¹ A proton enters the enzyme from the cytoplasm first through the hemichannel subunit a (panel A). The proton is then shuttled to the glutamate residues on subunits c and c'' (panel B) where it resides until release into the organelle. ATP hydrolysis on the interface of subunits A and B causes rotation of subunits c and c'' relative to subunit a (panel C). This rotation forces the realignment of the protein in such a way that the proton is shuttled from the glutamate residue back to subunit a, protonating the key arginine residue (panel D). The proton is then released into the organelle to complete the catalytic cycle.

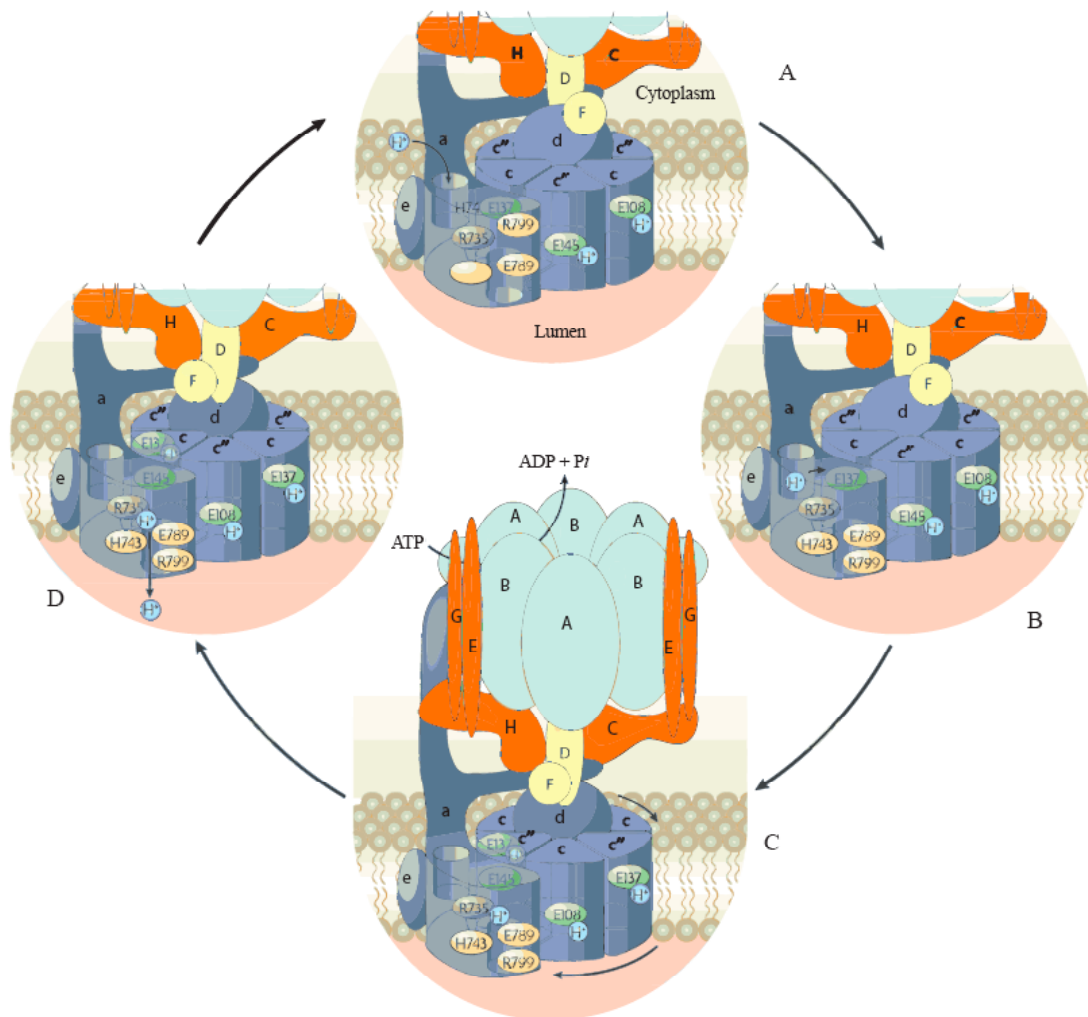


Figure 3. V-ATPase catalytic cycle³¹

Mammals express multiple isoforms of the V-ATPase subunits. The incorporation of different subunit isoforms does not alter the enzymatic mechanism. However, different isoforms are expressed in different membranes, potentially allowing for selective drug targeting. Two isoforms of subunit E are known, E1 and E2, but only E2 is expressed in the testis, creating a prospective opportunity for male contraceptive development.³⁷ Malfunction of specific isoforms may contribute to

certain diseases.³⁵ Mutation of the renal a (V₀) or B (V₁) subunit isoforms leads to distal renal tubule acidosis.³⁸ Hyperactivity or hypoactivity of V-ATPases in osteoclast cells leads to osteoporosis or osteopetrosis, respectively.³⁵

The V-ATPase system is important for normal human physiology but can be manipulated by various diseases.^{31,35} A basic cellular function of the V-ATPase system is to regulate the internalization of specific macromolecules through the endocytotic process. Certain viruses, such as the influenza virus, and certain bacterial toxins, such as diphtheria and anthrax, use this pathway to enter healthy cells.

The role of V-ATPases in cancer pathology is broad. Of the six hallmarks of cancer,³⁹ V-ATPase is involved in at least three – tissue invasiveness and metastasis, sustained angiogenesis and evasion of apoptosis.

V-ATPases are more expressed on highly metastatic cancer cell surfaces than on the surface of less metastatic cells.^{32,38} The increased V-ATPase population serves two symbiotic functions. Increased glycolysis rates inside the cancer cell lead to increased proton production.⁴⁰ However, an alkaline cytoplasmic pH is necessary for cancer cell survival.^{41,42} Pumping of these extra protons into the extracellular space generates an acidic environment for certain secreted proteins, such as cathepsins, to become active. These proteins are known to degrade the extracellular matrix surrounding cells, allowing metastasis to occur. It is unclear if cathepsin activation is the only extracellular role for V-ATPase activity in tumor metastasis. However, treatment of highly metastatic cells with V-ATPase inhibitors, such as the natural

product bafilomycin³⁸ or an indole compound,⁴³ greatly attenuated the migration and invasion of these cells.

The recruitment of new vasculature, the process known as angiogenesis, is required for tumor expansion. Direct access to the circulatory system also allows tumor metastasis to new sites in the body.^{44,45} Studies from the labs of Sennoune and Martinez-Zaguilan have shown that microvascular endothelial cells, cells instrumental in angiogenesis, overexpress V-ATPase enzymes on their plasma membrane similar to cancer cells.^{44,45} Thus, inhibiting migration of these endothelial cells to the growing tumor would prevent tumor expansion by cutting off its food and blood supply.

The mechanism by which V-ATPases cause apoptosis is not clearly defined and may involve more than one pathway. It is known that cellular acidosis, potentially resulting from increased glycolysis, leads to apoptosis.^{46,47} Inhibition of V-ATPases can also trigger apoptosis⁴⁸ through both caspase-dependent⁴⁹ and caspase-independent⁵⁰ pathways. Higher than normal V-ATPase levels have been seen on certain cancer cell types and may resist drug-induced apoptosis due to the presence of a non-P-glycoprotein multi-drug efflux pump.³⁶ It has been demonstrated that use of a V-ATPase inhibitor in combination with an anti-cancer agent increases cancer cell sensitivity towards chemotherapy,^{51,52} impacting cell viability at doses lower than the necessary dose for a single agent. This result highlights the potential impact of V-ATPase inhibitors on cancer chemotherapy.

V-ATPases also play a role in the complex autophagy pathway in eukaryotic cells. Autophagy is the intracellular degradation of proteins and organelles resulting from certain environmental stresses.⁵³ Cancer cells that avoid apoptosis use the autophagy pathway to recycle mutated proteins and protect the cell from metabolic stress.⁵⁴ The autophagy pathway can also destroy cancer cells.⁵⁵ Certain types of cancers such as breast⁵⁶ or prostate cancer⁵⁷ undergo cell death not by apoptosis but by autophagy following radiation or chemotherapeutic treatment.^{55,58} In these studies, co-administration of the V-ATPase inhibitor bafilomycin (**16**) with temozolomide led to increased cell death compared to use of temozolomide alone.⁵⁷ The exact role of autophagy in cancer cells is unknown, as inhibitors of autophagy are known to produce both cell death and cell growth.⁵⁵ V-ATPase inhibitors could be used to gain a better understanding of these complex processes.

1.3 V-ATPase Inhibitors – Investigation of Benzolactone Enamides

Although not all of the physiological consequences of V-ATPase modulation are understood, investigators have sought inhibitors of the enzyme. V-ATPases influence a variety of disease states and selective inhibition could have an impact in many therapeutic areas. Several synthetic compounds³⁴ and natural products^{4,34,59,60} have been discovered that bind selectively to V-ATPases. These molecules bind in the ATP binding site³⁴ or on various subunits.⁵⁹ Despite therapeutic potential towards a number of diseases, V-ATPase inhibitors have been mainly investigated as anti-osteoporosis or anti-cancer agents.

The first selective V-ATPase inhibitors, the plecomacrolides concanamycin^{26,28} (**17**) and bafilomycin^{23,24} (**16**, Figure 4) were identified in 1988. Concanamycin A selectively targets V-ATPases, displaying 250,000-fold selectivity for V-ATPases vs. K⁺ P-ATPases, while bafilomycin A is 7,200-fold selective for V-ATPases vs. K⁺ P-ATPases.²⁵ Neither molecule is active against F-ATPases. V-ATPase mutagenic studies demonstrated that the plecomacrolides bind in subunit c on the V₀ complex.⁶¹ Further photoaffinity labeling using a concanamycin analog confirmed this result.^{27,62} Analogs of bafilomycin A have been investigated for V-ATPase inhibitory properties.⁶³ Despite significant interest in these molecules, their *in vivo* toxicity has halted further development. The plecomacrolides were instrumental in demonstrating that V-ATPases are relevant biological targets for the treatment of cancer and osteoporosis, spawning further research.

Since the discovery of the plecomacrolides, other macrolides have been isolated that display V-ATPase inhibitory properties. The chondropsin class of macrolides (chondropsin B, **18**, Figure 4) was tested in the NCI 60-cell panel in 2003.⁶⁴ These molecules displayed potent cytotoxicity, exhibiting a mean GI₅₀ of 25.6 nM across the panel. Using a COMPARE correlation analysis, the chondropsins were identified as V-ATPase inhibitors and confirmed in subsequent biological assays. Archazolids A (**19**) and B (**20**) were isolated in 2003 from the culture broth of various myxobacteria species.⁶⁵ Ensuing studies revealed that these molecules, similar to the plecomacrolides, bind to the c subunit on the membrane-bound V₀ complex of V-ATPases.⁶⁶ Glycoside-containing archazolids C⁶⁷ (**21**) and D⁶⁸ (**22**) were isolated in

2007 and were shown to have attenuated biological properties compared to A (**19**) and B (**20**) (further analog development of the archazolids).⁶⁹ The iejimalides (**23** and **24**) were isolated in 2006 and exhibited mean log GI₅₀'s between -6.67 and -6.11 (correlating to 214 and 776 nM, respectively) across 39 different human cancer lines.⁷⁰ Interestingly, a COMPARE analysis did not suggest a mechanism of action despite the known V-ATPase inhibitor profile. However, testing of these molecules in V-ATPase assays by Kazami and coworkers demonstrated V-ATPase IC₅₀ values between 71 and 95 nM and that the iejimalies were potent anti-osteoporotic compounds.⁷¹ The most recently isolated V-ATPase-targeting macrolide is palmerolide A (**25**), isolated from Antarctic tunicates.⁷² This enamide-containing macrolide, while not potently cytotoxic (μ M IC₅₀ values across different cancer lines), is active against V-ATPases with an IC₅₀ value of 2 nM.

Small molecule synthesis groups at pharmaceutical companies have not ignored the promise of V-ATPase inhibition as a treatment for osteoporosis and cancer. Astellas Pharma Inc. in Japan recently detailed their novel quinoline compound FR202126 (**26**, Figure 4) as a potential treatment for periodontitis.⁷³ Periodontitis is the inflammation and infection of the ligaments and bones that support the teeth. This process is coupled with bone loss in the alveolar bone, similar to osteoporosis. FR202126 displayed an IC₅₀ of 99 nM in a proton transport assay using plasma membrane vesicles of murine osteoclasts. Further murine *in vivo* testing demonstrated blockage of bone resorption in alveolar bones, generating a proof of concept. A two-week murine toxicity test showed growth of a femoral bone

following treatment with FR202126. While the development of this compound was halted due to this side effect, it demonstrates that a selective V-ATPase inhibitor could be useful *in vivo* in treating bone loss. Inspired by bafilomycin, a series of indolyl compounds (**27**) were investigated for their bone antiresorptive properties.^{74,75} These compounds were selective for human osteoclast V-ATPases versus other human isoforms of the enzyme,⁷⁵ displaying nanomolar potency against osteoclast V-ATPases and in bone antiresorptive assays. Another synthetic indolyl compound, NiK-12192 (**28**, Figure 4), has been reported to potentiate the cytotoxic effects of camptothecin in both *in vitro* and *in vivo* models.⁷⁶ Further studies with this molecule displayed its ability to modulate the metastatic properties of lung carcinoma *in vitro* and *in vivo*. When a nude mouse was implanted with a human lung carcinoma, the tumor's metastasis was halted.⁴³ However, the implanted tumor continued to grow inside the target organ, potentially highlighting the limits for V-ATPase inhibition as an anti-cancer target. V-ATPase inhibitors may be useful anti-cancer agents when co-administered with other anti-cancer therapeutics, as previously discussed. Another deduction from these results is that more potent, irreversible compounds are required to ascertain substantial anti-cancer effects from V-ATPase inhibitors.

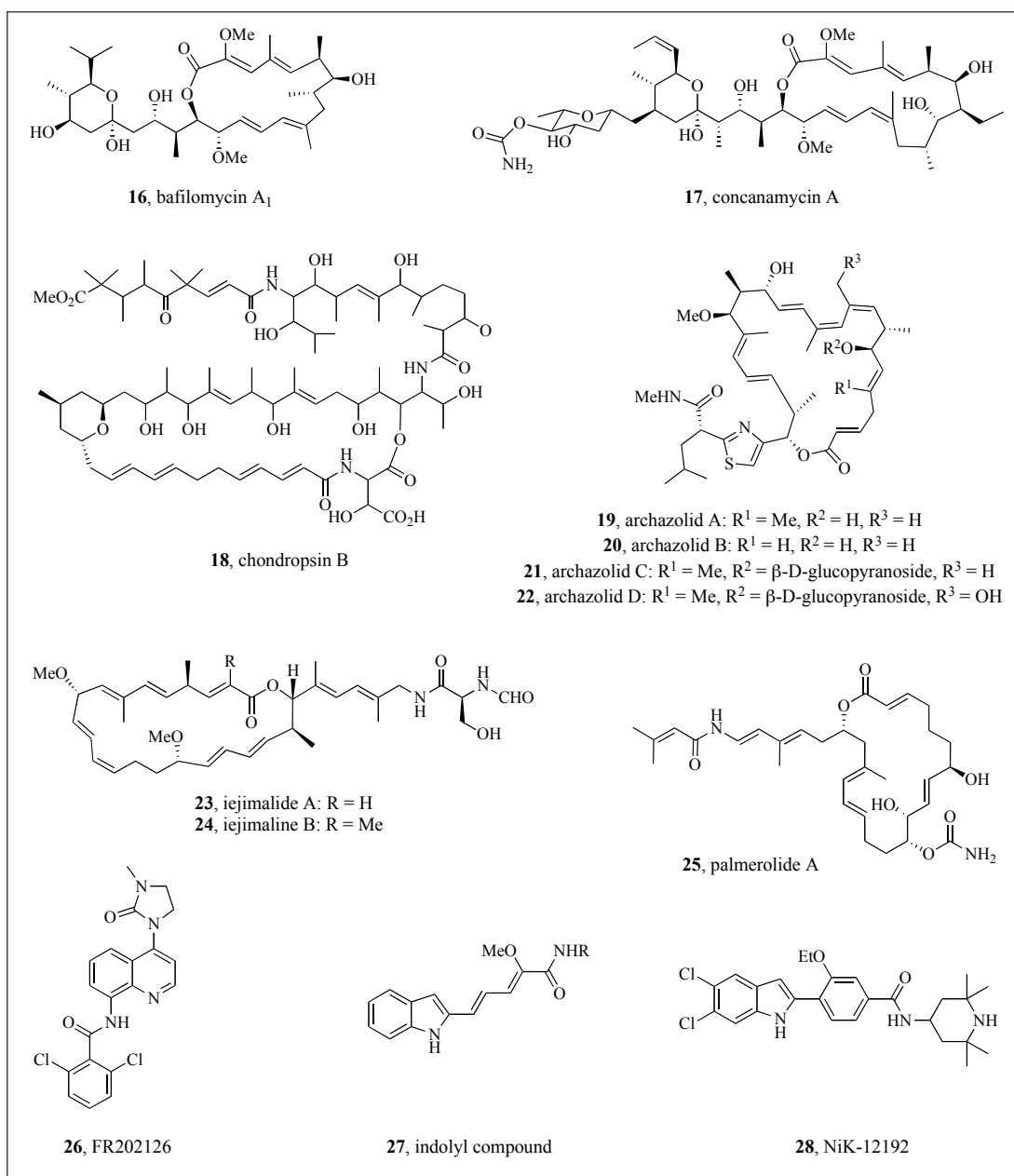


Figure 4. Reported V-ATPase inhibitors

The benzolactone enamides are the only known V-ATPase inhibitors that selectively target mammalian enzyme types.⁴ The reasoning behind this eukaryotic differentiation is unknown. Binding studies by Xie *et al.* have shown that this natural

product family binds somewhere in the membrane-bound V_0 region of the holoenzyme, similar to the plecomacrolides.⁷⁷ However, competitive binding studies have shown that salicylihalamide does not bind to the same binding site as bafilomycin or concanamycin.²⁷ The exact subunit targeted by the benzolactone enamides is still unknown despite their irreversible interaction with the enzyme.⁷⁷

The De Brabander group proposed a mechanism for irreversible inhibition based on *N*-acyl-iminium ion chemistry (Figure 5). Under acidic conditions, *N*-acyl enamides can form *N*-acyl-iminium ions.⁷⁸ Following protonation of the olefin, a stabilized carbocation is generated. This *N*-acyl iminium ion could then react with a variety of nucleophilic residues within the V-ATPase binding site. This mechanism was supported by analog studies by the group that demonstrated the necessity of an *N*-acyl enamide for irreversible binding to the enzyme.⁷⁷ Analogs lacking this functionality but containing a Michael-accepting hexadienyl side chain were not irreversible inhibitors.

To more thoroughly investigate this mode of action and to try to discover the residue responsible for covalent bond formation, the group synthesized a radiolabeled salicylihalamide analog.⁷⁷ Placement of the radiolabel on the enamide side chain and incubation with bovine brain V-ATPase surprisingly revealed only a small amount of radiolabeled protein despite high levels of proton pump inhibition, indicating that the side chain is most likely not covalently bound to the enzyme. These studies additionally could not deduce the subunit binding site or specific residue that bound the radiolabeled analog.

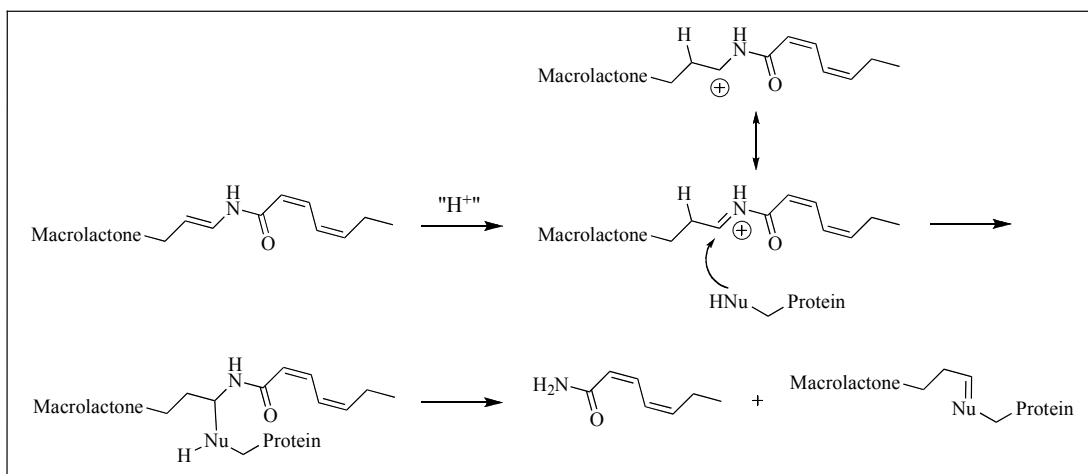


Figure 5. Proposed mechanism of inhibition by the enamide side chain⁷⁷

Prior to the mechanism of action studies by De Brabander, his group synthesized a series of analogs to develop the structure-activity relationship (SAR) for the enamide side chain. An easily synthesized enamide carbamate analog⁷⁹ (entry 7, Table 1) exhibited a similar biological profile compared to salicylihalamide A, with an IC_{50} of 1.6 nM against bovine brain V-ATPases and irreversible inhibition of the enzyme. While saturation of the macrolactone olefin (entry 8) only marginally reduced the V-ATPase inhibitory properties of the molecule, reduction of the enamide double bond (entry 9) resulted in a 10-fold shift in the V-ATPase inhibition.⁸⁰ This molecule also displayed reversible binding to the protein. Attempts to model the proposed electrophilicity of the generated *N*-acyl iminium ion through development of α,β -unsaturated carbonyl compounds were moderately successful. The α,β -unsaturated ketone derivative (entry 3) displayed good V-ATPase inhibition but was a reversible inhibitor in various assays. The enoate analog (entry 4) was much less potent. The differences displayed by these two analogs could be due to the placement

of the double bond or to the length of the side chain. The group also probed the size of the lipophilic side chain binding pocket. The saturated hexane side chain analog (entry 5) retained potent V-ATPase inhibition but was five-fold less active against the SK-MEL-5 melanoma cancer cell line compared to salicylihalamide A. A phenylacetylene derivative (entry 6) was similarly potent to the saturated hexane side chain analog and showed irreversible inhibition, again displaying the necessity for an enamide moiety for covalent bonding to the protein. While these analogs did not improve the anti-cancer properties of the natural product, the data suggests that covalent adduct formation is not necessary for successful V-ATPase inhibition by the benzolactone enamides.

Other analog studies probed the macrolactone core of salicylihalamide A. The absolute stereochemistry of the molecule is important. The unnatural enantiomer (entry 2, Table 1), (+)-salicylihalamide,⁸⁰ displayed greatly attenuated V-ATPase inhibitory activity (270 nM) and was ineffective at inhibiting the growth of SK-MEL-28 melanoma cancer cells at 20 μ M.⁸¹ Eliminating the hydrogen donating ability of either the phenol (entry 1, Table 2) or the secondary alcohol (entry 2) dramatically reduced the biological properties of the molecule. Smith and coworkers synthesized a modified macrolactone analog of the natural product, removing the alcohol and methyl groups (entry 4).⁸² This had a moderate effect on the GI₅₀ values, reducing the potency of the molecules against various cancer lines 10-fold compared to salicylihalamide A (entry 6). Reducing the C9-C10 macrolactone olefin (entry 5), allowing for more flexibility in the macrolactone, did not perturb the bioactivity of

the analog compared to the unsaturated analog (entry 4). Following this work, the De Brabander group synthesized a series of macrolactone ether analogs⁸³ lacking the methyl (entry 7) and hydroxyl (entry 8) groups appended to the core of salicylihalamide A. The benzoate compound lacking the phenol moiety (entry 8) was inactive in various biological assays, highlighting the necessity for hydrogen bonding of the phenol for bioactivity. The size requirement for the macrolactone is highlighted in entry 9. Against different cancer cell lines from the NCI 60-cell assay, this truncated analog was about 1000-fold less active than the parent natural product.⁸⁴ A fluorinated analog of salicylihalamide A (entry 10) has also been made in an attempt to use ¹⁹F NMR to elucidate the binding mode of the benzolactone enamides.⁸⁵ With an IC₅₀ of 2 nM, this molecule retained the potent anti-V-ATPase activity of the parent molecule. Further studies with this molecule have not been published.

Table 1. Salicylihalamide enamide analogs and biological activity

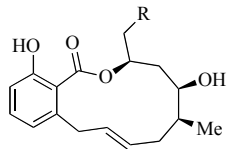
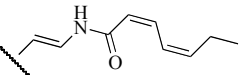
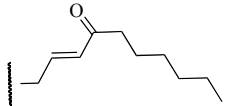
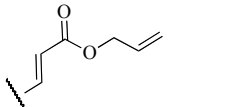
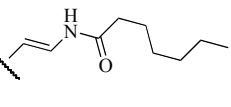
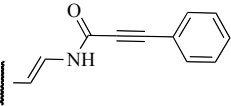
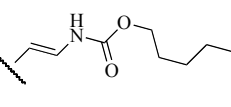
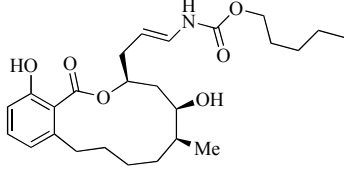
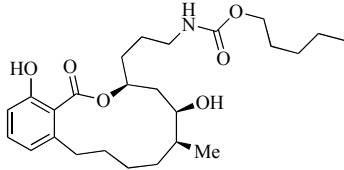
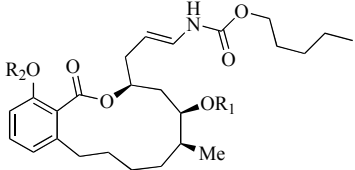
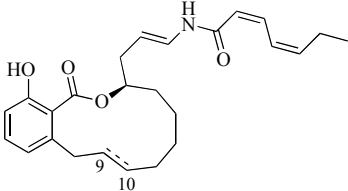
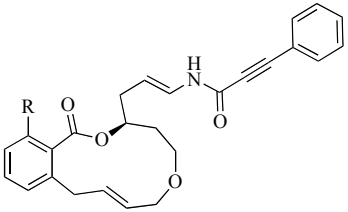
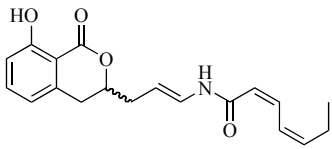
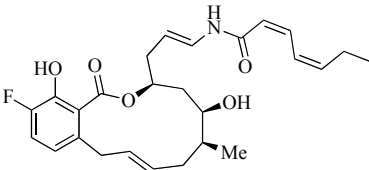
Entry	Analog Structure	V-ATPase IC ₅₀ (nM)	SK-Mel-5 Growth Inhibition (IC ₅₀ in μ M)	Binding Mode	Reference
					
	R = 				
1	1, (-)-salicylihalamide A	< 1	0.060	irreversible	80
2	(+)-salicylihalamide A	270	NA	NA	80
3		7.5	NA	reversible	77
4		230	> 20	NA	77
5		1	0.38	NA	77
6		< 1	0.3	irreversible	77
7		1.6	0.5	irreversible	77
8		3	8	NA	77
9		30	> 20	reversible	77

Table 2. Salicylihalamide core analogs and biological activity

Entry	Analog Structure	V-ATPase IC ₅₀ (nM)	Biological Activity	Reference
				
1	R ₁ = H, R ₂ = Bz	180	IC ₅₀ > 20 μM	80
2	R ₁ = Bz, R ₂ = H	300	IC ₅₀ = 1 μM	80
3	1 , salicylihalamide A	> 1	IC ₅₀ = 0.06 μM	80
				
4	C9-C10 <i>E</i> -olefin	NA	GI ₅₀ = 0.11-0.87 μg/mL	82
5	C9-C10 saturated analog	NA	GI ₅₀ = 0.37-0.88 μg/mL	82
6	1 , salicylihalamide A	NA	GI ₅₀ = 0.038-0.081 μg/mL	82
				
7	R = OH	4.5	IC ₅₀ = 0.20-1.03 μM	83
8	R = H	no inhibition at 1 μM	NA	83
				
9		NA	GI ₅₀ = 2-49 μM	84
				
10		2	NA	85

The six known lobatamide molecules are structurally different in only three positions as shown in Figure 1.¹⁰ It is unknown how the C30 hydroxyl group, the C24-C25 olefin configuration, or the orientation of the methyl oxime ether differentiates the biological activity between this series of natural products as no bioactivity data has been reported for these isolated molecules. To date, only lobatamide C (**7**) has been targeted for SAR development.⁸⁶ The Porco group focused mainly on open chain analogs of the diester macrocycle **7** (Table 3). They showed that open chain analogs lacking substitution at C7, such as entry 2, had no V-ATPase inhibitory properties at the concentrations tested. However, substitution at this carbon with a methyl group (entry 3), iodine (entry 4) or prenyl group (entry 5) restored biological activity.⁸⁷ In general, the IC₅₀ values decrease with increasing bulkiness at C20. The researchers attributed these results to the removal of the ester carbonyl from planarity with the benzene ring with the larger C20 substituents. The crystal structure of the bromophenyl acetate of lobatamide C helps support this hypothesis. In the crystal structure, the ester group lays 52° out of planarity with the aromatic ring.⁸⁶ How this deviation from planarity moderates interaction with V-ATPase is unknown. Similar to the salicylihalamide analog exploration, reducing the ring size eliminated V-ATPase inhibitory properties (entry 6), while removing the substitution on the macrolactone core dramatically reduced its biological properties (entry 7). The Porco group has also developed photoaffinity lobatamide molecules based upon their prenyl-substituted open chain analogs with the goal of identifying the protein binding site of the substrate.⁸⁸ A benzophenone-substituted⁸⁹ analog **29**

retained some anti-V-ATPase activity with an IC_{50} of 100 nM (Figure 6). Further biological results employing these potentially useful probes have not been published.

Table 3. Lobatamide analogs and biological activity

Entry	Structure	V-ATPase Inhibition (IC_{50} in μ M)
1	<p>Chemical structure of lobatamide (7), featuring a central chiral carbon atom bonded to a hydroxyl group, a methyl group, a propyl chain with a terminal methyl group, and a side chain containing a hydroxyl group, a carbonyl group, and a diene system with an N-methylamino group.</p>	0.0021
2	<p>General chemical structure of lobatamide analogs with substituents R_1 and R_2.</p>	
3	$R_1 = H$ $R_2 = Et$	18
4	$= Me$ $= Me$	0.10
5	$= I$ $= Me$	0.21
6	<p>Chemical structure of lobatamide analog 6, which is a complex molecule containing a bicyclic core, a hydroxyl group, a carbonyl group, and a diene system with an N-methylamino group.</p>	27% inhibition at 27 μ M
7	<p>Chemical structure of lobatamide analog 7, which is a complex molecule containing a bicyclic core, a hydroxyl group, a carbonyl group, and a diene system with an N-methylamino group.</p>	1.4

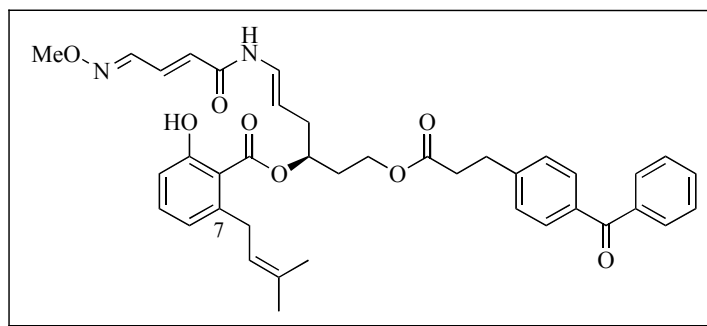


Figure 6. Lobatamide benzophenone photoaffinity compound **29**⁸⁸

The crystal structure of apicularen A furthered the understanding of the geometrical conformation of the benzolactone enamides. In the crystal structure of **11**, the ester carbonyl of apicularen A displayed a similar deviation from planarity as the lobatamide analog.¹⁴ The effect was more pronounced in apicularen A, as an 80° dihedral angle was observed between the ester carbonyl and the benzene ring.

Analog studies on apicularen A, similar to other benzolactone enamide SAR development campaigns, focused on the importance of the enamide side chain (Table 4).⁹⁰⁻⁹² Inverting the stereochemistry of either an olefin in the hexadienyl side chain (entry 2) or in the enamide olefin (entry 3) resulted in a 10- or 100-fold loss of potency, respectively. As seen with salicylihalamide A analogs, substitution of the hexadienyl side chain with a bulkier phenyl group was tolerated provided that a geometrically slender group (here a *trans* olefin) separated the benzene ring from the amide (entries 4 and 5). Methylation of the amide nitrogen dramatically decreased activity (entry 6), implicating the amide N-H in hydrogen bonding in the active site. Interestingly, substitution of the hexadienyl side chain found on the salicylihalamides and the apicularens with the oxime ether side chain of the lobatamides and

oximidines greatly reduced the activity of the analog (entry 7). Modification of the hydroxyl group on the tetrahydropyran (entries 8 and 9) had only a marginal effect on the biological activity. However, inversion of this hydroxyl stereocenter resulted in a 75-fold decrease in activity (not shown).⁹⁰ Opening of the pyran ring (entry 10) generates a molecule similar in structure to salicylihalamide A. However, this analog has greatly attenuated cytotoxic activity compared to the parent molecule, highlighting the importance of the 3-D conformation of the molecule for biological activity.

Table 4. Apicularen A analogs and biological activity

Entry	Analog Structure	Biological Activity (in nM)*	Reference
	R =	GI ₅₀ = 6.0	90
1		IC ₅₀ = 0.78 IC ₅₀ 's = 2.3-15.9	92 91
2		GI ₅₀ = 60	90
3		IC ₅₀ = 71	92
4		IC ₅₀ > 1500	92
5		IC ₅₀ = 50	92
6		IC ₅₀ 's = 550 - 1980	91
7		IC ₅₀ 's = 900 - 9000	91
8		IC ₅₀ = 3.2	92
9		IC ₅₀ 's = 2.4 - 19	91
10		IC ₅₀ 's = 180-1360	91

(*Compounds from reference 90 evaluated in SK-Mel-5 cells; reference 91 compounds evaluated in L929, Y1, KB-3-1, KB-VI cells; reference 92 compounds in 1A9 cells)

Cruentarens A and B (**30** and **31**, Figure 7), isolated in 2006, are structurally similar to the benzolactone enamides.^{93,94} Cruentaren A, containing a 12-membered macrolactone, is one of the most cytotoxic molecules isolated from myxobacteria, displaying an IC₅₀ of 1.2 ng/mL (2 nM) against murine L929 fibroblast cells. As seen with salicylilalamide analogs, the truncated lactone version cruentaren B displayed dramatically decreased biological activity.⁹⁴ Surprisingly, these molecules were found to inhibit F-ATPases, not V-ATPases as their structure suggests.⁹⁵ Although F-ATPases and V-ATPases are structurally similar, possessing lumen-exposed F₁ and V₁ domains and membrane-bound F₀ and V₀ domains, respectively, cruentaren A targets the F₁ complex. The benzolactone enamides target the V₀ complex.⁷⁷

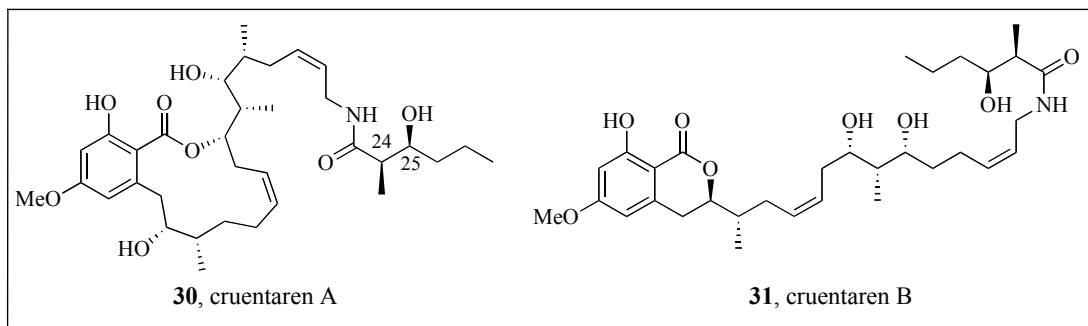


Figure 7. Cruentaren A and B

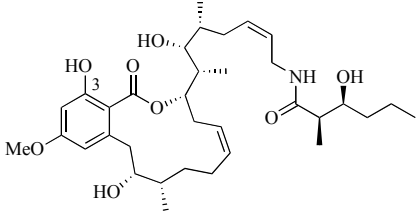
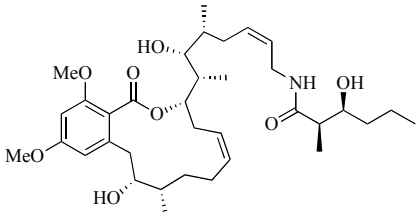
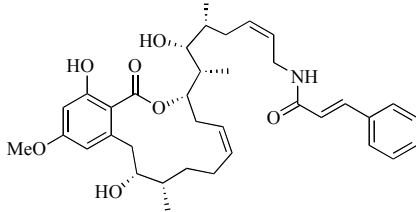
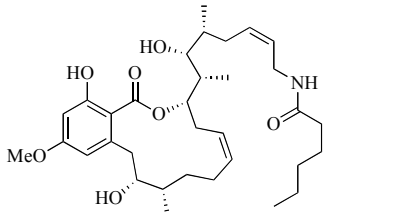
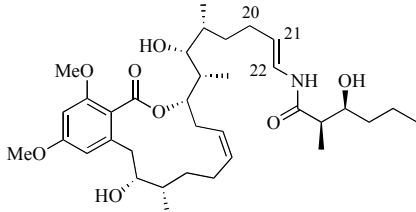
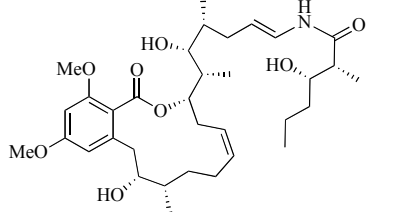
Four structural disparities could explain why these molecules interact with different cellular targets. The amide side chain of cruentaren A is bulkier than the benzolactone enamide side chains, substituted with a methyl group at C24 and a hydroxyl group at C25. There are three more carbons separating the amide from the benzoate in cruentaren A than in the benzolactone enamides. The cruentarens possess

an allylic amide side chain, prohibiting covalent bonding to the F-ATPase enzyme through the *N*-acyl iminium ion chemistry hypothesized for the benzolactone enamides. A crystal structure of cruentaren A supplied the final point of discrepancy between the molecules. Crystal structures of apicularen A and the lobatamide analog demonstrated a non-planar relationship between the ester carbonyl bond and the phenyl ring. However, the crystal structure of cruentaren A identified a hydrogen bond between the phenol hydrogen and the ester carbonyl oxygen, forming a six-membered ring. This intramolecular hydrogen bond generated co-planarity of the ester carbonyl and benzene ring.

Recent analog synthesis by the Maier laboratories has allowed insight into the SAR for the cruentaren molecule **30**.⁹⁶ Methylation of the phenol dramatically reduced the inhibitory properties against L929 murine fibroblast cells (Table 5, entry 2). Similar to the benzoylated salicylihalamide derivative (Table 2, entry 1), this change reduced the cytotoxicity 400-fold. However, this molecule retained the F-ATPase inhibitory properties of the parent molecule, displaying 42% inhibition at 0.1 μ M compared to 78% for cruentaren A at the same concentration. This result implies that the side chain may be the biggest structural contributor for potent F-ATPase inhibition. Modification of the amide side chain to substituents demonstrated to retain biological activity for apicularen A (styrenyl, entry 3) or salicylihalamide A (pentyl, entry 4) drastically reduced the cytotoxicity of the analogs, displaying the necessity of hydrogen bonding in the side chain for bioactivity. The group also investigated replacement of the allylic amide with the enamide functionality seen in the

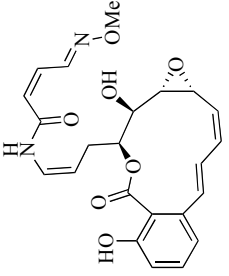
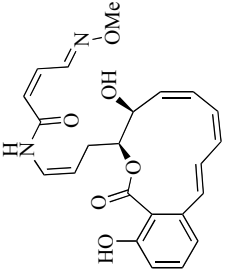
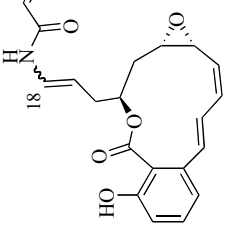
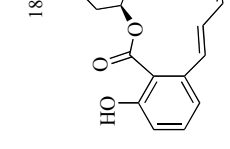
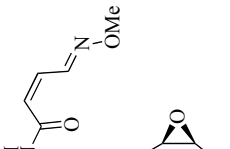
benzolactone enamides. These molecules (entries 5 and 6) displayed only micromolar cytotoxicity values. Further, these enamide analogs did not display any V-ATPase inhibitory properties. Based on the available data, it is unclear what contributes to the lack of activity of these enamide molecules.

Table 5. Cruentaren A (**30**) analogs and biological activity

Entry	Analog Structure	L929 Fibroblast Cells Inhibition (IC ₅₀ in μ M)
1		0.00071
2		0.028
3		10.3
4		4.5
5		5.0
6		5.1

The oximidines, unlike their benzolactone enamide counterparts, have not been the subject of rigorous SAR investigation. Oximidines II (**14**) and III (**15**) are generally twice as active as oximidine I (**13**) in various mutated rat 3Y1 cell lines (Table 6).^{15,17} The Porco group investigated the consequence of inverting the stereochemistry of both the enamide olefin and the epoxide on the V-ATPase inhibitory properties of oximidine III.⁹⁷ Inverting the epoxide from α -oriented to β -oriented had a minimal effect on the anti-V-ATPase properties (**15** vs. **33** and **32** vs. **34**). However, altering the stereochemistry of the enamide olefin from the native *E*-configuration to the *Z*-configuration caused a 15- to 30-fold decrease in the inhibitory property of the molecule (**15** vs. **32** and **33** vs. **34**). These results, coupled with Nicolaou's studies of apicularen A (entry 3, Table 4)⁹² hint that the enamide olefin configuration is important for proper alignment of the molecule in the active site.

Table 6. Biological activity of oximidines and oximidine III analogs

Oximidine Compound						
	13, oximidine I	14, oximidine II	15, oximidine III: 18E	32, 18Z	33, 18E	34, 18Z
Cell Line (IC ₅₀ in nM)						
Bovine V-ATPase	NA	NA	2.2	65	4.3	65
3Y1	510	270	140	NA	NA	NA
SV-3Y1	740	350	19	NA	NA	NA
E1A-3Y1	30	17	24	NA	NA	NA
Ad12-3Y1	62	36	31	NA	NA	NA
HR-3Y1	16	9.0	14	NA	NA	NA
SR-3Y1	27	14	4.5	NA	NA	NA
Reference	17	17	15, 97	97	97	97

Seeing an opportunity to expand the understanding of the SAR for the oximidines, we sought to develop an expedient route for their syntheses. We decided to target oximidine II due to the potential chemical instability of the epoxide moieties in oximidines I and III. Similar to previous SAR campaigns targeting the benzolactone enamides, we directed our attention at the enamide moiety. However, unlike previous campaigns, our goal was to not only develop more potent analogs, but also to develop more metabolically stable analogs. The acid-sensitive enamide moiety could be hydrolyzed *in vivo* to the corresponding aldehyde (Figure 8). Therefore, we chose to target an allylic amide homolog of oximidine II, inspired by the cruentaren molecule **30**. Following a successful synthesis of this analog, we planned to test oximidine II and the analog in various biological assays. First, we would probe the anti-cancer activity of both compounds by testing against melanoma cancer cells. If the analog displayed potency, we would investigate its mechanism of action by testing in both V-ATPase and F-ATPase inhibitory assays. Pertinent to the development of this analog is its metabolic stability, particularly its acid sensitivity. Finally, we would examine the stability of both molecules across a pH range relevant to *in vivo* systems.

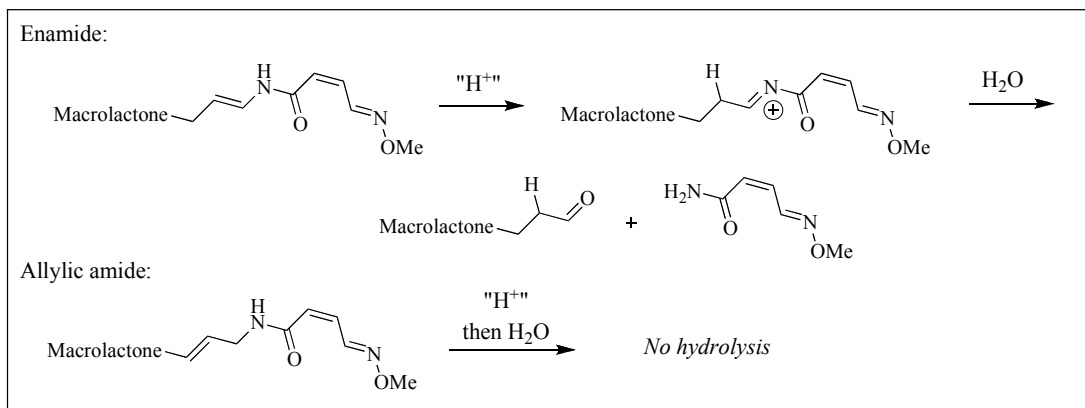
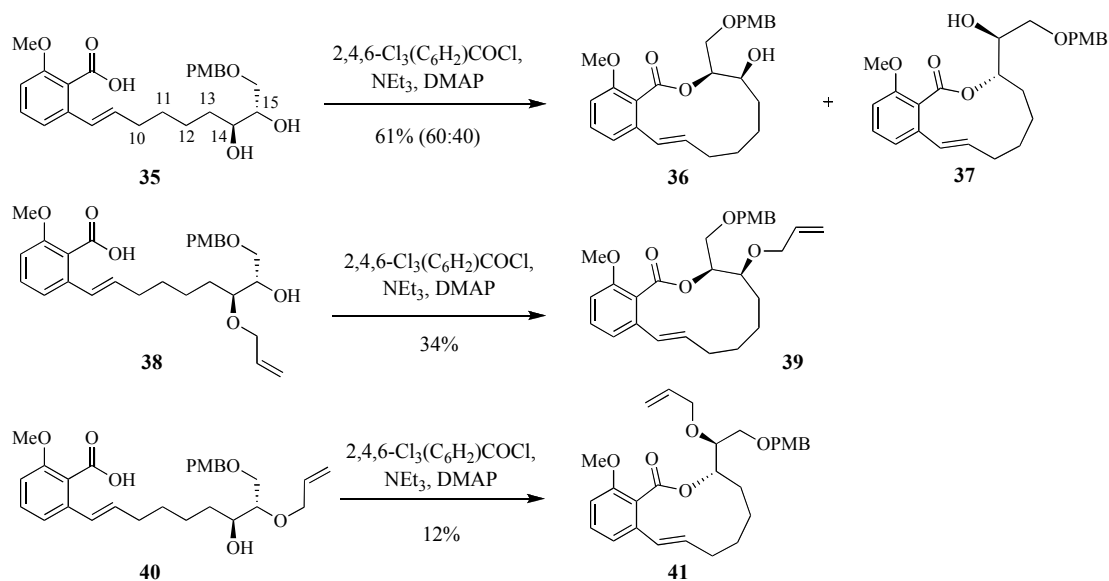


Figure 8. Predicted enamide *in vivo* hydrolysis and allylic amide stability

1.4 Previous Synthetic Studies of the Oximidines

In general, the most challenging step in synthesizing macrocycle natural products is the macrocyclization event. Typically, the loss of entropy from the open-chain cyclization precursor provides the resistance to macrocyclization.⁹⁸ An important fundamental discovery was the use of high-dilution conditions by Ziegler to help overcome the entropic barriers and prevent polymerization of the seco-cycle substrates.⁹⁸⁻¹⁰⁰ Several methodologies have been developed to aid organic chemists in forming large ring structures.^{98,101} Examples include ring-closing metathesis (RCM), palladium-mediated reactions (Heck, Suzuki-Miyaura, Stille, Tsuji-Trost allylation), Wittig/Horner-Wadsworth-Emmons (HWE)/Julia olefinations and macroaldolizations for C-C bond formation; macrolactonization (C-O bond formation) via Yamaguchi, Keck or Mitsunobu protocols;¹⁰² and macrolactamization (C-N bond formation) through the use of peptide coupling reagents.⁹⁸ Macrocyclization in the syntheses of the benzolactone enamides have utilized many of these methodologies.⁴

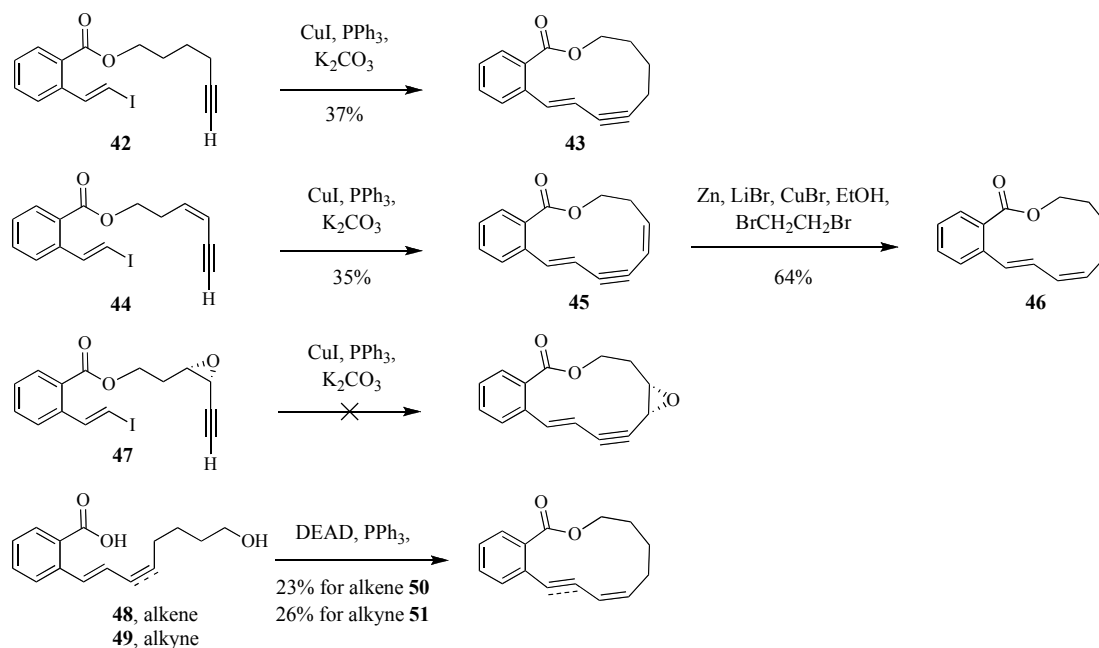
Scheufler and Maier published the first model study directed at the synthesis of the macrolactone of the oximidines in 2001.¹⁰³ Their strategy used C-O bond formation to accomplish the macrocyclization. Exposure of the seco-acid **35** to typical Yamaguchi macrolactonization conditions¹⁰⁴ gave a 60:40 ratio of desired (**36**) to undesired (**37**) macrolactone products in 61% combined yield (Scheme 1). This size ratio is not surprising given the thermodynamic and kinetic preference for 12-membered ring formation vs. 11-membered ring formation.^{101,105} To perturb this competition, the chemists protected the C14 alcohol as its allylic ether, generating compound **38**. Exposure of this seco-acid to Yamaguchi conditions generated only a 34% yield of the macrolactone product **39**. The authors did not detail the cause of the low yield. Interestingly, exposure of the C15 allyl ether compound **40** to Yamaguchi conditions generated only 12% of the desired 11-membered ring (**41**).



Scheme 1. Yamaguchi macrocyclization by Scheufler and Maier

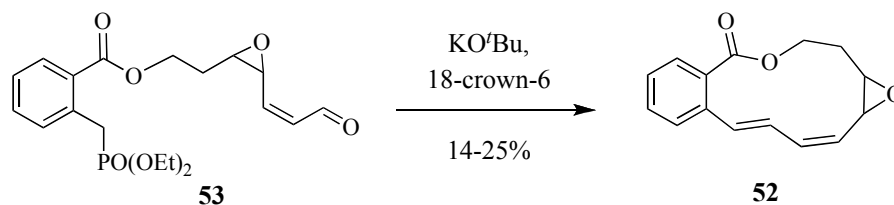
The model system developed by Coleman and Garg was the first to incorporate the nine consecutive sp^2 -hybridized carbon centers of oximidine II, exploring how a decrease in flexibility would affect the macrocyclization.¹⁰⁶ Exposure of the alkyne benzoate **42** to the Miura-modified Castro-Stephens conditions,¹⁰⁷ utilizing a catalytic amount of CuI in the presence of phosphine ligands and a stoichiometric amount of base in *N,N*-dimethylformamide (DMF), gave 37% of the enyne product **43** (Scheme 2). Macrolactone formation utilizing the Castro-Stephens reaction had been achieved only once prior to this report.¹⁰⁸ The related, palladium-mediated Sonogashira coupling reaction¹⁰⁹ was ineffective at generating the desired product. Addition of a *Z*-olefin to the alkyne chain (compound **44**) had a negligible effect on the yield of the macrocyclization (35%). The resultant dienyne

molecule (**45**) was chemo- and stereoselectively reduced under Boland reduction conditions¹⁸⁰ to give the macrocycle with the desired *E,Z,Z*-triene stereochemistry of oximidine II. Attempts to execute the macrocyclization with the epoxide-containing backbone of oximidine I (**46**) were unsuccessful, potentially due to the lability of the propargylic epoxide. Macrolactonization using the enyne (**48**) or diene (**49**) starting materials was successful only under Mitsunobu conditions, in contrast to Maier's previous report with Yamaguchi's protocol, and led to lower yields (26% for **50** and 23% for **51**, respectively) than the copper-mediated methodology. This report demonstrated the feasibility of using metal-mediated processes in the key macrocyclization reaction.



Scheme 2. Castro-Stephens approach by Coleman and Garg

In 2003, Taylor and coworkers were able to form the epoxide-containing nucleus of oximidine I using HWE technology.¹¹⁰ Anticipating the conversion of the epoxide of oximidine I to the alkene of oximidine II,¹¹¹ this group targeted the epoxide macrolactone (**52**, Scheme 3) in their model study. However, under a variety of basic conditions, high yields of the epoxide macrolactone **52** could not be realized from a HWE reaction of the phosphonate seco-cycle (**53**). The olefination cyclization was only successful when potassium bases, such as KHMDS or KO^tBu, were used.



Scheme 3. HWE macrocyclization by Harvey, Raw and Taylor

The total syntheses of the benzolactone enamides have not only been focused on macrocyclization strategies, but also the installation of the enamide side chain. Due to the potential chemical instability of this crucial functional group, it has typically been introduced near the end of a synthetic sequence. Three main strategies have prevailed for enamide installation (Figure 9): nucleophilic trapping of an isocyanate resulting from a Curtius rearrangement (method A),^{80-82,90} Lewis acid-mediated addition of an amide to an aldehyde followed by base-mediated elimination of the resultant hemi-aminal (method B),^{91,112,113} or copper-mediated coupling of an amide and vinyl iodide fragment (method C).^{86,92,114,115} Furthermore, these strategies

have proven applicable towards the synthesis of the oxime ether-containing side chains of the oximidines and lobatamides (method A,^{116,117} method B,⁹¹ method C).^{86,87,97,118}

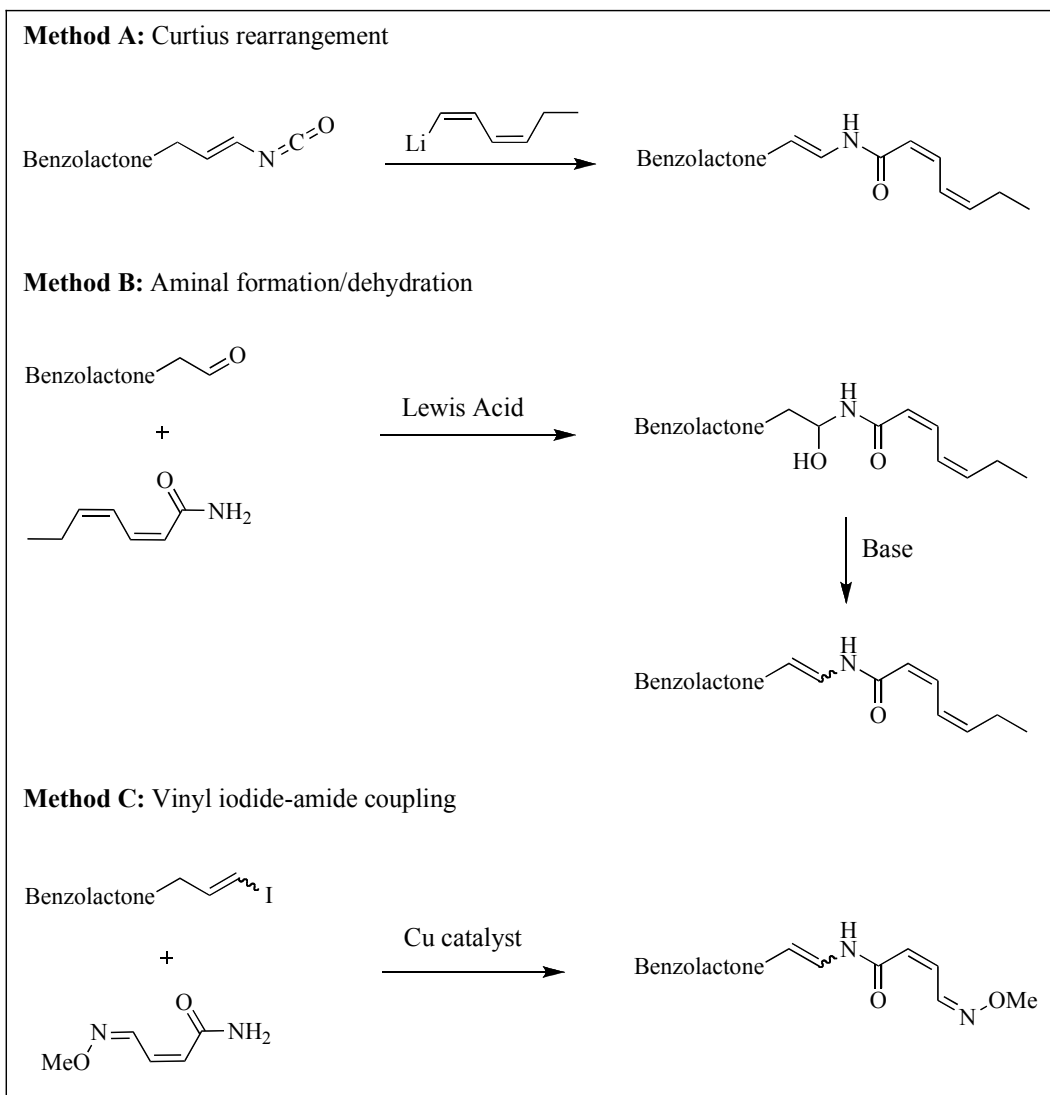


Figure 9. Methods of enamide side chain installation

Porco and Wang completed the first total synthesis of oximidine II in 2003.¹¹⁸ They disconnected the molecule into three fragments: an amide (**54**), an aromatic

salicylate (**55**), and an aliphatic alcohol (**56**) (Figure 10). Following their previous reports of enamide installation using copper thiophene carboxylate (CuTC, **57**)¹¹⁹ as the catalyst for amide-vinyl iodide coupling,¹²⁰ they planned to couple amide **54** and triene macrocycle **58** at the end of the synthesis. The macrocycle would be formed using a RCM reaction of seco-cycle **59**. A base-mediated transesterification reaction¹²¹ between salicylate fragment **55** and aliphatic fragment **56** would generate the RCM substrate.

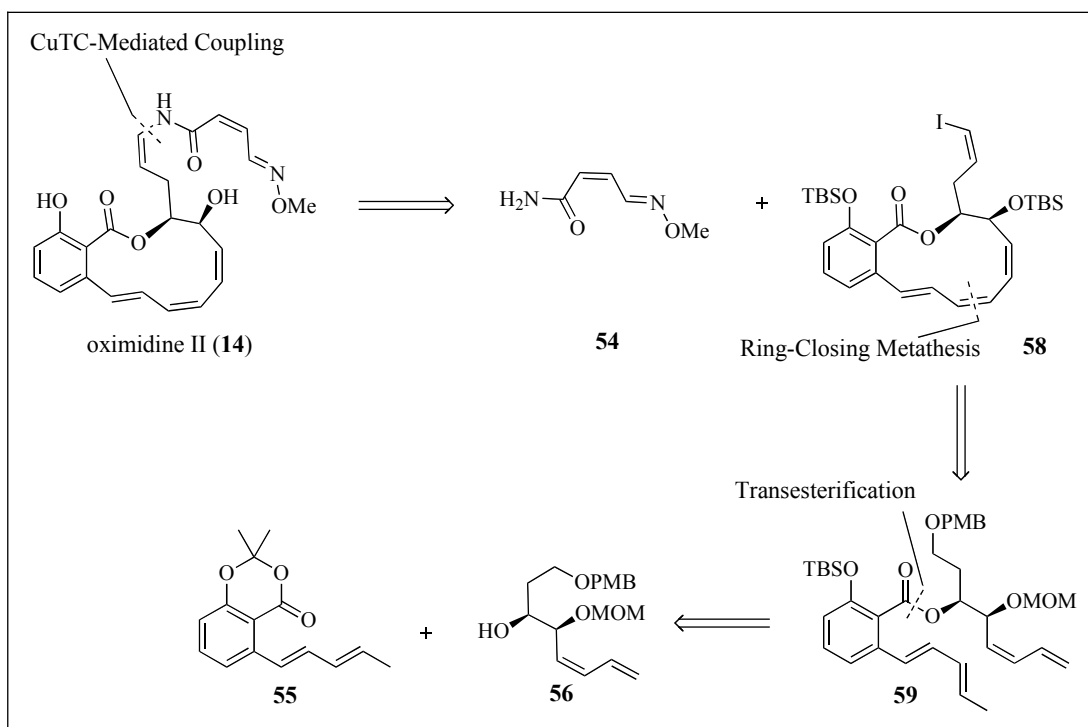
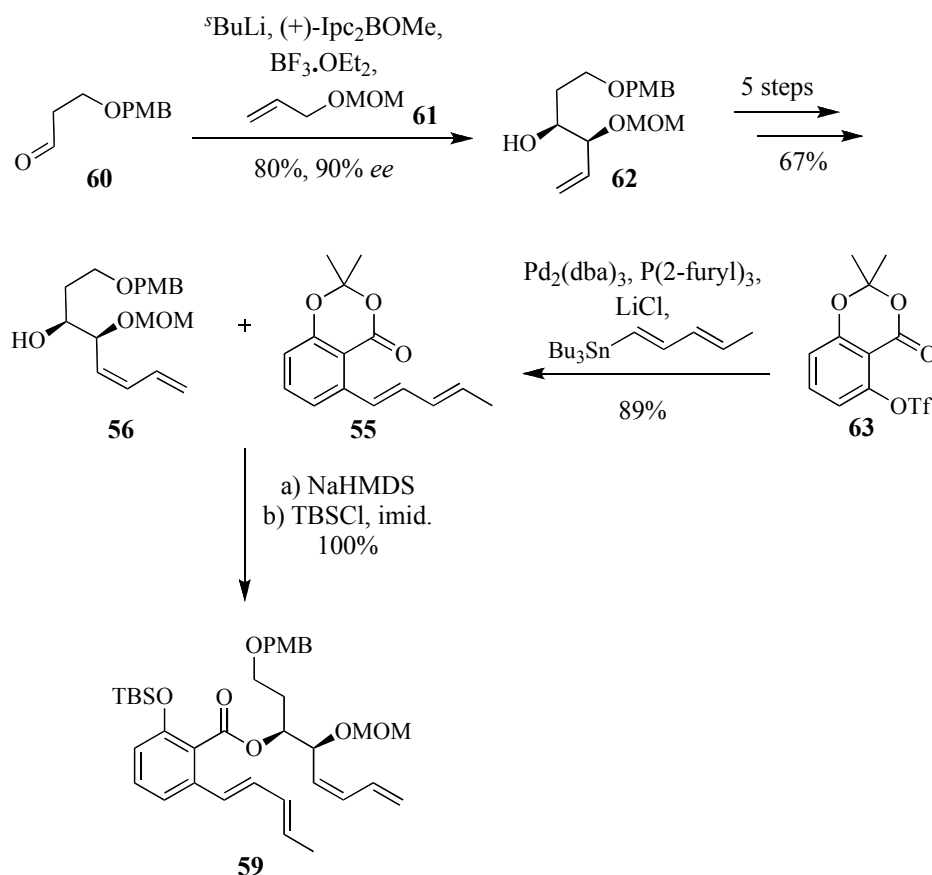


Figure 10. Oximidine II retrosynthesis by Porco and Shen

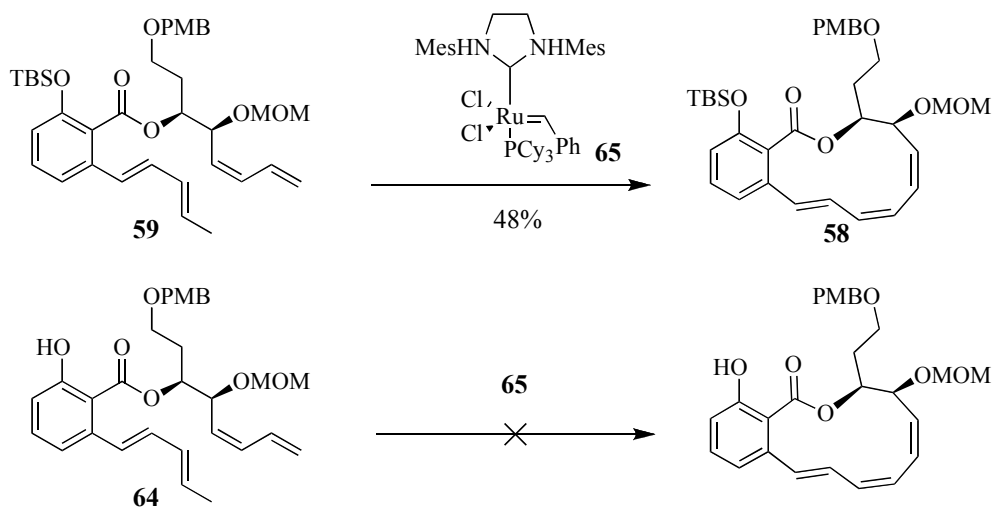
Their asymmetric synthesis began with a Brown allylation reaction¹²² between aldehyde **60** and allyl methoxymethyl ether **61**, generating the chiral product **62** in 90% ee (Scheme 4). The enantioenriched triol (**62**) was elaborated in five steps to the

aliphatic fragment **56**, ready for the transesterification reaction. Starting with the known aryl triflate **63**,¹²³ a Stille coupling formed the dienylyl acetonide **55**. Generation of the sodium alkoxide of **56** using sodium bis(trimethylsilyl)amide (NaHMDS) followed by addition of the acetonide generated a sodium phenolate that was silylated *in situ*, yielding seco-cycle **59**. The corresponding phenol compound (**64**) was also accessible by quenching the transesterification with water (not shown).



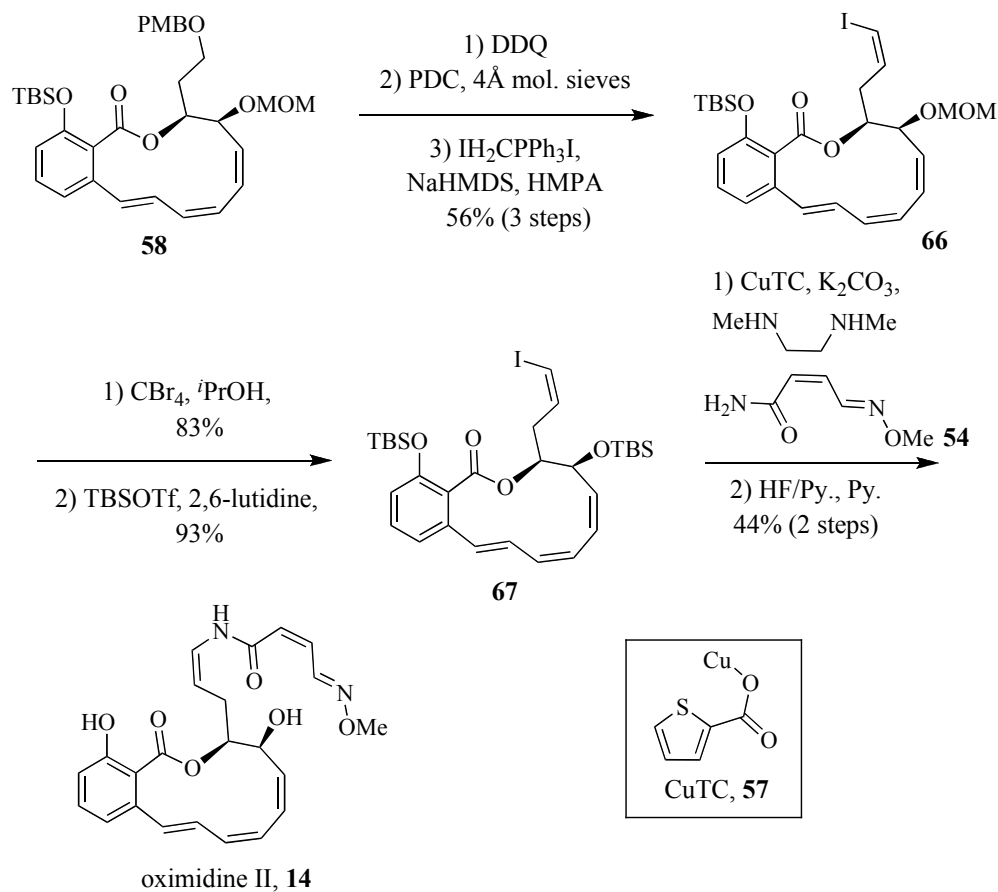
Scheme 4. Synthesis of RCM substrate **59** by Porco and Shen

Initial RCM studies employing Grubbs' 1st generation catalyst led to complex mixtures of desired and oligomeric products. Grubbs' 2nd generation catalyst (**65**) was more discriminating. Exposure of the TBS-protected compound **59** led to a 48% yield of the desired triene macrocycle following one recycle (Scheme 5). However, the phenol compound **64** generated no monomeric macrocycle under similar RCM conditions – only oligomeric products resulted from the reaction. Using Monte Carlo calculations on a model compound (not shown), the researchers demonstrated the importance of ester carbonyl-phenyl ring non-planarity for success in the RCM reaction. The large TBS group forces this non-planarity and subsequently forces the two reactive dienes into close proximity for a favorable RCM macrocyclization. This successful RCM reaction led to the *E,Z,Z*-triene stereochemistry of oximidine II. For the phenol substrate, the carbonyl and aromatic ring are nearly planar allowing for a different orientation of the dienes relative to each other. This orientation potentially leads to the formation of a hypothetically unstable *E,E,Z*-triene macrocycle that eventually oligomerizes. Similar phenol protecting group effects have been demonstrated during syntheses of salicylhalamide A that utilize a RCM macrocyclization approach.^{114,124,125} This RCM strategy also proved useful in Porco's synthesis of oximidine III.⁹⁷ In the macrocyclization leading to the core structure of oximidine III, the allylic epoxide proved stable to the reaction conditions.



Scheme 5. RCM macrocyclization by Porco and Shen

To prepare the substrate for installation of the enamide, the primary 4-methoxybenzyl ether was cleaved and the resultant alcohol was oxidized with PDC to the aldehyde. Stereoselective iodo-olefination under Stork-Zhao conditions,¹²⁶ employing the light sensitive iodomethyl(triphenyl)phosphonium iodide salt (IH₂CPh₃I),¹²⁷ generated the *Z*-vinyl iodide macrolactone **66**. Following protecting group interconversion, the macrolactone **67** was prepped for formation of the enamide. Employing CuTC (**57**) as the copper source, *N,N*-dimethylethylene-diamine as the ligand and K₂CO₃ as the base in deoxygenated *N,N*-dimethylacetamide (DMA),¹²⁰ the enamide was installed. Removal of the silyl protecting groups with a buffered solution of HF/Py. produced oximidine II (**14**) in a 44% yield over the final two steps.



Scheme 6. Completion of oximidine II by Porco and Shen

Following the model system developed by Coleman and Garg, the Georg group developed a synthesis employing the Castro-Stephens reaction as the macrocyclization method.¹²⁸ The retrosynthesis, displayed in Figure 11, shows a similar disconnection strategy compared to the Porco total synthesis. The enamide bond would be established using Porco's vinyl iodide-amide bond formation methodology. The Castro-Stephens macrocyclization reaction would join C9 and C10 of compound **69**, followed by a *cis*-selective reduction of the alkyne to the

corresponding alkene **68** to construct the *E,Z,Z*-triene stereochemistry of oximidine II. The final major disconnection in this synthesis is at the ester bond, joining together salicylate fragment **70** and enyne fragment **71** via an esterification reaction.

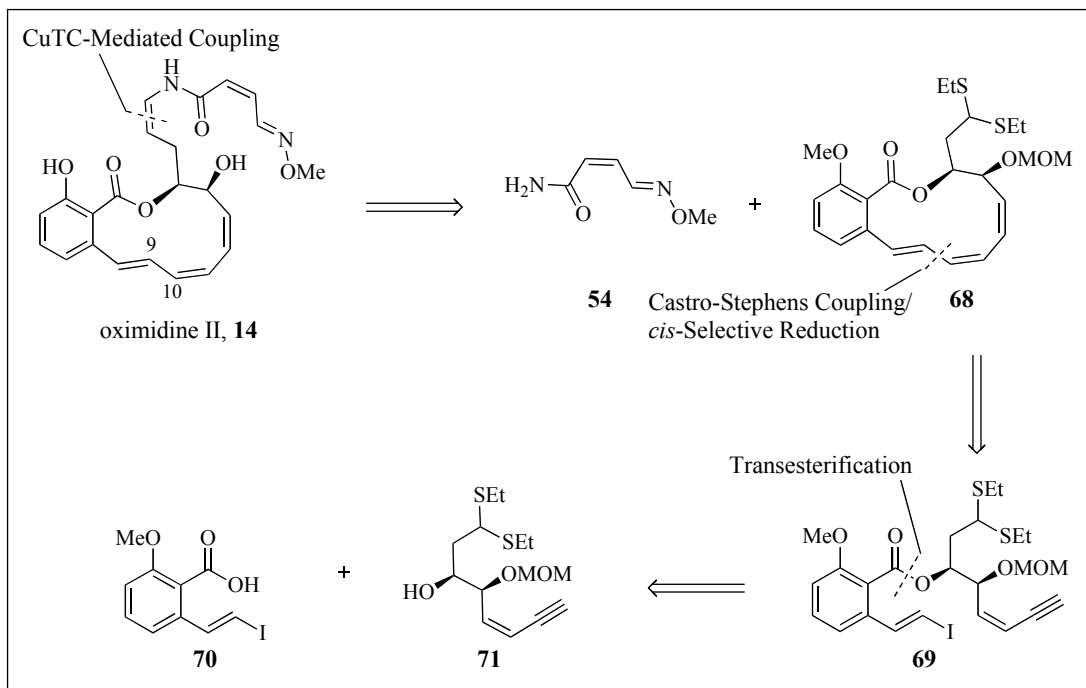
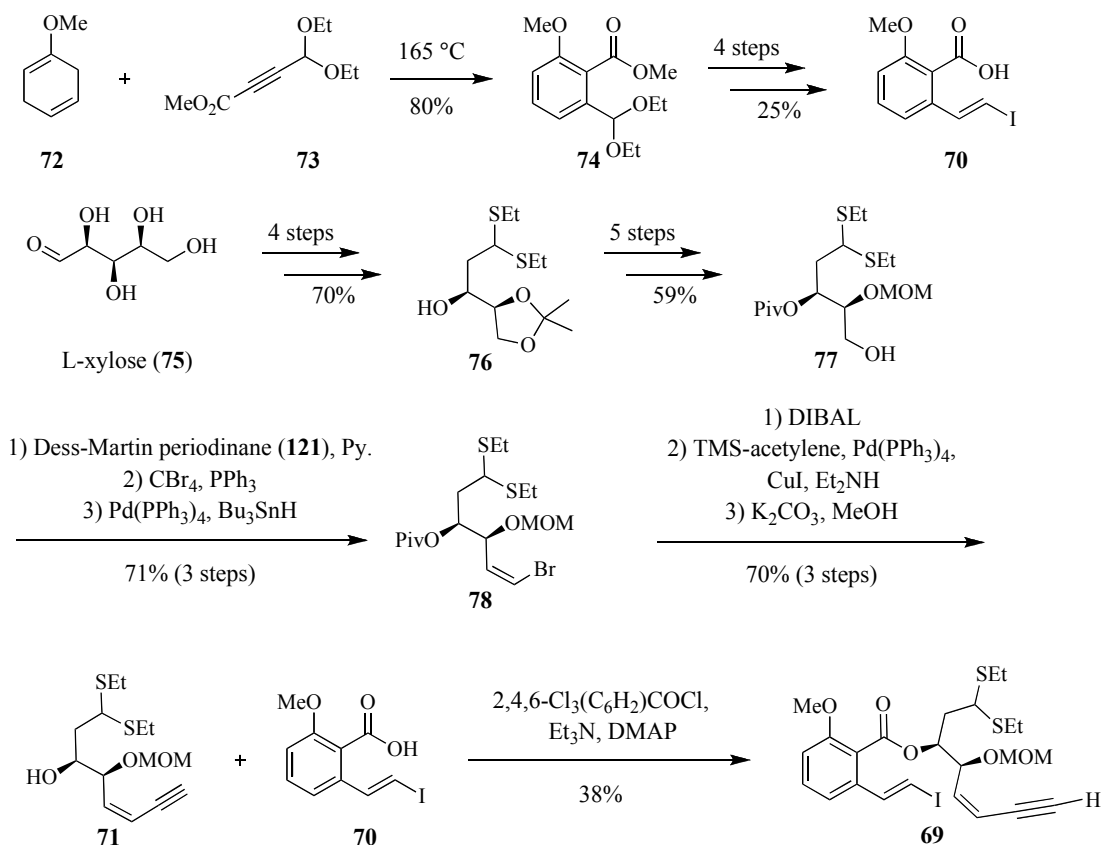


Figure 11. Oximidine II retrosynthesis by Georg group

The synthesis of the aryl salicylate fragment **70** was accomplished in five steps (Scheme 7), generating the trisubstituted aromatic ring via a Diels-Alder cycloaddition and the requisite *E*-vinyl iodide via a Takai olefination.¹²⁹ Using a chiral-pool strategy, the synthesis of the enyne aliphatic fragment began with L-xylose (**75**). In four steps,¹³⁰ the sugar was transformed into the 2-deoxysugar **76**. Protecting group interconversion transformed the acetonide **76** into primary alcohol compound **77** in five total steps. Oxidation of the primary alcohol to the corresponding aldehyde with Dess-Martin periodinane (**121**),^{131,132} Corey-Fuchs

dibromohomologation and stereoselective debromination yielded the *Z*-bromo olefin **78** in 71% yield over the three steps. Cleavage of the pivalate under reductive conditions, Sonogashira coupling with TMS-acetylene and removal of the alkyne protecting group readied the aliphatic fragment (**71**) for esterification with the aromatic fragment **70**. This esterification step proved difficult. Under Yamaguchi conditions,¹⁰⁴ the esterification reaction proceeded to give seco-cycle **69** in only 38% yield. The low yield realized in this reaction could be attributed to both steric (di-ortho-substituted acid substrate) and electronic (electron rich acid due to ortho-methoxy group) issues with the acid **70**.

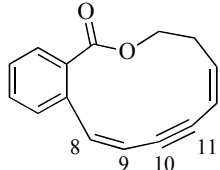
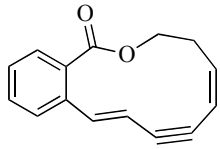


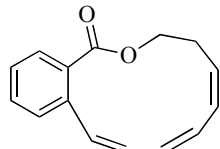
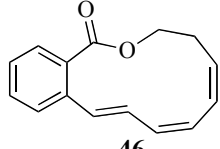
Scheme 7. Previous synthesis of Castro-Stephens substrate by Georg group

Rigorous investigation of the crude reaction mixture following exposure of the seco-cycle **69** to the Castro-Stephens reaction conditions, as described by Coleman and Garg, revealed two unexpected products (Scheme 8). In general, the Castro-Stephens coupling is stereospecific, generating products that retain the double bond geometry of the starting material.^{133,134} However, in this case, the C8-C9 double bond isomerized during the reaction, generating the *Z*-dienyne product **79** in 31% yield. A coupling constant of $^3J = 12$ Hz for the C8-C9 protons in the ^1H NMR suggested a *Z*-olefin geometry. A strong NOE between the C8 and C9 protons further supported this hypothesis. In Coleman's model study, the C8-C9 proton coupling constants were 16 Hz, values consistent with an *E*-configured olefin. Using Ramsey's non-relativistic approach¹³⁵ and the B3LYP/6-311G(d,p) basis sets,¹³⁶ computer calculations of the C8-C9 proton coupling constants were in agreement with the observed, experimental results. To investigate why double bond inversion occurred, molecular mechanics and quantum chemical relative energies were calculated. Table 7 displays the results from these calculations using three different calculation methods: MMFF, DFT, MP2. When the alkyne is present within the macrocycle, the C8-C9 *Z*-olefin (**80**) is thermodynamically favored versus the C8-C9 *E*-olefin (**81**) by 11-16 kcal/mol. However, upon stereoselective reduction of the macrocycle alkyne to the corresponding C10-C11 *Z*-alkene (**81**), this thermodynamic preference is reversed and the C8-C9 *E*-olefin geometry (**46**) is favored versus the C8-C9 *Z*-olefin **81**. Using the results from the MMFF calculations, the *Z*-dienyne Castro-Stephens product **79** was shown to be favored by 15.3 kcal/mol versus the corresponding *E*-

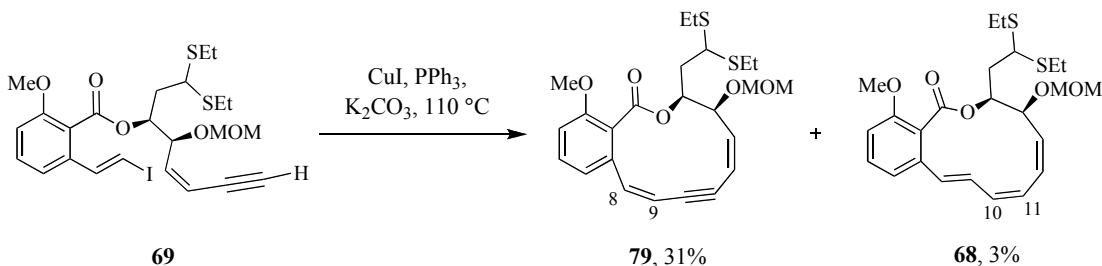
olefin, again supporting the experimental outcome. Considering the known stereospecificity of the Castro-Stephens reaction, the C8-C9 inversion most likely occurred after ring closure.

Table 7. Calculations of relative macrocycle stabilities

Macrocycle	MMFF (relative ΔE in kcal/mol)	DFT (relative ΔE in kcal/mol)	MP2 (relative ΔE in kcal/mol)
 80	0.0	0.0	0.0
 45	11.4	14.4	15.7

 81	4.8	2.6	2.4
 46	0.0	0.0	0.0

The second unexpected product isolated from the crude mixture was the partially reduced triene macrocycle **68**, albeit in a small, 3% yield (Scheme 8). The reductant source was unclear given the reaction conditions – one equivalent of seco-cycle **69**, 0.10 equivalents CuI, 0.20 equivalents PPh₃, 1.75 equivalents K₂CO₃ in 0.005 M anhydrous DMF heated at 110 °C for 26 h – and was not investigated further. The combined yield of the two functionalized products **68** and **79** (34%) was similar to that of Coleman and Garg’s model system (35%).



Scheme 8. Castro-Stephens macrocyclization by Haack and Georg

An inherent advantage in utilizing a Pd-mediated macrocyclization in the synthesis of oximidine II is that each of the three olefin geometries of the triene would be established prior to cyclization. This prefunctionalization would allow for stereospecific macrocycle formation with the triene in the correct geometry of oximidine II. Pd-mediated couplings have demonstrated success when used as the macrocyclization event in other benzolactone enamide syntheses.^{137,138} Utilizing the potassium organotrifluoroborate-modified conditions for the Pd-mediated Suzuki-

Miyuara coupling championed in his labs,¹³⁹ Gary Molander and Florian Dehmel completed a formal total synthesis of oximidine II.¹⁴⁰

Their synthetic strategy targeted a late stage intermediate of Porco's total synthesis of oximidine II and specifically focused on the key macrocyclization event. Thus, they envisioned that intermediate **82** could be advanced to a total synthesis of oximidine II following Porco's established methods (Figure 12). Protecting group manipulations following macrocyclization via a modified Suzuki-Miyuara coupling of triene **83** would yield intermediate **82**, constituting a formal total synthesis of the natural product. Although previous macrocyclizations linked C9 and C10, this first generation approach attempted to join C7 and C8. A transesterification reaction between dienynol **84** and the readily available salicylate fragment **85** followed by installation of the vinyl potassium trifluoroborate would ready the molecule **83** for Pd-mediated macrocyclization. The chiral dienynol is available following a diastereoselective addition of the alkyne **86** to the known benzylidene acetal aldehyde **87**.¹⁴¹

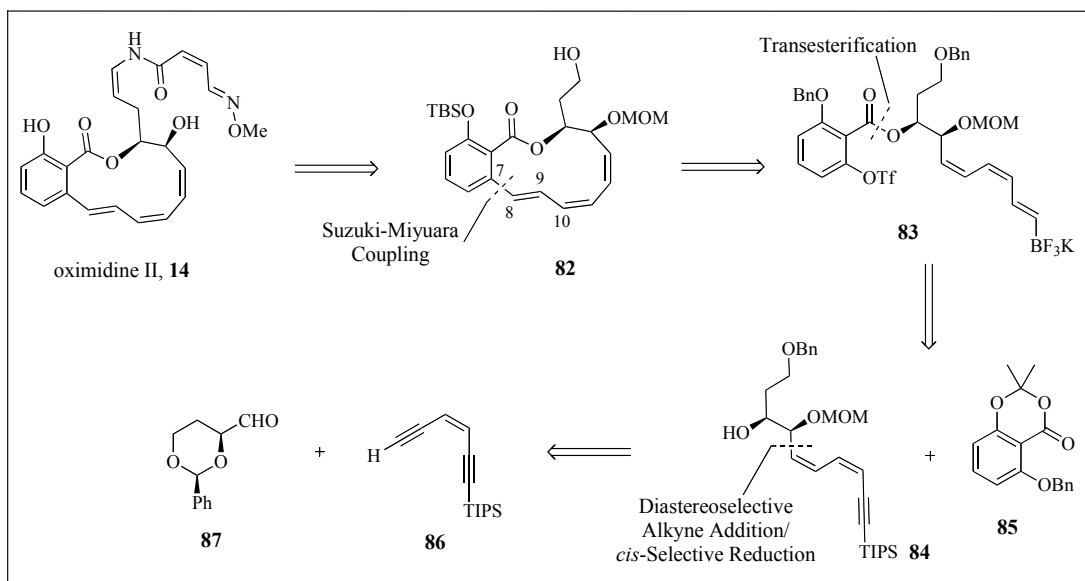
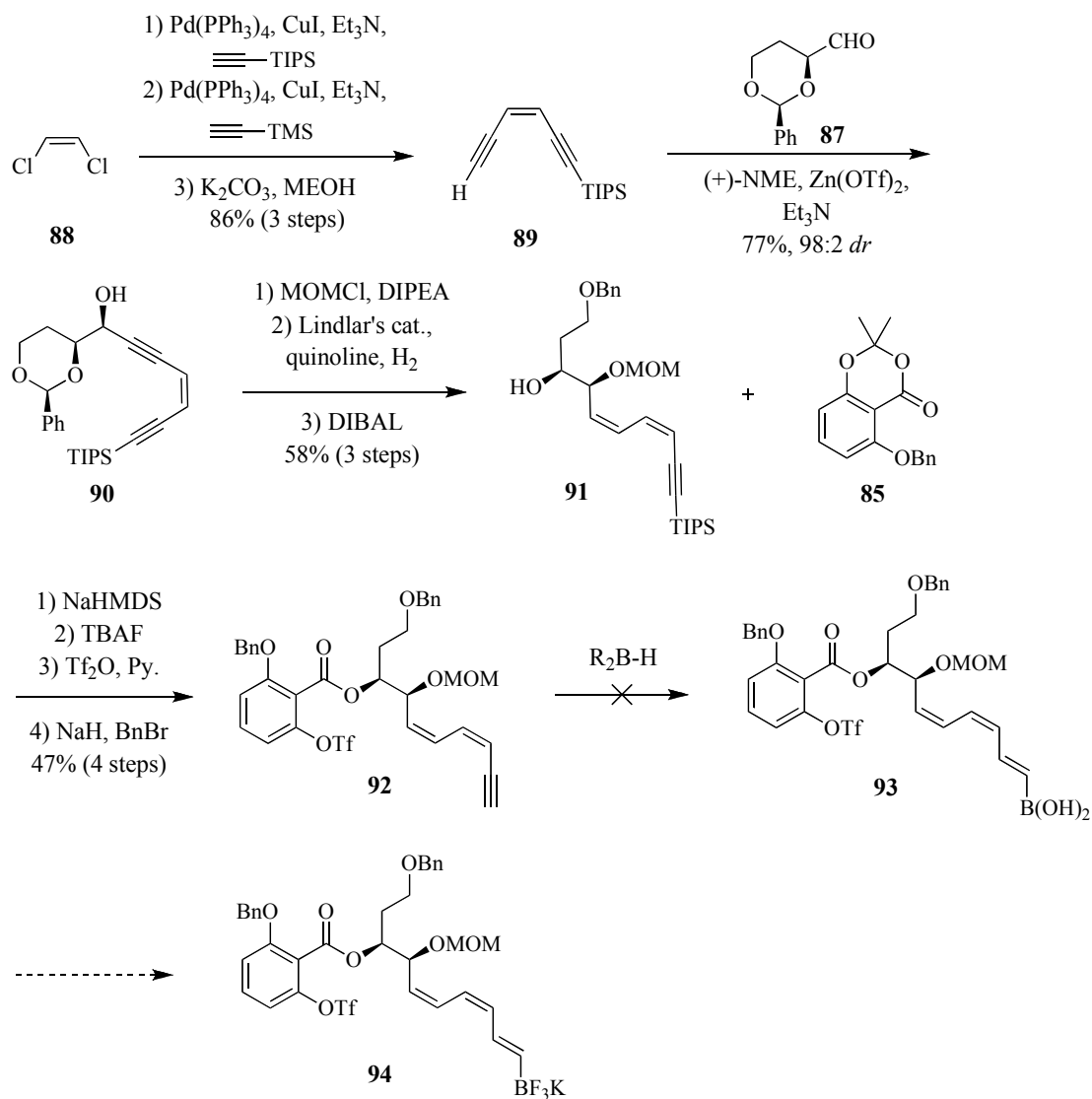


Figure 12. Oximidine II retrosynthesis by Molander and Dehmel

Beginning with *cis*-1,2-dichloroethylene (**88**), double Sonogashira coupling with silylated acetylenes followed by chemoselective hydrolysis of the TMS-protected alkyne afforded ene-diyne **89** (Scheme 9). Alkynylmagnesium or alkynyllithium reagents of **89** added to the chiral aldehyde **87**¹⁴¹ failed to deliver acceptable diastereoselectivities of the desired product **90**. However, application of Carreira's Zn-mediated conditions, employing the chiral ligand (+)-*N*-methylephedrine (NME),¹⁴² gave excellent diastereoselectivity (98:2 diastereomeric ratio (*dr*)) for the alkyne addition. Protection of the secondary alcohol (**90**), regio- and chemoselective reduction of the doubly-alkylated alkyne under Lindlar conditions, and regioselective reductive opening of the acetal directed by the methoxymethyl (MOM) protecting group delivered the alcohol **91**, ready for the transesterification reaction. Coupling of the alcohol **91** and acetone **85** (available in

one step from the known phenol¹⁴³) occurred following literature precedent.¹¹⁸ In three steps, the molecule **92** was prepared for selective hydroboration. Despite their experimentation, the alkynyl molecule **92** was either unreactive towards various hydroborating reagents or decomposed when attempting to oxidize the hydroborated product to the corresponding boronic acid (**93**).



Scheme 9. First generation synthesis by Molander and Dehmel

A new retrosynthesis was then developed, avoiding the obstacles of hydroborating the polyene-yne system **77** (Figure 13). Ring closure to form the C9-C10 olefin linkage was then explored. This strategy required only slight modification of their previous synthetic plan. Transesterification of the potassium

organotrifluoroborate-acetonide **95** with the secondary alcohol **96** would afford the precursor (**97**) for the Suzuki-Miyaura coupling. Using the Carreira protocol,¹⁴² the diol chirality would again be established through the diastereoselective addition of the alkyne **98** to the benzylidene acetal aldehyde **87**.¹⁴¹

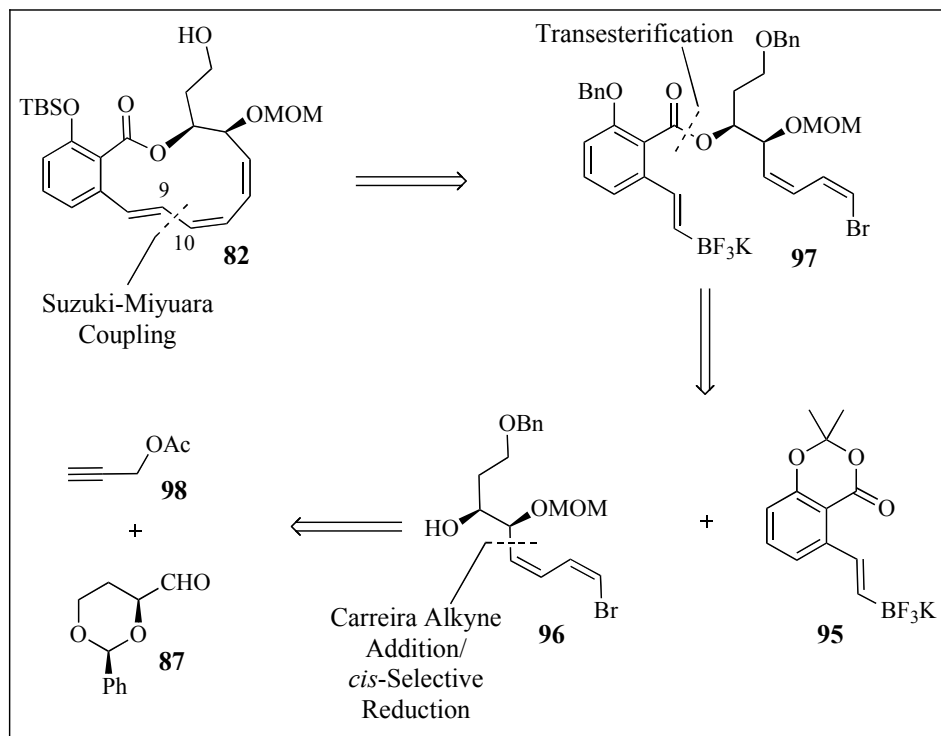
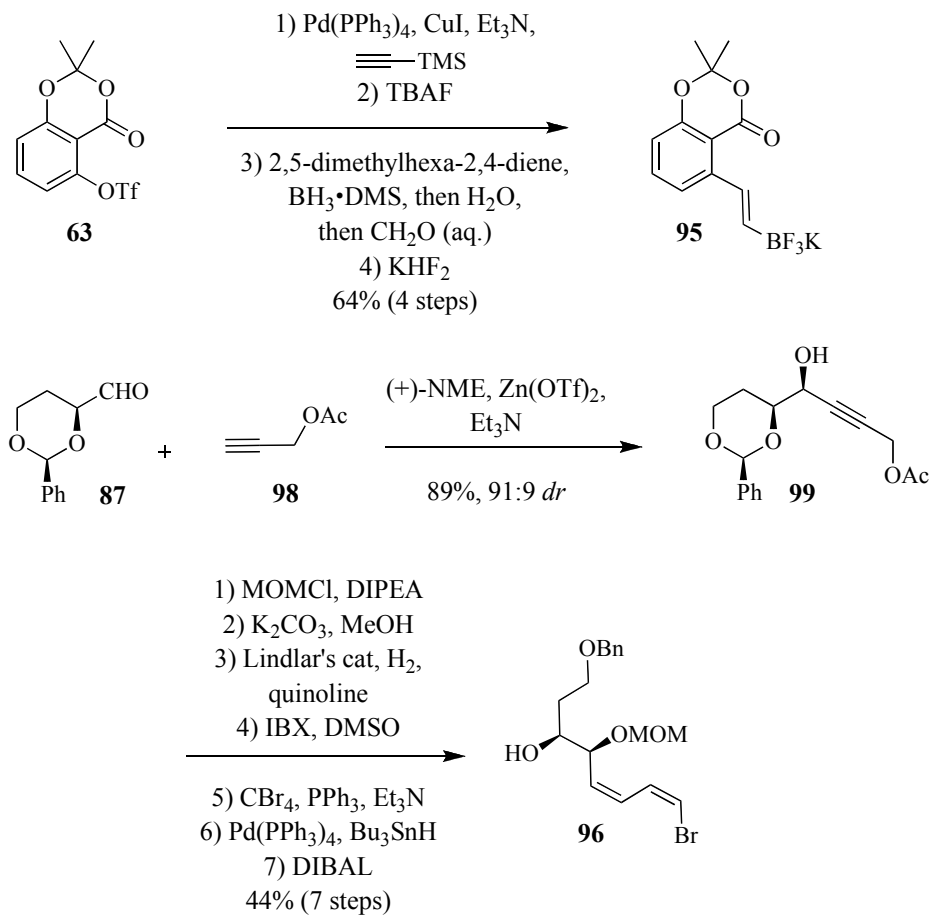


Figure 13. Second-generation retrosynthesis by Molander and Dehmel

In four steps, the known acetonide triflate **63**¹²³ was converted to the requisite transesterification partner **95** (Scheme 10). The synthesis of the aliphatic fragment **96** began with the Zn-mediated addition of propargyl acetate (**98**) to the chiral aldehyde **87**. This reaction proceeded with slightly diminished diastereoselectivity compared to the previous alkyne addition, delivering **99** in a 91:9 *dr*. Following seven

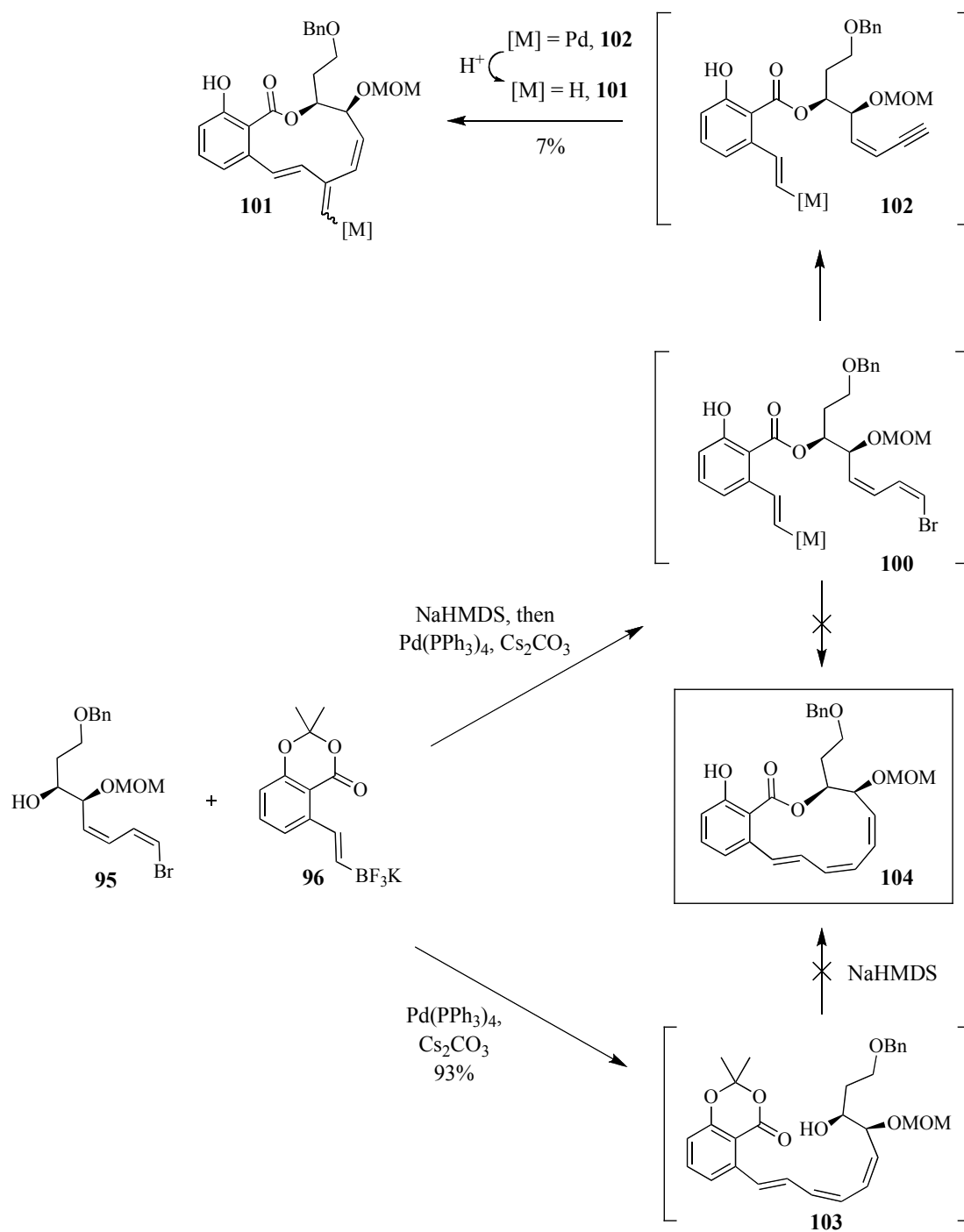
straightforward and high yielding steps, the secondary alcohol **96** was prepped for the ensuing transesterification.



Scheme 10. Synthesis of aromatic and aliphatic fragments by Molander and Dehmel

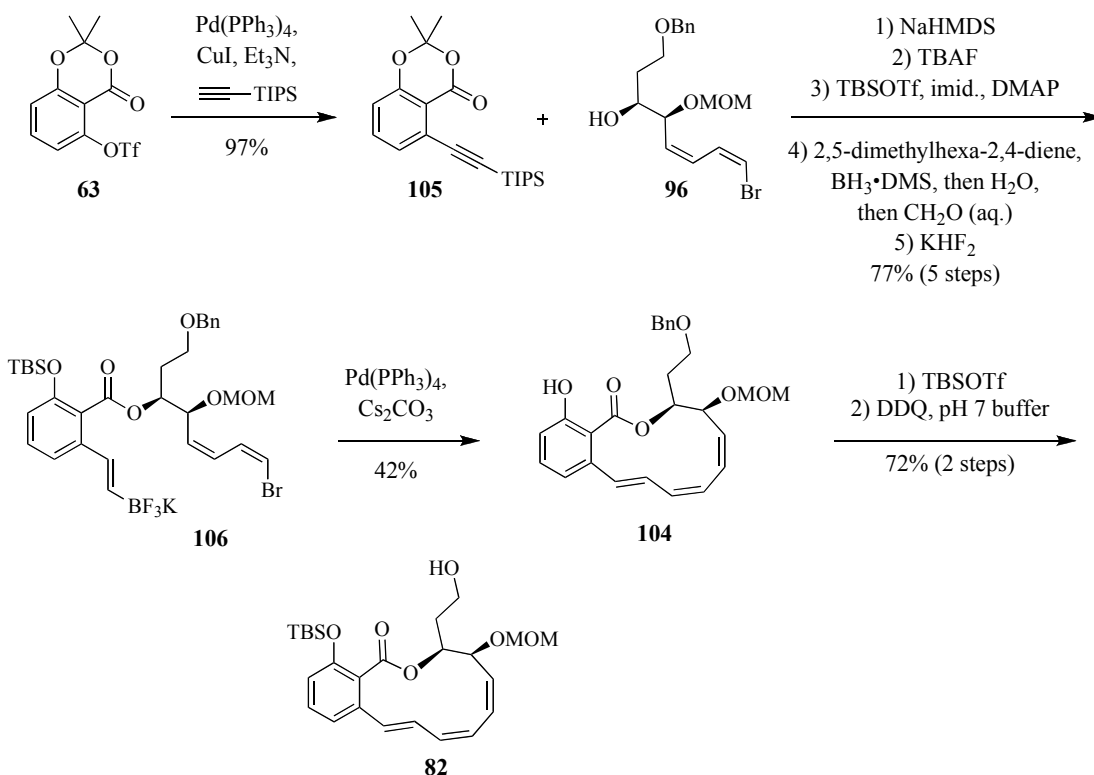
The synthesis again ran into a roadblock when attempting the transesterification reaction (Scheme 11). The aryl acetate **95** was added to the sodium alkoxide of **96**, presumably forming intermediate **100**. This intermediate (**100**) was immediately subjected to the cross-coupling conditions. However, an

unexpected exo-methylene product (**101**) formed. Presumably, this reaction occurs following the base-induced elimination of HBr from the *Z*-vinyl bromide, revealing an enyne subunit that can undergo a carbometallation event. Following protonation of the resultant palladium intermediate **102**, the observed 11-membered macrocycle **101** is formed. Alternatively, the group attempted to perform a macrolactonization following a successful Suzuki-Miyaura coupling. This route was also ineffective, presumably due to the developing ring strain when the sodium alkoxide attempted to add to the acetonide (**103**).



Scheme 11. Second-generation macrocyclization attempts by Molander and Dehmel

Assuming a later installation of the organotrifluoroborate would allow for successful macrocyclization, the group again altered their synthetic course (Scheme 12). Under basic conditions, the alkynyl-acetonide **105** was coupled to the alcohol **96**. A four-step protocol installed the requisite functionalized olefins, ready for Pd-catalyzed coupling to form the C9-C10 bond. This Suzuki-Miyaura coupling proceeded in a 42% yield, with the moderate yield realized again highlighting the difficulties associated with forming the strained triene core of oximidine II. The reaction was successful when substrate **106** was heated to reflux in a THF/H₂O mixture under high dilutions (1 mM) for 20 h in the presence of 10 mol % Pd(PPh₃)₄ and five equivalents of Cs₂CO₃. Alteration of the concentration, Pd species, or solvent mixture led to reduced product formation. During the course of the macrocyclization, the TBS-phenolic protecting group was removed. To complete the formal total synthesis, this phenol compound **104** was re-silylated and the primary benzyl ether was removed by 2,3-dichloro-5,6-dicyano-1,4-benzoquinone (DDQ) to deliver the target compound **82**.



Scheme 12. Completion of the formal total synthesis of oximidine II by Molander and Dehmel

1.5 Total Synthesis of Oximidine II

Our previous attempt at the total synthesis of oximidine II,¹²⁸ employing the Castro-Stephens macrocyclization, left behind opportunities for further investigation.

We embarked on a second-generation approach with the following goals in mind:

- 1) Develop efficient routes to the aliphatic and aromatic fragments
- 2) Improve the Castro-Stephens macrocyclization yield while investigating the reductive pathway leading to the *in situ* formation of the triene macrocycle
- 3) Complete the total synthesis of oximidine II

4) Develop an efficient synthesis of an allylic amide homolog of oximidine II, inspired by cruentaren A (**30**), to probe the importance of the enamide bond on the bioactivity of oximidine II

The retrosynthesis of our second-generation synthesis targeting oximidine II is displayed in Figure 14. The enamide bond would be installed using the Liebeskind catalyst, CuTC (**57**),¹¹⁹ following Porco's protocol,¹¹⁸ joining the oxime amide fragment **54** and the bis-TBS macrocycle **67**. The oxime amide **54** could be synthesized in two steps from commercially available maleimide (**107**), reducing the number of steps required by Porco's synthesis of the fragment.⁸⁶ The Molander and Dehmel synthesis of the triene macrocycle¹⁴⁰ demonstrated the necessity to join C9 and C10 during the macrocyclization. In their synthesis, attempting to link C7 and C8 in the ring-closure event was unsuccessful likely due to steric hindrance of the ortho ester group or to an overbearing amount of developing ring strain during the course of the reaction. With this knowledge in hand, we envisioned following our previous work and joining C9 and C10 with a Castro-Stephens coupling followed by a *cis*-selective reduction to create the triene macrolactone core of oximidine II. Following literature precedence, a transesterification reaction between aromatic fragment **108** and the aliphatic enynol molecule **109** would form the ester bond. Elaboration of the known aryl triflate **63**¹²³ via a Heck coupling would enable ready access to the aromatic acetonide compound **108**. A stereoselective Peterson olefination between 1,3-bis-TIPS-propyne (**110**)¹⁴⁴ and the enantioenriched aldehyde **111** was envisioned to generate the enyne moiety of the aliphatic fragment **109**.

Protecting group and oxidation state manipulations of the known diol ester **112** (or other ester oxidation states of **112**) would properly functionalize the aldehyde (**111**) prior to installation of the enyne. Paramount to our synthetic strategy is the orthogonal protection of a tetrol intermediate, allowing selective exposure of each hydroxyl group at various points during the synthesis. Further complicating the synthesis is the requirement of a MOM protecting group, or other small protecting group, on the alcohol at C14 to give high yields in the transesterification reaction.¹³⁸

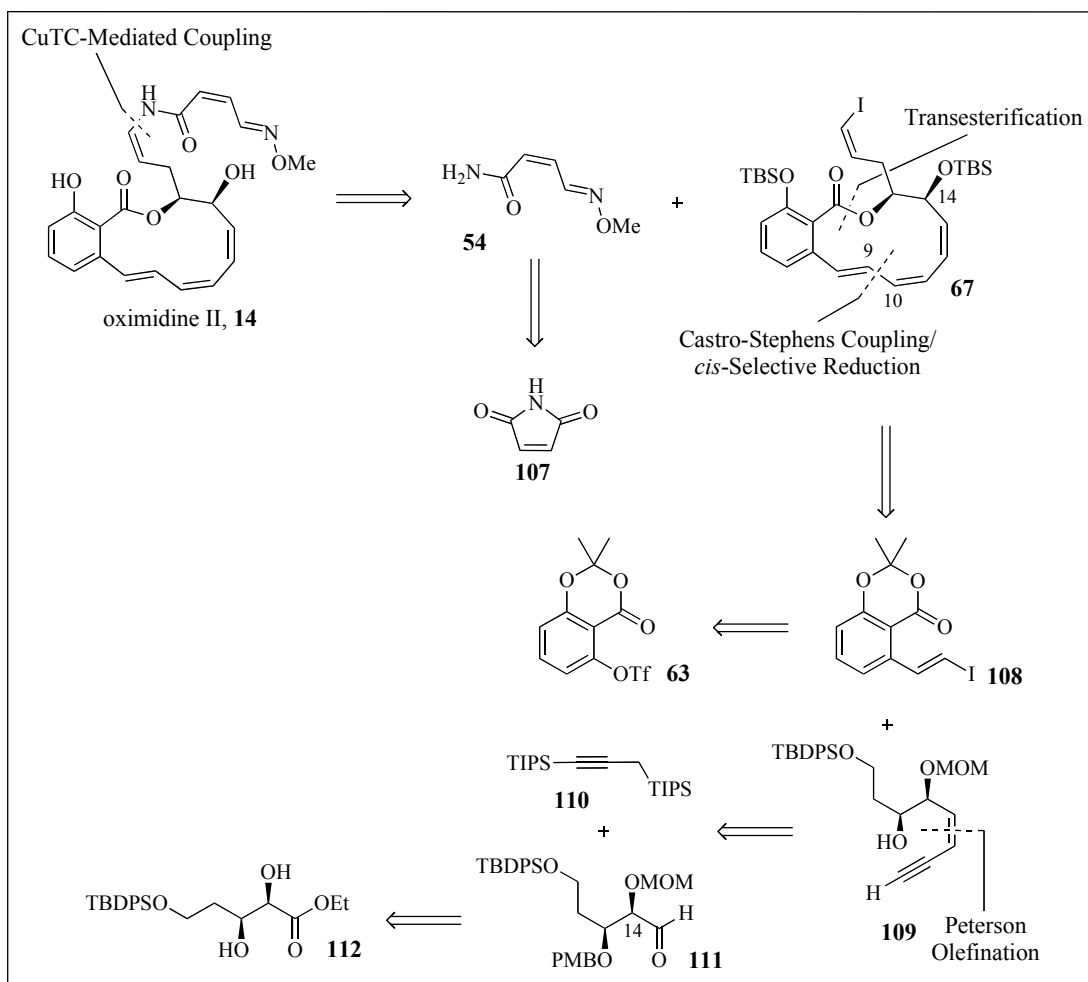
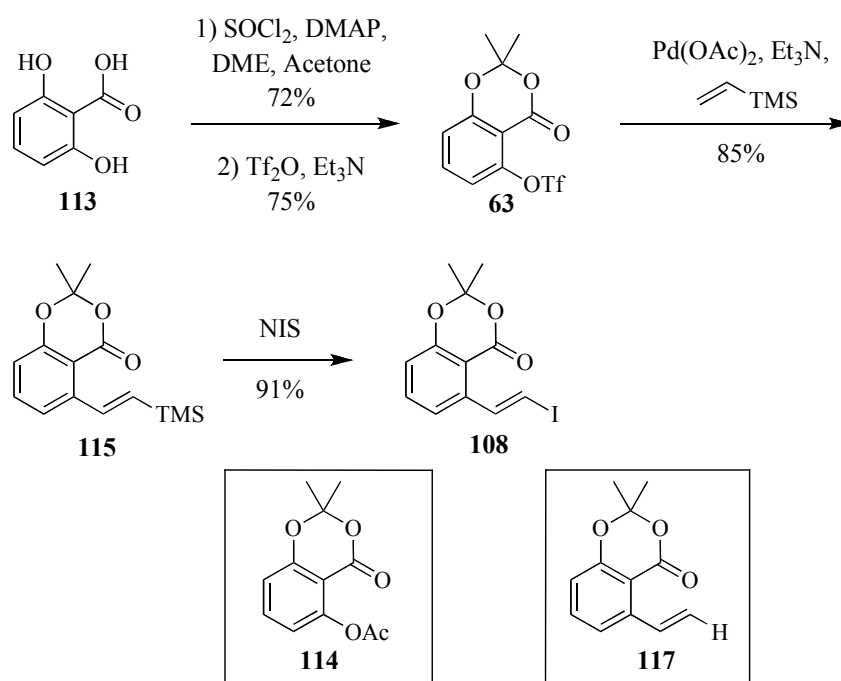


Figure 14. Our second-generation oximidine II retrosynthesis

The synthesis of the aryl fragment (**108**) began with acetone formation of commercially available 2,6-dihydroxybenzoic acid (**113**) (Scheme 13).¹⁴³ Triflation proceeded as previously described by Fürstner,¹²³ readying the molecule (**63**) for Heck coupling with vinyl(trimethyl)silane. Initially, Jeffery conditions,¹⁴⁵ employing ⁿBu₄NOAc to act both as a phase-transfer reagent and to generate a more reactive palladium species, were explored to catalyze this coupling. These conditions led to generation of equimolar amounts of an aryl acetate compound **114** (confirmed by ¹H

NMR and mass spectroscopy) in addition to the desired product **115**. Further catalyst system refinement led to use of 10 mol % Pd(OAc)₂, three equivalents of triethylamine (Et₃N) in DMSO at room temperature to provide the desired product **115**. A small amount (~5% by NMR) of desilylation occurred during this reaction, forming terminal alkene **117**. Ag salts are known to prevent this side reaction in Heck couplings with vinyl(trimethyl)silane,¹⁴⁶ but were unsuccessful in preventing the deleterious side reaction in this case. Iododesilylation following Kishi's protocol¹⁴⁷ led to formation of the vinyl iodide fragment **108** in 91% yield.



Scheme 13. Synthesis of aryl fragment **108**

The synthesis of the aliphatic piece began with protection of commercially available 1,3-propanediol (**118**) as its monosilyl ether (**119**).¹⁴⁸ The primary alcohol **119** was then oxidated to the corresponding aldehyde (**120**) by Dess-Martin periodinane (**121a**),^{131,132} homologated with a HWE reaction (**121**) and reduced with diisobutylaluminum hydride (DIBAL) to the *E*-allylic alcohol (**122**) following modification of the procedures of Baltas and coworkers (Scheme 14).¹⁴⁹ A Sharpless asymmetric dihydroxylation (SAD) of the allylic alcohol with AD mix- α in the presence of sulfonamide (MeSO₂NH₂) gave an excellent yield of the desired 1,2,3-triol **123**. Based upon studies by Sharpless¹⁵⁰ and Kumar¹⁵¹ on asymmetric dihydroxylation reactions of long chain allylic alcohols similar to our substrate **122**, we anticipated formation of the 2*S*,3*S* enantiomer **123** as drawn in Figure 15. The mnemonic developed by Sharpless¹⁵² predicts the stereochemical outcome of this asymmetric reaction (Figure 15). For our substrate, the hydroxymethylene group occupies the R_L position and the silyloxyethylene group occupies the R_M position, leading to the predicted diol stereochemistry. The presence of MeSO₂NH₂ speeds up the catalytic turnover of the reaction by cleaving osmate esters formed during the catalytic cycle of the reaction.¹⁵²

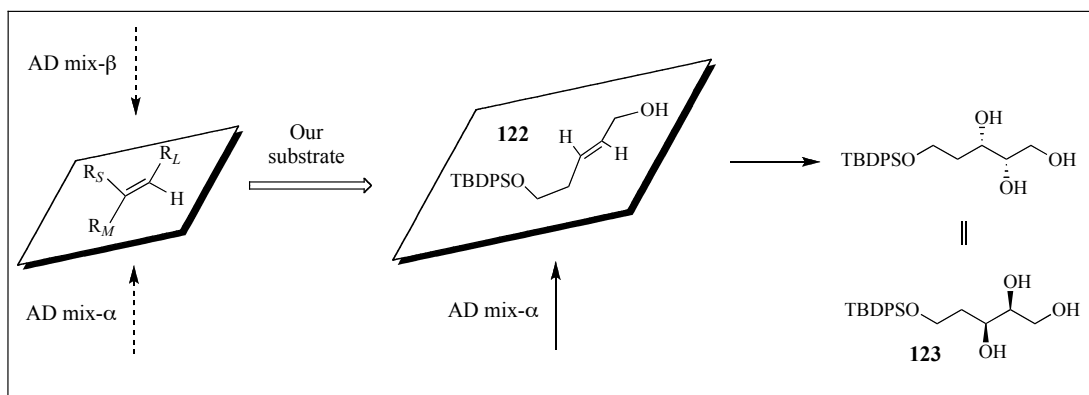


Figure 15. Sharpless's mnemonic device for asymmetric induction

The next challenge to conquer in the synthesis of the aliphatic piece was the selective formation of 1,3-benzylidene acetal **124** from the 1,2,3-triol **123**. Standard conditions for (*p*-methoxy)benzylidene acetal formation (*p*-methoxybenzaldehyde dimethyl acetal (PMB-dimethylacetal) with an acid catalyst)¹⁵³ gave near quantitative conversion of the starting material to a mixture of products, presumably 1,2-acetal **125**, 2,3-acetal **126**, and 1,3-acetal **124**, as inferred from the multitude of spots seen on TLC. A ¹H NMR spectra of the crude reaction revealed at least four major peaks with chemical shifts between 5 and 6 parts per million (ppm) corresponding to both five- and six-membered acetal rings. The relative stereochemistry of the major isomer generated by this reaction was confirmed by X-ray crystallography (Figure 16). Attempts to improve the ratio of 1,3-dioxane acetal **124** formation through variation of the acid, reaction time, temperature, solvent, or conversion to the corresponding tri-TMS variant following Noyori's protocol^{154,155} led to diminished conversion of starting material or to complete decomposition of the starting material. Additionally, the mixture of undesired acetal regioisomers was not stable under

ambient conditions. Isomerization of the mixture occurred with benchtop storage after four to eight weeks, leading to a ratio of acetals similar to that of the crude reaction mixture as determined by ^1H NMR. The isomerized mixture could then be purified by column chromatography and subjected to the next synthetic step. This recycling procedure could be repeated for up to six months following the initial acetal formation, after which time significant decomposition of the material occurred.

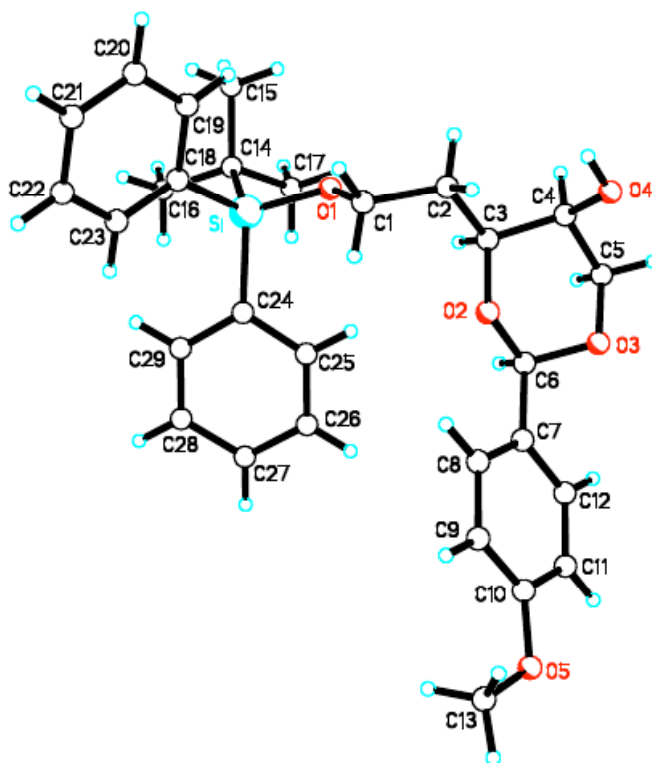
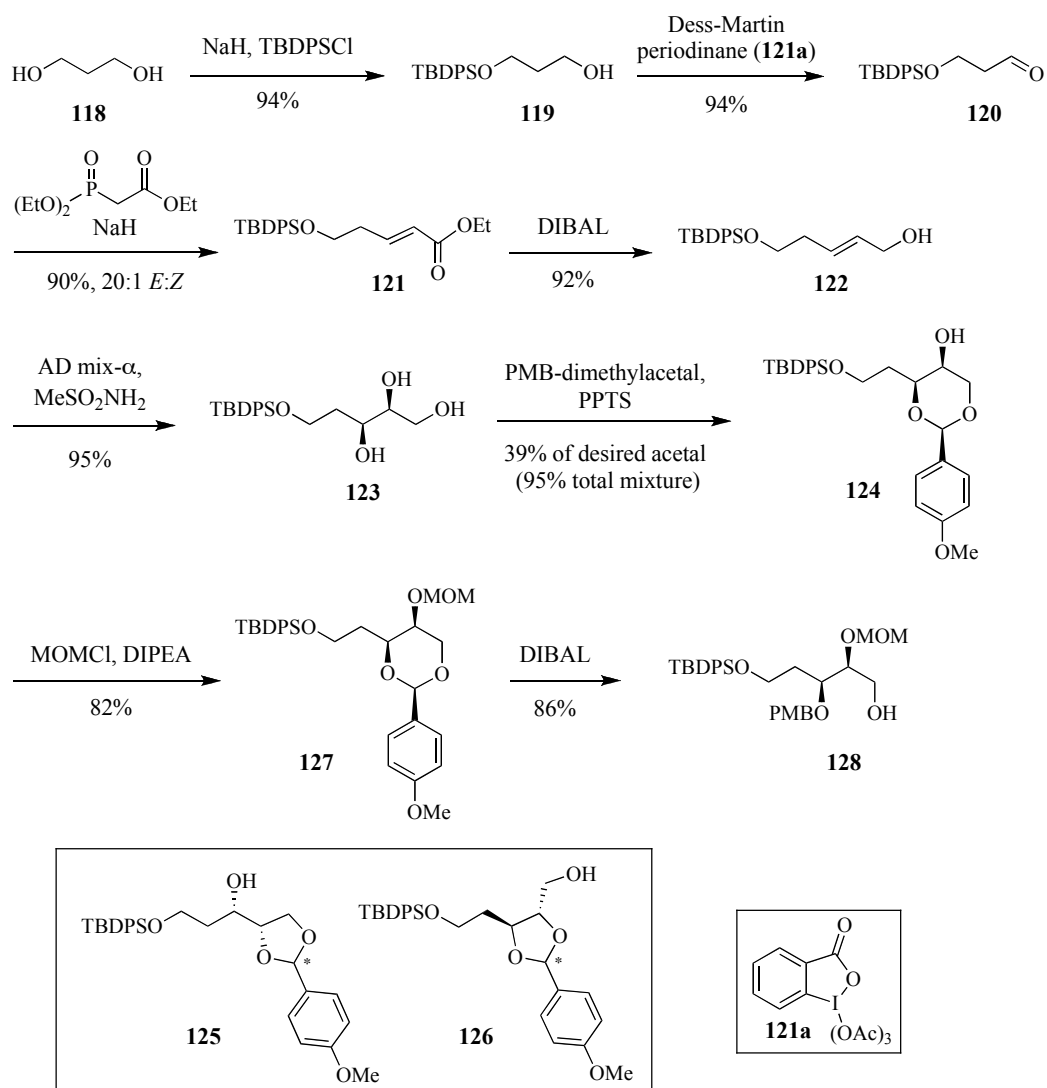


Figure 16. Crystal structure of desired acetal **124**

Immediately following chromatographic separation of the desired 1,3-benzylidene acetal **124** from the product mixture, the material was subjected to MOM ether formation (**127**). During this MOM protection step, some isomerization of the

1,3-benzylidene acetal occurred, contributing to the 82% yield for this step. This undesired regioisomeric material was easily removed by column chromatography. Regioselective reductive ring opening of acetal **127** with DIBAL generated the primary alcohol compound **128**.¹⁵⁶ While this route generated sufficient quantities to initially explore the formation of the enyne in subsequent steps, the prohibitive nature of the acetal protection step prompted us to revise our strategy for the synthesis of primary alcohol **128**.

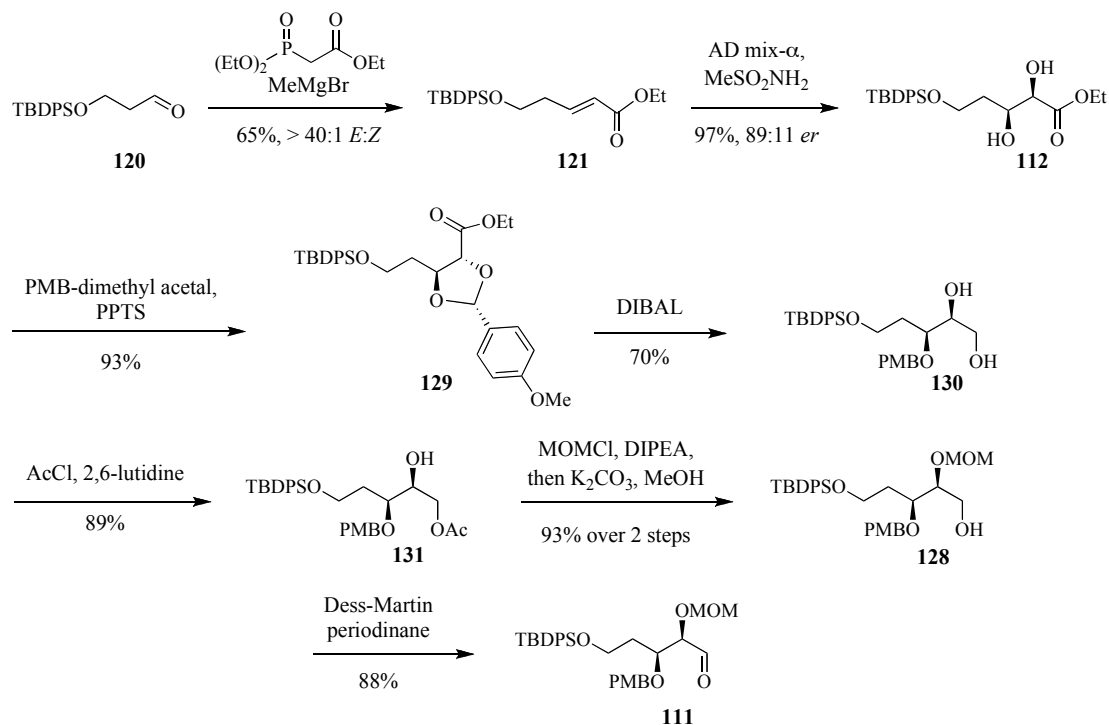


Scheme 14. Selective acetalization route towards the synthesis of alcohol **128**

We were able to evade the troublesome acetal protection step by changing the reaction sequence (Scheme 15). Using sodium hydride (NaH) as the base in the HWE reaction of aldehyde **120** gave high yields (<80%) on one to two mmol scale but gave diminished yields on larger scales necessary for material throughput (20-50

mmol scale). Following a recent report by Claridge *et al.*,¹⁵⁷ methyl magnesium bromide (MeMgBr) was employed as the base to give the desired homologated ester **121** in reproducible yields of 65% and high stereoselectivity (>40:1 *E:Z*). A SAD occurred without event to generate the known ester diol **112** in high yields with an enantiomeric ratio (*er*) of 89:11 (reported *er* of 95:5).¹⁵⁸ Not completely discouraged by our previous application of a benzylidene acetal protecting group, the diol was protected as its (*p*-methoxy)benzylidene acetal **129**. This acetal, similar to its predecessor **124**, was not stable at room temperature. We briefly explored conditions to reductively open the acetal, regioselectively generating the C15 (oximidine II numbering) PMB-ether, prior to ester reduction. This would then allow selective protection of the C14 alcohol as the MOM-ether. Boranes, often in conjunction with Lewis acids, are known to perform reductive ring opening transformations.¹⁵⁹ Also, boranes are generally unreactive towards esters at low temperatures. However, at low temperatures $\text{BH}_3 \cdot \text{SMe}_2$ or $\text{BH}_3 \cdot \text{THF}$ did not effect the desired ring opening transformation. Increasing the temperature or adding Lewis acids, such as AlCl_3 or $\text{BF}_3 \cdot \text{OEt}_2$,^{160,161} led to decomposition of the starting material mostly through the deprotection of the acetal. Other conditions employing hydrosilanes and AlCl_3 ¹⁶² or sodium cyanoborohydride and hydrochloric acid¹⁶³ were not explored because of the acid-sensitivity of the PMB-acetal **129**. A one-pot ester reduction/regioselective reductive acetal opening with DIBAL generated the diol **130**. While this work was ongoing, a similar sequence was developed by Brimble and coworkers.¹⁶⁴

Development of a three-step protection strategy was required to distinguish the primary and secondary alcohols. Freshly distilled acetyl chloride (AcCl) and 2,6-lutidine were necessary to achieve high levels of regioselectivity in the formation of secondary alcohol **131**. Use of acetic anhydride or less bulky bases, such as pyridine, was generally less selective for the primary alcohol and bis-acetylation was a common side reaction. MOM protection of the secondary alcohol **132** followed by methanolysis of the acetate yielded the desired primary alcohol **130**. Oxidation of alcohol **128** with Dess-Martin periodinane (**121a**) followed to generate the aldehyde **111**, ready for installation of the critical enyne moiety.



Scheme 15. Synthesis of aldehyde **111**

The demonstrated stereoselectivity of Peterson olefinations convinced us to explore the methodology for creation of the *Z*-enyne (Table 8).^{144,165-168} Treatment of a 1,3-bis-silyl-propyne (**110**) with an alkylolithium species, such as *n*-butyllithium (*n*BuLi), converts the starting material to the corresponding lithiated species, a nucleophilic propargyl anion. This lithiated species can be transmetalated with titanium^{169,170} or magnesium,¹⁷¹ leading to higher *Z:E* enyne ratios in certain instances upon treatment with an aldehyde or ketone. Corey¹⁴⁴ and Yamamoto¹⁷¹ have discussed the importance of bulkier 3-silyl groups on the stereoselectivity of this reaction. In general, bulkier silyl groups such as TIPS or TBDPS at this position give higher stereoselectivities (*Z:E* enyne ratios).

Our search for optimal conditions for the synthesis of enyne **133** began with the addition of a cooled solution (-78 °C) of 1-lithio-1,3-bis-TIPS-propyne to a precooled solution (-78 °C) of the aldehyde (**111**) (Table 8, entry 1). The overall yield for this reaction was low (35%) and generated a substantial amount (55% by ¹H NMR) of side product **134** formed by elimination of *p*-methoxybenzyl alcohol from the starting material (confirmed by ¹H and ¹³C NMR and mass spectroscopy). Eventually, it was discovered that a slow addition of the anion to the aldehyde at low temperatures reduced the production of the elimination product **134**. Even this procedural adjustment did not increase the yield or mass balance of the reaction, however. In these initial attempts, 1,3-bis-TIPS-propyne (formed by treatment of 3-lithio-1-TIPS-propyne with TIPS-OTf)¹⁴⁴ was purified by column chromatography. Although the ¹H NMR spectra of this columned product matched the reported spectra,

some impurity remained in the product leading to the diminished yields realized in the Peterson reaction. Distillation of the 1,3-bis-TIPS-propyne following its formation led to dramatically increased yields (60-80%) in the Peterson olefination (entry 2). Solvent effects were briefly explored. Use of diethyl ether (Et₂O) instead of tetrahydrofuran (THF) led to dramatically decreased reactivity. In this reaction, only 50% of the starting material reacted even after prolonged reaction times at room temperature. Presumably in THF, a solvent-ion pair (THF-Li) is formed and increases the nucleophilicity of the propargyl anion. However, in Et₂O, this effect is not present and the strength of the carbanion-Li bond hinders addition to the aldehyde. Although the activity in Et₂O is diminished, the stereoselectivity is greatly enhanced (entry 3). Addition of hexamethylphosphoramide (HMPA) to the reaction, functioning to sequester the lithium cation and create a more reactive carbanion, led to almost exclusive formation of the *E*-enyne by crude ¹H NMR (entry 4). Based upon this result, the addition of other cation sequestering reagents, such as *N,N,N',N'*-tetramethylethylenediamine, was not further explored. Variation of the counter ion had mixed results. The overall yield was similar for each of the reactions and a reduced amount of eliminated product was generated when MgBr₂•OEt₂ (entry 5) or Ti(O^{*i*}Pr)₄ (entry 6) were added to the reaction mixture. The Mg salt favored formation of the *E*-enyne, contrary to Yamamoto's previous report.¹⁷¹ Altering the quenching reagent (1N HCl, acetic acid (AcOH), aqueous NH₄Cl) had no effect on the *Z:E* ratio (not shown in Table). The best combination of yield and stereoselectivity resulted from a slow addition (1.5-2 h) of one equivalent of the

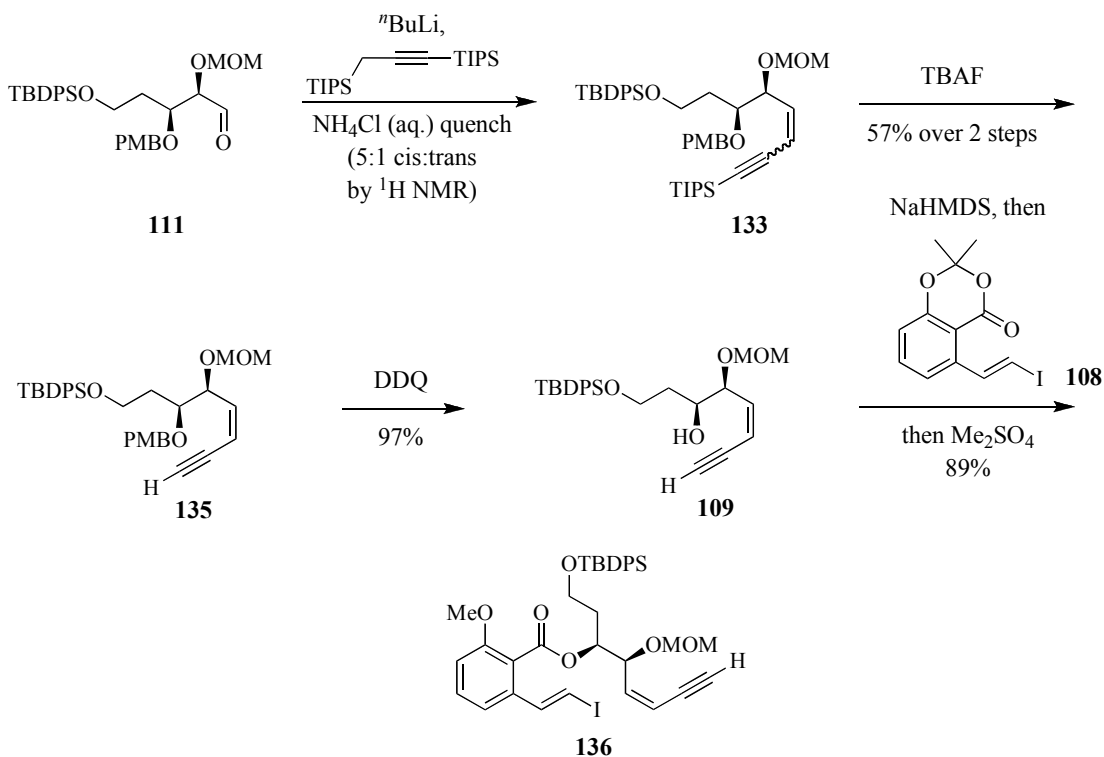
aldehyde to 1.8 equivalents of the anion generated from n BuLi at -78 °C (entry 2). Under these conditions, the reaction was complete within 30 min and gave a 5:1 *Z*:*E* ratio of unseparable enyne stereoisomers.

Table 8. Optimization of Peterson olefination

Entry	Additive	Solvent	% Yield (133 : 134)	<i>Z</i> : <i>E</i> Ratio of 133 (by 1 H NMR)
1	None	THF	35 (0.8:1)	4:1
2	None	THF	80 (10:1)	5:1
3	None	Et ₂ O	30 (1:2)	>20:1
4	HMPA	THF	15 (2:1)	1:20
5	MgBr ₂ •OEt ₂	THF	34 (20:1)	1:10
6	Ti(O ^{<i>i</i>} Pr) ₄	THF	40 (10:1)	5:1

Selective removal of the alkynyl-TIPS protecting group with tetra-*n*-butylammonium fluoride (TBAF) at 0 °C allowed for chromatographic separation of the previously unseparable *Z*- and *E*-enyne stereoisomer products (**135**, Scheme 16). Oxidative cleavage of the PMB ether with DDQ generated the *Z*-enynol **109** in 97% yield, ready for the transesterification reaction. Protection of the salicylate functional

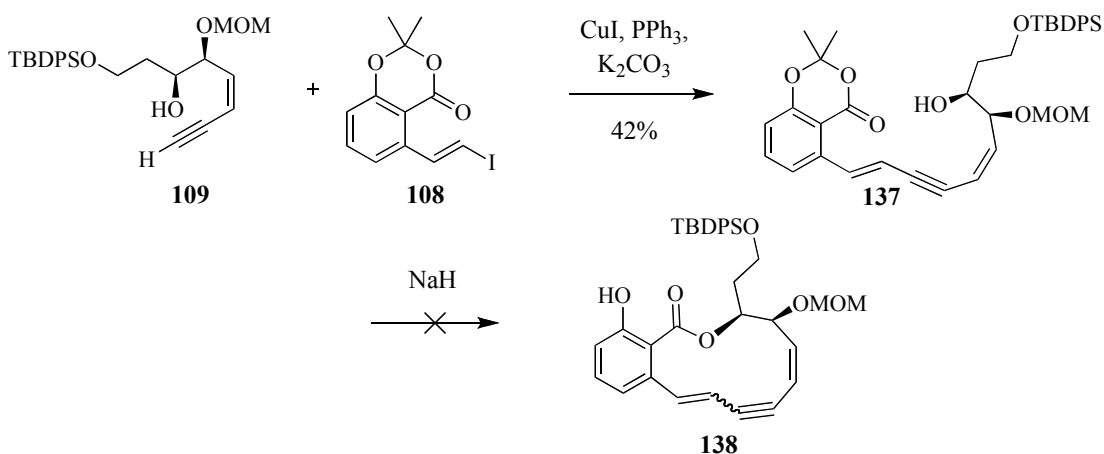
group as the corresponding acetonide generates an electrophile that, when treated with an alkoxide nucleophile, drives the coupling reaction towards product formation due to the increase in entropy gained from the liberation of acetone from the acetonide. The yields for this reaction were high provided that the alcohol **109** was dried by azeotropeing with toluene or benzene prior to deprotonation with NaHMDS.¹¹⁸ To this sodium alkoxide solution was added a solution of the acetonide (**108**), generating a phenolate anion that could be quenched *in situ* with a variety of electrophiles. For our total synthesis effort, we chose to use a methyl-protecting group because we hoped to remove both this aryl methyl ether and the MOM ether in one step later in the synthesis. We initially tried methyl iodide as the phenolate anion quenching source but the reaction was slow and often did not go to completion. Dimethyl sulfate (Me₂SO₄) was more expedient and complete in performing the methylation, forming the seco-cycle **136** in 89% yield.



Scheme 16. Synthesis of seco-cycle **136**

The biggest challenge of the synthesis was discovering and developing a more efficient macrocyclization approach based upon the Castro-Stephens coupling reaction. Our previous studies achieved only a 34% total yield of the ring-closing reaction – 15% lower than the standard set by Porco with a RCM reaction. In Molander’s synthesis, he demonstrated that ring-closure via a macrolactonization of the pre-formed triene **103** was unsuccessful in contrast to Maier’s previous work detailing a successful macrolactonization approach.¹⁰³ Curious of the effect of dienyne incorporation compared to a triene system on this macrolactonization approach, we first coupled the enynol **109** with the vinyl iodide **108** under Castro-

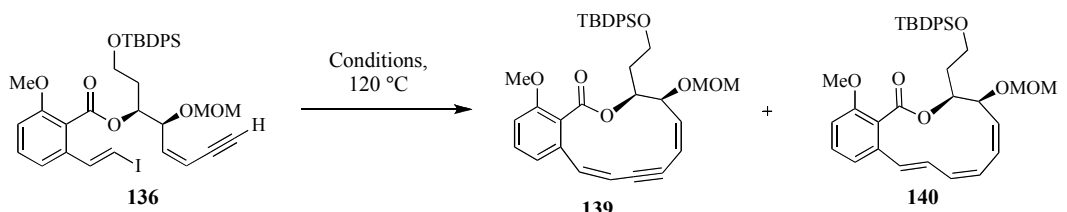
Stephens conditions, generating the dienyne open chain molecule **137** in 42% yield (unoptimized) (Scheme 17). Exposure of this molecule to NaH¹³⁸ led only to decomposition products, consistent with Molander's experimental results.



Scheme 17. Base-induced transesterification attempt

We then began investigating modifications to the Castro-Stephens reaction to increase the yield of either the dienyne **139** or triene **140** macrocycles (Table 9). Under non-catalytic conditions using one equivalent of CuI, the reaction produced an 18% yield of the dienyne **139** and an 8% yield of the reduced triene **140** (entry 1). As demonstrated previously,¹²⁸ the C8-C9 olefin inverted to the *cis* configuration during the course of the reaction. Exposing the seco-cycle **136** to the catalyst conditions described by Coleman and used in our first generation synthesis, 26% of the dienyne **139** was produced (entry 2). This yield is similar to our previous result (31%) demonstrating that the substitution at C17 (here OTBDPS, previously bis-SEt₂) has

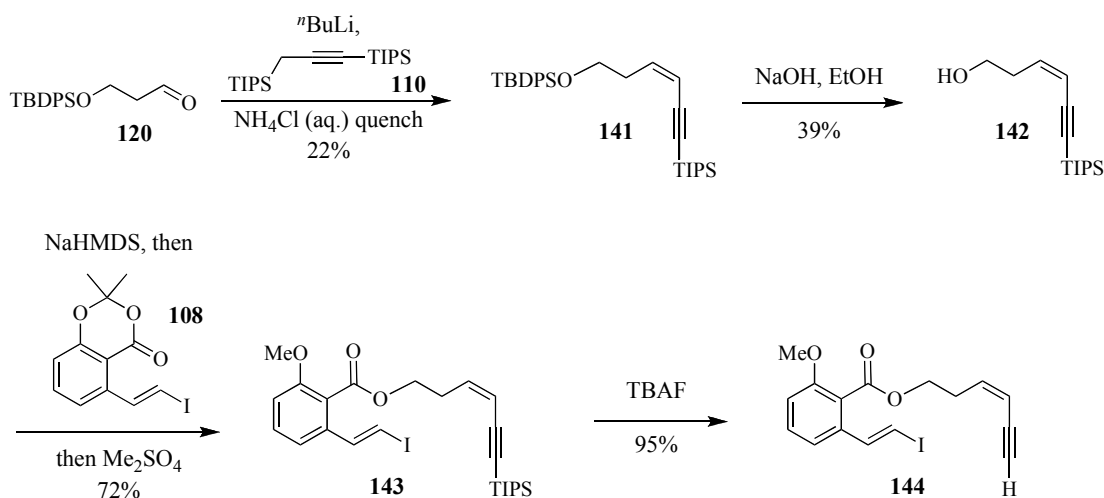
little effect on the cyclization. The reaction is successful in polar, coordinating solvents (entry 2 and 4), but not in non-polar solvents (entry 3). We then investigated the role of the phosphine ligand in the outcome of the reaction. Use of 2-(2',6'-dimethoxybiphenyl)dicyclohexylphosphine (S-Phos), a highly reactive Suzuki-Miyaura catalyst,¹⁷² left the starting material untouched (entry 5). Switching to P^tBu₃, a more bulky trialkylphosphine, generated a higher ratio of dienyne **139** to triene **140** as seen in the crude ¹H NMR, but was poor at converting the starting material to product. A catalyst system developed by Venkataraman and coworkers,¹⁷³ employing a bipyridine (bipy) ligand, gave similar results as the PPh₃ system (entry 8). Interestingly, the pre-catalyst complex Cu(PPh₃)₃Br used to form Cu(bipy)PPh₃Br showed only degradation products in the crude ¹H NMR (entry 7). Although only a small amount of starting material reacted by crude ¹H NMR analysis, switching the base to KO^tBu generated only the reduced product (entry 9). The significance of this result will be highlighted by forthcoming studies.

Table 9. Castro-Stephens macrocyclization optimization

Entry	Cu Source (equiv.)	Ligand	Base	Solvent	% Yield OR <i>136:139:140</i> by ¹ H NMR
1	CuI (1)	PPh ₃	K ₂ CO ₃	DMF	139 = 18 140 = 8
2	CuI (0.5)	PPh ₃	K ₂ CO ₃	DMF	26
3	CuI (0.5)	PPh ₃	K ₂ CO ₃	Toluene	NR
4	CuI (0.5)	PPh ₃	K ₂ CO ₃	DMSO	24
5	CuI (0.5)	S-Phos	K ₂ CO ₃	DMF	SM
6	CuI (0.5)	P ^t Bu ₃	K ₂ CO ₃	DMF	<i>10:3:1</i>
7	Cu(PPh ₃) ₃ Br (0.5)		K ₂ CO ₃	DMSO	<i>Degradation</i>
8	Cu(bipy)PPh ₃ Br (0.25)		K ₂ CO ₃	DMF	24
9	CuI (1)	PPh ₃	KO ^t Bu	DMF	<i>10:0:1</i>

These initial studies suggested that higher-yielding conditions for this macrocyclization would not be easily found. Therefore, we chose to develop a model system to investigate this key step (Scheme 18). A Peterson olefination installed the

requisite *Z*-enyne, forming the bis-silylated product **141** in low yield. The yield of this reaction could not be improved. As all starting material was consumed during the reaction, it is likely that the instability of the alkyl aldehyde **120** contributes to this result. Selective hydrolysis of the silyl ether (**142**),¹⁷⁴ one-pot transesterification/phenolate quench (**143**), and alkynyl-TIPS removal generated the seco-cycle **144** ready for optimization studies.



Scheme 18. Synthesis of model system for Castro-Stephens macrocyclization investigation

The results from this macrocyclization optimization study are displayed in Table 10. As previously seen, the solvent plays a critical role in the outcome of the reaction. When run in DMF (entry 1) or DMSO (entry 2), the Castro-Stephens coupling generated adequate yields of the dienyne macrocycle **145**. In less coordinating solvents, such as *N*-methylpyrrolidinone (NMP) (entry 3) or acetonitrile

(MeCN) (entry 4), or in a non-coordinating solvent (toluene, entry 5) no reaction occurred. Switching to the bipy-supported complex (entry 6) had little effect on the yield of the macrocyclization, as did changing the ligand to a dialkyl-aryl phosphine, 2-(di-*tert*-butyl)phosphino-2',4',6'-tri-isopropyl-biphenyl (DBPIB) (entry 7). Addition of Et₃N to the reaction completely halted activity (entries 8 and 9).

Shelting the Castro-Stephens reaction materials from light following a fast reaction workup and purification by chromatography allowed for the isolation of both the C8-C9 *Z*- and *E*-dienyne stereoisomers (**145** and **146**). After eight h as a CDCl₃ solution stored at 4 °C, the *E*-dienyne (**146**, Figure 17) inverted to the corresponding *Z*-dienyne cycle (**145**), confirmed by ¹H NMR. These observations prove the stereospecificity of the Castro-Stephens reaction of **144**.

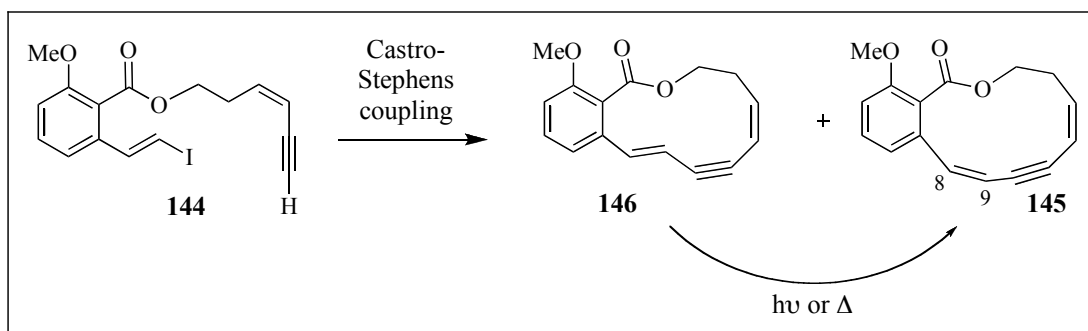


Figure 17. Castro-Stephens macrocyclization followed by C8-C9 olefin inversion

Table 10. Castro-Stephens optimization with model system **144**

Entry	Metal	Ligand/ Additive	Base	Solvent	Result (% Yield OR ¹ H NMR observation)
1	CuI	PPh ₃	K ₂ CO ₃	DMF	40
2	CuI	PPh ₃	K ₂ CO ₃	DMSO	37
3*	CuI	PPh ₃	K ₂ CO ₃	NMP	No Reaction (NR)
4	CuI	PPh ₃	K ₂ CO ₃	MeCN	NR
5	CuI	PPh ₃	K ₂ CO ₃	Toluene	NR
6	Cu(bipy)PPh ₃ Br		K ₂ CO ₃	DMF	29
7	CuI	DBPIB, ⁱ PrOH (2 equiv.)	K ₂ CO ₃	DMF	23
8	CuI	PPh ₃	Et ₃ N	DMF	NR
9	CuI	Et ₃ N	Et ₃ N	DMF	NR
10	Cp ₂ Zr(H)Cl	Pd(PPh ₃) ₂ Cl ₂ , DIBAL		THF	147 , X = H
11	[CuH(PPh ₃) ₆]	Pd(PPh ₃) ₂ Cl ₂ , DIBAL		Toluene	Mixture
12	[CuH(PPh ₃) ₆]			Toluene	148 , X = I
13	[CuH(PPh ₃) ₆]			DMF	148 , X = I

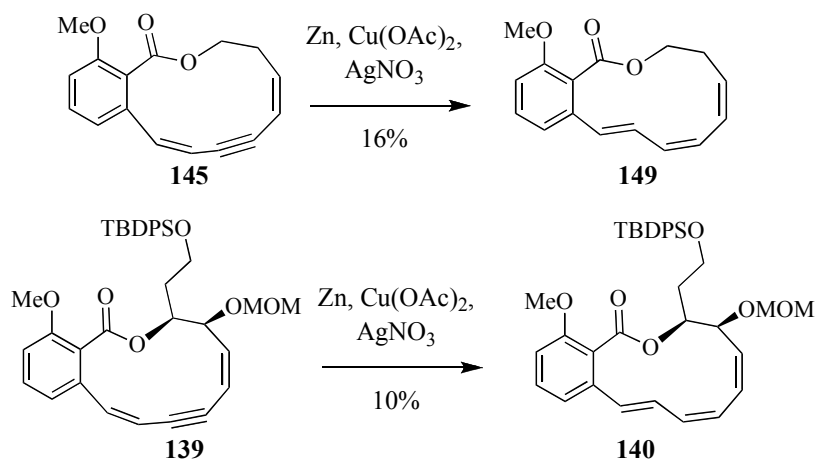
* Performed at 90 °C

With the oximidine system, we were able to isolate small amounts of the reduced, triene macrocycle (**140**) from the Castro-Stephens reaction (Table 9, entry 1). However, the model system (**144**) did not produce a similar result. Still intrigued

by the idea of performing a one-pot macrocyclization/alkyne reduction reaction, we explored chemistry developed by Negishi.¹⁷⁵⁻¹⁷⁷ Treatment of the model system **144** with Schwartz's reagent ($\text{Cp}_2\text{Zr(H)Cl}$) followed by a Pd-Al mixture generated a reduced, but un-cyclized product **147** (Table 10, entry 10). Presumably, this product arises from hydrozirconation of the alkyne and a Pd-mediated deiodination. Changing the alkyne-reducing reagent to Stryker's reagent ($[\text{CuH}(\text{PPh}_3)]_6$)^{178,179} followed by treatment with the Negishi Pd-Al mixture generated an unidentifiable mixture of products by crude ^1H NMR analysis (entry 11). Use of only Stryker's reagent in the catalyst system led only to reduction of the alkyne (**148**) (entries 12 and 13).

Although we were unable to find conditions to dramatically increase the yield of the Castro-Stephens macrocyclization, we proceeded forward with our synthetic strategy that required chemo- and stereoselective reduction of the alkyne macrocycle **145** to the corresponding *cis*-alkene macrocycle **149**. We also hoped that this reduction would also invert the C8-C9 *cis*-olefin to produce the thermodynamically more stable *E,Z,Z* triene configuration. Again using the model system as practice, we investigated various reduction methods. Coleman and Garg utilized a Boland reduction¹⁸⁰ to execute this transformation. Reduction of our alkyne macrocycle **145** was inconsistent with these conditions, generating a yield of only of 16% (50% based on recovered starting material) (Scheme 19). We explored other stereoselective alkyne-to-*Z*-alkene reduction methods, such as hydrogenation with the Lindlar catalyst, the Schwartz reagent, and samarium iodide-mediated reduction,¹⁰⁴ but these

were also ineffective. Low catalyst loading and running the reaction at room temperature in the Lindlar system gave no reaction, while increasing the catalyst loading and temperature resulted in degradation of the starting material (**145**). Understanding that the best model system is the actual system, the Boland and Lindlar reductions were performed on the dienyne macrocycle **139**. In this case, the model system proved to be true. The oximidine macrocycle **139** was reduced by the Boland reduction conditions to the desired triene macrocycle **140**, giving only 10% conversion to the product (Scheme 19). This result was not repeatable. Reduction attempts with the Lindlar catalyst were also futile. This apparent roadblock presented an opportunity to explore the mechanism leading to the formation of the triene macrocycle **140** produced in the Castro-Stephens reaction.



Scheme 19. Boland reduction of dienyne macrocycles **145** and **139**

Two potential reductive pathways for this transformation were investigated based upon both literature precedence and experimental observations. Our initial idea was that some oxidation state of copper was propagating the reduction. We had demonstrated the feasibility of Zn dust to reduce the alkyne to the alkene (Scheme 19), so possibly Cu, although having a lower reduction potential compared to Zn, could induce the reduction under the right conditions. Further, we noticed that the triene product was isolated in higher yields when CuI had been pre-activated by flame-drying under vacuum prior to utilization in the Castro-Stephens reaction. This pre-activation process left a metallic coating on the flask, indicating the CuI was being partially disproportionated into Cu(0) and Cu(II) species. CuI used directly from the vendor generated little or none of the reduction product in most cases. Application of CuI purified by precipitation with treatment of KI¹⁸¹ in the Castro-Stephens reaction produced no reduction product **140**. We reasoned that Cu(0) was most likely the reductant source and began investigating the use of this metal. Addition of Cu wire or Cu powder to the reaction, with and without various Cu(II) salts, generated similar ratios of dienyne product **139** and triene product **140** as previously seen with the flame-dried CuI system. The yields for these reactions were also comparable to previous results. The addition of Zn dust to the Castro-Stephens reaction led only to partial degradation of the starting material.

An alternative pathway involves copper-hydride (Cu-H) reduction of the alkyne to the corresponding *Z*-alkene. Cu-H species are well known to reduce alkynes to the corresponding *cis*-alkenes.¹⁷⁹ Support for our hypothesis that a Cu-H

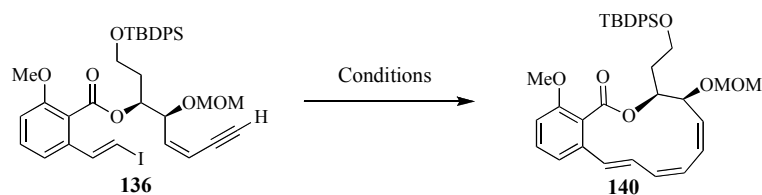
intermediate was responsible for the alkyne-to-alkene reduction arose from a previous result in which KO^tBu was employed as the base in the Castro-Stephens reaction. Compared to K₂CO₃, use of this base generated a higher ratio of the triene macrocycle **140** to dienyne macrocycle **139** (Table 9). Mixing KO^tBu with Cu(I) salts generates Cu(O^tBu), a complex used to make the Cu-H hexamer ([CuH(PPh₃)₆]).¹⁸² In Stryker's initial report, this Cu-H hexamer was made by mixing Cu(O^tBu) with PPh₃ under an atmosphere of hydrogen (H₂). In our system, DMF, the solvent of choice for the Castro-Stephens reaction, could decompose during the reaction to generate a hydride equivalent. Although unprecedented with copper salts, DMF is known to act as a hydride source when treated with various metals (Pd,¹⁸³ Fe,¹⁸⁴ and Rh¹⁸⁵). The triene product **140** was generated only when DMF was used as the solvent in the macrocyclization. Although unclear if DMF could be the hydride source in our case, we explored other conditions known to generate the Cu-H species.

The first conditions explored emulated those of Stryker's Cu-H formation paper.¹⁸² Stirring a DMF solution of CuI, PPh₃ and KO^tBu under an atmosphere of H₂ at 120 °C for 30 minutes followed by slow addition of a DMF solution of the seco-cycle **136** generated the desired, triene macrocycle **140** in 31% yield (Table 11, entry 1). No dienyne (**139**) was observed in the ¹H NMR spectra of the crude material. Further, this crude ¹H NMR spectrum displayed a clean reaction product – no degradation or side products were seen. Lowering the reaction temperature (entry 2) had a detrimental effect on the outcome of the reaction. These observations are contrary to literature reports that question the thermal stability of Cu-H species.¹⁸⁶

Seeking an easier reaction setup, the use of commercially available Stryker's reagent was investigated. Across a range of temperatures and in different solvents (entries 3-6), use of this reagent to perform the reductive ring-closure generated a complex mixture of products by crude ^1H NMR analysis. Other conditions known to generate reactive Cu-H species also produced complex ^1H NMR spectra (entries 7-9). Polymethylhydrosiloxane (PMHS) was investigated specifically due to its wide use in various literature preparations of Cu-H complexes.¹⁸⁷ Therefore, we were surprised to see its ineffectiveness in our system. Results from the application of the hydrosilane in model system reactions gave insight into its ineffectiveness (see below). Alteration of the base (entry 10) also dramatically reduced the yield of triene formation, demonstrating the need to generate the Cu(O^tBu) species, at least when H₂ was used as the hydride source. Formic acid (HCO₂H) or formate salts are commonly used in transfer hydrogenation reactions with Pd catalysts. Although unprecedented as the hydride source in Cu-H complex formation, addition of formic acid to the reaction mixture produced a 50% yield of only the desired triene macrocycle **140** (entry 11). No dienyne **139** was seen in the crude ^1H NMR spectrum. Key to success of the reductive macrocyclization was stirring the reagents together at 120 °C for 30 min prior to slow addition of the enyne seco-cycle **136** over one h. The yield was further increased by increasing the CuI:PPh₃ ratio from 1:2 to 1:3¹⁸⁸ and using sodium formate (HCO₂Na) (entry 12). The 67% yield realized by these conditions is almost 20% higher than the precedent set by Porco's RCM macrocyclization approach. Simplification of the reaction setup by using commercially available copper (II)

formate hydrate ($\text{Cu}(\text{O}_2\text{CH})_2 \cdot \text{H}_2\text{O}$) (entry 13) with the addition of PPh_3 generated the desired triene product by crude ^1H NMR analysis. However, crude ^1H NMR analysis also displayed a variety of side products and these conditions were not explored further. Another Cu(II) salt, $\text{Cu}(\text{OAc})_2 \cdot \text{H}_2\text{O}$, was investigated because of its demonstrated ability to form Cu-H species.^{189,190} This salt was also successful in catalyzing the reductive ring closure, albeit in a slightly lower yield than CuI (entry 14).

On reactions of less than 50 mg, CuI was reproducibly effective at catalyzing the reductive ring closure. For unknown reasons, on larger scales CuI generated mixtures of the triene and dienyne macrocycles (**140** and **139**, respectively). Fortunately, $\text{Cu}(\text{OAc})_2$ catalyzed the reductive macrocyclization on all reaction scales. Later investigations revealed that $\text{Cu}(\text{OAc})_2$ generates a catalyst with a rapid turnover rate. The reductive macrocyclization was often complete within 15 minutes of substrate addition to the $\text{Cu}(\text{OAc})_2$ catalyst solution. Further, the substrate could be added over a period of one to two minutes instead an hour as required for the CuI-catalyzed reaction. Other Cu(II) salts were not investigated.

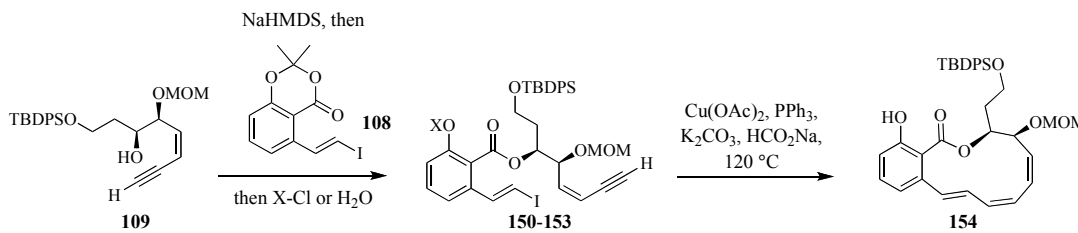
Table 11. Optimization of reductive macrocyclization

Entry	Cu Source	Base	Additive(s)	Solvent	Temp. (°C)	% Yield (isolated) OR Crude ¹ H NMR Analysis
1	CuI	KO ^t Bu	PPh ₃ , H ₂ (1 atm)	DMF	120	31
2	CuI	KO ^t Bu	PPh ₃ , H ₂ (1 atm)	DMF	90	NR
3	[CuH(PPh ₃) ₆]			DMF	90	mixture
4	[CuH(PPh ₃) ₆]			Toluene	90	mixture
5	[CuH(PPh ₃) ₆]			DMF	120	mixture
6	[CuH(PPh ₃) ₆]			DMF	50	mixture
7	CuCl	NaO ^t Bu	PPh ₃ , H ₂ (1 atm)	DMF	100	mixture
8	CuCl	NaO ^t Bu	PPh ₃ , PMHS	DMF	100	mixture
9	CuCl	NaO ^t Bu	PPh ₃ , PMHS	DMF	110	mixture
10	CuI	K ₂ CO ₃	PPh ₃ , H ₂ (1 atm)	DMF	120	some triene
11	CuI	K ₂ CO ₃	HCO ₂ H	DMF	120	50
12	CuI	K ₂ CO ₃	HCO ₂ Na	DMF	120	67
13	Cu(O ₂ CH) ₂		PPh ₃	DMF	120	triene
14	Cu(OAc) ₂	K ₂ CO ₃	HCO ₂ Na	DMF	120	55

Porco previously demonstrated the effect of the phenol protecting group on the yield of the RCM macrocyclization.¹¹⁸ The bulky TBS protecting group allowed the RCM reaction to occur, while lack of any phenol protecting group generated none of the desired macrocycle (Scheme 5). We investigated the steric and electronic role of the phenol protecting group on the Cu-mediated reductive macrocyclization. Quenching the transesterification reaction with TBDPS-Cl, TBS-Cl, Ac-Cl or H₂O

generated seco-cycles **150-153** (Table 12). These substrates each produced the phenol triene macrocycle **154** when subjected to the reductive macrocyclization conditions. The cyclization yields for the TBDPS- (entry 1), TBS- (entry 2) or hydroxyl (entry 4) seco-cycle reactions were approximately 60%, implying that cleavage of the silanes occurred prior to macrocyclization. The acetate-protected compound **152** (entry 3), however, yielded 80% of the phenol triene **154**, implying that electronics of the cyclization substrate may play an important role in this reaction.

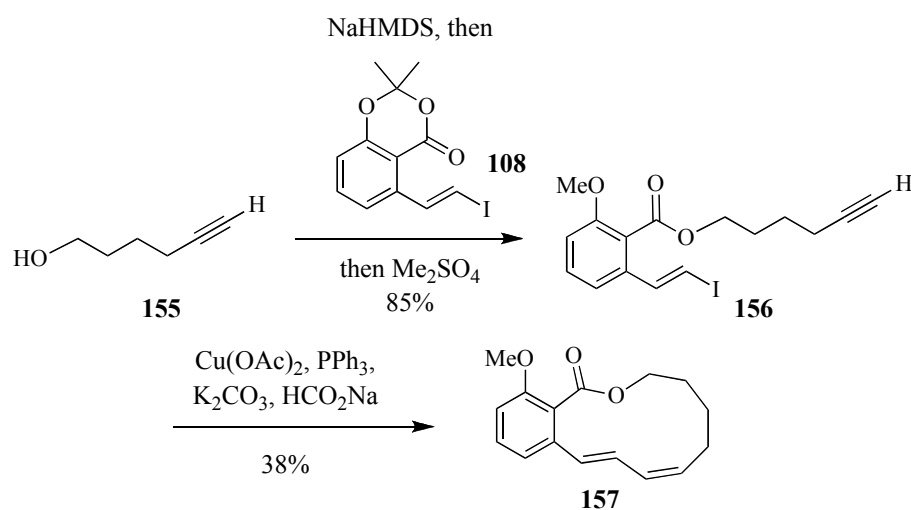
Table 12. Investigation of phenol protecting group on reductive macrocyclization



Entry	Transesterification Quenching Reagent	Transesterification % Yield	Macrocyclization % Yield
1	TBDPSCl (150)	51	62
2	TBSCl (151)	53	60
3	AcCl (152)	65	80
4	H ₂ O (153)	65	57

A simplified model system was developed to explore other conditions known to generate Cu-H species. Transesterification of the aryl acetonide **108** with 1-hexyn-1-ol (**155**) produced the seco-cycle **156** (Scheme 20). Exposure of the seco-cycle to the newly established reductive cyclization conditions (Cu(OAc)₂ (0.33 equivalents),

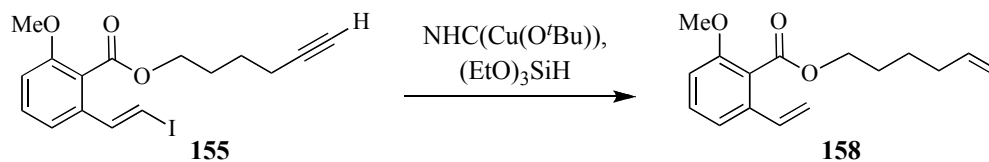
PPh₃ (one equivalent), K₂CO₃ (1.5 equivalents), HCO₂Na (four equivalents) generated the desired reduced macrocycle **157** in 38% yield. The macrocycle was the only product of the reaction based upon crude ¹H NMR analysis and it is unclear why the mass balance was low for the reaction. Nonetheless, the success of this reaction demonstrated that an enyne functionality was not required for reductive macrocyclization and that this simplified model system could be used in further optimization and mechanistic investigations.



Scheme 20. Reductive macrocyclization of alkyne model system

Besides phosphines, *N*-heterocyclic carbenes (NHC) have been used as ligands to support Cu-H species.^{187,189} In 2004, Sadighi and coworkers demonstrated the applicability of these ligands towards Cu-H generation.¹⁹¹ The researchers were able to hydrocuprate 1-hexyne using an NHC-Cu-H complex generated from NHC-Cu(OtBu) and (EtO)₃SiH. Crystal structure analysis of this vinylcopper product revealed the formation of a σ -bound organocopper molecule – the first evidence of

this intermediate that is likely involved in hydrogenation¹⁷⁹ or reductive coupling¹⁹² reactions involving Cu. Use of this NHC-Cu-H catalyst in the reductive macrocyclization of the model system **155** only generated product **158** based on crude ¹H NMR analysis, resulting from reduction of the vinyl iodide and partial reduction of the alkyne (Scheme 21). Use of hydrosilanes to generate the Cu-H species, whether from an NHC-Cu complex or from a mixture of CuI, PPh₃ and base, generated this non-cyclized, reduced product **158**. Based on these results, use of formate as the hydride source generates a catalyst with attenuated reductive capability compared to Cu-H species derived from hydrosilanes. This formate-derived Cu-H species is able to reduce only a highly strained alkynyl intermediate to the corresponding *Z*-olefin compound. Further mechanistic implications of this cyclization reaction will be discussed in a forthcoming section.



Scheme 21. Failed reductive macrocyclization with NHC-Cu-H complex

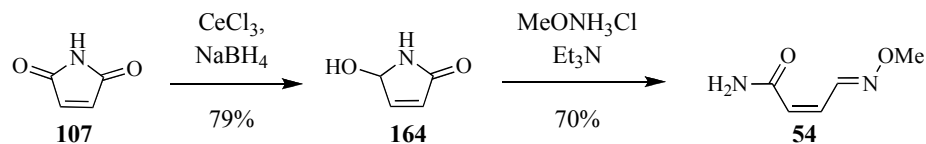
With a reliable synthesis of the triene macrocycle **140** in hand, we were able to complete the total synthesis of oximidine II (Scheme 23). Removal of the primary silyl ether (**159**) followed by oxidation by Dess-Martin periodinane (**121a**) generated aldehyde intermediate **160**. Following Porco's example, a Stork-Zhao-modified

Wittig olefination with $\text{IH}_2\text{CPh}_3\text{I}^{127}$ installed the Z-vinyl iodide (**161**),¹²⁶ required for late-stage amide coupling. At this point we decided to change our protecting group strategy because of potential issues arising from trying to remove alkyl ethers in the presence of the methyl oxime ether at the end of the synthesis.

Initial attempts to remove both alkyl ethers in one step (i.e. from **161** to **162** directly) with boron tribromide¹⁵³ or boron trichloride (BCl_3) were unsuccessful. Using either of these reagents generated an unidentifiable product as the major mass component. Therefore, a two-step protocol was developed. First, removal of the MOM-ether with carbon tetrabromide (CBr_4) in warm $^i\text{PrOH}$ generated the secondary alcohol **163**. This mixture of reagents presumably generates a small amount of hydrobromic acid that facilitates the deprotection.¹⁹³ The phenol (**162**) was exposed following treatment of the aryl methyl ether **163** with BCl_3 . This unstable diol was immediately bis-TBS protected, readying the molecule for installation of the amide side chain. With the formation of the bis-TBS ether **67**, our synthesis intersected with Porco's synthesis of oximidine II and allowed for both structure confirmation and establishment of optical purity (reported $[\alpha]_D^{25} = -171.3^\circ$ ($c = 2.00$, CHCl_3), observed $[\alpha]_D^{25} = -151.2^\circ$ ($c = 0.49$, CHCl_3)).¹¹⁸ Further, this intermediate would serve as the point of divergence towards the synthesis of the allylic amide analog.

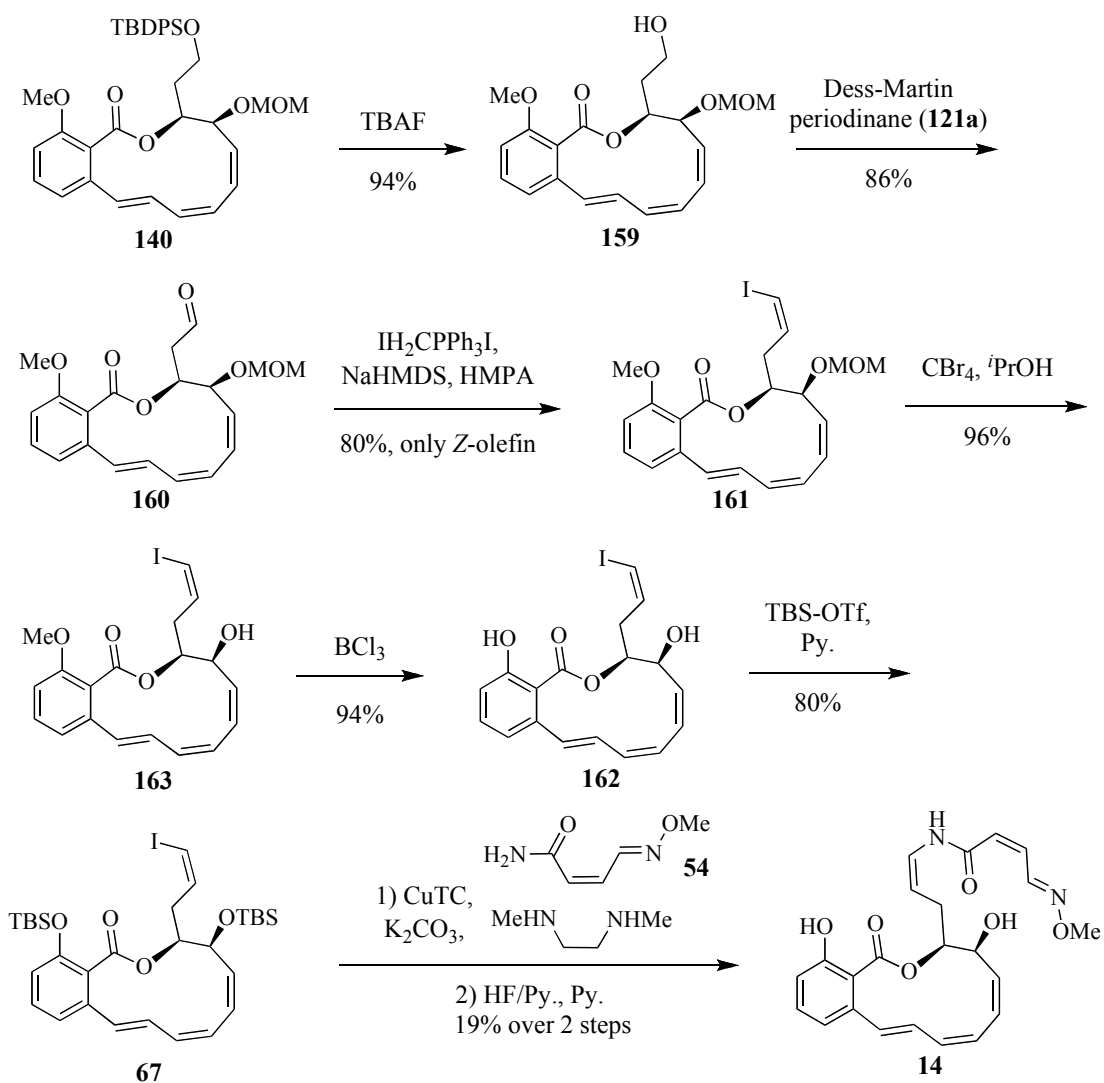
The oxime amide **54** was accessible in two steps from commercially available maleimide (**107**) following Coleman's work (Scheme 22).¹¹⁵ Selective reduction of maleimide under Luche conditions delivered the corresponding hydroxypyrrolone **164**. This masked aldehyde was condensed with methoxyammonium chloride

(MeONH₃Cl) to generate the oxime amide **54**. This synthesis of amide **54** is one step shorter and 20% higher-yielding than Porco's previous synthesis of the amide.⁸⁶



Scheme 22. Synthesis of oxime amide side chain **54**

Besides Porco's established conditions for enamide formation, we investigated conditions reported by Buchwald and Coleman. Coupling of the amide **54** to the *Z*-vinyl iodide **67** using Buchwald's conditions (CuI, *N,N'*-dimethylethylenediamine, K₂CO₃ in THF) returned only the starting materials.¹⁹⁴ The conditions developed by Coleman and coworkers (CuTC (**57**), *trans-N,N'*-dimethyl-1,2-cyclohexanediamine, K₃PO₄ in dioxane) generated some product by crude ¹H NMR.¹¹⁵ However, attempts to push the reaction to completion by increasing the amount of amide **54**, the amount of the catalyst system, or modifying the temperature were unsuccessful. Following Porco's two-step amide coupling/bis-silyl ether removal protocol, we synthesized oximidine II (**14**) in 19% yield over the final two steps (Scheme 23). The ¹H NMR and high-resolution mass spectrometry (HRMS) data of the synthesized oximidine II matched the literature values for the isolated natural product.¹⁷



Scheme 23. Completion of the total synthesis of oximidine II (**14**)

1.6 Synthesis and Biological Activity of Oximidine II Analogs

The retrosynthesis for our allylic amide homolog **165** is displayed in Figure 18. We envisioned installation of the amide side chain via modification of the corresponding allylic alcohol **166** followed by bis-TBS removal to generate the

desired analog **165**. Specifically, the amide could be obtained by: conversion of the allylic alcohol to the allylic amine **167** followed by an amide coupling reaction, similar to Maier's protocol for installing the allylic amide during his group's total synthesis of cruentaren A;¹⁹⁵ conversion of the allylic alcohol to a leaving group followed by S_N2 displacement by the amide or an amide surrogate; or by Mitsunobu coupling of the allylic alcohol with maleimide^{196,197} followed by modification of the maleimide moiety into the desired oxime amide similar to our strategy for formation of amide **54** (Scheme 22).

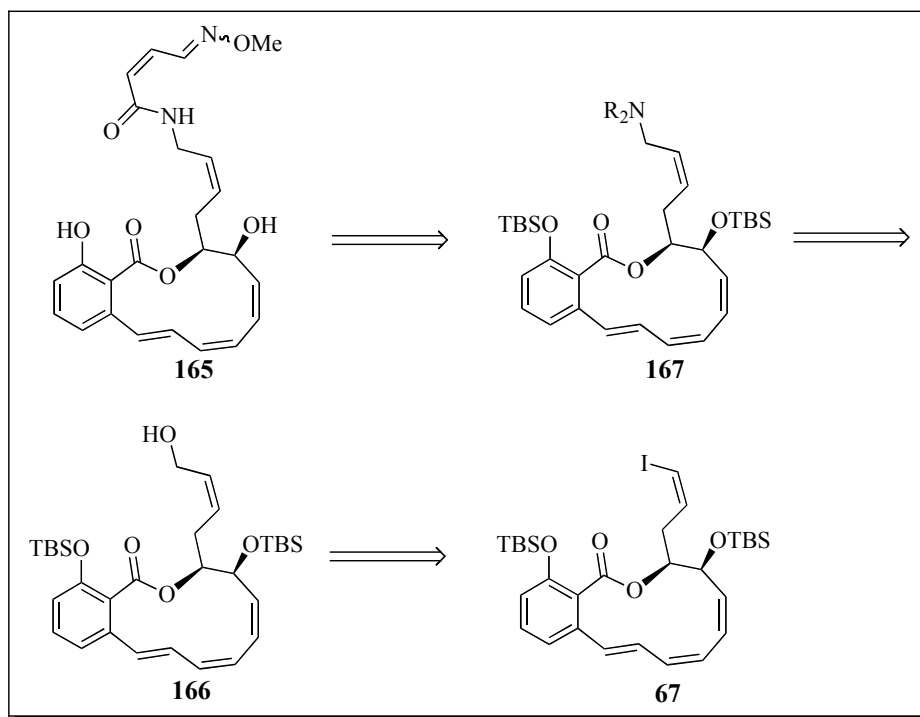
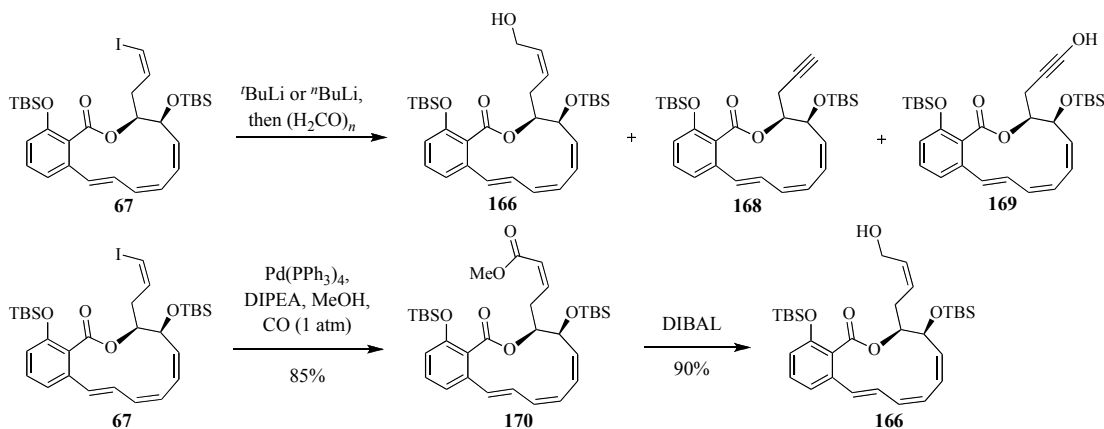


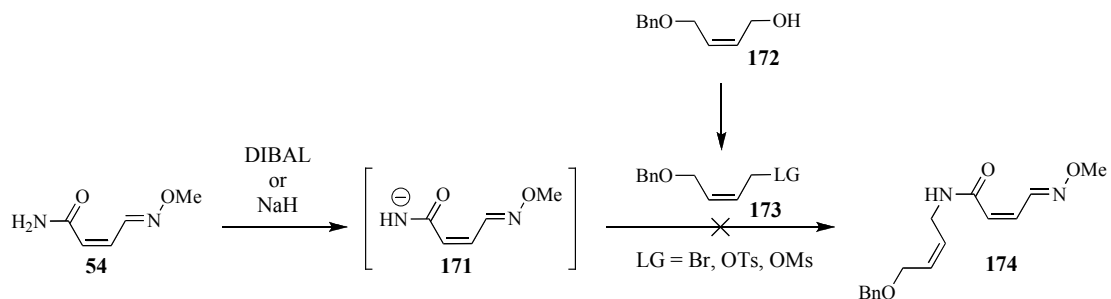
Figure 18. Retrosynthesis for allylic amide homolog

The first task was formation of the allylic alcohol **166** from the vinyl iodide **67** (Scheme 24). We initially attempted to add the hydroxymethylene group by lithium-iodine exchange followed by quenching the anion with paraformaldehyde (H_2CO)_n. However, the vinyl iodide moiety was prone to elimination. Analysis of crude reaction mixtures by ¹H NMR and HRMS revealed formation of the desired product **166** in addition to the alkynyl molecules **168** and **169**. Variation of the lithium base (^tBuLi or ⁿBuLi), solvent or temperature did not avert the formation of these undesired alkynyl side products. We then turned to a two-step protocol to install the hydroxymethyl group. The vinyl iodide **67** was transformed into the *cis*-enoate **170** by a Pd-catalyzed methoxycarbonylation reaction. Careful control of reaction time was necessary to prevent base-catalyzed isomerization of the *cis*-enoate olefin. Use of the bulkier amine base diisopropylethylamine (DIPEA) was also helpful in preventing this inversion. Reduction to the *Z*-allylic alcohol **166** was achieved with slow addition of DIBAL to a solution of the ester **170**.



Scheme 24. *Z*-Allylic alcohol (**166**) formation

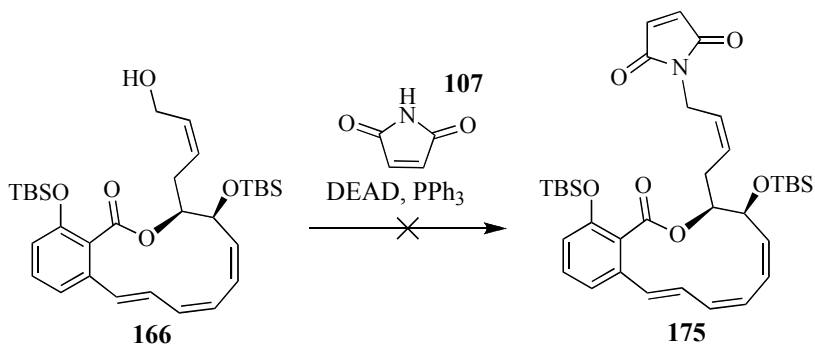
The next obstacle in the synthesis was conversion of the hydroxyl oxygen atom to a nitrogen atom. We again employed a model system to tackle this challenge. Commercially available (*Z*)-4-(benzyloxy)but-2-en-1-ol (**172**) was used to investigate a variety of the oxygen-to-nitrogen interconversion ideas. With an efficient synthesis of the oxime amide **54** in hand, we first explored conversion of allylic alcohol **172** to a leaving group followed by displacement with the anion of amide **171** (Scheme 25). While conversion of the alcohol (**172**) to a leaving group (LG = Br, OTs, OMs) (**173**) was facile, alkylation of the amide **54** was not. Generation of the amide anion **171** by deprotonation with NaH^{198,199} or DIBAL^{200,201} followed by addition of the allylation substrate **173** did not yield any of the desired amide-alkylated product **174**.



Scheme 25. Failed allylation of oxime amide **54**

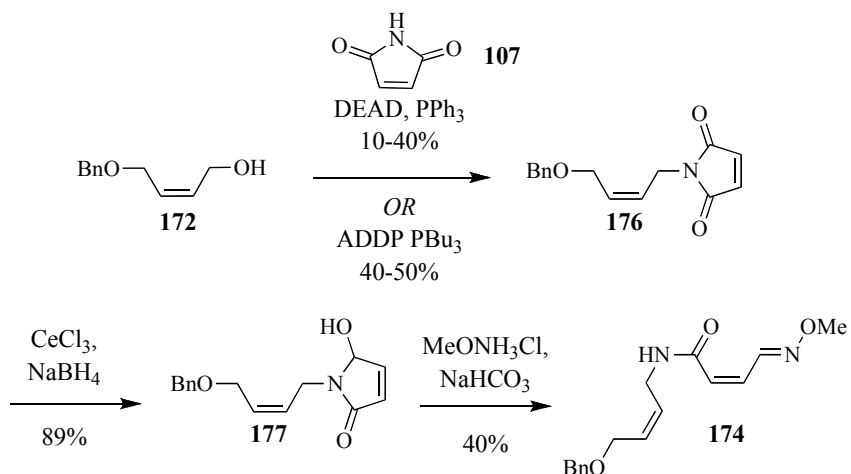
We then investigated construction of the allylic amide via a Mitsunobu reaction of the allylic alcohol with maleimide. Due to the relatively high pKa of maleimide (**107**), Mitsunobu reactions with this molecule are notoriously difficult.^{197,202} Using the procedure developed by Walker,¹⁹⁶ the Mitsunobu reaction between allylic alcohol **166** and maleimide was unsuccessful (Scheme 26). Variation

of solvent, time, temperature, maleimide or diethyl azodicarboxylate (DEAD)/PPh₃ equivalents failed to generate any product (**175**).



Scheme 26. Initial failed Mitsunobu reaction with DEAD/PPh₃ system

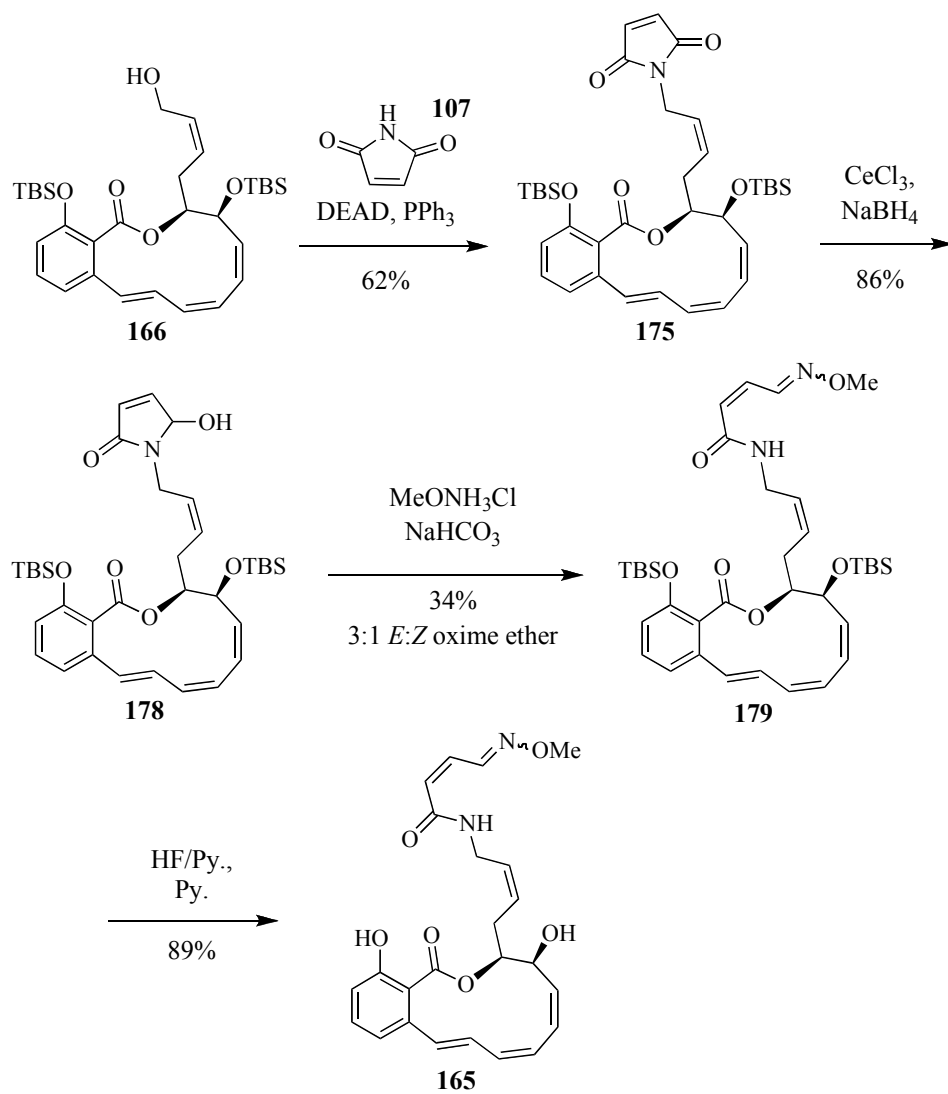
To further investigate this key reaction, we turned to the allylic alcohol model system for optimization studies (Scheme 27). Using the DEAD/PPh₃ activator system, the reaction inconsistently produced yields of compound **176** between 10-40% even with modification of the phosphine, solvent, time, temperature, or reagent order of addition. However, switching reagents system to 1,1'-(azodicarbonyl) dipiperidine/tri-*n*-butylphosphine (ADDP/PBu₃)²⁰³ increased the yield, reliably generating 40-50% of the desired product **176**. Reduction of the maleimide moiety to the corresponding 5-hydroxypyrrolone (**178**) was straightforward. Conversion to the corresponding allylic oxime amide **174** by condensing the pyrrolone with MeONH₃Cl was not. The base utilized in this reaction proved to be pivotal. Using bases other than sodium bicarbonate (NaHCO₃) produced a spectrum of products unidentifiable by NMR or MS.



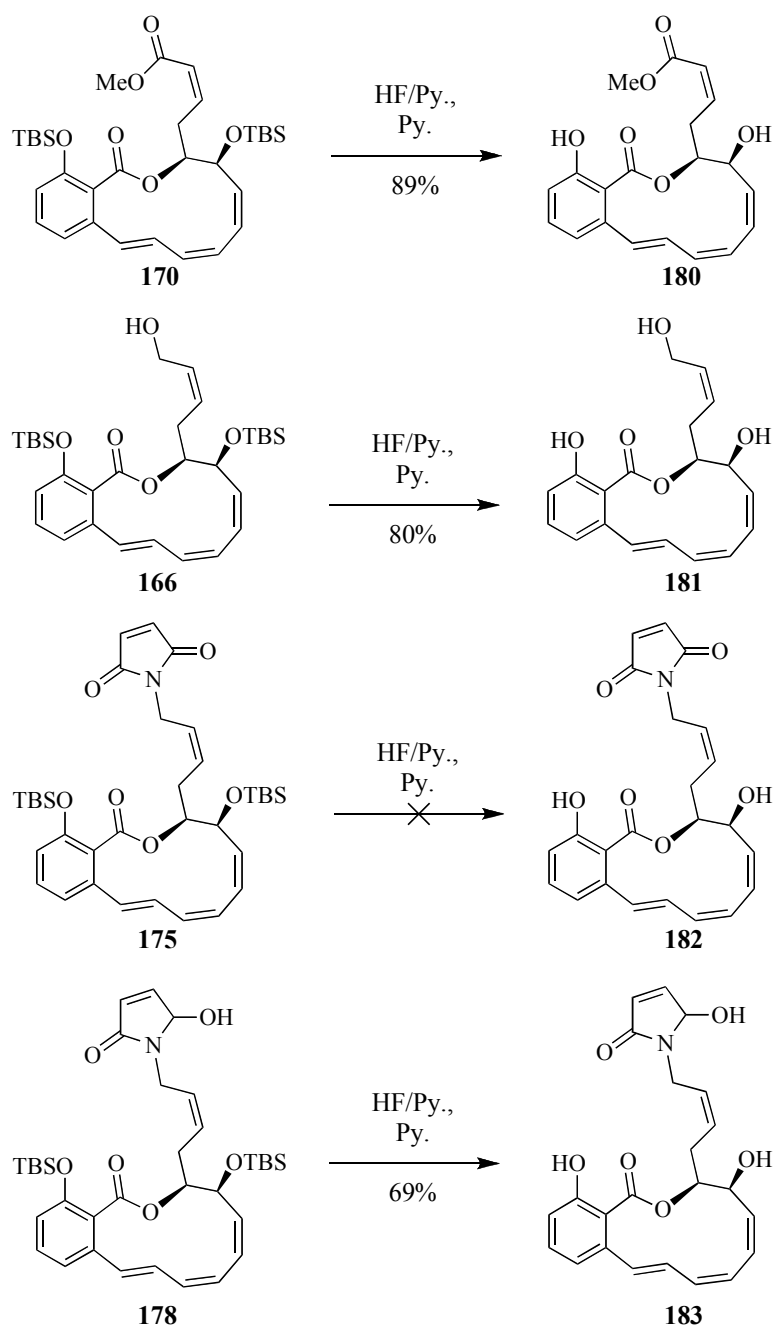
Scheme 27. Formation of allylic amide **174** with model system

With methodology to install the allylic amide in hand, we turned to synthesizing the target analog **165** (Scheme 28). We were disappointed to find that use of the ADDP/PBu₃ system generated low yields (10-20%) of the desired allylic maleimide compound **175**, resulting from low conversion of starting material even after increasing the equivalents of maleimide or activator reagents. Returning to the original DEAD/PPh₃ system, a slow addition of DEAD to a THF solution of maleimide, PPh₃, and the allylic alcohol gave a 62% yield of the Mitsunobu product **175**. Reduction of the maleimide to the corresponding 5-hydroxy-pyrrolone **178** by a Luche reduction occurred without incident. Condensation of the pyrrolone **178** with MeNH₃Cl was low yielding and gave a 3:1 ratio of *E*:*Z* oxime ether stereoisomers (**179**). The major oxime ether stereoisomer configuration was assigned as *trans* based upon previous ¹H NMR studies of the lobatamide oxime ethers.¹⁰ Lobatamides containing an *E*-oxime ether displayed a chemical shift of 8.9-9.0 ppm in the ¹H

NMR for the oxime C-H proton. The *Z*-oxime ether lobatamides displayed a chemical shift of 8.3-8.4 ppm for this proton. Finally, bis-TBS deprotection with a buffered solution of HF/Py. delivered the target allylic amide homolog of oximidine II (**165**). Using the same deprotection conditions intermediates **170**, **166**, **175**, and **178** were desilylated to give compounds **180-183**, increasing the amount of compounds available for biological testing (Scheme 29). The maleimide diol **182** rapidly degraded after bis-TBS deprotection and was not further investigated.



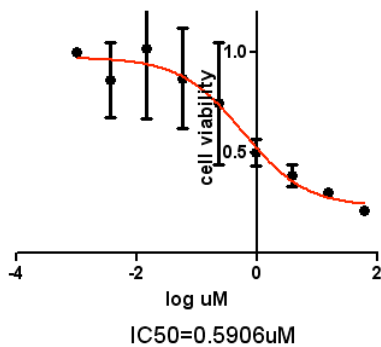
Scheme 28. Synthesis of allylic amide analog **165**



Scheme 29. Bis-silyl deprotection of allylic amide intermediates

Prior to biological testing, LC/MS analysis of oximidine II (**14**), the allylic amide homolog **165** and molecules **180**, **181** and **183** established purities between 82% and 95% for the molecules. Without further purification, the compounds were tested against melanoma cell lines SK-Mel-5 and SK-Mel-28. Figures 19 and 20 display the IC_{50} graphs for oximidine II (**14**) and the allylic amide analog **165**, respectively, against SK-Mel-5 cancer cells. Oximidine II realized an IC_{50} of 590 nM in this assay while the analog displayed only 40% inhibition at 100 μ M. Against the SK-Mel-28 cell line, known to be less sensitive towards the benzolactone enamides, oximidine II (Figure 19) and the analog **165** (Figure 20) were much less potent. Oximidine II displayed an IC_{50} of 100 μ M while the analog was barely active, exhibiting only 10% inhibition at 100 μ M. The other compounds, **180**, **181** and **183**, were inactive against both cell lines (not shown). As a control, Taxol® exhibited an IC_{50} value of 8.7 nM against the SK-Mel-5 cell line and 10% inhibition at 100 μ M against the SK-Mel-28 cells.

IC₅₀ assay of SK-MEL-5 treated by CSM11-225 for 48 hours



IC₅₀ assay of SK-MEL-28 treated by CSM11-225 for 48 hours

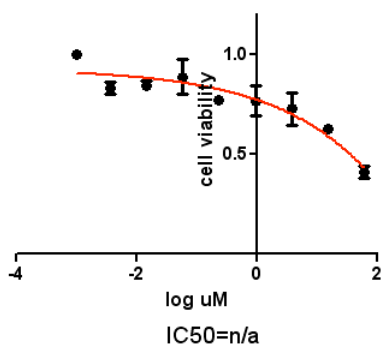
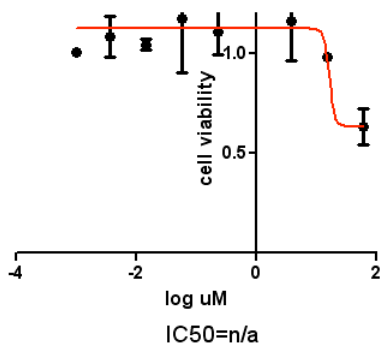


Figure 19. IC₅₀ graphs for oximidine II (**14**), tested against SK-Mel-5 (top) and SK-Mel-28 (bottom) melanoma cells

IC₅₀ assay of SK-MEI-5 treated by CMS11-223 for 48 hours



IC₅₀ assay of SK-MEI-28 treated by CMS11-223 for 48 hours

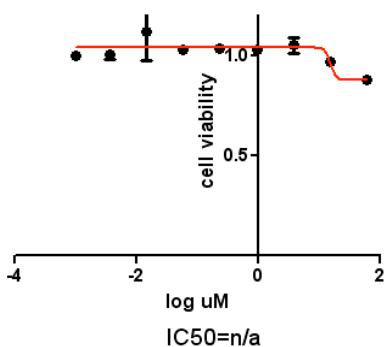


Figure 20. IC₅₀ graphs for allylic amide analog (**165**), tested against SK-Mel-5 (top) and SK-Mel-28 (bottom) melanoma cells

These results reiterate the necessity of the enamide moiety for bioactivity of this natural product class against melanoma cancer cells. Cruentaren A, containing the allylic amide moiety, has not been tested against either of these cell lines. To gain a more thorough understanding of the relationship between the structure of the macrolactone and the presence of either an enamide or an allylic amide, we planned to test both oximidine II and our homolog **165** against the mouse L929 fibroblast cell

line. Cruentaren A displays an IC_{50} of 1.2 ng/mL against this cell line.⁹³ These biological assays are currently underway.

1.7 Copper-mediated Reductive Ring-closure Mechanistic Investigation

The unprecedented nature of the copper-mediated reductive coupling reaction prompted mechanistic investigation. We hoped that an in-depth understanding of the mechanism would lead to expansion of the scope of the technology, with a particular interest in developing intermolecular vinyl or aryl iodide-alkyne reductive couplings towards diene synthesis. This reductive coupling reaction could become a powerful methodology in the toolbox of organic chemists.

Based upon previous studies, a Cu-H species was very likely responsible for the reduction of the alkyne to the alkene in the reaction. However, we were unsure if this reduction proceeded by a radical or non-radical pathway. Under the previously described reaction conditions ($Cu(OAc)_2$, PPh_3 , K_2CO_3 , HCO_2Na in DMF at 120 °C for 30 min), the cyclized, reduced macrocycle **157** is produced in 38% yield (Scheme 20). To probe the intermediacy of radicals, the radical-sequestering reagents hydroquinone and DDQ were added to the macrocyclization reaction.²⁰⁴ Addition of either radical-mediating reagent had no noticeable effect on either the reaction rate or the reaction yield, suggesting that radicals were not likely produced during the course of the reaction.

After ruling out the possibility of a radical-based mechanism, we focused on identifying the timing of the alkyne-to-alkene reduction, i.e. does the reduction occur prior to (path A) or after (path B) macrocyclization (Figure 21).

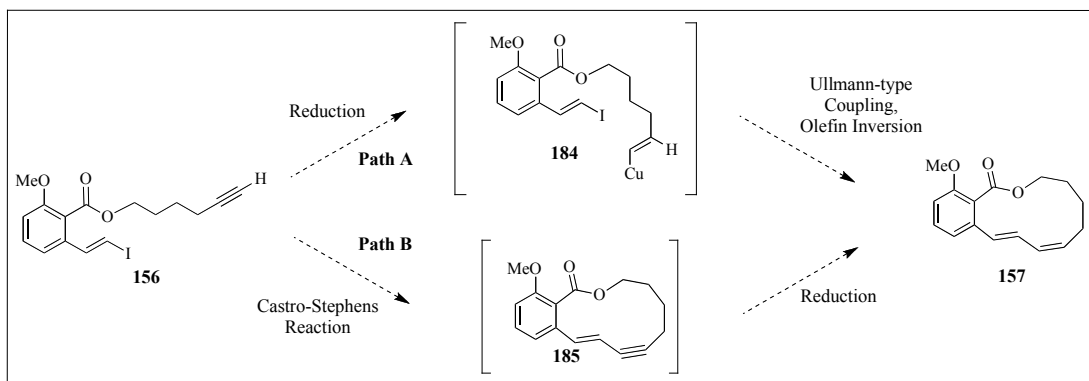
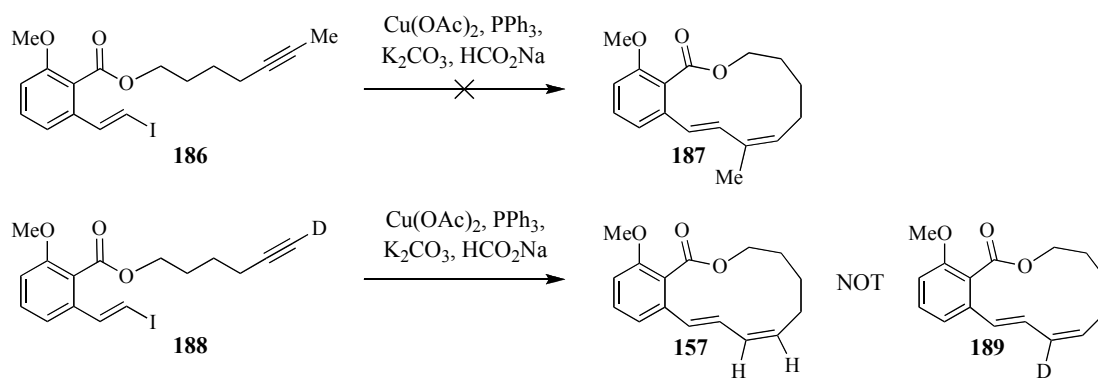


Figure 21. Possible reductive cyclization mechanisms

In order for path A to be active, the hydrocuprated intermediate **184** would undergo an Ullmann-like coupling reaction followed by a C10-C11 olefin inversion to generate the observed product **157**. We had observed reduction of the terminal alkyne to the corresponding terminal alkene (Scheme 21) when hydrosilanes were used as the hydride source in the reaction and believed that a vinylcopper species, generated from reduction of the alkyne, was the responsible intermediate. This hypothesis was further supported by Sadighi's crystal structure of the vinylcopper intermediate.¹⁹¹ To test the plausibility of this pathway, we exposed the methylated-alkyne molecule **186** to the reductive cyclization conditions (Scheme 29). However, this reaction generated none of the anticipated product **187**. No starting material was consumed during the course of the reaction. The deuterated alkyne **188** also did not produce the anticipated product – the C10-deuterated diene **189**. Instead, only the

bis-protonated macrocycle **157** resulted. Although suggestive that path B was operational, the outcomes of these two experiments did not completely rule out the possibility of path A. The reduction reaction could be specific for terminal alkynes, therefore making the methyl-alkyne **186** a poor substrate choice. Considering the deuterio-alkyne **188**, a proton-deuteron exchange could occur in the reaction, leading to the observed result. Copper acetylides result from the addition of a Cu(I) or Cu(II) salt to a solution of a terminal alkyne in the presence of a base.¹⁰⁷ Under the reaction conditions employing the monohydrate of Cu(OAc)₂ as the copper source, a kinetic quench of the copper acetylide **190** by water or another proton source could generate the protonated alkyne **156**, followed by reduction and cyclization to yield the observed product **157** (Figure 22).



Scheme 29. Path A investigation

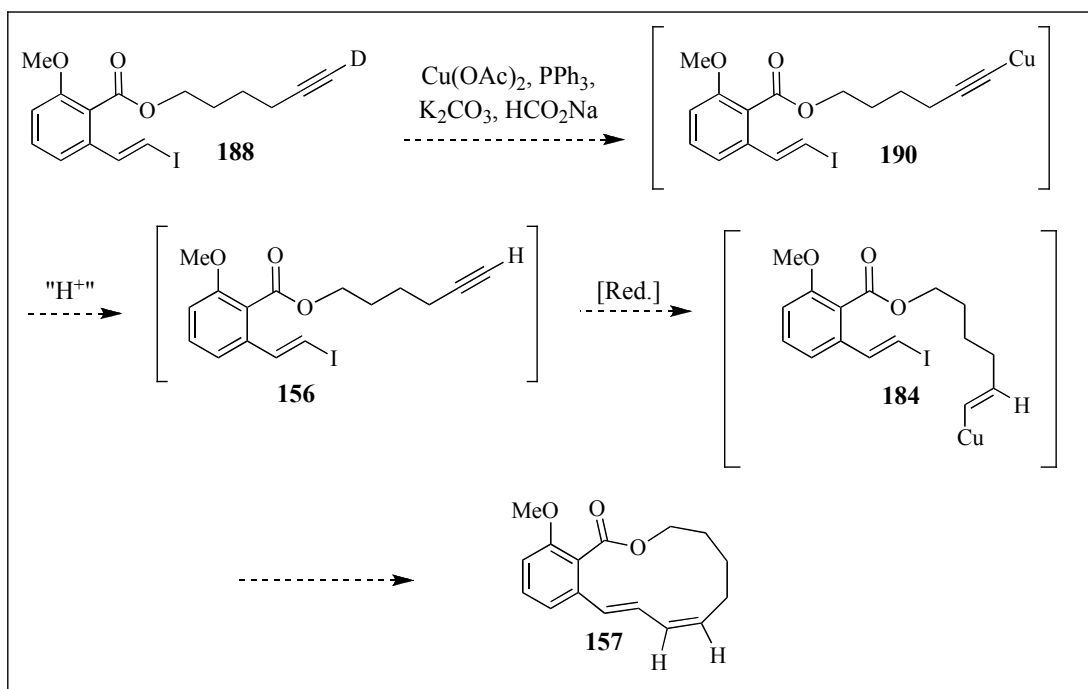
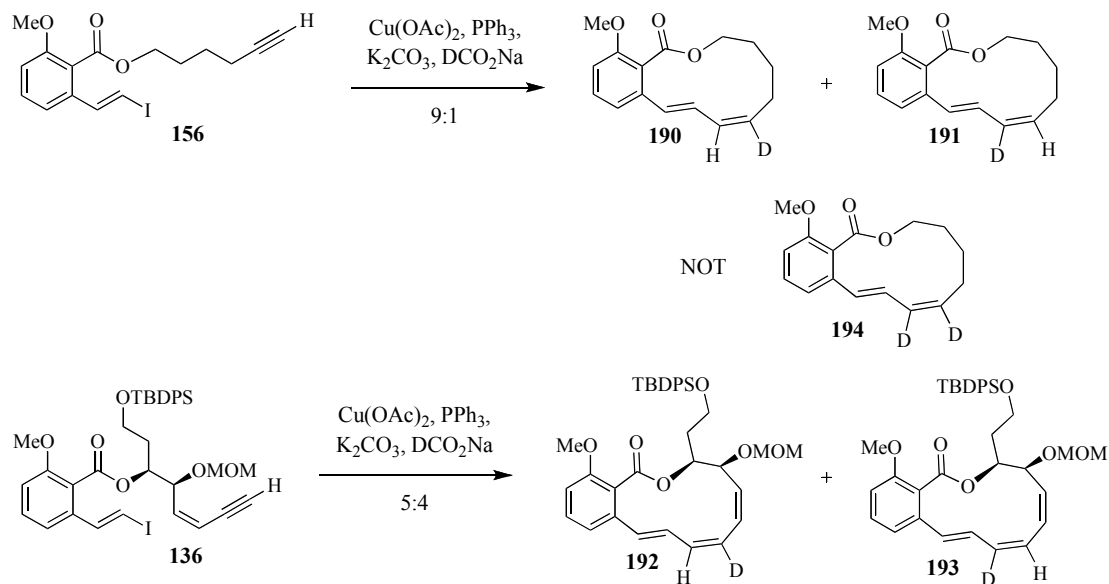


Figure 22. Potential deuterium-proton exchange pathway

Although no deuterium incorporation occurred when exposing **188** to the reductive cyclization conditions, we were able to incorporate deuterium by using DCO_2Na instead of HCO_2Na (Scheme 30). Analysis of the product ^1H NMR revealed that the deuterium was not regioselectively incorporated into the product as would be expected if path A were the mechanistic pathway. Instead, a 9:1 ratio of deuterated products **190** and **191** resulted from the macrocyclization. This regiochemical preference for deuterium incorporation implies that some steric or electronic force guides the reduction. Deuterium labeling of the oximidine system with DCO_2Na generated a 5:4 mixture of regioisomerically-deuterated products (**192:193**). The reduction does not occur through a conjugate addition pathway due to the formation of both deuterium regioisomer products and because the ester carbonyl

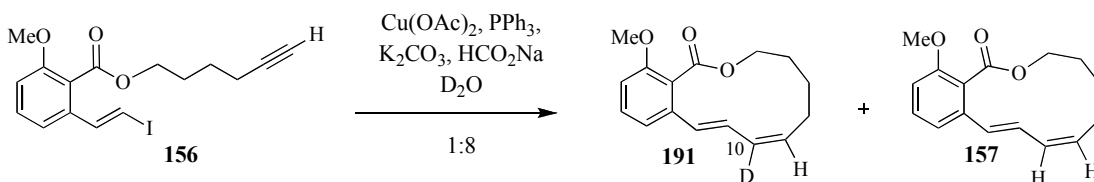
is presumably not co-planar with the aromatic ring based on the apicularen A crystal structure. Based on this evidence, we concluded that path B was most likely the operating mechanism.



Scheme 30. Deuterium incorporation during reductive cyclization

In mechanism B, a vinylcopper-macrocycle intermediate is generated that is quenched either during the reaction or during the reaction workup. Because no bis-deuterated product (**194**) was observed when DCO_2Na was used, we deduced that formate was not the quenching source. Quenching the reaction with D_2O also gave no bis-deuterated product. In Stryker's paper detailing the reduction of alkynes to the corresponding *cis*-alkenes with Cu-H ,¹⁷⁹ he observed that the presence of five to 10 equivalents of water in the reaction greatly increased yields compared to the complete exclusion of water. Presumably, water serves to quench the vinylcopper intermediate

resulting from Cu-H addition across the triple bond.¹⁷⁹ Further, adding more than five to 10 equivalents of water diminished the reactivity of the Cu-H species and prohibited conversion of the starting material to product. Similar to Stryker's observations, addition of 10 equivalents of D₂O to the catalyst solution prohibited the reductive cyclization. Addition of five equivalents of D₂O, however, generated a different result. Although 66% of the starting material (**156**) remained after two hours at 120 °C, 10-20% deuterium incorporation at C10 (**191**) was achieved when D₂O was added to the catalyst system employing HCO₂Na as the hydride source (Scheme 31). The quenching proton, generating the remaining 80-90% of the product (**157**), could come from water hydrating the Cu(OAc)₂ or from non-dry reagents or solvent. We have not yet ruled out any of these possibilities.



Scheme 31. Internal quench with D₂O

The complete mechanism, based on current evidence, is displayed in Figure 23. Following Cu-acetylide generation (**190**), a Castro-Stephens coupling¹⁰⁷ forms the C8-C9 *E*-dienyne macrocycle **196**. A moderate π -acid, Cu remains coordinated to the alkyne (**196**), stabilizing the intermediate and preventing the C8-C9 *E* to *Z* inversion. This intermediate stabilization is an important facet of the catalytic cycle.

Exposure of the *Z*-dienyne **139** to the reductive cyclization conditions generated none of the reduced triene product **140**, hinting that the energetic barrier of C8-C9 *Z*- to *E*-inversion is relatively high and that the reduction occurs due to ring-strain relief. It is presently unclear if the reactive Castro-Stephens catalyst species contains the Cu-H species (i.e. L = H in **190**) or if this species is generated somewhere along the catalytic cycle by loss of CO₂ from formate (**196** to **197**). In Figure 23, coordination of formate (**196**) followed by loss of CO₂ yields the requisite Cu-H intermediate **197**. 1,2-Addition of the Cu-H results in reduction of the alkyne to the *cis*-alkenylcopper species (**198**) that is internally quenched by a proton ("H⁺"), yielding the desired product (**157**) and regenerating the active Cu species.

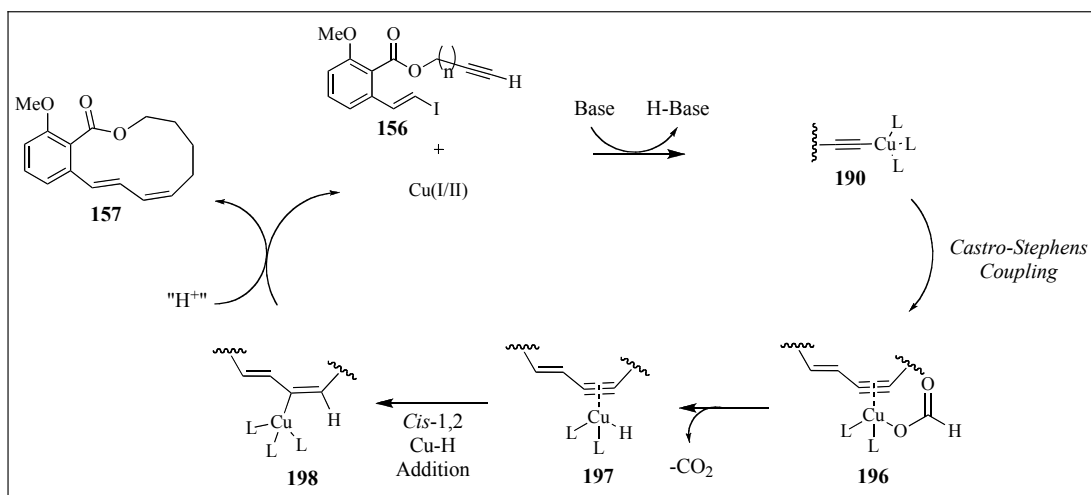


Figure 23. Proposed mechanism for copper-mediated reductive cyclization

Attempts to perform intermolecular reductive coupling reactions have thus far been unsuccessful, generating only the Castro-Stephens enyne product. Most likely, ring-strain relief drives the reduction of the alkyne to the *cis*-alkene in the previous

macrocyclization examples. Modifications to the catalyst system could lead to increasing the substrate scope for the reaction.

1.8 Conclusions

The third total synthesis of the benzolactone enamide oximidine II was achieved in 1.1% overall yield in 22 linear steps from commercially available 1,3-propanediol. The key macrocyclization step in the synthesis was performed by an unprecedented copper-mediated reductive vinyl iodide-alkyne coupling reaction. The 67% yield realized by this reaction was 20% higher than previous methodologies utilized to form the triene core of oximidine II. Based on current mechanistic evidence, this reductive macrocyclization is thought to occur as a consequence of ring-strain developed by stereospecific coupling of an *E*-vinyl iodide and an alkyne.

An allylic amide analog of oximidine II was synthesized to investigate the importance of the enamide side chain on biological activity of the benzolactone enamide natural product class. Against melanoma cancer cells, oximidine II was bioactive while the allylic amide analog displayed marginal bioactivity. Benzolactone enamides are known to exert their biological activity through inhibition of the V-ATPase enzyme. Further biological comparison of oximidine II and the allylic amide analog will determine if the allylic amide analog targets the V-ATPase enzyme or the F-ATPase enzyme – the biological target of cruentaren A, another allylic amide benzolactone molecule.

Chapter 2

The Search for New Antibiotics – New Inhibitors of the MurA Enzyme

2.1 Background

Many types of bacteria depend on humans for survival. Some of these prokaryotic microorganisms are symbiotic, such as *Bacteroides thetaiotaomicron*, functioning to digest polysaccharides inside the gastrointestinal tract, and some are harmful, such as the peptic ulcer-causing *Helicobacter pylori*.²⁰⁵ For bacteria to grow and thrive inside the body, they must be tolerant to a variety of physiological conditions. Unchecked bacterial infections can form rapidly. Mutations in bacterial genetic code occur partly because they replicate rapidly. These mutations can lead to no observable change in bacterial function, bacterial death, or to a worse extreme – drug resistance.²⁰⁵

It is these drug-adapted and damage-causing bacteria that have kept medicinal chemists at work for nearly a century.²⁰⁶ Sulfonamides (sulfacetamide, **199**, Figure 24), the first antimicrobials, were widely used beginning in the 1930's but are now generally used clinically for treating urinary tract infections (UTI's). This is due to the widespread development of resistance to the drug class. World War II helped spread the use of penicillin antibiotics following their discovery by Alexander Fleming in 1929. Initially, the original β -lactam drug Penicillin G (**200**) was successful at fighting mostly Gram-(+) bacteria. However, resistance to the drug soon occurred, forcing medicinal chemists to develop successive generations of the

drug class. Seeing that β -lactams would not be the end-all for antibiotic therapeutics, new classes with novel mechanisms of action were discovered and explored. These antibiotic classes include the quinolones (ciprofloxacin, **201**), tetracyclines (**202**), aminoglycosides (streptomycin, **203**), macrolides (erythromycin A, **204**) and oxazolidinones (linezolid, **205**), among others (Figure 24). Incurrence of resistance to antibiotic therapeutics by bacteria has led to the development of new agents by medicinal chemists.

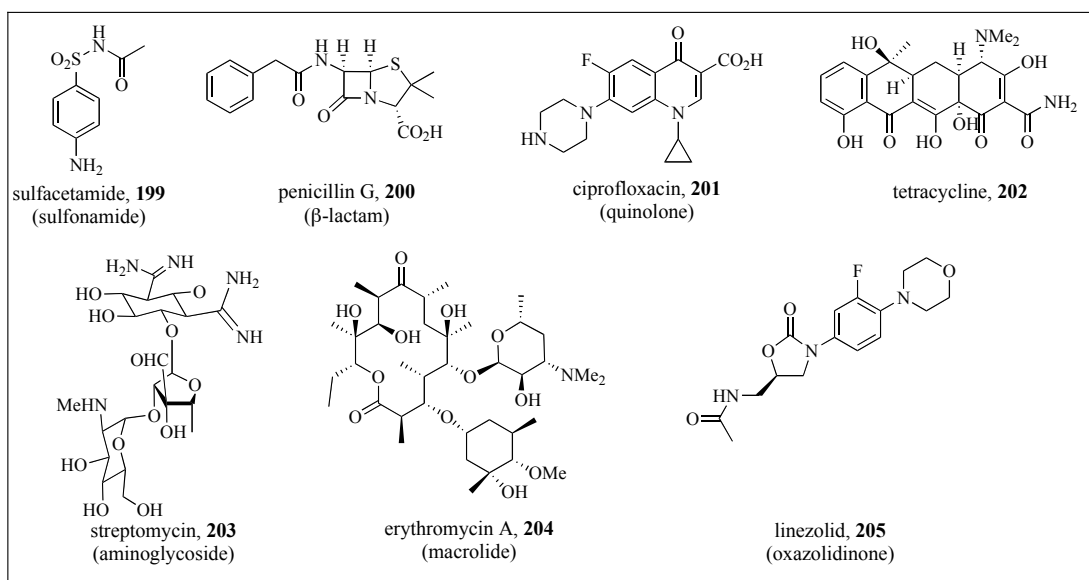


Figure 24. Examples of antibiotic therapeutics

Despite the extensive research in this area, there is again a growing need for new antibacterial targets and drugs. It is estimated that 70% of all hospital infection-causing bacteria are unaffected by at least one antibiotic and that about 90,000 people die each year in the U.S. from these “superbugs”.²⁰⁷ Even “drugs of last resort”, such as vancomycin, are becoming less clinically useful due to incurrence of resistance.

Furthermore, a worldwide increase in the incidence of certain bacterial infections previously considered cured, such as tuberculosis, is being attributed to bacterial resistance.

Antibiotics target a variety of enzymes resulting in the inhibition of many cellular processes. One of the most common processes targeted is biosynthesis of the cell wall, specifically construction of the peptidoglycan layer of the cell wall. The cell wall is responsible for maintaining cellular shape, maintaining an internal osmotic pressure, and acting as a barrier for xenobiotics, among other roles.²⁰⁸ This approach is attractive for many reasons. First, the cell wall and most of the enzymes responsible for its construction are necessary for bacterial survival. Selective therapeutic targeting is easily achievable because the enzymes responsible for constructing the peptidoglycan layer are not found in mammals. The peptidoglycan layer is comprised of a repeating linear *N*-acetylglucosamine (NAG) / *N*-acetylmuramic acid (NAM) dimer functionalized with a pentapeptide chain (Figure 25).²⁰⁹ The pentapeptide subunits serve to crosslink the glycan backbone, creating the 3-D peptidoglycan polymer that provides structural rigidity to the cell wall (Figure 26).²⁰⁸

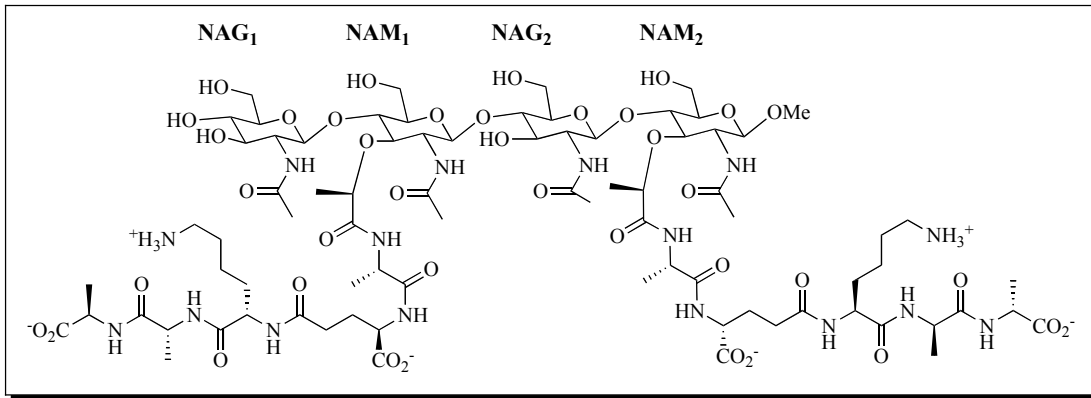


Figure 25. Dimer of peptidoglycan layer²⁰⁹

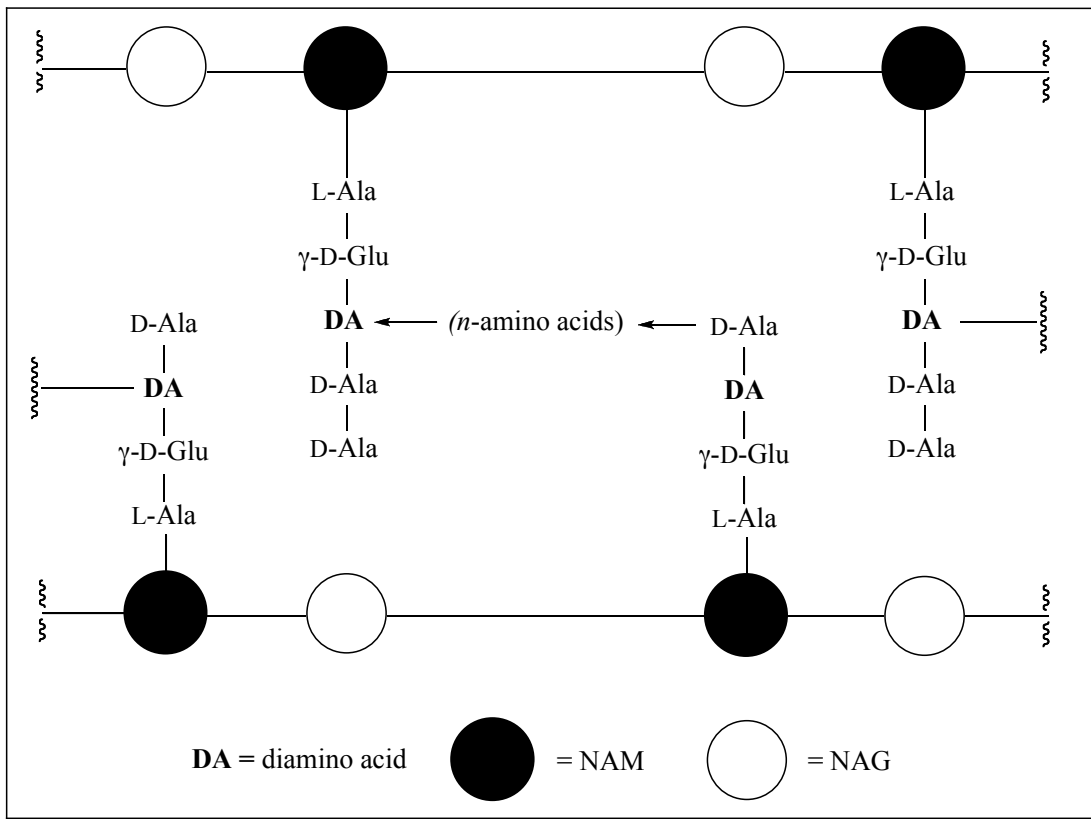


Figure 26. Crosslinking of peptidoglycan layer²⁰⁸

Catalyzing the first committed step in peptidoglycan biosynthesis is the cytoplasmic enzyme UDP-*N*-acetylglucosamine enolpyruvyl transferase (MurA).²¹⁰

This enzyme is necessary for cell survival and not present in humans,²¹¹ therefore an attractive antibiotic target. At steady state, MurA exists as two globular domains in an open conformation, shaped like a jellybean (Figure 27).²¹² Following UDP-*N*-acetylglucosamine (UNAG, **207**) binding, the two domains undergo a large structural change to form the closed, active state (Figure 28).²¹³ During this conformational change, a loop region closes the interdomain section, similar to a lid.²¹⁴ Upon binding of the second substrate, phosphoenolpyruvate (PEP, **206**), the loop undergoes another structural change following an induced-fit mechanism – a key consideration for antibiotic development.²¹³⁻²¹⁵ The loop is also significant because it contains the Cys115 (*E. coli* numbering) residue that is important for successful product release.²¹⁶ Cys115 is also the target amino acid for the known MurA inhibitor fosfomycin.²¹⁴

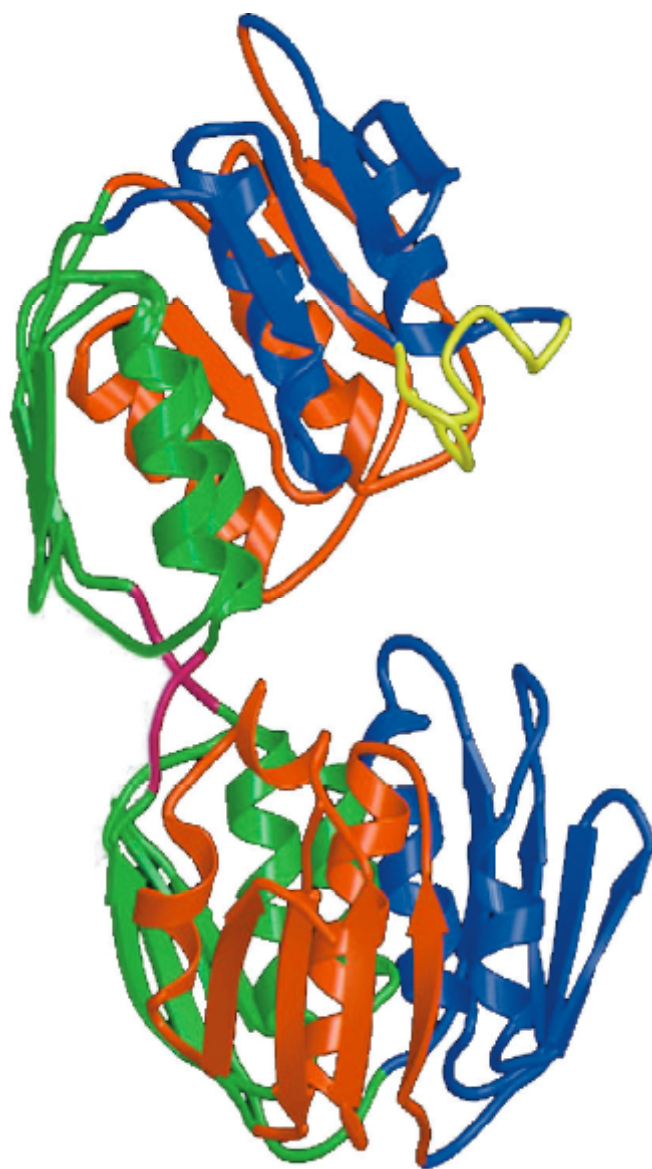


Figure 27. MurA in open state²¹²



Figure 28. MurA with UNAG bound²¹²

Figure 29 displays the unusual mechanism of enolpyruvyl transfer from PEP (206) to UNAG (207) catalyzed by MurA. This has been determined by both co-crystallization and synthetic studies.^{217,218} The reaction proceeds via a typical mechanism for vinyl ether transfer. First, protonation of the alkene of PEP generates an oxocarbenium ion 208. The reactive hydroxyl group on UNAG attacks this intermediate to generate a tetrahedral intermediate 209. Simultaneous collapse of the tetrahedral intermediate and release of inorganic phosphate (PO_4^{3-}) generates the enolpyruvyl-UDP-*N*-acetylglucosamine (EP-UNAG, 210) product. EP-UNAG is then released from the enzyme, relaxing the enzyme back to the open configuration.

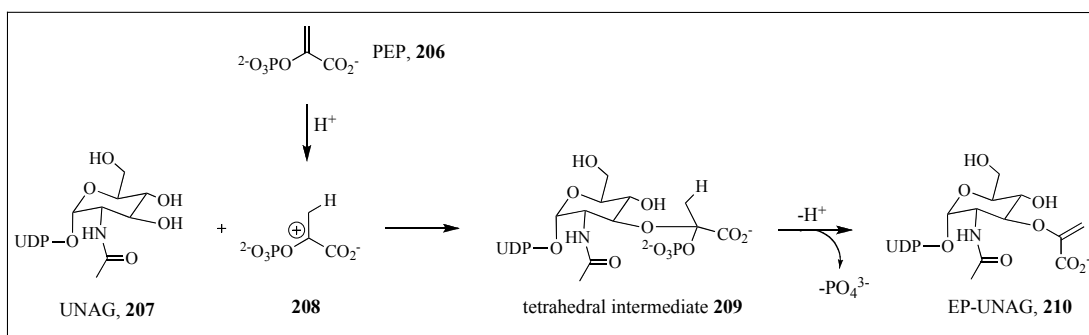


Figure 29. MurA-catalyzed conversion of UNAG to EP-UNAG (210)

5-Enolpyruvyl shikimate-3-phosphate synthase (EPSPS or AroA) is the only other member of the enolpyruvyl transferase family.²¹⁹ This family is unusual as it utilizes PEP as an enolpyruvyl donor. In all other known PEP-dependent reactions, its P-O bond is cleaved and a phosphoryl moiety is transferred to the substrate. AroA is the sixth enzyme in the shikimate pathway – the pathway responsible for constructing aromatic compounds in bacteria and plants.²¹⁹

The development of inhibitors of these enzymes has led to a deeper understanding of the catalysis mechanism for MurA and AroA (Figure 30). Glyphosate (**211**), the active ingredient of the herbicide Roundup™, is a potent and exclusive inhibitor of AroA.²²⁰ Discovered in 1969 by Hendlin and coworkers,²²¹ fosfomycin (**212**) inhibits MurA. Fosfomycin is currently the only marketed inhibitor of MurA and is the active ingredient in MouroI™.²²² Interestingly, glyphosate and fosfomycin are mutually exclusive in inhibiting only AroA and MurA, respectively, although both enzymes proceed through a similar tetrahedral intermediate. This is attributed to the differences in amino acids in the active site.²¹⁷

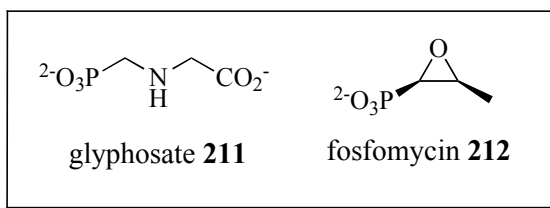


Figure 30. Inhibitors of the enolpyruvyl transferase enzyme family

Fosfomycin, a phosphonate epoxide, forms a covalent adduct with the Cys115 residue (numbering according to *E. coli* sequencing) in the active site via opening of the epoxide.²¹⁴ The drug is specific for MurA with reported IC₅₀ values of 0.40-12 μM.²²³ Despite the reactive epoxide moiety, the molecule does not function as a group specific reagent in alkylating other nucleophilic amino acids in the body. Although the antibiotic is active against both Gram-(+) and Gram-(−) bacteria, the high water solubility of fosfomycin limits its clinical applicability and it is used

worldwide only in treating UTI's. It is also used in Japan as the drug of choice for treating Shiga-like toxin-producing *E. coli*.²²⁴

Similar to other antibiotic treatments, resistance is building against this MurA inhibitor through a variety of mechanisms. Fosfomycin is actively transported across the bacterial cell wall.^{225,226} Bacterial genetic changes result in either decreased fosfomycin binding to the transporter proteins or to obstruction of drug uptake. Second, a fosfomycin-resistance protein, FosA, has recently been identified. This enzyme uses glutathione as a nucleophile to open up the epoxide and form a covalent adduct to deactivate the drug.²²⁷⁻²²⁹ Lastly, is the mutation of the Cys115 residue to an aspartate amino acid leaves the enzyme catalytically active but renders fosfomycin inactive.^{230,231}

2.2 Generation of HTS-Inspired Library

The limited scope of fosfomycin and its incurrence of bacterial resistance coupled with a wealth of recently uncovered structural biology information about MurA from crystallographic studies has led to increased interest in MurA inhibitor exploration. High-throughput screening (HTS) by various pharmaceutical companies has revealed several new structures with MurA inhibitory activity (Figure 31).^{223,232-234} Preincubation of the bacterial cells with UNAG prior to administering these lead candidates was necessary to achieve nanomolar IC₅₀ values, suggesting that these compounds (**213-218**) bind to a UNAG-activated enzyme complex. Unfortunately, development of the entire RWJ series (**213-215**) was halted due to unspecific

inhibition of DNA, RNA, protein and cell wall biosynthesis.²²³ Natural products have also been reported to inhibit the bacterial enzyme, most notably the sesquiterpene cnicin 216.^{235,236} X-ray crystallography revealed that this molecule works in an interesting manner, forming a covalent 1,3-adduct (**219**) with UNAG instead of the expected 1,4-adduct as the result of a typical Michael addition (Figure 32).²³⁵ The vicinal diol moiety is thought to imitate the phosphate moiety in the tetrahedral intermediate (**220**) of the MurA catalytic cycle, allowing the unusual adduct to form. Despite the recent activity targeting MurA, no lead candidate has emerged leaving an opportunity to discover and develop new inhibitors of the enzyme.

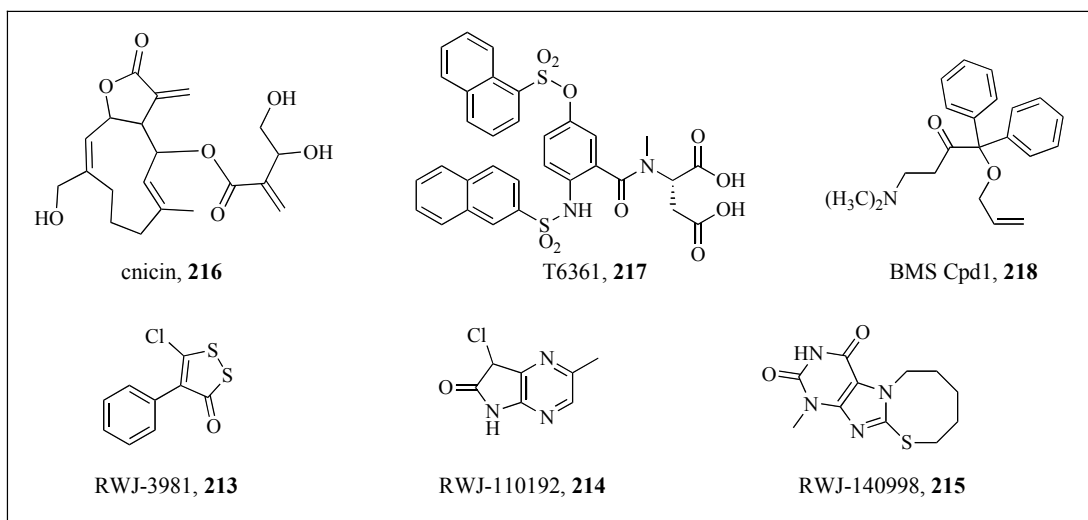


Figure 31. Recently reported MurA inhibitors

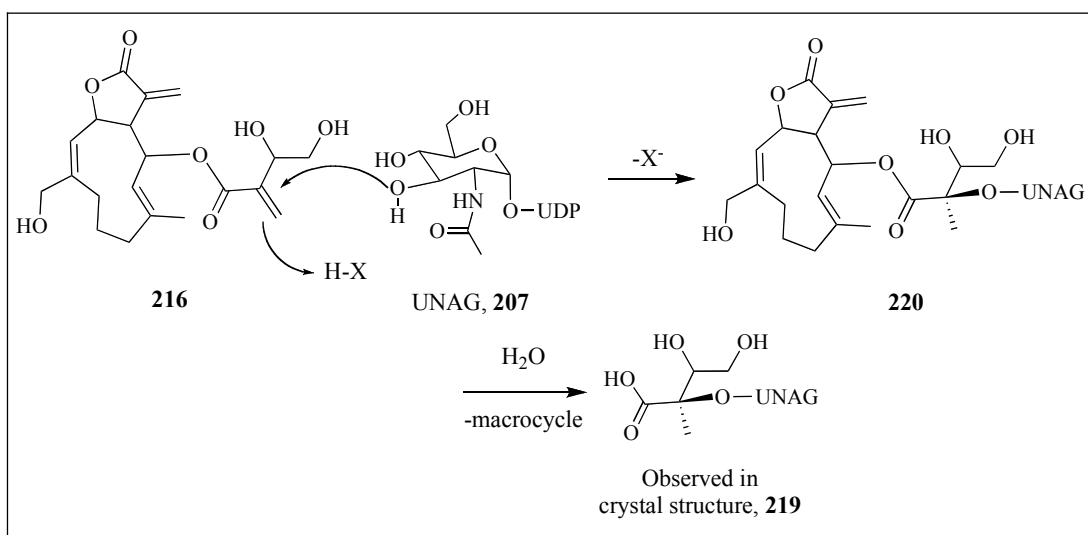


Figure 32. Unusual mechanism for enicin binding

Our search for new MurA inhibitors began with an HTS campaign performed at the KU HTS facility. A Lanzetta assay²³⁷ was used to identify possible lead structures in this screening campaign. The Lanzetta assay uses color changes to quantify amounts of inorganic phosphate present in solution. Therefore, a decrease in phosphate production compared to a control would correspond to inhibition of the

MurA catalytic pathway (Figure 29). During this screening campaign, five different scaffolds (**221-225**) were identified with IC_{50} values of 2-41 μ M (Figure 33). The similarities between **221** and **224** – benzoic acids substituted with the isosteric heteroaromatics pyrrole or furan, respectively – prompted closer examination.

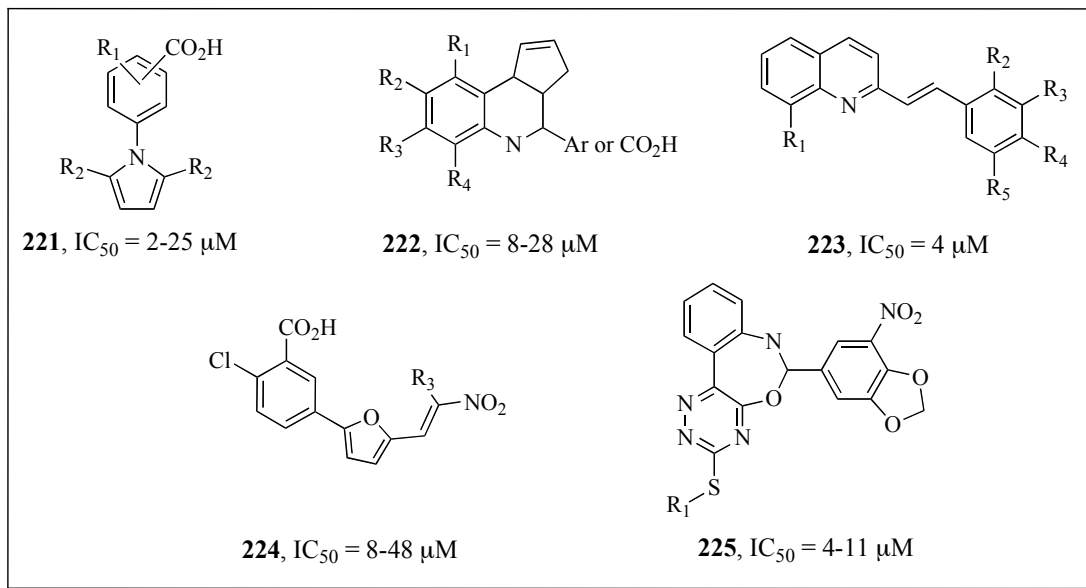


Figure 33. MurA HTS hits

We followed up on the pyrrol-benzoic acid scaffold (compounds **226-228**, Figure 34) for SAR development. The relatively small number of compounds from this class present in the screening collection did not allow for an easily discernable SAR (Figure 34). Furthermore, the lack of step-by-step functional group substitution on each of the rings prevented a clear correlation of functionality to activity. Carboxyl substitution, either on positions C3 or C4, appeared necessary although no C2-carboxylated ligands were examined. It was unclear whether a carboxyl bioisostere, such as a nitro group, could be tolerated. Some steric bulk was tolerated

on the pyrrole ring at positions C1' and C4'. Other *N*-heteroaromatic compounds were not represented in the collection.

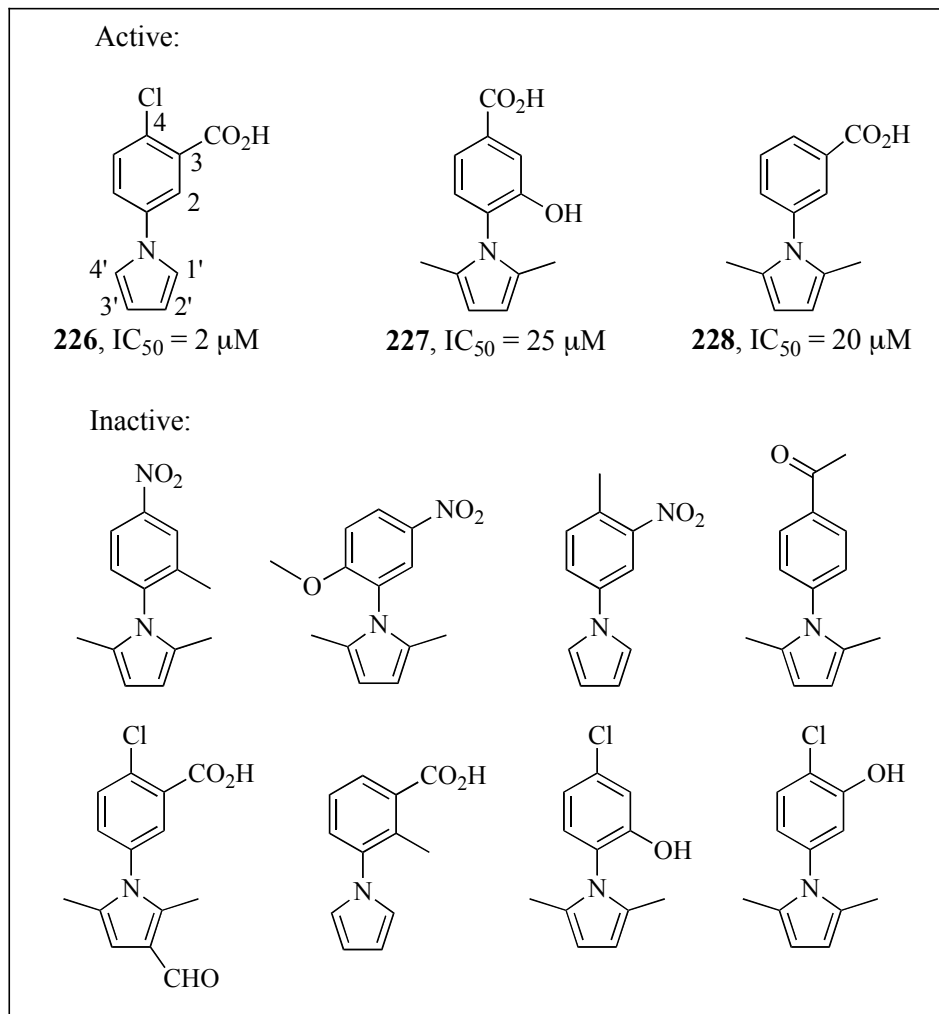


Figure 34. HTS compounds from lead series 1

Pyrrole-benzoic acids can be synthesized in a variety of ways (Figure 35). The first synthesis of substituted pyrroles appeared in 1884 from the independent labs of Paal and Knorr.^{238,239} Condensation of 1,4-diketone derivatives with amines in the presence of acid led to the desired *N*-heteroaromatic compounds. However, this

procedure was limited to the synthesis of 1,4-disubstituted pyrroles due to the instability of 1,4-dialdehydes under the harshly acidic reaction conditions. In 1952, the lab of Clausen-Kaas developed the reagent 2,5-dimethoxytetrahydrofuran (**229**) as a surrogate for the labile succinaldehyde.²⁴⁰ This Clausen-Kaas modification of the Paal-Knorr pyrrole synthesis allows for formation of a variety of unsubstituted pyrroles via the acid-mediated condensation of primary amines and 2,5-dimethoxytetrahydrofuran (route A). This procedure is limited by the harsh reaction conditions necessary for product formation.

Quenching phenyl anions with carbon dioxide (CO₂) produces benzoic acids. Regiospecific lithiation of substituted *N*-phenyl pyrroles can be achieved through variation of the lithiation conditions (route B).²⁴¹

Copper and palladium are also known to mediate the coupling of amines to various halogenated or pseudohalogenated aryl or vinyl species (route C).²⁴²⁻²⁴⁴ The use of copper for this cross coupling reaction was first reported by Ullmann²⁴⁵ in 1903 then by Goldberg in 1906.²⁴⁶ The reaction was recently improved by the Buchwald labs through incorporation of diamine ligands into the reagent system,²⁴⁷ leading to lower catalyst loadings and broadening of the substrate scope. Palladium is also an effective catalyst for pyrrole cross coupling.²⁴⁸⁻²⁵¹ This Buchwald-Hartwig chemistry is attractive because the ligand can be optimized for specific substrates. Copper is used in stoichiometric quantities to couple aryl and vinyl boronic acids to amines in the Chan-Lam coupling reaction (route D).^{252,253} A limitation of the metal mediated

reactions is that free carboxylic acids are not suitable substrates for the couplings, requiring an additional hydrolysis step to reveal the desired acid compound.

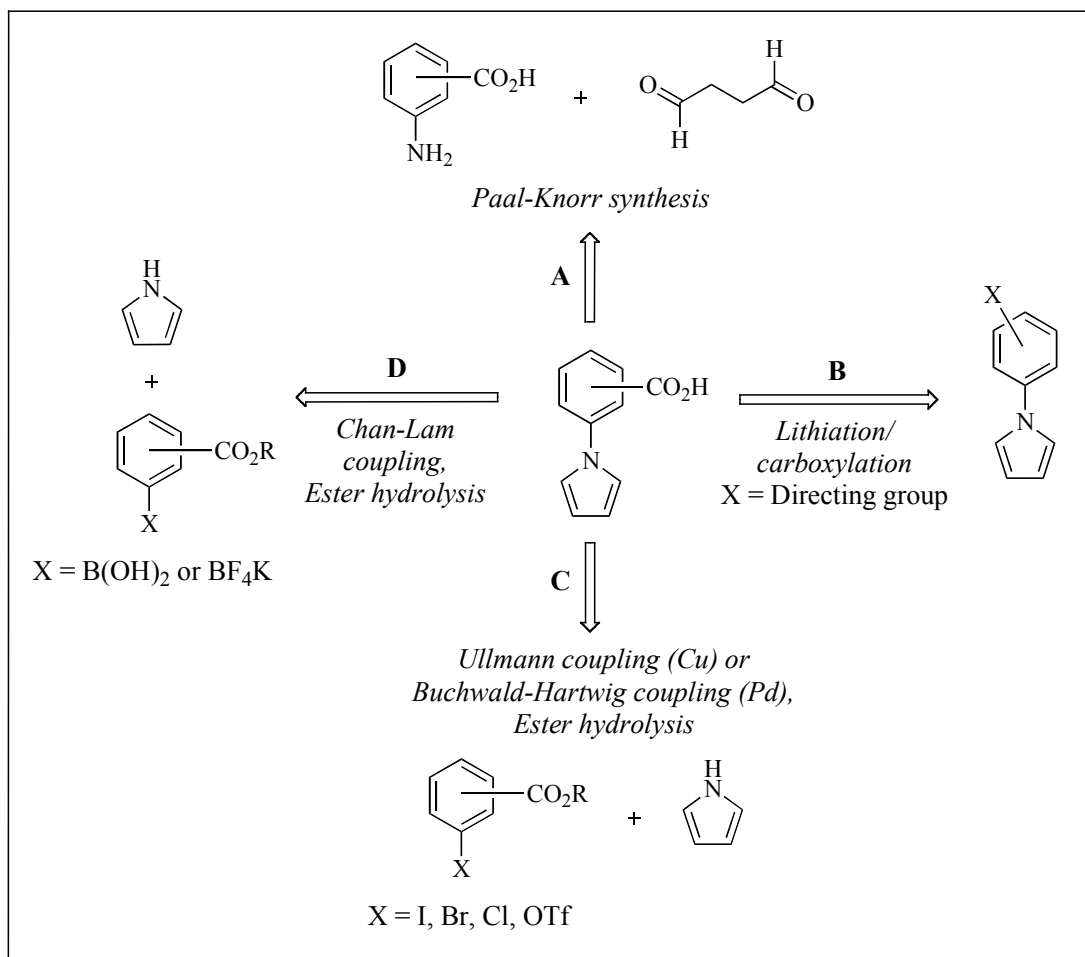
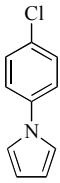
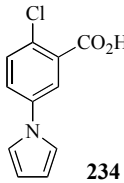
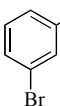
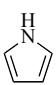
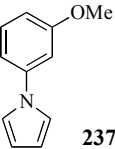
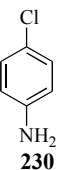
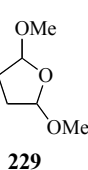
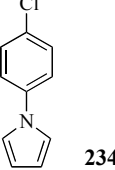
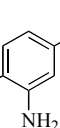
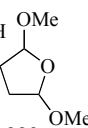
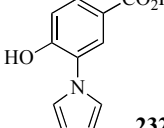
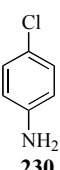
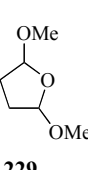
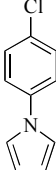
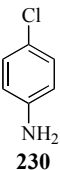
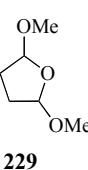



Figure 35. Pyrrole-benzoic acid synthetic strategies

We initially explored the lithiation-carboxylation route (route B, Table 13, entry 1). However, we were unable to achieve the levels of regioselectivity required for the expedient synthesis of a library of pyrrole-benzoic acids and abandoned this route. Buchwald-Hartwig protocol²⁵⁰ was briefly explored (entry 2). Various Pd-

mediated protocols generated a complex mixture of products as seen in the crude ^1H NMR's and this strategy was also abandoned. The Clausen-Kaas protocol was then employed (entries 3-6).^{240,254} This strategy allowed for rapid analog access due to the commercial availability of a variety of aniline derivatives and the simple one-step condensation procedure. As yields were not important in this study, we set to establish a protocol that would provide clean compounds with minimal purification efforts. Our first attempt utilized an uncatalyzed, direct condensation of the amino-benzoic acid with 2,5-dimethoxytetrahydrofuran, adding 4Å molecular sieves to soak up methanol and drive the reaction equilibrium towards product formation. While this procedure worked well for 4-chloro-aniline (**230**) (Table 13, entry 3), carboxyl substitution on the benzene ring (**231**) led to isolation of only starting materials and delivered no product (**232**) (entry 4). We then turned to acid catalyzed variants of the reaction. Following the precedent of Ottenheijm and coworkers,²⁵⁵ phosphorus pentoxide (P_2O_5) did provide the desired pyrrole product (**233**) by ^1H NMR (entry 5), but multiple chromatographies could not deliver pure material. We then turned to acetic acid as the catalyst.²⁵⁴ Indeed, refluxing the aniline **230** and tetrahydrofuran **229** in glacial acetic acid for one h followed by column chromatography delivered the desired pyrrole (**233**) in 78% yield. This technology was easily transferred to other amino-benzoic acid starting materials, albeit in modest yields.

Table 13. Optimization of pyrrole-benzoic acid formation

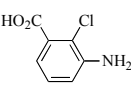
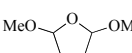
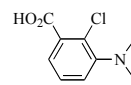
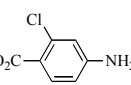
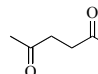
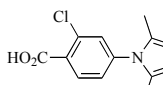
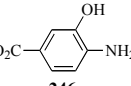
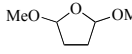
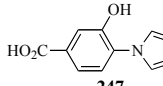
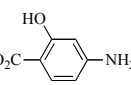
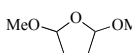
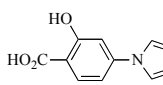
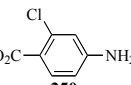
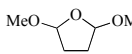
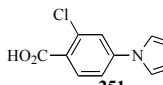
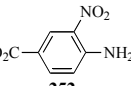
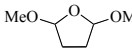
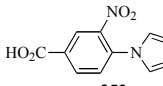
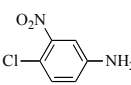
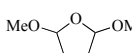
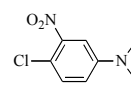
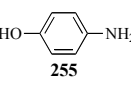
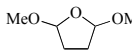
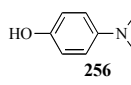
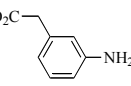
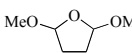
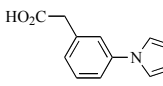
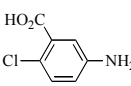
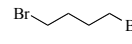
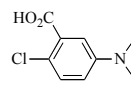
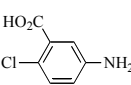
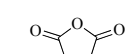
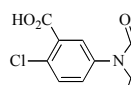
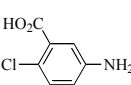
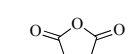
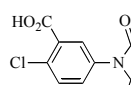
Entry	Substrate(s)	Conditions	Desired Product	Result
1	 233	1) TMP, <i>n</i> BuLi, THF, -78 °C 2) CO ₂ (s), Et ₂ O 3) 10% citric acid (aq.)	 234	Complex mixture by TLC and ¹ H NMR analysis
2	 235 +  236	Pd ₂ (dba) ₃ , P(<i>t</i> Bu) ₃ , Cs ₂ CO ₃ , Tol., 100 °C <i>OR</i> Pd(OAc) ₂ , DPPF, NaO ^{<i>t</i>} Bu, Tol., 120 °C	 237	Complex mixture by TLC and ¹ H NMR analysis
3	 230 +  229	4Å mol. sieves, Tol., 120 °C	 234	55% isolated yield
4	 230 +  229	4Å mol. sieves, Tol., 120 °C	 232	Starting material
5	 230 +  229	P ₂ O ₅ , Tol., 60 °C --> 110 °C	 233	Desired product + inseparable undesired products
6	 230 +  229	HOAc, 120 °C	 233	78% isolated yield

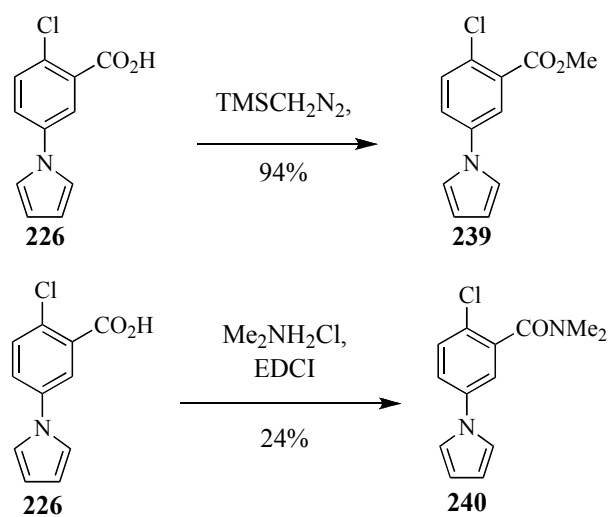
Using this standard protocol, a variety of substituted anilines and electrophiles were reacted to generate a 14-membered library for biological testing (Table 14). The

yields are variable for these compounds (3–67%). In general, the electron deficient anilines gave poorer yields of the condensation products (entry 2) compared to the more electron rich substrates (entry 8). Also, sterically hindered anilines generated lower yields of the pyrroles (entries 1, 3 and 6). Consumption of the starting material occurred in each reaction. While decomposition of the starting materials cannot be ignored as a potential cause for the low yields realized, the most likely cause is decomposition of the pyrrole products. Pyrroles are known to be unstable and can react with aldehyde substrates to undergo electrophilic aromatic substitution reactions, leading to polypyrrole compounds such as porphyrins.²⁵⁶

The analogs synthesized addressed a variety of issues generated by the HTS campaign. The role of an electron-withdrawing group was probed, replacing the carboxyl group of **226** with a nitro group (**238**, entry 7). The anionic character of the carboxyl group was also probed. Methylation of the benzoic acid with trimethylsilyldiazomethane gave the corresponding methyl ester **239** (Scheme 32). Using a *N*-(3-dimethylaminopropyl)-*N'*-ethylcarbodiimide hydrochloride (EDCI) coupling,²⁵⁷ the acid **226** was converted to the *N,N'*-dimethylamide **240** for testing (Scheme 32). Non-pyrrole *N*-substituted heterocycles were also synthesized following the acid-mediated protocol (entries 10-12).²⁵⁸

Table 14. Pyrrole benzoic acid analogs

Entry	Aniline	+	Electrophile	$\xrightarrow[100\text{ }^\circ\text{C, 2 h}]{\text{HOAc}}$	Product	Yield %
1						14
2						3
3						8
4						67
5						10
6						3
7						30
8						49
9						20
10						12
11						40
12						5



Scheme 32. Synthesis of ester and amide analogs

Despite the modifications to the lead scaffold, only the maleimide analog **265** displayed significant MurA inhibitory properties when tested at 100 μM in the Lanzetta assay (Figure 36), at least initially. The exact IC_{50} value was determined by varying the concentration of compound **265** in the Lanzetta assay, producing an IC_{50} of about 25 μM (Figure 37). The maleimide **265** displayed equipotency when compared to HTS lead compound **226**. This result, however, was discovered to be a false positive.

Maleimides are known to be good Michael acceptors and we hypothesized that the observed biological activity could result from this reactive moiety. However, the purple color of the maleimide DMSO solution used in the biological assay suggested that decomposition of some component had occurred. A multitude of peaks seen in the ^1H NMR of the decomposed product further supported this

hypothesis. Attempts to analytically identify compounds in the mixture were unsuccessful. The maleimide compound **265** was synthesized again, spectroscopically confirmed as the desired structure, and tested in the Lanzetta assay. The biological activity displayed by the initial, decomposed compound was not reproduced by the newly synthesized maleimide **265**. Further, this new product proved to be stable to a variety of conditions present while as a DMSO solution awaiting biological testing, such as exposure to UV light or heat.

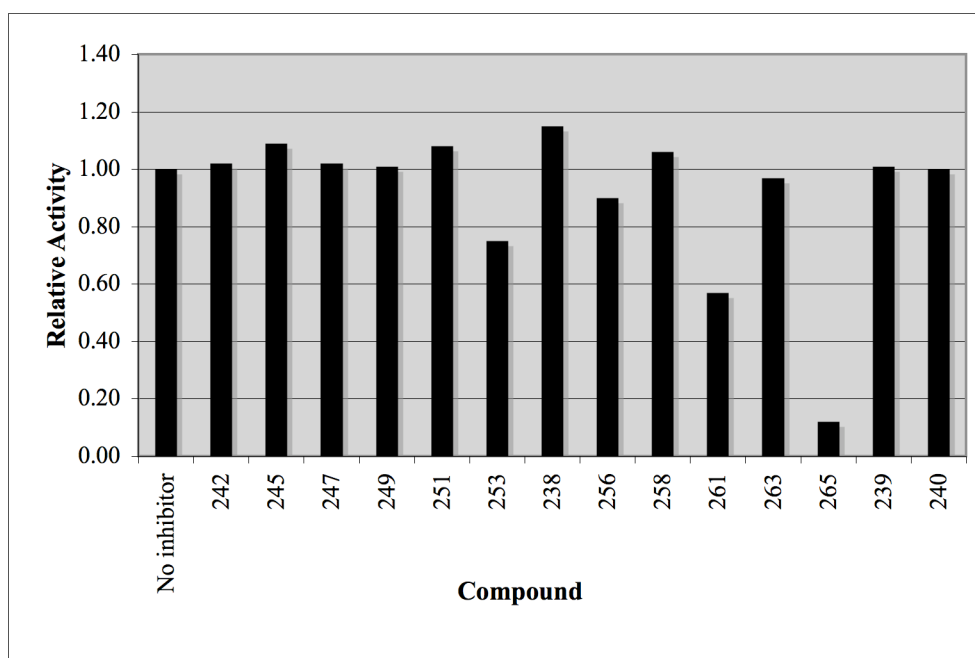


Figure 36. Relative MurA inhibitory activity for synthesized analogs

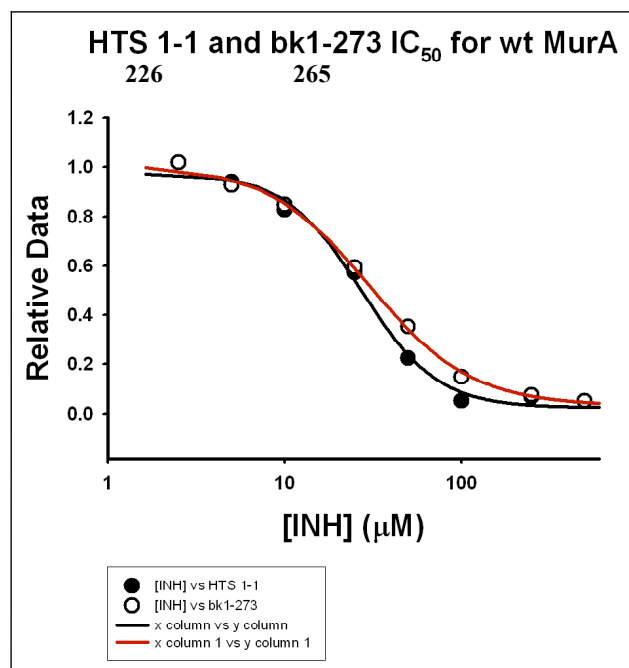


Figure 37. Initial IC₅₀ determined for compound **265** vs. **226**

As our analog campaign failed to construct a quantifiable SAR, we assumed that these compounds possessed a flat SAR and halted further analog exploration. Still determined to find a new MurA inhibitor, structure-based drug design was then explored.

2.3 Structure-Based / Fragment-Based Drug Design Approach

Hemoglobin was the first target for structure-based drug design.²⁵⁹ In 1975, Beddell *et al.* detailed their rational development of new binders of the iron-containing protein based upon interactions seen in the X-ray crystal structure. It is important to note that these new molecules were not analogs of the native substrate

2,3-diphosphoglycerate and therefore most likely would not have been discovered following medicinal chemistry practices of that era.

As both X-ray crystallography and computational methodology became cheaper and easier to perform, the use of structure-based drug design grew.²⁶⁰ The basic premise of structure-based drug design is to use protein structural information, generally acquired from an X-ray crystal structure or NMR spectroscopy, to design molecules that form key binding interactions with the protein. Commonly, this practice is coupled with computer modeling to speed the discovery process. Structure-based drug design has been successfully applied in the development of many drugs including the neuraminidase inhibitor Relenze®, an influenza treatment.²⁶¹

A related drug design strategy, fragment-based drug design, has also grown rapidly in recent years due to technological advances. A benefit of a fragment-based approach is that a relatively small amount of compounds need to be screened to find a hit compared with the standard HTS practice.^{262,263} The basic concept of fragment-based drug design is to find small molecules, generally less than 250 Da in molecular weight, with high micromolar to millimolar activity against a specific biological target.²⁶⁴ These weak binders can then be elaborated upon in a ligand efficient manner^{265,266} to generate nM inhibitors of the target enzyme.²⁶⁷ To be considered “ligand efficient”, each non-hydrogen atom added to the scaffold should increase the free binding energy by approximately $1.5 \text{ kcal mol}^{-1}$. This generates a nM inhibitor from a 250 Da fragment with an initial K_d or IC_{50} value of $100 \mu\text{M}$.²⁶⁶ The fragments

forming interactions with the target protein are identified by a variety of biophysical methods, such as high throughput X-ray crystallography, high-throughput NMR spectroscopy or isothermal calorimetry. In addition to the cutting-edge technology required for a successful fragment-based screening program, this technique is limited towards proteins that can be easily purified in large quantities.

As there is a wealth of MurA structural information in the literature, we chose to utilize these two methods in the search for new MurA inhibitor scaffolds. Crystal structures are solved with MurA in both the open and closed forms and with various ligands docked in each form.²⁶⁸ We envisioned that virtual screening of fragment libraries against the crystal structures would generate leads with μM binding affinities. However, these weak binders would reveal chemical functionality pertinent for ligand-protein interactions to aid the discovery process. Based on these modeling results, establishment of an SAR would lead to the design of more potent inhibitors. Important to this structure-based drug design approach is confirmation of our modeling hits with follow-up testing in MurA inhibitory assays and, ultimately, co-crystallization with the enzyme.

In 2006, Klein and Bachelier reasoned that, while many crystal structures of MurA have been solved, only the closed form structures would be useful for *in silico* inhibitor development.²⁶⁸ In the open form, the enzyme's loop region is flexible in solution. Binding to this loop requires a large loss of entropic freedom from the enzyme, therefore requiring high affinity compounds for MurA inhibition. Further, the positioning of the loop region in various crystal structures is influenced by several

crystal contacts. This implies that the crystal structure conformation is likely not the conformation present in solution. The authors also reasoned that targeting the loop is undesirable due to the observed lack of residue conservation. For example, the C115D mutation is present in about 20% of known MurA enzymes. Based on these hypotheses, we began our search by looking at the closed form of the enzyme, specifically the 1RYW crystal structure.²¹⁶

We predicted that a successful MurA inhibitor would induce the open/closed conformational change similar to the native MurA substrates UNAG and PEP. Therefore, binding to the closed state was imperative. MurA was co-crystallized with the reaction product EP-UNAG in the 1RYW crystal structure, forming an active site ready for ligand docking studies. The 1RYW crystal structure contains a C115S mutation. This mutation was not expected to be detrimental towards our *in silico* approach as the cysteine residue is required only for product release.²¹⁶ Use of this structure may actually be beneficial towards MurA inhibitor development due to the known prevalence of mutation for this residue.

Our high-throughput virtual screening campaign began by generating a receptor model of the enzyme in the modeling program SYBYL.²⁶⁹ The reaction product EP-UNAG, the liberated phosphate molecule, and crystallographic waters were removed from the crystal structure. Valence protons were added according to standard physiological conditions (pH = 7.4). Gasteiger-Marsili formalism was used to assign partial atomic charges.²⁷⁰ We docked ligands using the Autodock

program²⁷¹, requiring 10 poses per ligand. The results were evaluated using default Lamarckian genetics algorithms search specifications.

Prior to beginning the screening campaign, we validated the receptor model by docking EP-UNAG into the receptor site. This docking simulation generated EP-UNAG poses comparable – less than 2.0Å root mean squared positional deviation – to the crystallographic EP-UNAG molecule. According to the Autodock scoring function, this result corresponds to an exothermic -10 kcal mol⁻¹ binding energy.

The ligands used in the virtual screen were extracted from the ChemNavigator iResearch Library collection, comprised of commercially available and synthetically feasible molecules.²⁷² As this was a fragment-based screening approach, we used the UNITY program²⁷³ to mine only the molecules with molecular weight less than 150 Da. This size criterion allows for a small amount of structural complexity but plenty of room to evaluate and build larger molecules in line with the Lipinski rules.³ A total of 3,692 compounds fit this molecular weight criterion. Using the Concord program,²⁷⁴ we then converted these compounds into 3D structures and assigned atomic charges again using the Gasteiger-Marsili formalism, ready for docking in the receptor model analogously to the EP-UNAG study. This *in silico* screen revealed 331 compounds with a predicted docking energy of greater than -8.0 kcal mol⁻¹ and 19 compounds with greater than -9.0 kcal mol⁻¹ docking energy (Figure 38). Autodock estimated K_i values between 125 and 318 nM for these 19 compounds.

The 331 hit molecules displayed a variety of functionality. At least one hydrogen-bonding element was required for activity. Amines and amides were well

represented. The 19 most potent inhibitors generally contained at least two hydrogen-bonding functionalities.

As shown in Figure 38, the ligands expectedly clustered around the outside of the EP-UNAG-formed binding pocket. UNAG is displayed in the center of the Figure as a reference. The individual residues are not numbered in this Figure, but their labeling allows for some structural understanding. In particular, a majority of the ligands bind near a tryptophan residue at the bottom of the Figure. As this amino acid (Trp95) may be important for the open to closed conformational change, we visually dissected the 331 compounds and removed the compounds that did not bind within five angstroms of the W residue. This left behind 255 compounds, 18 with greater than $-9.0 \text{ kcal mol}^{-1}$ binding energy, for further docking investigation.

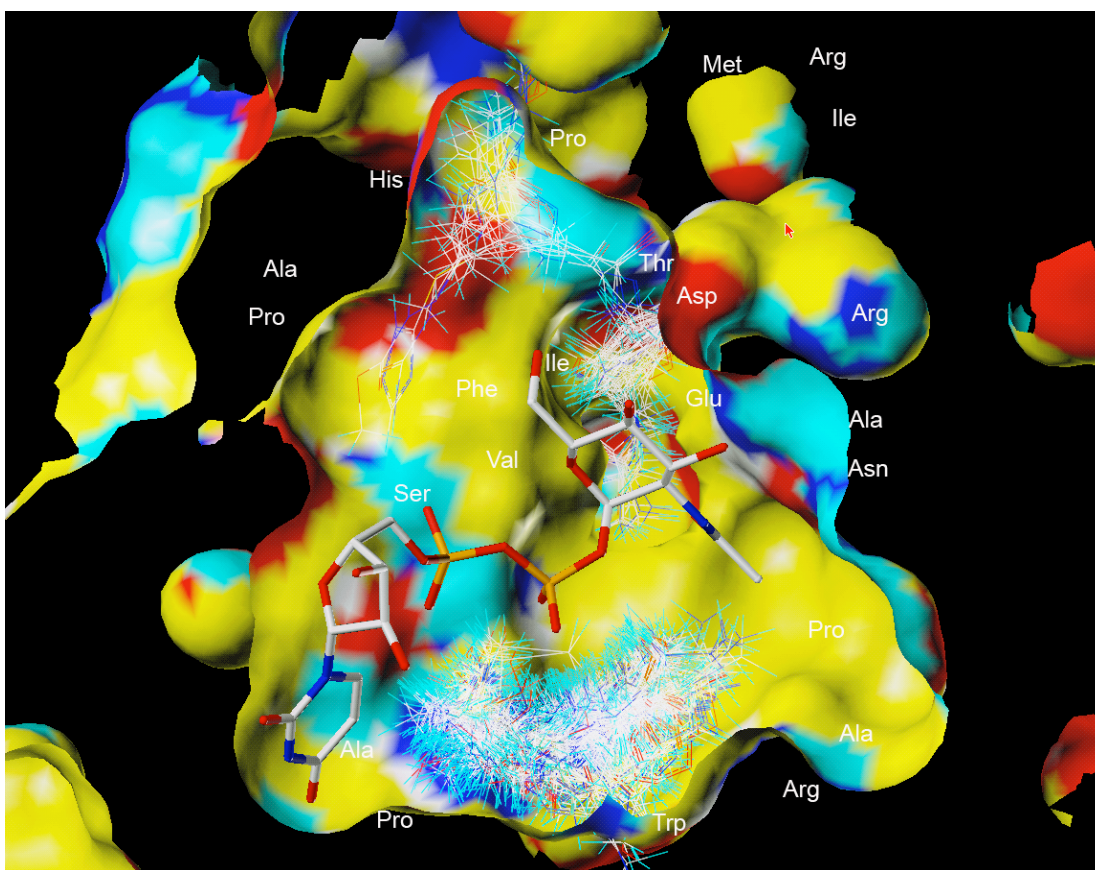


Figure 38. MurA docking results

The 255 compounds were then virtually screened in four different open conformation MurA crystal structures: 1EYN,²⁷⁵ 1YBG,²⁷⁶ 1EJC²⁷⁷ and 1EJD.²⁷⁷ A known MurA inhibitor, Aventis compound T6361 (compound **217**), was co-crystallized with the enzyme in crystal structure 1YBG and was removed using a similar protocol for EP-UNAG as above. Similarly, the fluorescence probe 8-anilino-1-naphthalene-sulfonate (ANS (**226**), Figure 39) was removed from crystal structure 1EYN. Method validation by virtual docking of these compounds into their respective crystal structures was difficult. The Aventis inhibitor (**217**) did bind in the

correct active site compared to the 1YBG crystal structure, but in a different orientation. Hydrogen bonding and π - π stacking interactions previously thought to be key for **217** binding to MurA based on the co-crystal structure were not present in the docking simulation. ANS did not dock in the correct site altogether. This result could be attributed to tightly-formed binding pocket of ANS in the crystal structure. We did not perform follow-up molecular dynamics simulations to relax the crystal in an attempt to promote ANS docking.

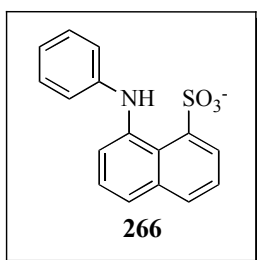


Figure 39. Structure of ANS

Using the Trp95 residue as the bullseye for compound docking, we again visually dissected the virtual screening results. Crystal structures 1YBG and 1EYN docked a majority of the compounds, 133 and 255 respectively, within five angstroms of the Trp95 residue. Without a co-crystallized molecule to define an active site, crystal structures 1EJC and 1EJD were more discriminate. Only two compounds docked within 5Å of Trp95 in 1EJC and only three compounds fit this criterion in 1EJD.

Comparing the hit fragments from the 1EJC and 1EJD docking studies with the hit fragments from the 1RYW, 1EYN and 1YBG virtual screens gave four

compounds that were successfully docked within five angstroms of Trp95 in two or more of the X-ray structures. These molecules (**267-270**) are shown in Figure 40. In general, the fragments contain a lipophilic side chain appended to a hydrogen bond donor in the center. As none of these molecules were commercially available, a similar molecule *N*-(2-methylpropyl)-1-butanamide (**271**) was purchased and tested for MurA inhibitory activity. Even at five mM concentrations, this molecule displayed no activity. Further, it did not display activity when UNAG was added to the assay. This compound did not appear as a hit in the initial 331 fragments and it is unclear whether this molecule was present in the initial 3,692 compounds virtually screened.

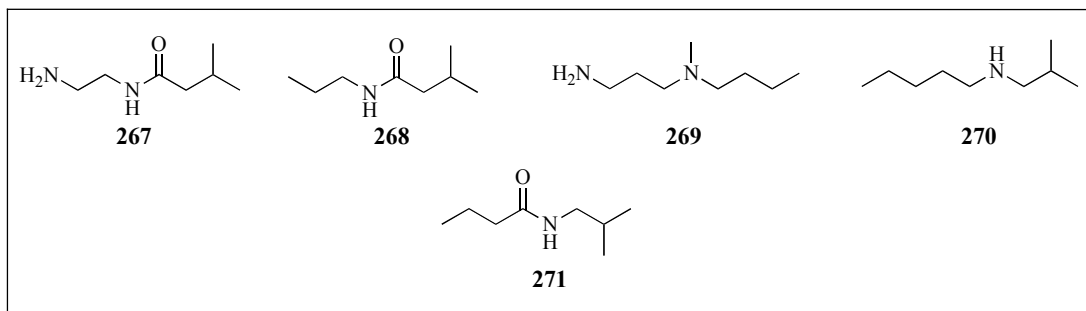


Figure 40. Virtual screen hits **267-270** and analog **271** tested for MurA inhibition

2.4 Conclusions

The bacterial enzyme MurA was targeted for new antibiotic development. A few inhibitors of the enzyme are known and only one, fosfomycin, is currently marketed as a therapeutic. The limited applicability of fosfomycin coupled with a thorough understanding of the enzymatic role in bacteria presented an opportunity to discover new inhibitors of this enzyme. We began our search for original MurA

inhibitors with an HTS campaign that identified five scaffolds for further investigation. The pyrrole-benzoic acid series was chosen for SAR development. We synthesized 14 analogs using Clauson-Kaas methodology. These analogs probed the role of the carboxylic acid and tolerance of other phenyl ring functionality. Various *N*-heterocycles were also explored. However, these analogs displayed no MurA inhibitory activity. Subsequently, we turned to other investigatory tools to probe MurA. Structure-based drug design using *in silico* screening of small molecules in various MurA X-ray structures identified four structurally similar molecules that could be used as starting points for further inhibitor discovery.

Chapter 3

Synthesis and Initial Biological Evaluation of 2,3,7,8-Tetrachlorophenothiazine

3.1 Background

Dioxins are environmental pollutants comprised of a polychlorinated aromatic structure, with 2,3,7,8-tetrachlorodibenzo-*p*-dioxin (TCDD (**272**)) being the one of the most potent congeners. Formation of these toxic molecules occurs via various manufacturing processes, including chlorine bleaching of paper, via burning of solid waste, even resulting from volcanic eruptions and forest fires.²⁷⁸ These lethal chemicals enter the body mainly through the consumption of animal-based foods²⁷⁹ but can also enter via inhalation of polluted air. Highly chemically stable,²⁸⁰ their slow metabolism and excretion coupled with a highly lipophilic nature leads to the ready accumulation of dioxins in fat cells. For example, TCDD has an elimination half-life of 7.8 years²⁸⁰ and a *c*LogP value of 7.05. The calculated LD₅₀ of six mg kg⁻¹ in humans makes TCDD especially dangerous^{281,282} yet widely studied because of its intriguing biological profile.

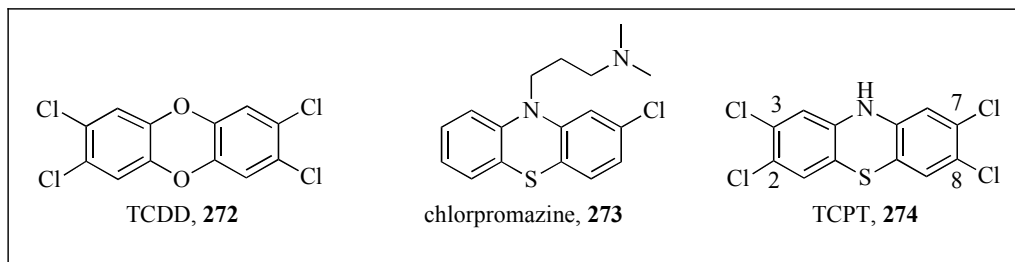


Figure 41. Structures of TCDD (**272**), chlorpromazine (**273**), and TCPT (**274**)

Dioxins exert a range of biological activities dependent upon dose size. At high doses, these compounds can be lethal by causing wasting syndrome²⁸³ or cancer.²⁸⁴ Medium dose effects include liver injury, immunosuppression,²⁸⁵ debilitating reproductive effects,²⁸⁶ and reduced serum IGF-1 (insulin-like growth factor-1) levels.²⁸⁷ However, at low doses, TCDD has been shown to reduce age-related tumor occurrence,²⁸⁴ reduce body weight²⁸⁸ and inhibit ovulation.²⁸⁹ A shift of body homeostasis could explain the biological activity differential in relation to potency.²⁹⁰ At low doses, dioxins could cause a slight fluctuation in body equilibrium. This flux forces the body to adapt by turning on or off certain pathways to eliminate the xenobiotic, affecting downstream biological pathways that lead to desirable therapeutic effects. However, at high doses, the body could not recover from the influx of toxic xenobiotics and harmful side effects result.²⁹⁰

This broad range of biological effects has prompted various mechanism of action studies on dioxins.²⁹¹⁻²⁹³ It is widely hypothesized that TCDD binds to the aryl hydrocarbon receptor (AhR) due to its planar geometry, exerting the observed biological effects through interaction with this receptor. The AhR is well known to bind planar molecules. Indeed, TCDD is a strong AhR binder with a K_i of 0.54 nM.²⁹⁴ However, recent evidence has challenged this hypothesis.²⁹⁵ Saturation of the rat AhR system by TCDD occurs at a dose of 0.2-0.3 $\mu\text{g}/\text{kg}$,²⁹⁶ but the LD_{50} is 10-50 $\mu\text{g}/\text{kg}$ for most rat variants,²⁹⁷ suggesting that binding to the AhR may occur but is not the ultimate source for dioxin toxicity.²⁹⁴ The AhR receptor can activate the p450 enzyme CYP1A1.^{298,299} Activation of this enzyme could induce metabolism of

various carcinogens resulting in decreased cancer rates.²⁸⁴ Pharmaceutical companies view binding and activation of the CYP1A1 enzyme as disastrous for a prospective drug candidate because metabolites produced by this enzyme could be carcinogenic.³⁰⁰ However, case studies refute this school of thought. The best example is a study published in 2005 by Rozman *et al.*³⁰¹ A higher chlorinated dioxin, 1,2,3,4,6,7,8-heptachlorodibenzo-*p*-dioxin, tested in rats was found to induce CYP1A1 but produced lower incidences of cancer compared to the control group.

Dioxins have been shown to decrease IGF-1 levels.²⁸⁷ IGF-1 is responsible for mediating a variety of body processes, such as stimulating mitosis, inhibiting apoptosis, stimulating glucose uptake and increasing protein biosynthesis.²⁸⁷ Therefore, the reduction in body weight and inhibition of ovulation observed when TCDD is administered to female rats most likely results from reduced IGF-1 levels.^{302,303} However, due to the wide range of bioactivity exerted by these molecules, it is possible that several mechanisms are responsible.

Given the therapeutic potential for a compound that could harvest the beneficial low-dose effects of dioxins while avoiding the harmful medium- and high-dose effects, could a molecule be developed with these goals in mind? Development of a TCDD analog, a tetra-chlorinated phenothiazine compound, served to probe this question. Many factors made this bioisoelectronic approach desirable. Phenothiazines have been used as antihistaminic and antipsychotic drugs since the 1930's with the first antipsychotic phenothiazine, chlorpromazine (**273**, Figure 41), being approved by the FDA in 1954.²⁸¹ While searching for novel antihistaminic and

antipsychotic therapeutics, researchers have carved out an extensive SAR for this class of compounds while demonstrating that these compounds generally possess acceptable absorption, distribution, metabolism, and excretion (ADME) properties – important for drug candidate development.²⁸¹ The parent molecule of this class is a known anthelmintic compound,³⁰⁴ but analogs lacking substitution on the aniline nitrogen are generally unexplored due to the general lack of antihistaminic or antipsychotic activity. Increased chlorine substitution on the phenothiazine ring system is also generally unexplored. Another reason for choosing a phenothiazine as the basis for the analog is its non-planar butterfly molecular geometry.³⁰⁵ The dihedral angle, or fold angle, of these tricyclic molecules is defined as the angle between the bridging heteroatom and each of the phenyl rings. Chlorpromazine displays a fold angle of 134°. ³⁰⁵ Comparatively, the fold angle for TCDD is near 180°. ³⁰⁶ The non-planar geometrical orientation of phenothiazines should lead to decreased interaction with the AhR. Hoping to meld the low-dose effects of dioxins with the ADME properties of phenothiazines, 2,3,7,8-tetrachlorophenothiazine (TCPT (**274**), Figure 41) was designed and synthesized.

3.2 TCPT Synthesis

As phenothiazines have been known for many years, many methods exist for their synthesis (Figure 42).^{307,308} Each strategy relies upon the formation of a diphenyl-heteroatom (N or S) intermediate prior to phenothiazine ring closure. No previous strategy consistently generates high yields (>50%) of the desired

heterocycle. One of the harshest methods is the cyclization of diphenylamines in the presence of a sulfur reagent and a catalyst (method **A**).³⁰⁹ The triethyl phosphite-mediated reductive cyclization of *o*-nitro-diphenylsulfides (method **B**), while generating decent yields of the desired product, is known to form rearranged products as side products.³¹⁰ The requirement of a certain substitution pattern on the nitrophenyl ring of the diphenylsulfide starting material limits the Smiles rearrangement approach (method **C**).³¹¹ 2-Azidodiphenylsulfide compounds undergo a rearrangement followed by loss of nitrogen gas under thermal conditions to afford phenothiazines (method **D**).³⁰⁸ Condensing thiozincate anilines with quinones substituted with a leaving group (LG) in the 2-position generates a cyclic imine intermediate that can then be reduced to generate the target tricyclic compounds (method **E**).³⁰⁸ The only proven transition metal catalyzed approach is the copper-mediated Ullmann coupling (method **F**),³¹² also requiring high temperatures and generally resulting in low yields. The application of many methodologies for phenothiazine synthesis suggests that a superior methodology has not yet been developed.

One previous synthesis of TCPT is reported in the literature in which unsubstituted phenothiazine is exposed to chlorine gas in the presence of a Friedel-Crafts catalyst (D-X Li).³¹³ Attempts to repeat this chemistry resulted only in the formation of 1,3,7,9-tetrachlorophenothiazine.³¹⁴ A new route towards the synthesis of TCPT was subsequently designed.

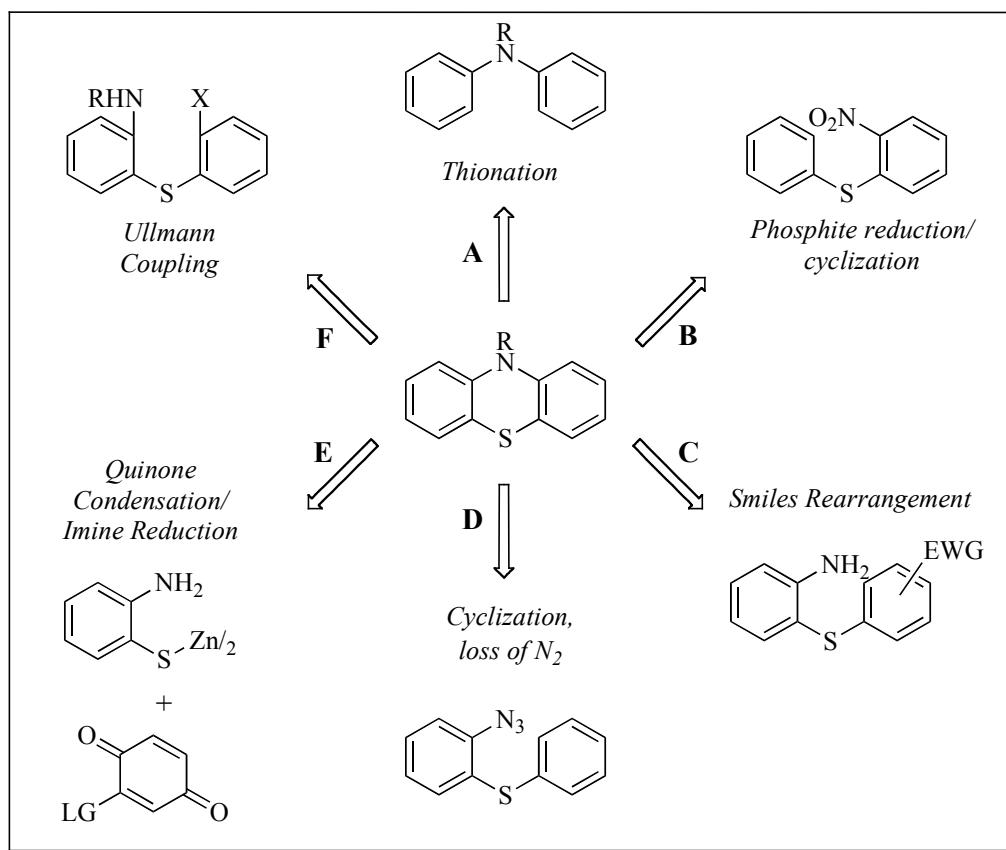
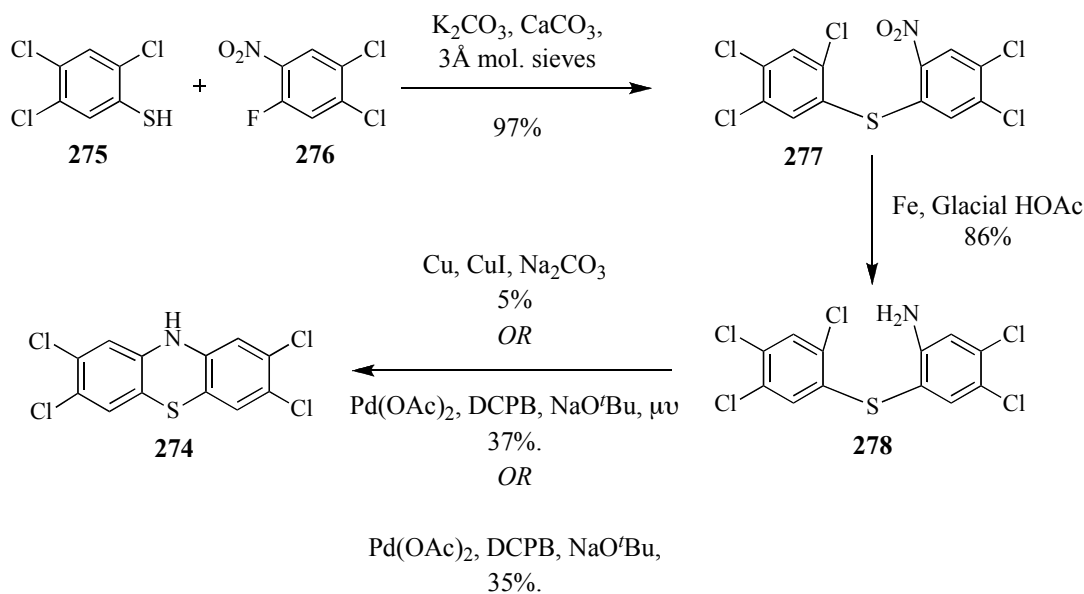


Figure 42. Synthetic strategies for phenothiazine synthesis

The recently developed Buchwald-Hartwig coupling holds the potential as the superior technology for phenothiazine synthesis.^{249,251} This palladium-mediated carbon-heteroatom bond forming reaction has never been used in the synthesis of phenothiazines. One limitation in the application of this strategy towards the synthesis of TCPT, as with any metal-catalyzed strategy, is the possibility for dechlorination at positions 2, 3, 7 or 8. However, we reasoned that the Pd(0) species could be directed towards oxidative insertion into the desired aryl-chloride bond by

either the sulfur or nitrogen atom, decreasing the probability of this deleterious side reaction.

Condensation of the commercially available 2,4,5-trichlorobenzenethiol (**275**) with 1,2-dichloro-4-fluoro-5-nitrobenzene (**276**) generated the diphenylsulfide compound (**277**) in 97% yield (Scheme 32). Reduction of the nitro group with Fe filings in acetic acid (HOAc)³¹⁵ yielded the aniline compound **278** prepped for the key cyclization step. Before turning to the Buchwald-Hartwig reaction, we attempted to use the established Ullmann coupling technology³¹² to generate TCPT. Refluxing diphenylsulfide **278**, Cu powder, CuI, and Na₂CO₃ in DMF generated only 5% of the desired phenothiazine compound **274**. As all the starting material was consumed during the reaction, we reasoned that the product was being degraded by the reaction conditions leading to the observed low yields. In an attempt to speed up the reaction and reduce the amount of degradation, we turned to microwave technology. In fact, Ullmann couplings performed under microwave irradiation have been reported to decrease reaction time and increase yields.³¹⁶ However, the Ullmann coupling of **278** performed in the microwave returned only starting material. Because of the confidence that long reaction times under harsh conditions degraded TCPT, we rationalized that a Buchwald-Hartwig coupling performed in the microwave would generate higher yields of TCPT.



Scheme 32. Synthesis of TCPT

Due to the electronics and sterics of the cyclization substrate **278**, specific parameters in a catalytic system were sought. The strength of the aryl carbon-chloride bond generally makes the oxidative insertion of Pd(0) difficult. However, based on studies performed by Buchwald and coworkers, we anticipated that the electron deficient nature of the trichlorosubstituted aryl ring would help to promote this step of the Pd catalytic cycle.²⁵¹ The ortho-located thiobenzene group could sterically impede the Pd-insertion. The Buchwald laboratories have also shown that substituents placed ortho to the desired reactive aryl C-halogen bond can be problematic.³¹⁷ With these electronic and steric constraints in mind, a Pd-catalyst system using 2-(dicyclohexylphosphino)-biphenyl (DCPB) as the ligand developed by Maes and coworkers was selected for testing.³¹⁸ This system has demonstrated the ability to

couple both activated and non-activated aryl chlorides, as well as sterically hindered aryl chlorides, under microwave irradiation.^{318,319}

Table 15 summarizes the results for our Buchwald-Hartwig cyclization studies. The reagents comprising the catalyst system were not altered during these studies. We chose to focus on catalyst to substrate ratio, time, temperature, and solvent in the optimization of this reaction. In a successful reaction employing a 10% catalyst loading ratio, 0.1 equivalents of Pd(OAc)₂ and 0.2 equivalents of DCPB were dissolved in DMF and added to a DMF solution containing one equivalent of cyclization substrate **278** and 1.3 equivalents of NaO^tBu. The solution was flushed with argon for five minutes before heating. Following microwave irradiation for two minutes at 200 °C, the starting material was completely consumed and TCPT was isolated in a 37% yield following column chromatography and recrystallization from CHCl₃ (entry 3). Reducing the reaction temperature and the amount of catalyst from 10% to 1% (entries 1 and 2) gave no conversion to product, even after prolonged heating times. Increasing the reaction time from two minutes led to decreased yields (entries 4 and 5), presumably due to degradation of the product as previously described. The optimal solvent for the reaction was DMF. Reactions in the less polar solvents dioxane and toluene failed to consume starting material. To determine if microwave effects were responsible for the increased yields of TCPT, the reaction was performed using traditional oil bath heating (entry 6). Following the addition and purging procedure previously described, diphenylsulfide **278** was heated at 150 °C for one h, a time and temperature corresponding to two minutes at 200 °C in the

microwave. Despite the presence of starting material in the crude reaction as determined by TLC analysis, the reaction produced a 35% yield of TCPT following purification, demonstrating that no microwave effects were responsible for forming TCPT.

Table 15. Optimization of reaction parameters for TCPT formation

Entry	Time(min.)	Temp (°C)	% Catalyst	Yield
1	5	150	1	No Reaction
2	10	150	1	No Reaction
3	2	200	10	37% after recrystallization
4	4	200	10	27% after recrystallization
5	5	200	10	26% after recrystallization
6	60	150	10	35% after recrystallization ^a

^a The reaction was run under normal reflux conditions.

Before TCPT could be tested in biological assays, an additional obstacle remained. Degradation studies demonstrated that TCPT was light sensitive and unstable as a solid or as a solution in THF or acetone. These facts help support our rationale behind the moderate yields realized in the cyclization reaction. However, TCPT is light stable as a DMSO solution, solving a potential problem for biological testing.

3.3 Initial Biological Evaluation of TCPT

Prior to testing TCPT in *in vitro* and animal models, the crystal structure for TCPT was solved. The crystal structure revealed a fold angle of 161.5° (Figure 43), hinting at the possibility for a decreased interaction with the AhR. If there is a decreased interaction with the AhR, downstream effects mediated by activation of the AhR, such as CYP1A1 induction, should also be reduced.

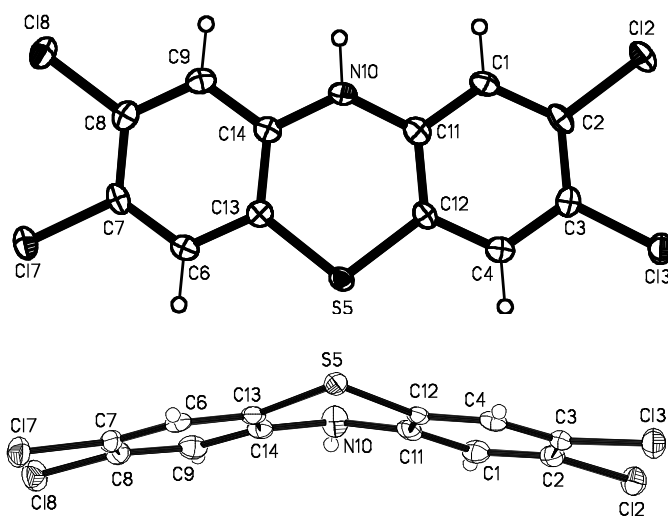


Figure 43. Crystal structure of TCPT

TCPT was first evaluated in an ethoxyresorufin-*O*-deethylase (EROD) assay,^{320,321} an assay is commonly used to measure CYP1A1 activity. As expected, TCDD induced CYP1A1 activity over time (Figure 44). However, induction of the enzyme with TCPT decreased after 24 h with almost complete loss of activity after 72 h. This suggests that TCPT is metabolized to inactive compounds by hepatocytes. After 24 h, the ED₅₀ for induction of EROD by TCDD was calculated to be 0.23

pg/well while TCPT was calculated at 85.1 pg/well – representing a 370-fold reduction in CYP1A1 induction potency for TCPT. This loss in potency, however, was not completely mirrored by a loss in efficacy. Maximal induction of EROD after 24 h for TCDD was determined to be 637 pmol min⁻¹ mg protein⁻¹. TCPT presented a maximum induction of 494 pmol min⁻¹ mg protein⁻¹ after 24 h, representing a 77.6% efficacy compared to TCDD. These findings show that the therapeutic window for CYP1A1 induction has been greatly broadened by TCPT compared with TCDD.

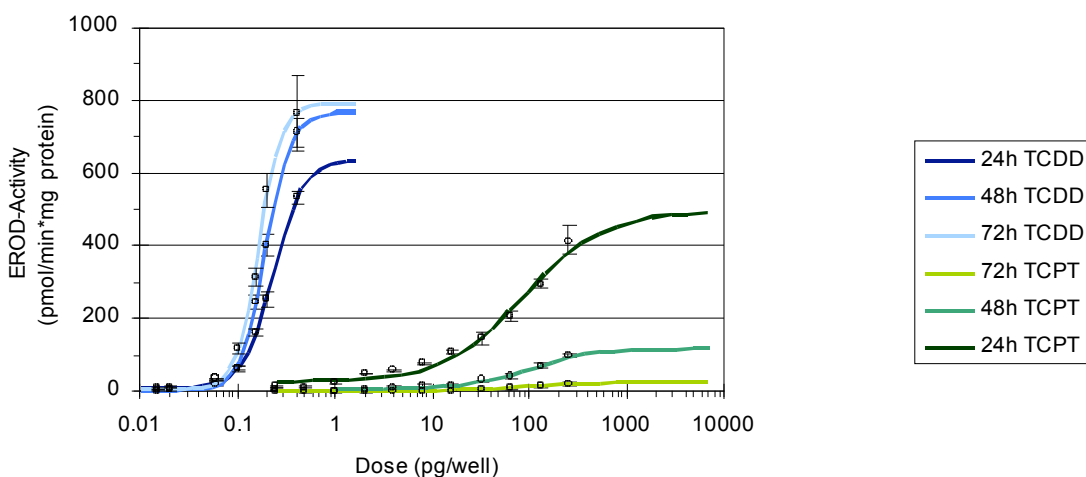


Figure 44. *In vitro* EROD activity of TCDD (left, blue) and TCPT (right, green)

TCPT was evaluated in a radiolabel displacement assay to evaluate AhR binding.²⁹⁴ Displacement of ³H-TCDD by increasing concentrations of TCDD or TCPT determined the binding constant K_i . The K_i 's for TCDD and TCPT were found to be 0.54 nM and 1.08 nM, respectively.²⁹⁴ Given the results of the EROD assay, these results are astonishing as the binding affinity for the AhR for TCPT is only two

times higher than TCDD. Methylcholanthrene is the only other compound known to display such a divergence between AhR binding and EROD activity.³²² These results suggest that a more complicated mechanism exists between AhR binding and CYP1A1 induction. Also, AhR binding may induce other enzymatic pathways leading to the demonstrated dioxin toxicity. More investigation is necessary to address this issue.

As pharmacokinetics are an important aspect of drug development, TCPT was evaluated in rats and guinea pigs for distribution and elimination properties. TCPT was administered to the animals via i.v. as an acetone solution. Using classic curve feathering and a computational regression analysis following a two-compartment model analysis, TCPT was found to have a distribution half-life ($t_{1/2}$) of 0.8 h and an elimination $t_{1/2}$ of 5.4 h in rats (Figure 45). In guinea pigs, these numbers were 0.4 h and 2.7 h, respectively (Figure 46). The clinically used phenothiazine **273** has an elimination $t_{1/2}$ of 9.1 h in similar rat strains,³²³ corresponding to a $t_{1/2}$ of 30 h in humans.²⁸¹ Correlating the known $t_{1/2}$ of **273** in rats to TCPT's determined $t_{1/2}$ in rats suggests an elimination half-life of 18 h for humans. This drastic decrease in $t_{1/2}$ cannot be attributed only to a decrease in the $c\text{LogP}$ for TCPT compared to TCDD, as the $c\text{LogP}$'s vary by only 0.5 log units (7.05 for TCDD and 6.65 for TCPT). The observed decrease achieves one of the goals for the design of TCPT – improved pharmacokinetics compared to TCDD.

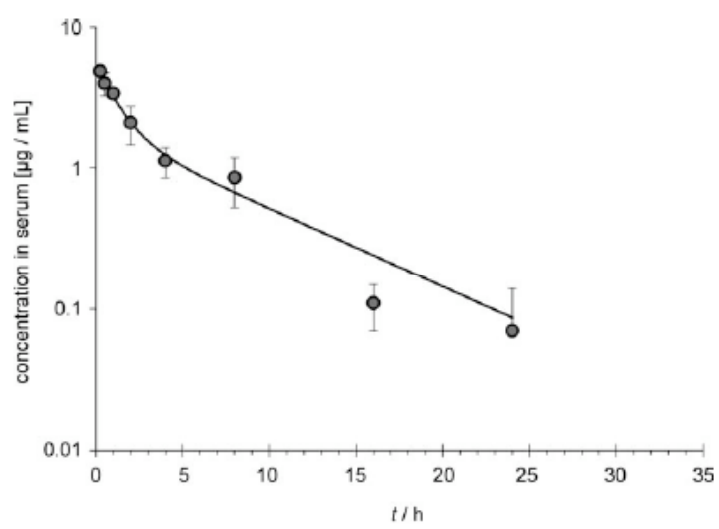


Figure 45. Serum profile of TCPT in rats after i.v. administration

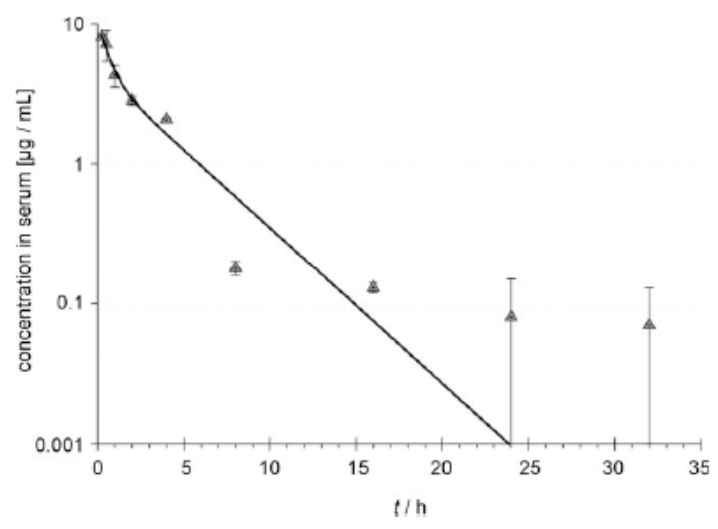


Figure 46. Serum profile of TCPT in guinea pigs after i.v. administration

3.4 Conclusions

Achieving selectivity for the therapeutically beneficial low dose effects of dioxins over the harmful higher dose effects was explored with the development of TCPT. The synthesis of this new phenothiazine compound was completed in a 31% overall yield over three steps utilizing a Buchwald-Hartwig coupling to perform the crucial ring-closing step. This protocol had previously not been explored and should prove useful in future phenothiazine syntheses. Initial biological evaluation of TCPT indicates that the compound has good pharmacokinetic properties. While the analog was expected to bind substantially less to the AhR compared to TCDD due to its non-linear molecular geometry, this hypothesis was proven incorrect in a competitive binding assay. However, a dramatically lowered induction of EROD, suggesting lowered CYP1A1 activity, was seen for TCPT compared to TCDD. This finding, coupled with the observed reduction in $t_{1/2}$ for TCPT, suggests that the phenothiazine is being metabolized whereas TCDD generally is not. These results prompt further biological investigation as TCPT is explored as both a tool to probe the source dioxin toxicity as well as a being potential drug lead for the treatment of various diseases.

Chapter 4

Experimental Data

4.1 Materials and Methods

Melting points were determined using a melting point apparatus and are reported uncorrected. Infrared (IR) spectra were recorded on an FT-IR instrument from thin films on NaCl plates. Proton (^1H) and carbon (^{13}C) NMR experiments were recorded on either 400 or 500 MHz spectrometers as noted. All chemical shifts are reported as parts per million (ppm) using the solvent residual peak as the internal standard. Samples obtained in CDCl_3 were referenced to 7.27 ppm for ^1H and 77.0 ppm for ^{13}C . Samples obtained in d_6 -DMSO were referenced to 2.50 ppm for ^1H and 39.5 ppm for ^{13}C . Coupling constants (J) are reported in Hz. The multiplicities of the signals are assigned using the following abbreviations: s = singlet, d = doublet, t = triplet, q = quartet, qu = quintet, se = sextet, br = broad. Optical rotations were recorded using a polarimeter at room temperature. LRMS and HRMS were obtained using the electrospray ionization (ESI) technique.

Moisture sensitive reactions were run in flame-dried glassware under an atmosphere of nitrogen or argon unless otherwise specified. THF, CH_2Cl_2 , Et_2O and toluene were dried and deoxygenated by passing the nitrogen-purged solvents through activated alumina columns on a solvent purification system. DMF was similarly dried by passing through a column of activated 4Å molecular sieves. 5M HF/Py. solution was made by mixing HF/Py. (70% HF, 1 mL), Py. (2 mL), and THF (5 mL).¹¹⁸ All other reagents and solvents were used as received from commercial

sources unless otherwise noted. Reaction progress was monitored by thin layer chromatography (TLC, silica gel, 10 x 20 cm, 250 micron), visualizing with UV light (254 nm) and developing the plates with Hanessian's stain (blue stain). All compounds were purified by distillation or by column chromatography with 230-400 mesh silica gel as described. All compounds were concentrated using standard rotary evaporator and high-vacuum techniques. HPLC analysis was conducted on an HPLC system equipped with a photodiode array detector according to the conditions described. UPLC-MS analysis was used to determine product purities prior to biological testing where noted.

4.2 Biological Procedures

Cytotoxicity Assay. The human cancer cell lines SK-Mel-5 and SK-Mel-28 were obtained from the NCI and grown in normal RPMI 1640 culture medium containing 10% fetal bovine serum. The cells, in exponential-phase maintenance culture, were dissociated with 0.25% trypsin and harvested at 125xg for five min. Trypsin was removed and the cells were resuspended in new culture medium. The cell density was adjusted to 1×10^5 and dispensed in triplicate on 96-well plates in 50 μ L volumes. After incubation overnight at 37 °C under 5% CO₂, 50 μ L of culture medium containing various concentrations of the test compounds were added. Paclitaxel (Taxol®) and colchicine were used as positive controls. After 48 h incubation, the relative cell viability in each well was determined by using the AlamarBlue Assay Kit. Optical densities were then measured photometrically

(excitation = 530 nm, emission = 590 nm) on the plate reader. The IC₅₀ of each compound was determined by fitting the relative viability of the cells to the drug concentration using a dose-response model.

MurA Inhibition Assay.²¹² Inhibition studies were performed by assaying the activity of MurA in 100 µL of 50 mM HEPES (pH = 7.5) and two mM dithiothreitol at 20 °C when exposed to varying concentrations of the inhibitor by determining the amount of phosphate produced in the reaction using the Lanzetta reagent. The Lanzetta reagent was prepared using plastic-ware according to the literature protocol.²³⁷ All assays were started with the addition of MurA to a solution containing one mM PEP, 0.025 – five mM UNAG and various concentrations of a DMSO solution of the inhibitor. The enzyme, substrates and inhibitors were allowed to react for 3 min before addition of 800 µL of the Lanzetta reagent, which halted the reaction. Color development was stopped after five min by the addition of 100 µL of 34% (w/v) sodium citrate. Changes in optical density were measured at 660 nm using a spectrometer. The amount of phosphate produced in the reaction was determined by comparison to phosphate standards. The relative activity was determined by comparing the optical density of the enzyme solution lacking inhibitor to solutions containing inhibitors. Data evaluation was performed with SigmaPlot (SPSS Science, Chicago, IL, USA). IC₅₀ values were determined by fitting the data to the following equation:

$$v = V_{\min} + \frac{V_{\max} - V_{\min}}{1 + \left(\frac{[I]}{IC_{50}} \right)^n}$$

where v is the initial velocity, V_{\max} is the maximum velocity, V_{\min} is the minimum velocity, $[I]$ is the concentration of inhibitor and n is the hill slope.

***In Vitro* Enzyme Induction.**³²⁴ An *in vitro* ethoxyresorufin-O-deethylase (EROD) assay was conducted with H4IIEC/T3 rat hepatoma cells^{320,321} in 96-well plates according to standard procedures.³²⁵ Cells were plated at a density of about 10,000 cells/well and cultured for 72 h prior to exposure. TCPT was then added in concentrations of 0.25–256 pg/well (2.5–2560 ng/L). TCDD served as positive control in concentrations of 0.015–0.4 pg/well (0.15–4 ng/L). Plates were incubated at 37 °C and 7% CO₂ for 24, 48, and 72 h. After incubation, media was discarded and hepatocytes were exposed to 7-ethoxyresorufin for 30 min. Subsequently, the generated resorufin was quantified by detecting fluorescence at 590 nm after excitation at 535 nm. Protein content was measured with the bicinchoninic acid protein assay and absorption was measured at 540 nm.³²⁶ Cytotoxicity was determined by the resazurine assay. Data was processed using the Microsoft Excel Solver option, which was applied to yield a sigmoidal regression to a four-parameter equation. Each concentration was measured in quadruplicate and error bars depict the standard deviation.

Serum Kinetic in Rats and Guinea Pigs after Intravenous Injection. All animal studies were approved by the University of Kansas Medical Center Institutional Animal Care and Use Committee. Female Sprague-Dawley rats (228 – 264 g) and

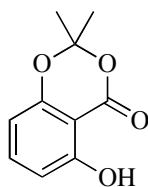
female Dunkin-Hartley guinea pigs (445 – 461 g) were purchased from Harlan, Indianapolis, Indiana, and Charles River Laboratories, Wilmington, Maine, respectively. Animal numbers were two per species, based on inherently low interindividual variability regarding kinetics. In both species, the *Vena jugularis* was cannulated by the supplier. Animals were housed in a climate-controlled facility with 12 h dark/light cycle and *ad libidum* access to feed and water. Rats were administered five mg/kg TCPT i.v. in freshly prepared acetone solution (1 mL acetone/kg), guinea pigs received 10 mg/kg TCPT i.v. in acetone (0.5 mL/kg). Blood samples were drawn in 500 μ L volumes from both species at 0.25, 0.50, 1, 2, 4, 8, 16, and 24 h, and 36 h (guinea pigs only) after dosing and stored on ice. The sample volume withdrawn was replaced by saline injections. Coagulated blood samples were centrifuged at 9,000 g at 4 °C for 16 min, and serum stored at -80 °C until analysis.

Analytics were performed by reverse-phase HPLC, using a 655A-11 liquid chromatograph, L-5000 LC controller with D-6000 interface, L-3000 photo diode array detector, and the software D-6000 HPLC Manager version 2 (Merck-Hitachi, Darmstadt, Germany). The analytical column Nukleosil C18 5 μ , 250 x 4.0 mm (VDS Optilab Chromatographie Technik GmbH, Berlin, Germany) was temperature-controlled at 25 °C and protected by an upstream Security Guard C18 ODS 4 x 3 mm (Phenomenex, Aschaffenburg, Germany). All samples were prepared online using the alkyl-diol-silica (ADS) technology developed by Boos *et al.*^{327,328} The cartridge employed was LiChroCART 25-4 LiChrospher RP-4 ADS, generously provided by Prof. Dr. Boos, Klinikum Großhadern, Ludwig-Maximilians-Universität München,

Germany and protected by an upstream inline filter ADS (Merck KGaA, Darmstadt, Germany). Solvents for analytics (water and MeOH) were of HPLC grade (Fisher Scientific, Loughborough, Leicestershire, UK). Calibration was conducted with nine concentrations from 0.01–20 µg/mL TCPT in rat serum ($R^2 = 0.99$) and five standards of 0.1–20 µg/mL in guinea pig serum ($R^2 = 0.99$). Limit of quantification was set at 0.05 µg/mL. Curve regression was performed by manual curve feathering and computational regression according to one-compartment ($C_p = C_1e^{-k_1t}$), two-compartment ($C_p = C_1e^{-k_1t} + C_2e^{-k_2t}$), and three-compartment models ($C_p = C_1e^{-k_1t} + C_2e^{-k_2t} + C_3e^{-k_3t}$) using Sigma Plot 4.0 (SPSS Inc., Chicago, Illinois), where C_p = concentration in plasma, $C_{1,2,3}$ = concentrations in compartments, $k_{-1,-2,-3}$ = compartmental rate constants, and t = time.

4.3 Experimental Procedures

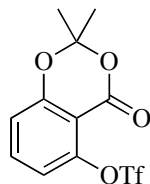
4.3.1 Chapter 1



5-Hydroxy-2,2-dimethyl-4H-benzo[d][1,3]dioxin-4-one (116). 2,6-

Dihydroxybenzoic acid **113** (10.0 g, 64.9 mmol) and DMAP (0.396 g, 3.25 mmol) were dissolved in anhydrous DME (22.0 mL) in a three-neck flask equipped with an internal thermometer. To this solution was added acetone (6.20 mL, 84.4 mL),

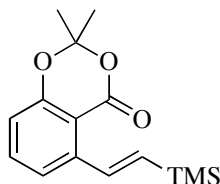
followed by dropwise addition of SOCl_2 (6.60 mL, 90.8 mmol) from a plastic needle over a one h period, ensuring that the internal reaction temperature never rose higher than 30 °C. After addition of the SOCl_2 , the reaction was stirred for one h then concentrated by blowing a stream of air into the flask. The crude, red material was then subjected to flash column chromatography (hexanes/EtOAc, 100:0 – 85:15) to yield 9.03 g of an off-white solid (72%). TLC (hexane/EtOAc, 80:20): $R_f = 0.60$. Spectral data was identical to literature reported values:¹⁴³ ^1H NMR (400 MHz, CDCl_3) δ 10.34 (s, 1H), 7.41 (t, $J = 8.2$ Hz, 1H), 6.63 (dd, $J = 8.2, 0.8$ Hz, 1H), 6.44 (dd, $J = 8.2, 0.8$ Hz, 1H), 1.75 (s, 6H).



2,2-Dimethyl-4-oxo-4H-benzo[d][1,3]dioxin-5-yl Trifluoromethanesulfonate (63).

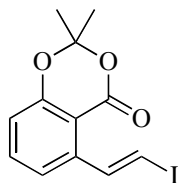
The acetonide phenol **116** (865 mg, 4.45 mmol) was dissolved in CH_2Cl_2 (18.0 mL) and cooled to 0 °C. To this solution was added Et_3N (0.750 mL, 5.34 mmol) dropwise followed by a slow, dropwise addition of Tf_2O (0.900 mL, 5.34 mmol). After stirring for 45 min, the volatiles were removed by rotary evaporation and the crude material was subjected to flash column chromatography (hexanes/EtOAc, 80:20) to yield 1.29 g of a pale yellow solid (89%). TLC (hexane/EtOAc, 80:20): $R_f = 0.30$. Spectral data was identical to literature reported values:¹²³ ^1H NMR (400 MHz,

CDCl₃) δ 7.65 (t, J = 8.2 Hz, 1H), 7.14 (dd, J = 8.2, 1.0 Hz, 1H), 7.02 (d, J = 8.2 Hz, 1H), 1.75 (s, 6H).

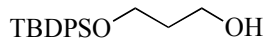


(E)-2,2-Dimethyl-5-(2-(trimethylsilyl)vinyl)-4H-benzo[d][1,3]dioxin-4-one (115).

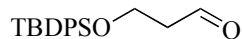
To a DMSO (246 mL) solution of the aryl triflate **63** (8.02 g, 24.6 mmol) was added Pd(OAc)₂ (0.55 g, 2.46 mmol), vinyl(trimethyl)silane (10.7 mL, 73.8 mmol), and triethylamine (10.3 mL, 73.8 mmol). The mixture was heated at 55 °C for 2.5 h, then cooled to room temperature. The reaction was diluted with water and extracted with 50:50 hexanes/Et₂O (3x). The combined organic extracts were washed with brine, dried over MgSO₄ and purified via flash column chromatography (hexanes/EtOAc, 100:0 – 90:10) to provide 5.76 g of the desired compound as a white powder (85%). TLC (hexane/EtOAc, 80:20): R_f = 0.65; IR (thin film) ν_{\max} = 2999, 2955, 1739, 1603, 1573, 1389, 1317, 1277, 1248, 1204, 1044, 867, 842 cm⁻¹; ¹H NMR (400 MHz, CDCl₃) δ 7.93 (d, J = 19 Hz, 1H), 7.45 (dt, J = 8.0, 0.8 Hz, 1H), 7.31 (d, J = 8.0 Hz, 1H), 6.86 (dd, J = 8.0, 0.8 Hz, 1H), 6.47 (d, J = 19 Hz, 1H), 1.71 (s, 6H), 0.19 (s, 9H); ¹³C NMR (100 MHz, CDCl₃) δ 160.2, 156.6, 143.3, 141.8, 135.0, 134.9, 121.3, 116.3, 110.8, 105.2, 25.6, -1.3; HRMS (ESI⁺), m/z calcd for C₁₅H₂₁O₃Si: 277.1260 (M+H); found, 277.1257; melting point 59-61 °C.



(E)-5-(2-Iodovinyl)-2,2-dimethyl-4H-benzo[d][1,3]dioxin-4-one (108). The vinyl silane **115** (1.00 g, 3.62 mmol) was dissolved in anhydrous MeCN (36.2 mL) and the flask wrapped in aluminum foil to prevent light exposure. *N*-Iodosuccinimide (4.00 g, 18.1 mmol) was added in one portion and the reaction stirred for eight h at room temperature. The reaction was diluted with a saturated solution of Na₂SO₃ and extracted with EtOAc (3x). The combined organic extracts were washed with brine, dried over MgSO₄ and purified via flash column chromatography (hexanes/EtOAc, 100:0 – 90:10) to provide 1.09 g of the desired compound as a white powder (91%). TLC (hexane/EtOAc, 80:20): R_f = 0.50; IR (thin film) ν_{\max} = 3059, 2996, 1738, 1606, 1571, 1477, 1319, 1268, 1230, 1211, 1047, 941, 818 cm⁻¹; ¹H NMR (400 MHz, CDCl₃) δ 8.45 (d, *J* = 15 Hz, 1H), 7.47 (t, *J* = 8.0 Hz, 1H), 7.12 (d, *J* = 7.8 Hz, 1H), 6.92 (dd, *J* = 8.2, 0.7 Hz, 1H), 6.87 (d, *J* = 15 Hz, 1H), 1.72 (s, 6H); ¹³C NMR (100 MHz, CDCl₃) δ 160.0, 156.7, 143.1, 141.3, 135.4, 121.5, 117.2, 110.0, 105.5, 80.9, 25.6; HRMS (ESI⁺), *m/z* calcd for C₁₂H₁₂O₃I: 330.9831 (M+H); found, 330.9832; melting point 119-121 °C.

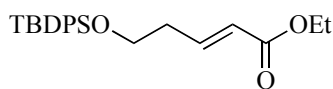


3-(*tert*-Butyldiphenylsilyloxy)propan-1-ol (119). To a rapidly stirring suspension of NaH (2.14 g, 53.5 mmol, 60% suspension in mineral oil) in anhydrous THF (107 mL) at room temperature was slowly added 1,3-propanediol (**118**) (3.87 mL, 53.5 mmol). After stirring for approximately 45 min, during which time a substantial amount of white precipitate had formed, TBDPSCl (14.0 mL, 54.6 mmol) was slowly added. Vigorous stirring continued for two h, after which time the solution was poured into Et₂O, washed with 10% K₂CO₃ solution, water and brine. The ethereal layer was dried over MgSO₄, concentrated and purified by flash column chromatography (Hexanes:EtOAc 100:0 – 70:30) to yield 15.8 g of the title compound (94%). Spectral data was identical to literature reported values:¹⁴⁹ ¹H NMR (400 MHz, CDCl₃) δ 7.68-7.66 (m, 4H), 7.46-7.38 (m, 6H), 3.87-3.83 (m, 4H), 2.36 (t, *J* = 5.6 Hz, 1H), 1.81 (qu, *J* = 5.6 Hz, 2H), 1.05 (s, 9H).

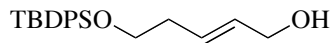


3-(*tert*-Butyldiphenylsilyloxy)propanal (120). Alcohol **119** (4.70 g, 14.9 mmol) was dissolved in CH₂Cl₂ (140 mL) at room temperature and Dess-Martin periodinane (**121a**, prepared according to Ireland¹³²) (9.50 g, 22.4 mmol) added in one portion. After 30 min of stirring, the reaction mixture was filtered through a plug of silica gel, eluted with hexanes/EtOAc (80:20) to give 4.4 g of the crude aldehyde (94%) that was used without further purification in subsequent reactions. Spectral data was

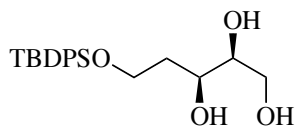
identical to literature reported values:¹⁴⁹ ¹H NMR (400 MHz, CDCl₃) δ 9.83 (t, *J* = 2.3 Hz, 1H), 7.65-7.63 (m, 4H), 7.45-7.37 (m, 6H), 4.03 (t, *J* = 6.0 Hz, 2H), 2.60 (td, *J* = 6.0, 2.3 Hz, 2H), 1.05 (s, 9H).



(*E*)-Ethyl 5-(*tert*-Butyldiphenylsilyloxy)pent-2-enoate (121). To a room temperature solution of triethylphosphonoacetate (18.3mL, 91.2 mmol) in anhydrous THF (560 mL) was added MeMgBr (65.0 mL, 91.2 mmol, 1.4M in 3:1 toluene/THF) dropwise. This mixture was stirred for 15 min, after which time a solution of aldehyde **120** (29.6 g, 94.7 mmol in 400 mL THF) was added dropwise over the course of 30 min. This mixture was heated at reflux for one h, then cooled to room temperature and quenched with an aqueous solution of NH₄Cl. The mixture was extracted with Et₂O (3x). The combined organic extracts were washed with brine, dried over MgSO₄ and concentrated. Purification by flash column chromatography (hexanes/Et₂O 100:0 – 95:5) yielded 24.0 g of the pure *trans*-ester (65%). Crude NMR revealed 40:1 *E:Z* enoate ratio. Spectral data was identical to literature reported values:¹⁴⁹ ¹H NMR (400 MHz, CDCl₃) δ 7.71-7.64 (m, 4H), 7.45-7.35 (m, 6H), 6.98 (td, *J* = 16, 7.2 Hz, 1H), 5.85 (d, *J* = 16 Hz, 1H), 4.18 (q, *J* = 7.2 Hz, 2H), 3.75 (q, *J* = 7.2 Hz, 2H), 2.43 (t, *J* = 6.4 Hz, 2H), 1.28 (t, 7.2 Hz, 1H), 1.05 (s, 9H).

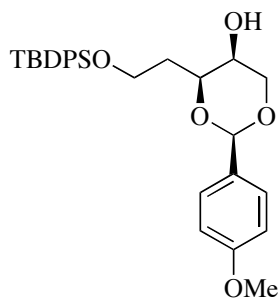


(E)-5-(tert-Butyldiphenylsilyloxy)pent-2-en-1-ol (122). The ester **121** (13.7 g, 35.8 mmol) was dissolved in anhydrous toluene (143 mL) and cooled to -60 °C. DIBAL (80 mL, 80.0 mmol, 1M in hexanes) was added dropwise over 30 min, after which stirring continued for two h followed by warming to 0 °C and additional stirring for two h. The reaction was quenched by the addition of EtOAc followed by water (32 mL) with stirring for 15 min, 2N NaOH solution (32 mL) with stirring for 15 min, and water (8 mL) with stirring for 15 min. The complexed aluminates were sequestered by the slow addition of solid MgSO₄ (*Caution: reaction is exothermic*) with stirring for two h at room temperature. The solids were filtered off and rinsed with EtOAc. The crude material was subjected to flash column chromatography (hexanes/EtOAc, 80:20) to yield 11.2 g of the desired allylic alcohol **1** as a yellow oil (92%): TLC (hexanes/EtOAc, 80:20): R_f = 0.15; Spectral data was identical to literature reported values:¹⁴⁹ ¹H NMR (400 MHz, CDCl₃) δ 7.68-7.65 (m, 4H), 7.44-7.35 (m, 6H), 5.67 (m, 2H), 4.09-4.05 (m, 2H), 3.71 (t, *J* = 6.4 Hz, 2H), 2.33-2.28 (m, 2H), 1.29-1.15 (m, 1H), 1.05 (s, 9H).

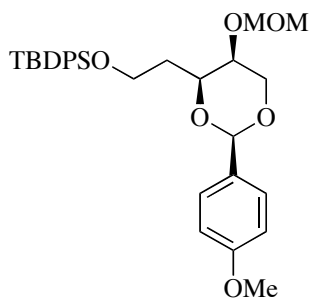


(2S,3S)-5-(tert-Butyldiphenylsilyloxy)pentane-1,2,3-triol (123). AD mix-α (28.0 g) was suspended in a vigorously stirred water/^tBuOH mixture (1:1, 112 mL total

volume) at room temperature. MeSO₂NH₂ (2.66 g, 22.4 mmol) was added in one portion and the resulting heterogeneous mixture was stirred until homogenous, after which time the solution was cooled to 0 °C. The olefin **122** (7.62 g, 22.4 mmol) was dissolved in ^tBuOH (80 mL with two 10 mL flask rinses) and added to the reagent solution. Water (100 mL) was then added and the solution stirred in the refrigerator (2-4 °C) for 24 h. The reaction was quenched with solid sodium sulfite (28.0 g) and stirred for one h, after which time the reaction was extracted with EtOAc (3x). The combined organic extracts were washed with brine, dried over MgSO₄ and purified via flash column chromatography (hexanes/EtOAc, 70:30 – 50:50) to give 7.99 g of the triol as an opaque amorphous solid (95%): TLC (hexane/EtOAc, 50:50): R_f = 0.10; [α]_D²⁵ = +3.56 (*c* = 1.01, CHCl₃); IR (thin film) ν_{max} = 3360 (br), 2954, 2930, 2887, 1632, 1427, 1321, 1138, 1111, 1090, 702 cm⁻¹; ¹H NMR (400 MHz, CDCl₃) δ 7.68-7.66 (m, 4H), 7.47-7.38 (m, 6H), 4.02-3.98 (m, 1H), 3.92-3.88 (m, 2H), 3.75-3.73 (m, 2H), 3.69 (d, *J* = 2.8 Hz, 1H), 3.58-3.54 (m, 1H), 2.92 (d, *J* = 6.4 Hz, 1H), 2.31 (t, *J* = 6.0 Hz, 1H), 1.99-1.90 (m, 1H), 1.71-1.65 (m, 1H), 1.06 (s, 9H); ¹³C NMR (100 MHz, CDCl₃) δ 135.5, 135.5, 130.0, 130.0, 127.9, 73.7, 72.9, 64.8, 63.0, 35.0, 26.8; HRMS (ESI⁺⁺), *m/z* calcd for C₂₁H₃₁O₄Si (M+H): 375.1992; found, 375.1989.

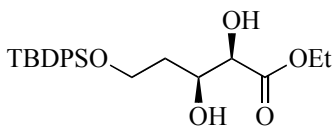


(2*R*,4*S*,5*S*)-4-(2-(*tert*-Butyldiphenylsilyloxy)ethyl)-2-(4-methoxyphenyl)-1,3-dioxan-5-ol (124). Triol **123** (4.30 g, 11.6 mmol) was dissolved in MeCN (232 mL) and stirred at room temperature. PPTS (1.40 g, 5.80 mmol) was added in one portion followed by *p*-methoxybenzyl-dimethyl acetal (2.00 mL, 13.9 mmol). After stirring for 15 min, the reaction mixture was poured into water, extracted with Et₂O (3x) and the combined organic extracts washed with brine, dried over MgSO₄ and concentrated. The product mixture was subjected to flash column chromatography (hexanes/EtOAc, 90:10 – 75:25) and only pure fractions containing the desired product were collected for use in the subsequent reaction, resulting in 1.20 g of the acetal as a colorless oil (21%). The remaining mixed fractions were collected (3.02 g, 74% total yield) allowed to remain on the benchtop for 2 weeks, and then subjected to flash column chromatography as before. This recycling process could be repeated many times over the course of 6-12 months. A clear oil: IR (thin film) ν_{\max} 3437 (br), 2957, 2930, 2856, 1614, 1518, 1427, 1385, 1250, 1111, 1086, 1034 cm⁻¹; HRMS (ESI⁺), m/z calcd for C₂₉H₃₆O₅SiNa: 515.2230 (M+Na); found, 515.2233.



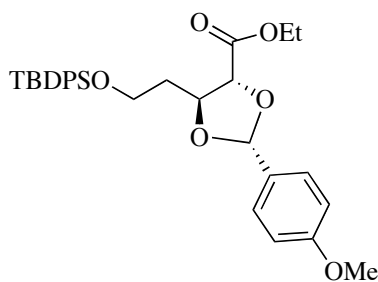
***tert*-Butyl-(2-((2*R*,4*S*,5*S*)-5-(methoxymethoxy)-2-(4-methoxyphenyl)-1,3-dioxan-4-yl)ethoxy)diphenylsilane (127).** MOMCl (0.081 mL, 0.64 mmol) was added to a 0 °C pre-cooled solution of the acetal **124** (52 mg, 0.11 mmol) in DIPEA (0.53 mL) and stirred overnight with gradual warming to room temperature. After stirring for 15 h, EtOAc was added to the solution and washed with water. The aqueous layer was extracted with EtOAc (2x), and the combined organic extracts were washed with brine, dried over MgSO₄ and subjected to flash column chromatography (hexanes/EtOAc 90:10 – 80:20) to give 52 mg of the title compound (91%) as a bright yellow oil: TLC (hexane/EtOAc, 80:20): R_f = 0.25; [α]_D²⁵ = +0.900 (*c* = 2.03, CHCl₃); IR (thin film) ν_{max} = 2957, 2932, 2887, 2856, 1616, 1518, 1427, 1250, 1151, 1095, 1036, 702 cm⁻¹; ¹H NMR (400 MHz, CDCl₃) δ 7.68-7.63 (m, 4H), 7.42-7.37 (m, 6H), 7.32-7.28 (m, 2H), 6.86 (d, *J* = 8.8 Hz, 2H), 5.51 (s, 1H), 4.82 (d, *J* = 7.0 Hz, 1H), 4.67 (d, *J* = 7.0 Hz, 1H), 4.37 (dd, *J* = 12, 1.3 Hz, 1H), 4.25 (m, 1H), 3.97 (d, *J* = 9.0 Hz, 1H), 3.96-3.90 (m, 1H), 3.81-3.78 (m, 1H), 3.80 (s, 3H), 3.40 (s, 4H), 2.15-2.08 (m, 1H), 1.89-1.81 (m, 1H), 1.06 (s, 9H); ¹³C NMR (100 MHz, CDCl₃) δ 159.8, 135.5, 135.5, 133.7, 133.6, 130.8, 129.6, 129.6, 127.7, 127.6, 127.4, 113.3,

101.1, 95.4, 75.5, 70.4, 69.4, 59.4, 55.8, 55.3, 34.3, 26.9, 19.3; HRMS (ESI⁺), *m/z* calcd for C₃₁H₄₀O₆SiNa: 559.2492 (M+Na); found, 559.2480.



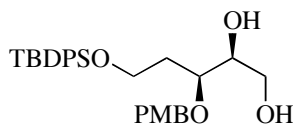
(2*R*,3*S*)-Ethyl 5-(*tert*-Butyldiphenylsilyloxy)-2,3-dihydroxypentanoate (112). AD mix- α (20.3 g) was suspended in a vigorously stirred water/^tBuOH mixture (1:1, 80 mL total volume) at room temperature. MeSO₂NH₂ (1.61 g, 16.9 mmol) was added in one portion and the resulting heterogeneous mixture was stirred until homogenous, after which time the solution was cooled to 0 °C. The olefin **121** (6.48 g, 16.9 mmol) was dissolved in ^tBuOH (30.0 mL with two 8.00 mL flask rinses) and added to the reagent solution. Water (40.0 mL) was then added and the solution stirred in the refrigerator (2-4 °C) for 15 h. The reaction was quenched with solid sodium sulfite (20.3 g) and stirred for one h, after which time the reaction was extracted with EtOAc (3x). The combined organic extracts were washed with brine, dried over MgSO₄ and purified via flash column chromatography (hexanes/EtOAc, 80:20 – 70:30) to give 6.87 g of the diol ester as a yellow oil (97%): TLC (hexane/EtOAc, 70:30): R_f = 0.25; $[\alpha]_D^{25} = -10.8$ (*c* = 1.09, CHCl₃); IR (thin film) $\nu_{\max} = 3475$ (br), 1737, 1428, 1212, 1112, 1028, 703 cm⁻¹; ¹H NMR (400 MHz, CDCl₃) δ 7.68-7.66 (m, 4H), 7.44-7.37 (m, 6H), 4.30 (q, *J* = 7.2 Hz, 2H), 4.29-4.24 (m, 1H), 4.08 (dd, *J* = 6.8, 2.0 Hz, 1H), 3.93-3.83 (m, 2H), 3.12 (d, *J* = 6.8 Hz, 1H), 2.96 (d, 5.7 Hz, 1H), 2.04-1.95 (m, 1H), 1.80-1.73 (m, 1H), 1.33 (t, *J* = 7.2 Hz, 3H), 1.05 (s, 9H); ¹³C NMR (100 MHz,

CDCl₃) δ 173.4, 135.7, 135.7, 133.3, 133.1, 130.0, 130.0, 127.9, 73.7, 71.8, 62.4, 62.1, 35.5, 27.0, 19.2, 14.3; HRMS (ESI⁺), m/z calcd for C₂₃H₃₃O₅Si (M+H): 417.2097; found, 417.2086; Chiral HPLC analysis (Diacel Chiracel OD (250 mm x 4.6 mm), 5% *i*PrOH in hexanes, one mL/min, 254 nm, major isomer, t_R = 14.9 min, minor isomer, t_R = 12.2 min, *e.r.* = 89:11).



(4*R*,5*S*)-Ethyl 5-(2-(*tert*-Butyldiphenylsilyloxy)ethyl)-2-(4-methoxyphenyl)-1,3-dioxolane-4-carboxylate (129). Diol ester **112** (14.1 g, 33.8 mmol) was dissolved in MeCN (169 mL) at room temperature. To this solution was added PPTS (4.25 g, 16.9 mmol) then *p*-methoxybenzyl-dimethyl acetal (13.0 mL, 77.8 mmol). The mixture was stirred for 45 min, after which time the reaction was quenched with water and extracted with Et₂O (3x). The combined organic extracts were washed with brine, dried over MgSO₄ and concentrated. The crude material was partially purified via flash column chromatography (hexanes/EtOAc, 100:0 – 85:15). The mixed fractions containing the desired acetal **129** and *p*-methoxybenzaldehyde were collected, re-dissolved in CH₂Cl₂ and stirred with PS-TsNHNH₂ until no *p*-methoxybenzaldehyde was detected by TLC analysis. The polystyrene beads were removed by vacuum filtration and washed with CH₂Cl₂. Following concentration, 16.8 g of the desired

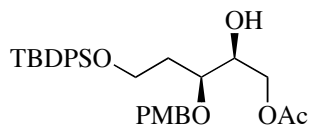
acetal ester was collected as a bright yellow oil (93%): TLC (hexanes/EtOAc, 70:30): $R_f = 0.65$; $[\alpha]_D^{25} = -7.4$ ($c = 0.89$, CHCl_3); IR (thin film) $\nu_{\text{max}} = 1735, 1615, 1250, 1112, 1034 \text{ cm}^{-1}$; $^1\text{H NMR}$ (400 MHz, CDCl_3) δ 7.68-7.65 (m, 4H), 7.50 (d, $J = 7.6$ Hz, 1H), 7.42-7.35 (m, 7H), 6.92-6.88 (m, 2H), 5.95 (s, 1H), 4.63-4.61 (m, 0.5H), 4.43-4.38 (m, 1.5H), 4.30-4.22 (m, 2H), 3.90-3.85 (m, 2H), 3.81 (s, 3H), 2.14-2.12 (m, 0.5H), 2.05-1.99 (m, 1.5H), 1.32-1.27 (m, 3H), 1.04 (d, $J = 3.6$ Hz, 9H); $^{13}\text{C NMR}$ (100 MHz, CDCl_3) δ 171.1, 160.6, 135.5, 133.6, 133.5, 129.6, 128.5, 128.3, 127.6, 113.7, 104.7, 104.2, 79.2, 78.6, 77.8, 77.1, 61.4, 60.2, 60.1, 55.3, 36.5, 35.8, 26.8, 26.8, 19.2, 14.2, 14.2; HRMS (ESI^+), m/z calcd for $\text{C}_{31}\text{H}_{39}\text{O}_6\text{Si}$: 535.2516 (M+H); found, 535.2502.



(2*S*,3*S*)-5-(*tert*-Butyldiphenylsilyloxy)-3-(4-methoxybenzyloxy)pentane-1,2-diol

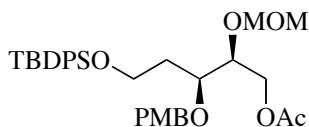
(130). The acetal ester **129** (6.20 g, 11.6 mmol) was dissolved in anhydrous CH_2Cl_2 (116 mL) and cooled to -78 °C. DIBAL (81 mL, 81.0 mmol, 1M in hexanes) was added dropwise over 30 min, after which stirring continued for three h followed by warming to 0 °C and additional stirring for two h. The reaction was quenched by the addition of EtOAc followed by water (32 mL) with stirring for 15 min, 2N NaOH solution (32 mL) with stirring for 15 min, and water (8 mL) with stirring for 15 min. The complexed aluminates were sequestered by the slow addition of solid MgSO_4 (*Caution: reaction is exothermic*) with stirring for two h at room temperature. The

solids were filtered off and rinsed with EtOAc. The crude material was subjected to flash column chromatography (hexanes/EtOAc, 80:20 – 50:50) to yield 3.98 g of the desired diol **130** as a yellow oil (70%): TLC (hexanes/EtOAc, 50:50): $R_f = 0.25$; $[\alpha]_D^{25} = +22.7$ ($c = 1.05$, CHCl_3); IR (thin film) $\nu_{\text{max}} = 3430$ (br), 1612, 1248, 1111, 1023 cm^{-1} ; $^1\text{H NMR}$ (400 MHz, CDCl_3) δ 7.67-7.64 (m, 4H), 7.45-7.36 (m, 6H), 7.17 (dd, $J = 6.8, 2.0$ Hz, 2H), 6.84 (dd, $J = 6.8, 2.0$ Hz, 2H), 4.55 (d, $J = 11$ Hz, 1H), 4.37 (d, $J = 11$ Hz, 1H), 3.79 (m, 5H), 3.70 (dd, $J = 10, 6.0$ Hz, 1H), 3.62 (br m, 3H), 2.75 (br, 1H), 2.14 (br, 1H), 1.86 (m, 2H), 1.06 (s, 9H); $^{13}\text{C NMR}$ (100 MHz, CDCl_3) δ 159.4, 135.6, 133.5, 133.4, 130.1, 129.8, 129.6, 127.7, 113.9, 72.9, 72.0, 64.1, 60.2, 55.3, 33.2, 26.9, 19.1; HRMS (ESI^+), m/z calcd for $\text{C}_{29}\text{H}_{39}\text{O}_5\text{Si}$ ($\text{M}+\text{H}$): 495.2567; found, 495.2560.



(2*S*,3*S*)-5-(*tert*-Butyldiphenylsilyloxy)-2-hydroxy-3-(4-methoxybenzyloxy)pentyl Ethanoate (131**).** The diol **130** (1.63 g, 3.29 mmol) was dissolved in freshly distilled 2,6-lutidine (16.5 mL) and cooled to 0 °C. Freshly distilled AcCl (0.258 mL, 3.62 mmol) was added dropwise. After 30 min, EtOAc and 1N HCl were added and the solution stirred for one h with warming to room temperature. The organic layer was washed with 1N HCl solution (1x), then brine and dried over MgSO_4 . The crude material was purified by flash column chromatography (hexanes/EtOAc, 90:10 – 70:30) to yield 1.29 g of the title compound as a bright yellow oil (89%): TLC

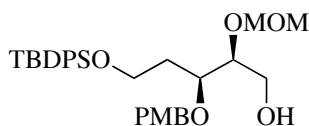
(hexanes/EtOAc, 70:30): $R_f = 0.25$; $[\alpha]_D^{25} = +13.3$ ($c = 1.25$, CHCl_3); IR (thin film) $\nu_{\text{max}} = 3467$ (br), 1740, 1612, 1250, 1112, 1023 cm^{-1} ; ^1H NMR (400 MHz, CDCl_3) δ 7.67-7.64 (m, 4H), 7.45-7.36 (m, 6H), 7.18 (d, $J = 8.4$ Hz, 2H), 6.84 (d, $J = 8.4$ Hz, 2H), 4.55 (d, $J = 11$ Hz, 1H), 4.42 (d, $J = 11$ Hz, 1H), 4.13 (d, $J = 5.6$ Hz, 2H), 3.83-3.77 (m, 6H), 3.76-3.72 (m, 1H), 2.60 (d, $J = 6.4$ Hz, 1H), 2.05 (s, 3H), 1.94-1.79 (m, 2H), 1.06 (s, 9H); ^{13}C NMR (100 MHz, CDCl_3) δ 171.0, 159.4, 135.6, 135.5, 133.4, 130.1, 129.8, 129.6, 127.7, 113.9, 75.3, 72.3, 71.1, 65.7, 60.1, 55.3, 33.3, 26.9, 20.9, 19.2; HRMS (ESI^+), m/z calcd for $\text{C}_{31}\text{H}_{41}\text{O}_6\text{Si}$: 537.2672 (M+H); found, 537.2665.



(2S,3S)-5-(tert-Butyldiphenylsilyloxy)-3-(4-methoxybenzyloxy)-2-

(methoxymethoxy)pentyl Ethanoate (132). The secondary alcohol **131** was dissolved in freshly distilled DIPEA and cooled to 0 °C. MOMCl was added and the reaction stirred for 15 h with gradual warming to room temperature. The reaction was diluted with water, extracted with EtOAc (3x). The combined organic extracts were washed with brine, dried over MgSO_4 and purified by flash column chromatography (hexanes/EtOAc, 80:20) to collect the title compound as a colorless oil (*Note: in practice, the crude material was taken on to the acetate hydrolysis step without column purification*): TLC (hexanes/EtOAc, 70:30): $R_f = 0.70$; $[\alpha]_D^{25} = -17.2$ ($c = 2.00$, CHCl_3); IR (thin film) $\nu_{\text{max}} = 2931$, 1743, 1247, 1155, 1110, 1036 cm^{-1} ; ^1H

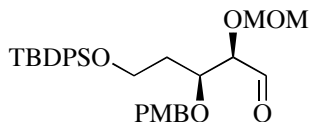
NMR (400 MHz, CDCl₃) δ 7.67-7.63 (m, 4H), 7.44-7.34 (m, 6H), 7.18 (td, *J* = 8.4, 2.0 Hz, 2H), 6.82 (td, *J* = 8.4, 2.0 Hz, 2H), 4.69 (dd, *J* = 16, 6.8 Hz, 2H), 4.51 (dd, *J* = 29, 11 Hz, 2H), 4.29 (dd, *J* = 12, 3.6 Hz, 1H), 4.13 (dd, *J* = 12, 6.8 Hz, 1H), 3.94-3.86 (m, 2H), 3.82-3.74 (m, 5H), 3.36 (s, 3H), 2.03 (s, 3H), 1.96-1.87 (m, 1H), 1.72-1.4(m, 1H), 1.05 (s, 9H); ¹³C NMR (100 MHz, CDCl₃) δ 170.8, 159.2, 135.6, 133.7, 130.4, 129.7, 129.6, 127.7, 127.7, 113.8, 96.7, 75.8, 74.5, 72.5, 64.0, 60.2, 55.7, 55.3, 32.9, 26.9, 20.9, 19.2; HRMS (ESI⁺), *m/z* calcd for C₃₃H₄₅O₇Si: 581.2935 (M+H); found, 581.2938.



(2*S*,3*S*)-5-(*tert*-Butyldiphenylsilyloxy)-3-(4-methoxybenzyloxy)-2-

(methoxymethoxy)pentan-1-ol (128). To a solution of the protected tetrol **132** (1.48 g, 2.55 mmol) in MeOH (26 mL) was added K₂CO₃ (3.5 g, 25.5 mmol) at room temperature. The mixture was stirred for two h, diluted with water and extracted with EtOAc. The combined organic extracts were washed with brine and dried over MgSO₄ to yield 1.28 g (2.37 mmol) of the title compound as a colorless oil (93%). *Alternatively:* Acetonide **127** (788 mg, 1.47 mmol) was dissolved in 29 mL of CH₂Cl₂ and cooled to -78 °C. DIBAL (4.40 mL, 4.40 mmol, 1M in hexanes) was added dropwise over 30 min with vigorous stirring. After one h, the solution was warmed to -40 °C and stirred at this temperature for six h. EtOAc was then added to the reaction mixture, the temperature raised to 0 °C, and water (1.8 mL) was added with stirring

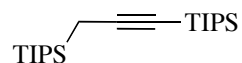
for 15 min, followed by addition of 2N NaOH solution (1.8 mL) with stirring for 15 min, and finally addition of water (0.44 mL) with stirring for 15 min. The complexed aluminates were sequestered by the slow addition of solid MgSO₄ (*Caution: reaction is exothermic*) with stirring for at least two h at room temperature. The solids were filtered off and rinsed with EtOAc. The crude material was subjected to flash column chromatography (hexanes/EtOAc, 80:20 – 70:30) to yield 720 mg of the desired diol **1** as a colorless oil (91%): TLC (hexanes/EtOAc, 70:30): R_f = 0.30; [α]_D²⁵ = -12.0 (*c* = 1.00, CHCl₃); IR (thin film) ν_{max} = 3470 (br), 2955, 2932, 1612, 1514, 1248, 1109, 1036, 702 cm⁻¹; ¹H NMR (400 MHz, CDCl₃) δ 7.67-7.63 (m, 4H), 7.43-7.35 (m, 6H), 7.17 (dt, *J* = 8.4, 2.0 Hz, 2H), 6.82 (dt, *J* = 8.4, 2.0 Hz, 2H), 4.73 (d, *J* = 6.8 Hz, 1H), 4.64 (d, *J* = 6.8 Hz, 1H), 4.48 (dt, *J* = 11, 5.2 Hz, 2H), 3.85-3.80 (m, 1H), 3.78 (s, 3H), 3.78-3.70 (m, 2H), 3.69-3.62 (m, 3H), 3.40 (s, 3H), 2.89 (br m, 1H), 1.92-1.85 (m, 1H), 1.75-1.67 (m, 1H), 1.05 (s, 9H); ¹³C NMR (100 MHz, CDCl₃) δ 157.9, 134.2, 132.3, 132.3, 128.9, 128.3, 126.3, 112.4, 96.0, 79.9, 74.3, 71.0, 61.4, 58.9, 54.4, 53.8, 31.5, 25.5, 17.8; HRMS (ESI⁺), *m/z* calcd for C₃₁H₄₃O₆Si: 539.2829 (M+H); found, 539.2806.



(2*R*,3*S*)-5-(*tert*-Butyldiphenylsilyloxy)-3-(4-methoxybenzyloxy)-2-

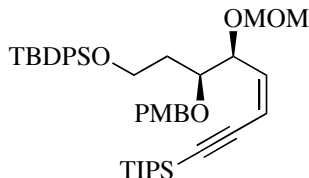
(methoxymethoxy)pentanal (111). To a solution of the alcohol **128** (813 mg, 1.51 mmol) in DCM (15 mL) was added Dess-Martin periodinane (1.30 g, 3.02 mmol) at

room temperature. The reaction was stirred for 20 min, diluted with EtOAc, washed with saturated NaHCO₃ solution (2x), washed with brine, dried over MgSO₄ and purified by flash column chromatography (hexanes/EtOAc, 80:20) to collect 715 mg of the title compound as a pale yellow oil (88%): TLC (hexanes/EtOAc, 70:30): R_f = 0.50; [α]_D²⁵ = +1.60 (*c* = 1.20, CHCl₃); IR (thin film) ν_{max} = 2954, 2932, 2889, 2856, 1734, 1612, 1514, 1248, 1111, 1038, 702 cm⁻¹; ¹H NMR (400 MHz, CDCl₃) δ 9.67 (s, 1H), 7.65-7.62 (m, 4H), 7.45-7.36 (m, 6H), 7.16 (d, *J* = 8.4 Hz, 2H), 6.82 (d, *J* = 8.4 Hz, 2H), 4.72 (d, *J* = 6.8 Hz, 1H), 4.65(d, *J* = 6.8 Hz, 1H), 4.47 (s, 2H), 4.13-4.11 (br m, 1H), 3.97 (d, *J* = 4.0 Hz, 1H), 3.82-3.76 (m, 2H), 3.78 (s, 3H), 3.70 (se, *J* = 5.2 Hz, 1H), 3.37 (s, 3H), 1.95-1.81 (m, 2H), 1.05 (s, 9H); ¹³C NMR (100 MHz, CDCl₃) δ 202.7, 159.3, 135.6, 133.6, 133.5, 129.9, 129.7, 127.7, 113.8, 97.2, 83.1, 75.4, 72.5, 60.0, 56.2, 55.3, 33.3, 26.9, 19.2; HRMS (ESI⁺), *m/z* calcd for C₃₁H₄₀O₆SiK: 575.2231 (M+K); found, 575.2249.



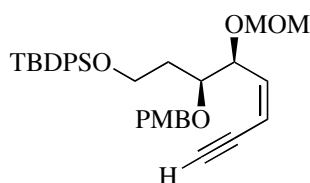
Prop-1-yne-1,3-diylbis(triisopropylsilane) (110). 1-(triisopropyl)-1-propyne (6.10 mL, 25.5 mmol) was dissolved in anhydrous THF (51 mL) and cooled to -20 °C. *n*BuLi (15.9 mL, 25.5 mmol, 1.6 M in hexanes) was added dropwise and stirring continued for 20-30 min, then the anion solution cooled to -78 °C. Triisopropyl trifluoromethylsulfonate (7.16 mL, 26.7 mmol) was added dropwise and the solution stirred for one h at -78 °C followed by warming to room temperature with stirring for two h. The THF was removed by rotary evaporation and the crude residue distilled

under reduced pressure (100 °C), collecting the distillate at 100 °C as a clear oil. Spectral data was identical to literature reported values:¹⁴⁴ ¹H NMR (400 MHz, CDCl₃) δ 1.59 (s, 2H), 1.19-1.11 (m, 6H), 1.10-0.84 (m, 36H); boiling point 130-135 °C (reduced pressure).



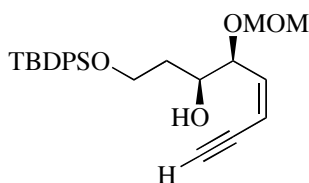
(5*S*,6*S*)-6-(4-Methoxybenzyloxy)-11,11-dimethyl-10,10-diphenyl-5-((*Z*)-4-(triisopropylsilyl)but-1-en-3-ynyl)-2,4,9-trioxa-10-siladodecane (133). Prop-1-yne-1,3-diylbis(triisopropylsilane) **110** (444 mg, 1.26 mmol) was dissolved in anhydrous THF (10 mL) and cooled to -20 °C. *n*BuLi (0.788 mL, 1.26 mmol, 1.6M in hexanes) was added dropwise over five min, stirred for 30 min, then cooled to -78 °C. The aldehyde **111** (390 mg, 0.727 mmol), as a solution in THF (7 mL), was added dropwise to the anion solution over 1.5 h. After additional stirring for 30 min, the reaction was quenched at -78 °C with saturated NH₄Cl solution and warmed to room temperature. Following extraction with EtOAc (3x), washing of combined organic extracts with brine, and drying over MgSO₄, the crude material was purified via flash column chromatography (hexanes/EtOAc, 100:0 – 90:10) to yield 352 mg of a yellow oil (68%). The enyne product was isolated as an inseparable 5:1 *Z*:*E* olefin ratio, as determined by ¹H NMR: TLC (hexanes/EtOAc, 80:20): R_f = 0.80; IR (thin film) ν_{\max} = 2943, 2865, 2147, 1613, 1514, 1249, 1112, 1036, 702 cm⁻¹; ¹H NMR

(400 MHz, CDCl₃) δ 7.59-7.56 (m, 4H), 7.36-7.27 (m, 6H), 7.09 (d, $J = 8.6$, 2H), 6.71 (d, $J = 8.6$, 2H), 5.82 (dd, $J = 11$, 9.5 Hz, 1H), 5.70 (d, $J = 11$ Hz, 1H), 4.74 (dd, $J = 9.2$, 5.6 Hz, 1H), 4.64 (d, $J = 6.4$ Hz, 1H), 4.53 (d, $J = 6.4$ Hz, 1H), 4.38 (d, $J = 11$ Hz, 1H) 3.73 (s, 3H), 3.72-3.65 (m, 4H) 3.27 (s, 3H), 1.89-1.79 (m, 1H), 1.68-1.61 (m, 1H), 1.01 (s, 21H), 0.98 (s, 9H); HRMS (ESI⁺), m/z calcd for C₄₃H₆₂O₅Si₂Na: 737.4033 (M+Na); found, 737.4014.



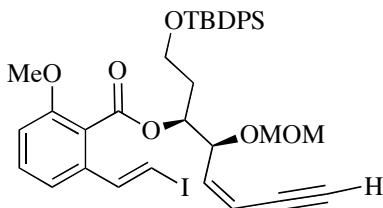
(5*S*,6*S*)-5-((*Z*)-But-1-en-3-ynyl)-6-(4-methoxybenzyloxy)-11,11-dimethyl-10,10-diphenyl-2,4,9-trioxa-10-siladodecane (135). The enyne **133** (1.21 g, 1.69 mmol), as a mixture of olefin isomers, was dissolved in anhydrous THF (17 mL) and cooled to 0 °C. TBAF (1.72 mL, 1.72 mmol, 1M in THF) was added dropwise. After 15 min, the reaction quenched with silica gel and THF removed by rotary evaporation. Purification of the crude mixture via flash column chromatography (hexanes/Et₂O, 100:0 – 80:20) yielded 560 mg of pure *Z*-enyne as a yellow oil (59%, 47% over two steps from aldehyde **111**): TLC (hexanes/Et₂O, 70:30): $R_f = 0.20$ for *Z*-enyne, 0.23 for *E*-enyne; $[\alpha]_D^{25} = +35.4$ ($c = 1.70$, CHCl₃); IR (thin film) $\nu_{\max} = 3286, 2955, 2931, 2887, 2858, 1613, 1514, 1248, 1111, 1035, 703$ cm⁻¹; ¹H NMR (400 MHz, CDCl₃) δ 7.67-7.64 (m, 4H), 7.42-7.34 (m, 6H), 7.19 (dd, $J = 6.8, 2.0$ Hz, 2H), 6.80 (dd, $J = 6.8, 2.0$ Hz, 2H), 5.96 (dd, $J = 10, 0.8$ Hz, 1H), 5.68 (dd, $J = 10, 2.0$ Hz, 1H), 4.77

(dd, $J = 9.2, 5.2$ Hz, 1H), 4.71-4.66 (m, 2H), 4.60 (d, 7.6 Hz, 1H), 4.47 (d, $J = 11$ Hz, 1H), 3.89-3.84 (m, 1H), 3.83-3.72 (m, 5H), 3.36 (s, 3H), 3.09 (dd, $J = 2.4, 0.8$ Hz, 1H), 1.94-1.85 (m, 1H), 1.76-1.68 (m, 1H), 1.05 (s, 9H); ^{13}C NMR (100 MHz, CDCl_3) δ 159.1, 142.1, 135.6, 133.9, 133.9, 130.8, 129.7, 129.6, 127.7, 127.6, 113.7, 112.2, 94.9, 82.9, 79.5, 77.3, 75.8, 73.3, 60.3, 55.7, 55.3, 33.9, 26.9, 19.2; HRMS (ESI $^+$), m/z calcd for $\text{C}_{34}\text{H}_{42}\text{O}_5\text{SiNa}$: 581.2699 (M+Na); found, 581.2699.



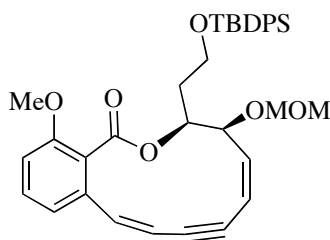
(5S,6S)-5-((Z)-But-1-en-3-ynyl)-11,11-dimethyl-10,10-diphenyl-2,4,9-trioxa-10-siladodecan-6-ol (109). The enyne **135** (283 mg, 0.506 mmol) was dissolved in DCM (5.10 mL) and water (0.510 mL) and cooled to 0 °C. DDQ (230 mg, 1.01 mmol) was added in three aliquots over 20 min. The solution was stirred for two h, diluted with EtOAc, washed with saturated NaHCO_3 (3x), brine, dried over MgSO_4 and purified by flash column chromatography to collect 216 mg of the enynol **109** as a yellow oil (97%): TLC (hexanes/EtOAc, 80:20): $R_f = 0.20$; $[\alpha]_D^{25} = +39$ ($c = 0.83$, CHCl_3); IR (thin film) $\nu_{\text{max}} = 3491$ (br), 3288, 3071, 2931, 2858, 1606, 1589, 1472, 1428, 1258, 1111, 1031 cm^{-1} ; ^1H NMR (400 MHz, CDCl_3) δ 7.71-7.7.67 (m, 4H), 7.46-7.37 (m, 6H), 5.98 (dd, $J = 11, 9.6$ Hz, 1H), 5.74 (dd, $J = 11, 2.4$ Hz, 1H), 4.74 (d, $J = 6.4$ Hz, 1H), 4.64 (d, $J = 6.4$ Hz, 1H), 4.54 (dd, $J = 9.2, 6.0$ Hz, 1H), 3.98-3.90 (m, 2H), 3.87-3.82 (m, 1H), 3.42 (s, 3H), 3.12 (dd, $J = 6.4, 0.8$ Hz, 1H), 3.04 (br d, J

=3.6 Hz, 1H), 1.84-1.75 (m, 2H), 1.06 (s, 9H); ^{13}C NMR (100 MHz, CDCl_3) δ 141.7, 135.6, 135.6, 133.5, 133.4, 129.7, 127.7, 112.7, 95.0, 83.1, 79.3, 77.9, 71.8, 61.8, 55.9, 35.0, 26.8, 19.1; HRMS (ESI^+), m/z calcd for $\text{C}_{26}\text{H}_{35}\text{O}_4\text{Si}$: 439.2305 (M+H); found, 439.2293.



(5*S*,6*S*)-5-((*Z*)-But-1-en-3-ynyl)-11,11-dimethyl-10,10-diphenyl-2,4,9-trioxa-10-siladodecan-6-yl 2-((*E*)-2-Iodovinyl)-6-methoxybenzoate (136). The enyne **109** (489 mg, 1.11 mmol) was azeotroped with toluene under reduced pressure, then diluted with anhydrous THF (12 mL) and cooled to 0 °C. NaHMDS (1.17 mL, 1.17 mmol, 1M in THF) was added dropwise and the mixture stirred at 0 °C for one h. A THF solution (10 mL) of the vinyl iodide **108** (385 mg, 1.17 mmol) was added dropwise to the anion solution, with continued stirring for two h at 0 °C. Me_2SO_4 (0.42 mL, 4.44 mmol) was added to quench the resultant phenolate anion and the reaction was warmed to room temperature. After three h of stirring, the reaction was quenched with water and extracted with EtOAc (3x). The combined organic extracts were washed with brine, dried over MgSO_4 and purified via flash column chromatography (hexanes/EtOAc, 95:5 – 80:20) to provide 713 mg of the desired compound as a pale yellow oil (89%): TLC (hexane/EtOAc, 80:20): R_f = 0.30; $[\alpha]_D^{25}$ = -1.80 (c = 1.65, CHCl_3); IR (thin film) ν_{max} = 3291, 3070, 2931, 2856, 1732, 1602,

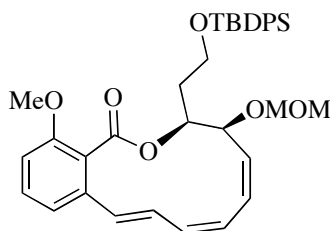
1590, 1571, 1471, 1271, 1111, 1033, 703 cm^{-1} ; ^1H NMR (400 MHz, CDCl_3) δ 7.72-7.69 (m, 4H), 7.50 (d, $J = 15$ Hz, 1H), 7.42-7.32 (m, 6H), 7.28 (t, $J = 8.0$ Hz, 1H), 6.99 (d, $J = 8.0$ Hz, 1H), 6.87 (d, $J = 15$ Hz, 1H), 6.79 (d, $J = 8.4$ Hz, 1H), 4.82 (dd, $J = 8.8, 5.6$ Hz, 1H), 4.73 (d, $J = 4.0$ Hz, 1H), 4.64 (d, $J = 4$ Hz, 1H), 3.95-3.83 (m, 2H), 3.56 (s, 3H), 3.32 (s, 3H), 3.13 (dd, $J = 2.4, 0.8$ Hz, 1H), 2.07-2.01 (m, 2H), 1.07 (s, 9H); ^{13}C NMR (100 MHz, CDCl_3) δ 166.8, 141.7, 141.0, 136.1, 135.7, 135.6, 134.0, 130.4, 129.5, 127.6, 117.5, 113.4, 110.5, 94.7, 83.8, 80.2, 74.8, 73.1, 59.7, 55.8, 55.5, 34.1, 26.8, 19.2; HRMS (ESI $^+$), m/z calcd for $\text{C}_{36}\text{H}_{41}\text{O}_6\text{SiNa}$: 747.1615 (M+Na); found, 747.1607.



(3*S*,4*S*,5*Z*,9*Z*)-3-(2-(*tert*-Butyldiphenylsilyloxy)ethyl)-14-methoxy-4-(methoxymethoxy)-3,4-dihydro-1-oxabenzocyclododeca-5,9-dien-7-ynone (139).

The enyne precycle **136** (27 mg, 0.037 mmol), PPh_3 (20 mg, 0.075 mmol), and K_2CO_3 (8 mg, 0.056 mmol) were suspended in anhydrous DMF (1.00 mL). CuI (7 mg, 0.037 mmol) was then added to this solution and the solution was heated for four h at 120 $^\circ\text{C}$. After heating, the solution was cooled to room temperature, quenched by adding water, then extracted with Et_2O (3x). The combined organic layers were washed with brine and dried over MgSO_4 . Purification of the crude material by flash column chromatography (hexanes/ EtOAc , 90:10 – 80:20) yielded 4 mg of the dienyne

cycle as a gold oil (18%): $[\alpha]_D^{25} = -70$ ($c = 0.60$, CHCl_3); IR (thin film) $\nu_{\text{max}} = 1722$, 1575, 1472, 1434, 1278, 1106, 1071, 1037, 743, 697 cm^{-1} ; ^1H NMR (400 MHz, CDCl_3) δ 7.72-7.67 (m, 4H), 7.42-7.28 (m, 7H), 6.85 (d, $J = 12$ Hz, 1H), 6.76 (d, $J = 8.0$ Hz, 1H), 6.71 (d, $J = 8.0$ Hz, 1H), 6.06 (dd, $J = 10, 8.0$ Hz, 1H), 5.86 (d, 8.0 Hz, 1H), 5.67 (br d, $J = 10$ Hz, 1H), 5.44 (ddd, $J = 11, 4.5, 1.5$ Hz, 1H), 5.30 (dd, $J = 10, 4.8$ Hz, 1H), 4.74 (dd, $J = 7.6, 6.4$ Hz, 2H), 3.94-3.90 (m, 2H), 3.42 (s, 3H), 3.24 (s, 3H), 2.32-2.24 (m, 1H), 1.91-1.82 (m, 1H), 1.05 (s, 9H); ^{13}C NMR (100 MHz, CDCl_3) δ 167.4, 158.0, 142.2, 138.8, 137.0, 135.6, 133.9, 130.8, 129.5, 127.6, 122.4, 121.5, 113.2, 111.1, 110.7, 95.7, 92.1, 91.5, 74.0, 73.0, 60.2, 55.7, 55.2, 31.0, 26.7, 19.2; HRMS (ESI⁺), m/z calcd for $\text{C}_{36}\text{H}_{41}\text{O}_6\text{Si}$: 597.2697 (M+H); found, 597.2659.

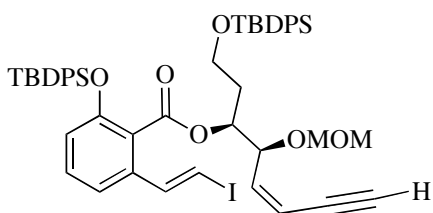


(3*S*,4*S*,5*Z*,7*Z*,9*E*)-3-(2-(*tert*-Butyldiphenylsilyloxy)ethyl)-14-methoxy-4-(methoxymethoxy)-3,4-dihydro-1*H*-benzo[*c*][1]oxacyclododecin-1-one (140).

CuI (4.3 mg, 0.023 mmol), PPh_3 (18 mg, 0.069 mmol), K_2CO_3 (14 mg, 0.10 mmol) and HCO_2Na (15 mg, 0.22 mmol) were suspended in anhydrous DMF (7 mL) (*Note: Cu(OAc)₂ was used for reactions greater than 0.1 mmol scale*). This suspension was heated at 120 °C for 30 min, during which time a black precipate formed. The cycle precursor **136** (45 mg, 0.062 mmol) was dissolved in DMF (7 mL) and added dropwise over one h. The reaction was stirred for an additional two h at 120 °C, then

cooled to room temperature. To the cooled reaction mixture was added Et₂O and saturated NH₄Cl solution. This mixture was stirred for two h, whereupon a white precipitate formed. The aqueous layer was extracted with Et₂O (2x), the combined organic layers were washed with brine and dried over MgSO₄. The crude material was purified by flash column chromatography (hexanes/EtOAc, 90:10 – 85:15) to yield 25 mg of the triene cycle as a bright yellow oil (67%). Boland reduction conditions: Zn dust (466 mg, 7.12 mmol) was suspended in water and the mixture purged with N₂ for 15 min. Cu(OAc)₂ (47 mg, 10% wt Zn) was added and the mixture stirred for 15 min. AgNO₃ (47 mg, 10% wt Zn) was then added, producing an exothermic reaction, and stirred for 30 min. The solution was then filtered and the activated Zn was washed with water, MeOH, acetone and Et₂O. The Zn was quickly transferred to a water:MeOH solution (1:1 mixture, 2.8 mL total) of the dienyne **139** (17 mg, 0.0285 mmol). The reaction was heated at 40 °C for 12 h. The solids were removed by filtration and rinsed with Et₂O. The ethereal layer was washed with water then brine and dried over MgSO₄. Crude ¹H NMR of the resulting material displayed a 10% conversion of the starting material to the desired product **140**: TLC (hexane/EtOAc, 80:20): R_f = 0.33; [α]_D²⁵ = -118 (c = 0.520, CHCl₃); IR (thin film) ν_{max} = 3011, 2930, 2857, 1733, 1599, 1572, 1468, 1428, 1301, 1271, 1090, 1030, 1000 cm⁻¹; ¹H NMR (400 MHz, CDCl₃) δ 7.72-7.69 (m, 4H), 7.41-7.33 (m, 6H), 7.23 (t, J = 8.0 Hz, 1H), 7.00 (dd, J = 16, 12 Hz, 1H), 6.78 (d, J = 8.0 Hz, 1H), 6.70 (d, J = 8.0 Hz, 1H), 6.65 (d, J = 16 Hz, 1H), 6.35 (t, J = 11 Hz, 1H), 6.16 (dd, J = 12, 3.9 Hz, 1H), 5.91 (dd, J = 11, 3.5 Hz, 1H), 5.69 (t, J = 12 Hz, 1H), 5.55 (ddd, J = 12, 3.4, 1.6

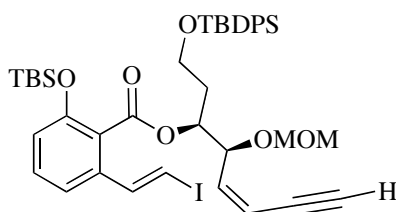
Hz, 1H), 4.56 (dd, $J = 11, 3.4$ Hz, 1H), 4.55 (dd, $J = 8.7, 6.5$ Hz, 2H), 3.94-3.85 (m, 2H), 3.40 (s, 3H), 3.36 (s, 3H), 2.35-2.27 (m, 1H), 2.10-2.01 (m, 1H), 1.07 (s, 9H); ^{13}C NMR (100 MHz, CDCl_3) δ 168.3, 156.0, 135.6, 134.0, 133.0, 132.1, 130.8, 129.6, 129.6, 127.7, 127.6, 127.4, 123.6, 120.4, 109.2, 93.3, 74.2, 68.4, 60.6, 55.4, 55.3, 31.2, 26.8, 19.2; HRMS (ESI $^+$), m/z calcd for $\text{C}_{36}\text{H}_{43}\text{O}_6\text{Si}$: 599.2829 (M+H); found, 599.2820.



(5*S*,6*S*)-5-((*Z*)-But-1-en-3-ynyl)-11,11-dimethyl-10,10-diphenyl-2,4,9-trioxa-10-siladodecan-6-yl 2-(*tert*-butyldiphenylsilyloxy)-6-((*E*)-2-iodovinyl)benzoate (150).

The enyne **109** (150 mg, 0.342 mmol) was azeotroped with toluene under reduced pressure, then diluted with anhydrous THF (1.00 mL) and cooled to 0 °C. NaHMDS (0.349 mL, 0.349 mmol, 1M in THF) was added dropwise and the mixture stirred at 0 °C for 1 h. A THF solution (0.70 mL) of the vinyl iodide **108** (119 mg, 0.359 mmol) was added dropwise to the anion solution, with continued stirring for two h at 0 °C. Approximately 0.21 mL of this phenolate solution (0.043 mmol phenolate) was withdrawn via syringe and added to an empty flask. With stirring, the phenolate anion was quenched with TBDPS-Cl (34.0 mg, 0.123 mmol), allowed to warm to room temperature over four h, after which time water was added and the mixture was extracted with EtOAc (3x). The combined organic extracts were washed with brine,

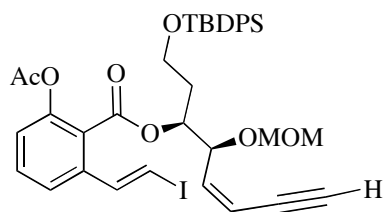
dried over MgSO₄ and purified via flash column chromatography (hexanes/EtOAc, 95:5 – 80:20) to provide 21.0 mg of the desired compound as a pale yellow oil (51%): TLC (hexane/EtOAc, 80:20): R_f = 0.40; ¹H NMR (400 MHz, CDCl₃) δ 7.76-7.71 (m, 8H), 7.52 (d, *J* = 14 Hz, 1H), 7.44-7.34 (m, 12H), 6.88-6.86 (m, 1H), 6.84 (dd, *J* = 9.8, 7.7 Hz, 1H), 6.77 (d, *J* = 14 Hz, 1H), 6.35 (dd, *J* = 7.6, 1.4 Hz, 1H), 6.07 (dd, *J* = 10, 9.6 Hz, 1H), 5.76 (dd, *J* = 11, 2.0 Hz, 1H), 5.54 (dt, *J* = 6.2, 4.0 Hz, 1H), 4.95 (dd, *J* = 7.0, 3.8 Hz, 1H), 4.71 (d, *J* = 6.8 Hz, 1H), 4.60 (d, *J* = 6.8 Hz, 1H), 3.96-3.84 (m, 2H), 3.30 (s, 3H), 3.01 (d, *J* = 2.2 Hz, 1H), 2.24 (q, *J* = 6.4 Hz, 2H), 1.08 (s, 9H), 1.04 (s, 9H); ¹³C NMR (100 MHz, CDCl₃) δ 166.5, 152.6, 142.3, 141.1, 136.5, 135.7, 135.6, 135.4, 135.4, 133.8, 133.6, 132.2, 131.9, 130.0, 129.7, 129.6, 127.9, 129.6, 127.9, 127.9, 127.6, 124.0, 119.1, 118.0, 113.1, 94.7, 83.9, 79.8, 78.9, 74.7, 73.5, 60.3, 55.9, 33.9, 26.9, 26.3, 19.4, 19.2; HRMS (ESI⁺), *m/z* calcd for C₅₁H₅₈IO₆Si₂: 949.2817 (M+H); found, 949.2825.



(5*S*,6*S*)-5-((*Z*)-But-1-en-3-ynyl)-11,11-dimethyl-10,10-diphenyl-2,4,9-trioxa-10-siladodecan-6-yl 2-(*tert*-butyldimethylsilyloxy)-6-((*E*)-2-iodovinyl)benzoate (151).

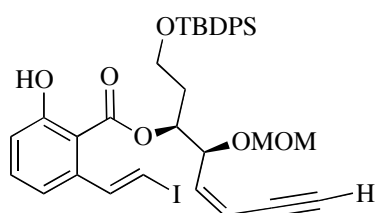
The enyne **109** (150 mg, 0.342 mmol) was azeotroped with toluene under reduced pressure, then diluted with anhydrous THF (1.00 mL) and cooled to 0 °C. NaHMDS (0.349 mL, 0.349 mmol, 1M in THF) was added dropwise and the mixture stirred at 0

°C for one h. A THF solution (0.70 mL) of the vinyl iodide **108** (119 mg, 0.359 mmol) was added dropwise to the anion solution, with continued stirring for two h at 0 °C. Approximately 0.21 mL of this phenolate solution (0.043 mmol phenolate) was withdrawn via syringe and added to an empty flask. With stirring, the phenolate anion was quenched with TBS-Cl (19.0 mg, 0.123 mmol), allowed to warm to room temperature over four h, after which time water was added and the mixture was extracted with EtOAc (3x). The combined organic extracts were washed with brine, dried over MgSO₄ and purified via flash column chromatography (hexanes/EtOAc, 95:5 – 80:20) to provide 19.0 mg of the desired compound as a pale yellow oil (53%): TLC (hexane/EtOAc, 80:20): R_f = 0.50; ¹H NMR (400 MHz, CDCl₃) δ 7.72-7.70 (m, 5H), 7.46 (d, *J* = 14 Hz, 1H), 7.43-7.37 (m, 7H), 7.19 (t, *J* = 8.0, 1H), 6.97 (d, *J* = 7.8 Hz, 1H), 6.80 (d, *J* = 14 Hz, 1H), 6.78 (d, *J* = 8.0 Hz, 1H), 5.99 (ddd, *J* = 11, 9.0, 0.7 Hz, 1H), 5.78 (dd, *J* = 11, 2.4 Hz, 1H), 5.46 (q, *J* = 5.7 Hz, 1H), 4.86 (dd, *J* = 9.0, 4.3 Hz, 1H), 4.68 (d, *J* = 6.8 Hz, 1H), 4.57 (d, *J* = 6.8 Hz, 1H), 3.90 (m, 2H), 3.27 (s, 3H), 3.02 (dd, *J* = 2.4, 0.8 Hz, 1H), 2.18-2.05 (m, 2H), 1.07 (s, 9H), 0.96 (s, 9H), 0.22 (s, 3H), 0.22 (s, 3H); ¹³C NMR (100 MHz, CDCl₃) δ 166.6, 152.8, 142.2, 141.1, 136.5, 135.7, 135.6, 134.8, 133.8, 133.6, 130.0, 129.6, 129.6, 127.7, 127.6, 124.8, 118.9, 118.1, 113.1, 94.6, 83.8, 79.8, 78.9, 74.1, 73.6, 60.2, 55.8, 33.9, 26.8, 25.8, 19.2, 18.4, -4.1, -4.1; HRMS (ESI⁺), *m/z* calcd for C₄₁H₅₄IO₆Si₂: 825.2504 (M+H); found, 825.2504.



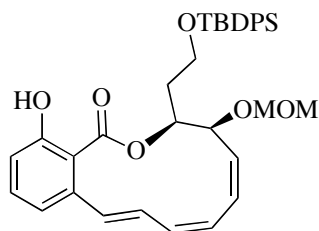
(5*S*,6*S*)-5-((*Z*)-but-1-en-3-ynyl)-11,11-dimethyl-10,10-diphenyl-2,4,9-trioxo-10-siladodecan-6-yl 2-(ethanoxyloxy)-6-((*E*)-2-iodovinyl)benzoate (152**).** The enyne **109** (150 mg, 0.342 mmol) was azeotroped with toluene under reduced pressure, then diluted with anhydrous THF (1.00 mL) and cooled to 0 °C. NaHMDS (0.349 mL, 0.349 mmol, 1M in THF) was added dropwise and the mixture stirred at 0 °C for one h. A THF solution (0.70 mL) of the vinyl iodide **108** (119 mg, 0.359 mmol) was added dropwise to the anion solution, with continued stirring for two h at 0 °C. Approximately 0.21 mL of this phenolate solution (0.043 mmol phenolate) was withdrawn via syringe and added to an empty flask. With stirring, the phenolate anion was quenched with freshly distilled AcCl (0.009 mL, 0.123 mmol), allowed to warm to room temperature over four h, after which time water was added and the mixture was extracted with EtOAc (3x). The combined organic extracts were washed with brine, dried over MgSO₄ and purified via flash column chromatography (hexanes/EtOAc, 95:5 – 80:20) to provide 21.0 mg of the desired compound as a pale yellow oil (65%): TLC (hexane/EtOAc, 80:20): R_f = 0.20; ¹H NMR (400 MHz, CDCl₃) δ 7.70-7.66 (m, 4H), 7.64 (d, *J* = 15 Hz, 1H), 7.42-7.33 (m, 7H), 7.28 (d, *J* = 7.6 Hz, 1H), 7.09 (dd, *J* = 8.0, 0.8 Hz, 1H), 6.82 (d, *J* = 15 Hz, 1H), 5.97 (dd, *J* = 10, 8.2 Hz, 1H), 5.78 (dd, *J* = 11, 2.2 Hz, 1H), 5.58 (dt, *J* = 6.7, 5.0 Hz, 1H), 4.82 (dd, *J* =

9.0, 5.2 Hz, 1H), 4.70 (d, $J = 6.8$ Hz, 1H), 4.61 (d, $J = 6.8$ Hz, 1H), 3.86-3.77 (m, 2H), 3.30 (s, 3H), 3.09 (dd, $J = 2.3, 0.7$ Hz, 1H), 2.14 (s, 3H), 2.11-2.05 (m, 1H), 2.01-1.94 (m, 1H), 1.06 (s, 9H); ^{13}C NMR (100 MHz, CDCl_3) δ 169.0, 164.5, 148.4, 142.1, 140.8, 137.9, 135.6, 135.6, 133.6, 133.5, 130.8, 129.6, 127.7, 124.4, 123.8, 122.9, 113.4, 94.7, 84.0, 80.5, 78.9, 74.5, 73.7, 59.8, 55.8, 33.8, 26.8, 20.8, 19.2; HRMS (ESI⁺), m/z calcd for $\text{C}_{37}\text{H}_{42}\text{IO}_7\text{Si}$: 753.1744 (M+H); found, 753.1725.



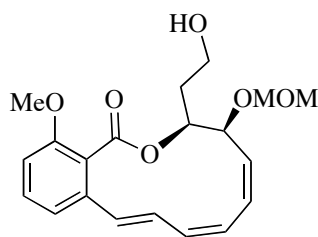
(5*S*,6*S*)-5-((*Z*)-But-1-en-3-ynyl)-11,11-dimethyl-10,10-diphenyl-2,4,9-trioxa-10-siladodecan-6-yl 2-Hydroxy-6-((*E*)-2-iodovinyl)benzoate (153). The enyne **109** (150 mg, 0.342 mmol) was azeotroped with toluene under reduced pressure, then diluted with anhydrous THF (1.00 mL) and cooled to 0 °C. NaHMDS (0.349 mL, 0.349 mmol, 1M in THF) was added dropwise and the mixture stirred at 0 °C for one h. A THF solution (0.70 mL) of the vinyl iodide **108** (119 mg, 0.359 mmol) was added dropwise to the anion solution, with continued stirring for two h at 0 °C. Approximately 0.21 mL of this phenolate solution (0.043 mmol phenolate) was withdrawn via syringe and added to an empty flask. With stirring, the phenolate anion was quenched with water and allowed to warm to room temperature over four h, after which time the mixture was extracted with EtOAc (3x). The combined organic extracts were washed with brine, dried over MgSO_4 and purified via flash

column chromatography (hexanes/EtOAc, 95:5 – 80:20) to provide 17.0 mg of the desired compound as a pale yellow oil (65%): TLC (hexane/EtOAc, 80:20): $R_f = 0.85$; $^1\text{H NMR}$ (400 MHz, CDCl_3) δ 11.47 (s, 1H), 7.86 (d, $J = 15$ Hz, 1H), 7.65-7.62 (m, 2H), 7.57-7.55 (m, 2H), 7.38-7.32 (m, 4H), 7.30-7.26 (m, 1H), 7.23-7.19 (m, 2H), 6.99 (dd, $J = 8.4, 0.9$ Hz, 1H), 6.75 (d, $J = 7.4$ Hz, 1H), 6.25 (d, $J = 4.6$ Hz, 1H), 5.97 (dd, $J = 10, 0.8$ Hz, 1H), 5.76 (ddd, $J = 11, 2.3, 0.6$ Hz, 1H), 5.69-5.64 (m, 1H), 4.94 (dd, $J = 9.2, 5.6$ Hz, 1H), 4.72 (d, $J = 6.8$ Hz, 1H), 4.66 (d, $J = 6.8$ Hz, 1H), 3.82-3.77 (m, 1H), 3.69-3.63 (m, 1H), 3.35 (s, 3H), 2.99 (dd, $J = 2.3, 0.7$ Hz, 1H), 2.18-2.12 (m, 1H), 2.02-1.95 (m, 1H), 1.02 (s, 9H); $^{13}\text{C NMR}$ (100 MHz, CDCl_3) δ 170.1, 162.7, 146.9, 141.5, 140.4, 135.5, 135.5, 134.6, 133.5, 133.2, 129.6, 129.5, 127.6, 127.5, 120.1, 117.9, 113.6, 109.7, 95.0, 83.7, 78.8, 74.2, 73.5, 59.4, 55.9, 32.2, 26.8, 19.1; HRMS (ESI⁺), m/z calcd for $\text{C}_{35}\text{H}_{40}\text{IO}_6\text{Si}$: 711.1639 (M+H); found, 711.1650.

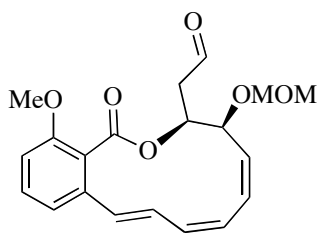


(3S,4S,5Z,7Z,9E)-3-(2-(*tert*-Butyldiphenylsilyloxy)ethyl)-14-hydroxy-4-(methoxymethoxy)-3,4-dihydro-1H-benzo[*c*][1]oxacyclododecin-1-one (154). CuI (1.4 mg, 0.0072 mmol), PPh_3 (5.6 mg, 0.022 mmol), K_2CO_3 (5.0 mg, 0.036 mmol) and HCO_2Na (6.5 mg, 0.096 mmol) were suspended in anhydrous DMF (2.8 mL). This suspension was heated at 120 °C for 30 min, during which time a black precipitate formed. The cycle precursor **153** (17 mg, 0.024 mmol) was dissolved in

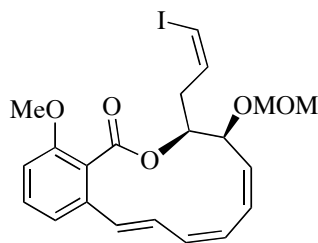
DMF (2.4 mL) and added dropwise over one h. The reaction was stirred for an additional two h at 120 °C, then cooled to room temperature. To the cooled reaction mixture was added Et₂O and saturated NH₄Cl solution. This mixture was stirred for two h, whereupon a white precipitate formed. The aqueous layer was extracted with Et₂O (2x), the combined organic layers were washed with brine and dried over MgSO₄. The crude material was purified by flash column chromatography (hexanes/EtOAc, 90:10 – 85:15) to yield 8.0 mg of the triene cycle as a bright yellow oil (57%): TLC (hexane/EtOAc, 80:20): R_f = 0.25; ¹H NMR (400 MHz, CDCl₃) δ 7.71-7.68 (m, 4H), 7.42-7.36 (m, 9H), 7.25-7.19 (m, 2H), 6.75-6.71 (m, 3H), 6.66-6.60 (m, 1H), 6.28 (t, *J* = 10 Hz, 1H), 6.20 (dd, *J* = 13, 3.2 Hz, 1H), 5.89 (dd, *J* = 11, 3.4 Hz, 1H), 5.61 (t, *J* = 11 Hz, 1H), 5.57 (br, 1H), 4.60 (dd, *J* = 10, 3.2 Hz, 1H), 5.54 (dd, *J* = 21, 6.6 Hz, 2H), 3.85 (br m, 2H), 3.34 (s, 3H), 2.29-2.19 (br, 1H), 2.00-1.93 (m, 1H), 1.06 (s, 9H); ¹³C NMR (100 MHz, CDCl₃) δ 170.0, 162.8, 146.8, 141.5, 138.4, 135.5, 134.6, 133.4, 133.2, 129.5, 127.5, 120.1, 118.0, 115.6, 109.7, 101.7, 94.6, 74.0, 73.2, 59.4, 55.6, 32.4, 26.7, 19.0, 18.5, 11.2, 0.0.



(3*S*,4*S*,5*Z*,7*Z*,9*E*)-3-(2-Hydroxyethyl)-14-methoxy-4-(methoxymethoxy)-3,4-dihydro-1*H*-benzo[*c*][1]oxacyclododecin-1-one (159). The triene cycle **140** (167 mg, 0.279 mmol) was dissolved in anhydrous THF (1.40 mL) at room temperature. TBAF (0.300 mL, 0.300 mmol, 1M in THF) was added dropwise. After 1.5 h, the reaction was quenched with silica gel and the THF was removed by rotary evaporation. The crude mixture was purified via flash column chromatography (hexanes/EtOAc, 90:10 – 50:50) to collect 95 mg of **159** as an opaque oil (94%): TLC (hexanes/EtOAc, 50:50): $R_f = 0.15$; $[\alpha]_D^{25} = -205$ ($c = 1.05$, CHCl_3); IR (thin film) $\nu_{\text{max}} = 3448$ (br), 2943, 2888, 1732, 1599, 1572, 1468, 1271, 1089, 1058, 1029 cm^{-1} ; ^1H NMR (400 MHz, CDCl_3) δ 7.28 (t, $J = 8.0$ Hz, 1H), 7.00 (dd, $J = 16, 12$ Hz, 1H), 6.83 (t, $J = 8$ Hz, 1H), 6.78 (d, $J = 12$ Hz, 1H), 6.37 (t, $J = 11$ Hz, 1H), 6.21 (dd, $J = 12, 3.6$ Hz, 1H), 5.90 (dd, $J = 11, 3.6$ Hz, 1H), 5.72 (t, $J = 11$ Hz, 1H), 5.55 (dt, $J = 11, 3.2$ Hz, 1H), 4.66 (dd, $J = 11, 3.6$ Hz, 1H), 4.58 (d, $J = 6.0$ Hz, 1H), 4.53 (d, $J = 6.0$ Hz, 1H), 3.92-3.90 (br m, 2H), 3.85 (s, 3H), 3.38 (s, 3H), 2.39 (br t, $J = 6.4$ Hz, 1H), 2.25-2.15 (m, 1H); ^{13}C NMR (100 MHz, CDCl_3) δ 168.2, 155.7, 138.5, 133.3, 132.7, 130.7, 129.9, 129.5, 127.8, 126.9, 123.3, 120.8, 109.4, 93.4, 76.7, 68.4, 61.3, 55.8, 55.5, 30.7; HRMS (ESI⁺), m/z calcd for $\text{C}_{20}\text{H}_{25}\text{O}_6$: 361.1651 (M+H); found, 361.1647.

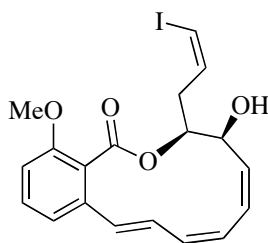


2-((3S,4S,5Z,7Z,9E)-14-Methoxy-4-(methoxymethoxy)-1-oxo-3,4-dihydro-1H-benzo[c][1]oxacyclododecin-3-yl)ethanal (160). To a solution of the alcohol **159** (180 mg, 0.499 mmol) in DCM (5.00 mL) was added Dess-Martin periodinane (**121a**) (318 mg, 0.749 mmol) at room temperature. The reaction was stirred for one h. The solvent was removed by rotary evaporation and the crude material purified by flash column chromatography (hexanes/EtOAc, 80:20 – 70:30) to collect 154 mg of the title compound as an opaque oil (86%): TLC (hexanes/EtOAc, 50:50): $R_f = 0.50$; $[\alpha]_D^{25} = -199$ ($c = 0.400$, CHCl_3); IR (thin film) $\nu_{\text{max}} = 2942, 2842, 1732, 1599, 1572, 1469, 1438, 1271, 1251, 1090, 1057, 1027 \text{ cm}^{-1}$; $^1\text{H NMR}$ (400 MHz, CDCl_3) δ 9.77 (t, $J = 2.0$ Hz, 1H), 7.27 (t, $J = 8.0$ Hz, 1H), 6.99 (dd, $J = 16, 12$ Hz, 1H), 6.81 (d, $J = 8.0$ Hz, 1H), 6.79 (d, $J = 8.0$ Hz, 1H), 6.68 (d, $J = 16$ Hz, 1H), 6.38 (t, $J = 11$ Hz, 1H), 6.24 (dd, $J = 12, 4.0$ Hz, 1H), 5.98 (dt, $J = 9.6, 4.0$ Hz, 1H), 5.90 (dd, $J = 11, 3.2$ Hz, 1H), 5.59 (t, $J = 11$ Hz, 1H), 4.71 (dd, $J = 10, 3.6$ Hz, 1H), 4.57 (d, $J = 6.4$ Hz, 1H), 4.52 (d, $J = 6.4$ Hz, 1H), 3.80 (s, 3H), 3.38 (s, 3H), 3.00-2.88 (m, 2H); $^{13}\text{C NMR}$ (100 MHz, CDCl_3) δ 199.5, 167.9, 156.1, 138.2, 133.3, 132.9, 131.0, 129.9, 129.8, 127.4, 126.3, 123.1, 120.5, 109.6, 93.3, 71.8, 68.0, 55.8, 55.6, 42.1; HRMS (ESI^+), m/z calcd for $\text{C}_{20}\text{H}_{23}\text{O}_6$: 359.1495 (M+H); found, 359.1477.



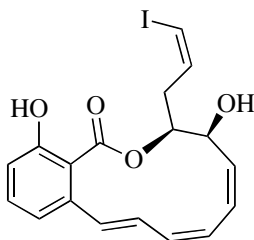
(3*S*,4*S*,5*Z*,7*Z*,9*E*)-3-((*Z*)-3-Iodoallyl)-14-methoxy-4-(methoxymethoxy)-3,4-dihydro-1*H*-benzo[*c*][1]oxacyclododecin-1-one (161). Freshly prepared IH_2CPh_3 (35 mg, 0.0653 mmol) was suspended in THF (0.131 mL), cooled to 0 °C and protected from light. NaHMDS (0.0650 mL, 0.0653 mmol, 1M in THF) was added dropwise, stirred for five min, and warmed to room temperature over 30 min. HMPA (0.0170 mL, 0.0980 mmol) was added, the resulting solution stirred for five min at room temperature, then cooled to -78 °C. The aldehyde **160** (13.0 mg, 0.0363 mmol) was dissolved in anhydrous DMF (0.182 mL) and added dropwise to the anion solution. After 30 min of stirring at -78 °C, the solution was warmed to room temperature and stirred for 30 min, after which time the reaction was filtered through a plug of silica and eluted with hexanes/EtOAc (50:50). Removal of the solvent followed by purification by flash column chromatography (hexanes/EtOAc 95:5 – 90:10) yielded 14.0 mg of the desired vinyl iodide as a yellow oil (80%): TLC (hexanes/EtOAc, 80:20): $R_f = 0.20$; $[\alpha]_D^{25} = -129$ ($c = 1.43$, CHCl_3); IR (thin film) $\nu_{\text{max}} = 3008, 2942, 2887, 1733, 1599, 1572, 1468, 1438, 1300, 1271, 1251, 1153, 1107, 1089, 1061, 1038 \text{ cm}^{-1}$; $^1\text{H NMR}$ (400 MHz, CDCl_3) δ 7.28 (t, $J = 8.0$ Hz, 1H), 7.03 (dd, $J = 16, 7.2$ Hz, 1H), 6.82 (d, $J = 2.4$ Hz, 1H), 6.80 (d, $J = 2.4$ Hz, 1H), 6.67 (d, $J = 16$ Hz, 1H), 6.44-6.34 (m, 3H), 6.23 (dd, $J = 12, 3.6$ Hz, 1H), 5.91 (dd, $J = 11,$

4.0 Hz, 1H), 5.73 (t, $J = 11$ Hz, 1H), 5.48 (dt, $J = 11, 3.2$ Hz, 1H), 4.64 (dd, $J = 11, 3.6$ Hz, 1H), 4.57 (dd, $J = 14, 6.4$ Hz, 1H), 3.82 (s, 3H), 3.38 (s, 3H), 2.84-2.78 (m, 1H), 2.69-2.61 (m, 1H); ^{13}C NMR (100 MHz, CDCl_3) δ 168.3, 156.0, 138.1, 137.5, 133.1, 132.6, 130.9, 129.7, 129.5, 127.6, 126.8, 123.4, 120.6, 109.5, 93.4, 84.2, 76.1, 68.6, 55.8, 55.5, 33.8; HRMS (ESI⁺), m/z calcd for $\text{C}_{21}\text{H}_{24}\text{O}_5$: 483.0669 (M+H); found, 483.0671.



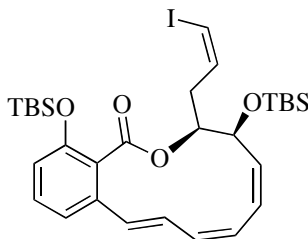
(3S,4S,5Z,7Z,9E)-4-Hydroxy-3-((Z)-3-iodoallyl)-14-methoxy-3,4-dihydro-1H-benzo[c][1]oxacyclododecin-1-one (163). To a *i*PrOH (0.830 mL) solution of the vinyl iodide **161** (40.0 mg, 0.0830 mmol) was added CBr_4 (110 mg, 0.332 mmol) in one portion. The mixture was heated at 75 °C for two h, after which time the reaction was cooled to room temperature, the solvent removed by rotary evaporation, and the reaction mixture was purified by flash column chromatography (hexanes/EtOAc, 90:10 – 80:20) to yield 35.0 mg the desired alcohol **163** as a colorless oil (96%): TLC (hexanes/EtOAc, 70:30): $R_f = 0.40$; $[\alpha]_D^{25} = -107$ ($c = 0.720$, CHCl_3); IR (thin film) $\nu_{\text{max}} = 3445$ (br), 3007, 2924, 2850, 1731, 1599, 1572, 1468, 1271, 1107, 1088, 1061, 1000 cm^{-1} ; ^1H NMR (400 MHz, CDCl_3) δ 7.28 (t, $J = 8.0$ Hz, 1H), 7.02 (dd, $J = 16, 11$ Hz, 1H), 6.83 (t, $J = 2.0$ Hz, 1H), 6.81 (t, $J = 2.7$ Hz, 1H), 6.67 (t, $J = 16$ Hz, 1H), 6.43-6.39 (m, 2H), 6.35 (t, $J = 11$ Hz, 1H), 6.12 (dd, $J = 12, 3.8$ Hz, 1H), 5.93-5.86

(m, 2H), 5.44 (td, $J = 11, 3.1$ Hz, 1H), 4.75 (br d, $J = 9.9$ Hz, 1H), 3.82 (s, 3H), 2.89-2.84 (m, 1H), 2.68-2.60 (m, 1H); ^{13}C NMR (100 MHz, CDCl_3) δ 168.4, 156.0, 138.0, 137.4, 133.1, 131.1, 130.9, 129.7, 129.5, 129.2, 127.5, 123.4, 120.6, 109.5, 84.3, 77.2, 65.8, 55.8, 33.1; HRMS (ESI^+), m/z calcd for $\text{C}_{19}\text{H}_{20}\text{O}_4\text{I}$: 439.0406 (M+H); found, 439.0401.



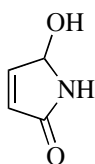
(3S,4S,5Z,7Z,9E)-4,14-Dihydroxy-3-((Z)-3-iodoallyl)-3,4-dihydro-1H-benzo[c][1]oxacyclododecin-1-one (162). Alcohol **163** (98.0 mg, 0.224 mmol) was dissolved in anhydrous CH_2Cl_2 (22.0 mL) and cooled to -78 °C. BCl_3 (2.24 mL, 2.24 mmol, 1M in CH_2Cl_2) was added dropwise and the reaction stirred for 10 min then warmed to room temperature. The reaction was quenched with water then extracted with EtOAc (3x). The combined organic extracts were washed with brine, dried over MgSO_4 and purified by flash column chromatography (hexanes/EtOAc, 85:15 – 75:25) to yield 89.0 mg of the desired diol as an unstable yellow oil (94%): TLC (hexanes/EtOAc, 70:30): $R_f = 0.30$; ^1H NMR (400 MHz, CDCl_3) δ 10.37 (s, 1H), 7.30 (t, $J = 8.0$ Hz, 1H), 6.88 (d, $J = 8.2$ Hz, 1H), 6.80-6.70 (m, 3H), 6.37 (d, $J = 7.6$ Hz, 2H), 6.21 (br, 2H), 6.07 (br d, $J = 12$ Hz, 1H), 5.79 (dd, $J = 12, 4.7$ Hz, 1H), 5.54 (br t, $J = 6.6$ Hz, 1H), 4.38 (br, 1H), 2.85 (br, 1H), 2.64 (br t, $J = 6.6$ Hz, 2H); ^{13}C

NMR (100 MHz, CDCl₃) δ ; HRMS (ESI⁺), m/z calcd for C₁₈H₁₈O₄I: 425.0250 (M+H); found, 425.0259.

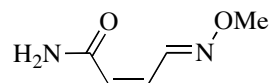


(3S,4S,5Z,7Z,9E)-4,14-Bis(*tert*-butyldimethylsilyloxy)-3-((Z)-3-iodoallyl)-3,4-dihydro-1H-benzo[*c*][1]oxacyclododecin-1-one (67). The diol **162** (89.0 mg, 0.210 mmol) was dissolved in CH₂Cl₂ (2.00 mL), followed by the addition of Py. (0.120 mL, 1.47 mmol) and cooled to 0 °C. TBS-OTf (0.335 mL, 1.47 mmol) was added dropwise and the reaction was allowed to warm to room temperature during the course of 15 h. EtOAc was added and the organic mixture was washed with saturated NaHCO₃ solution. The aqueous layer was re-extracted with EtOAc (2x), the organic extracts combined, washed with brine, dried over MgSO₄ and purified by flash column chromatography (hexanes/EtOAc, 100:0 – 95:5) to yield 110 mg of the title compound as a yellow oil (80%): TLC (hexanes/EtOAc, 80:20): R_f = 0.85; $[\alpha]_D^{25} = -151.2$ ($c = 0.49$, CHCl₃), (lit. $[\alpha]_D^{25} = -171$ ($c = 2.00$, CHCl₃)); IR (thin film) $\nu_{\max} = 3010, 2929, 2885, 2857, 1732, 1599, 1571, 1463, 1361, 1251, 1100, 1062, 1000$ cm⁻¹; ¹H NMR (400 MHz, CDCl₃) δ 7.17 (t, $J = 8.0$ Hz, 1H), 7.05 (dd, $J = 16, 11$ Hz, 1H), 6.79 (d, $J = 6.6$ Hz, 1H), 6.74 (d, $J = 8.0$ Hz, 1H), 6.64 (d, $J = 16$ Hz, 1H), 6.47 (dt, $J = 7.6, 5.2$ Hz, 1H), 6.37-6.31 (m, 2H), 5.99 (dd, $J = 12, 4.1$ Hz, 1H), 5.87 (t, $J = 11,$

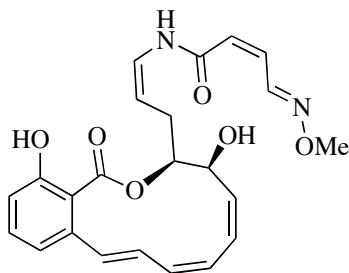
4.1 Hz, 1H), 5.79 (t, $J = 11$ Hz, 1H), 5.21 (dt, $J = 9.3, 3.5$ Hz, 1H), 4.63 (dd, $J = 10, 3.1$ Hz, 1H), 2.95-2.88 (m, 1H), 2.63-2.55 (m, 1H), 0.98 (s, 9H), 0.90 (s, 9H), 0.22 (s, 3H), 0.19 (s, 3H), 0.11 (s, 3H), 0.02 (s, 3H); ^{13}C NMR (100 MHz, CDCl_3) δ 168.3, 152.3, 138.0, 132.4, 130.7, 130.7, 129.7, 129.3, 128.6, 128.0, 126.4, 121.2, 117.9, 83.8, 78.4, 66.5, 33.8, 25.8, 25.8, 18.4, 17.9, -4.1, -4.1, -4.5, -4.9; HRMS (ESI^+), m/z calcd for $\text{C}_{30}\text{H}_{46}\text{O}_4\text{Si}_2$: 653.1979 (M+H); found, 653.1963.



5-Hydroxy-1H-pyrrol-2(5H)-one (164). Maleimide (**107**) (1.00 g, 10.3 mmol) and $\text{CeCl}_3 \cdot 7\text{H}_2\text{O}$ (2.50 g, 10.3 mmol) were dissolved in anhydrous MeOH (129 mL) and cooled to 0 °C. To this solution was added NaBH_4 (0.390 g, 10.3 mmol) with vigorous stirring. Upon consumption of the starting material (one to two h), the reaction mixture was diluted with MeOH and the solvent removed by rotary evaporation. This process was repeated twice, then the resulting material was loaded onto silica gel and purified by column chromatography ($\text{CH}_2\text{Cl}_2/\text{MeOH}$, 90:10) to yield 805 mg of the desired compound as a white solid (79%). TLC ($\text{CH}_2\text{Cl}_2/\text{MeOH}$, 90:10): $R_f = 0.20$; IR (thin film) $\nu_{\text{max}} = 3293$ (br), 1682, 1400, 1291, 1081 cm^{-1} ; ^1H NMR (400 MHz, d_6 -Acetone) δ 7.51 (br, 1H), 7.00 (td, $J = 6.0, 1.6$ Hz, 1H), 5.97 (td, $J = 6.0, 1.6$ Hz, 1H), 5.62 (d, $J = 8.0$ Hz, 1H), 5.05 (d, $J = 8.8$ Hz, 1H); ^{13}C NMR (100 MHz, d_6 -Acetone) δ 172.3, 149.5, 128.4, 81.2; melting point 96-98 °C.



(2Z,4E)-4-(Methoxyimino)but-2-enamide (54). The pyrrolone **164** (160 mg, 1.60 mmol), MeONH₃Cl (1.21 g, 14.5 mmol), and Et₃N (2.04 mL, 14.5 mmol) were dissolved in anhydrous MeOH (32 mL). After heating at 70 °C for three h, the volatiles were removed by rotary evaporation. The crude mixture was dissolved in EtOAc and washed once with brine. The organic layer was dried over MgSO₄ and purified by flash column chromatography (hexanes/EtOAc, 30:70 – 20:80) to yield 143 mg of the desired amide as an off-white solid (70%). TLC (EtOAc, 100): R_f = 0.45; IR (thin film) ν_{\max} = 3400 (br), 1667, 1437, 1340, 1044 cm⁻¹; ¹H NMR (400 MHz, CDCl₃) δ 8.97 (d, *J* = 10 Hz, 1H), 6.51 (dd, *J* = 12, 10 Hz, 1H), 5.97 (d, *J* = 12 Hz, 1H), 3.92 (s, 3H); ¹³C NMR (100 MHz, CDCl₃) δ 167.3, 148.4, 134.0, 127.3, 62.3; melting point 85-87 °C.

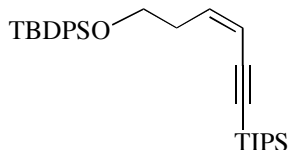


(2Z,4E)-N-((Z)-3-((3S,4S,5Z,7Z,9E)-4,14-Dihydroxy-1-oxo-3,4-dihydro-1H-benzo[c][1]oxacyclododecin-3-yl)prop-1-enyl)-4-(methoxyimino)but-2-enamide (14). Oxime amide **54** (22 mg, 0.172 mmol), CuTC (**57**) (14 mg, 0.0730 mmol), and K₂CO₃ (18 mg, 0.129 mmol) were added to an empty flask following Porco's

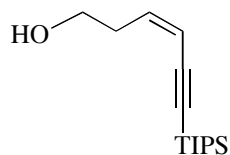
protocol.¹¹⁸ The flask was flushed rigorously with N₂. To the flask was added DMA (freshly distilled from BaO) (0.115 mL). The solution was vacuum degassed (house vacuum pressure) for 30 min. To this suspension was then added *N,N'*-dimethylethylenediamine (13 mg, 0.016 mL, 0.146 mmol) and the mixture was stirred for one h at room temperature. The vinyl iodide **67** (28 mg, 0.0430 mmol) was dissolved in DMA (0.086 mL) and added at once to the catalyst solution. After heating the solution for 16 h at 50 °C, it was cooled to room temperature and EDTA (107 mg, 0.365 mmol) was added and stirred for 10 min. Saturated NH₄Cl solution was then added to the quenched reaction and stirred for 30 min. The aqueous layer was extracted with EtOAc (3x), the organic extracts combined, washed with brine and dried over MgSO₄.

To a crude enamide/THF (0.43 mL) solution was added 5M HF/Py. (0.263 mL). The reaction was stirred at room temperature until TLC showed consumption of starting material, about seven h, after which time the reaction was quenched with the addition of pH 7 buffer and stirred for two h. The aqueous layer was extracted with EtOAc (3x), the organic extracts combined, washed with brine, dried over MgSO₄ and purified by prep TLC (hexanes/EtOAc, 40:60) to yield 3.5 mg of an off-white powder (19% from vinyl iodide **67**): ¹H NMR (400 MHz, CDCl₃) δ 10.77 (s, 1H), 9.04 (d, *J* = 10.3 Hz, 1H), 8.38 (d, *J* = 10.0 Hz, 1H), 7.34 (t, *J* = 8.0 Hz, 1H), 6.97-6.86 (m, 3H), 6.76 (d, *J* = 6.4 Hz, 1H), 6.77-6.70 (m, 1H), 6.52 (t, *J* = 11.0 Hz, 1H), 6.42 (t, *J* = 10.0 Hz, 1H), 6.31 (d, *J* = 11.0 Hz, 1H), 6.11 (d, *J* = 12.5 Hz, 1H), 5.93 (d, *J* = 11.5 Hz, 1H), 5.74 (dd, *J* = 12.5, 3.4 Hz, 1H), 5.30 (dd, *J* = 10.5, 4.6 Hz, 1H), 4.85 (qu, *J* =

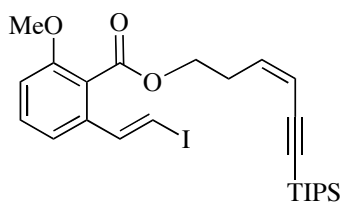
8.6 Hz, 1H), 4.35 (d, $J = 9.7$ Hz, 1H), 3.95 (s, 3H), 3.20 (d, $J = 11.0$ Hz, 1H), 2.67-2.58 (m, 1H), 2.33-2.26 (m, 1H); HRMS (ESI⁺), m/z calcd for C₂₃H₂₅N₂O₆: 425.1713 (M+H); found, 425.1707. UPLC-MS analysis revealed 91.5% purity prior to biological testing.



(Z)-tert-Butyldiphenyl(6-(triisopropylsilyl)hex-3-en-5-ynoxy)silane (141). Prop-1-yne-1,3-diylbis(triisopropylsilane) (**110**) (5.30 g, 15.05 mmol) was dissolved in anhydrous THF (125 mL) and cooled to -20 °C. *n*BuLi (9.40 mL, 15.05 mmol, 1.6M in hexanes) was added dropwise over 10 min, stirred for 30 min, then cooled to -78 °C. The aldehyde **120** (3.92 g, 12.55 mmol), as a solution in THF (125 mL), was added dropwise to the anion solution over 30 min. After additional stirring for five h, the reaction was allowed to warm to room temperature and stirred for an additional 10 h. The reaction was then quenched with saturated NH₄Cl solution. Following extraction with EtOAc (3x), washing of combined organic extracts with brine, and drying over MgSO₄, the crude material was purified via flash column chromatography (hexanes/CH₂Cl₂, 100:0 – 95:5) to yield 1.659 g of the pure *Z*-enyne as a yellow oil (22%): TLC (hexanes/EtOAc, 80:20): R_f = 0.80; ¹H NMR (400 MHz, CDCl₃) δ 7.59-7.56 (m, 4H), 7.36-7.27 (m, 6H), 6.05 (td, $J = 11, 7.2$ Hz, 1H), 5.59 (d, $J = 11$ Hz, 1H), 3.94 (t, $J = 6.0$ Hz, 2H), 2.63 (q, $J = 6.0$ Hz, 2H), 1.09 (s, 9H).

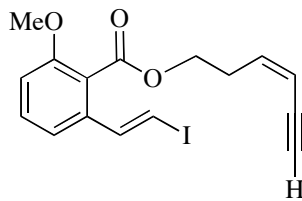


(Z)-6-(Triisopropylsilyl)hex-3-en-5-yn-1-ol (142). The silyl ether **141** (1.66 g, 3.38 mmol) was dissolved in anhydrous THF (3 mL) at room temperature. To this solution was added 0.4 mL of a 5% NaOH solution (13.5 mmol NaOH) in absolute ethanol, then the solution was heated at 55 °C for 12 h. After heating, the solution was cooled to room temperature, dissolved in EtOAc and washed with saturated NaHCO₃ solution. The aqueous phase was reextracted with EtOAc and the combined organic extracts were washed with brine and dried over MgSO₄. The crude material was purified via flash column chromatography (hexanes/EtOAc, 95:5 – 85:15) to yield 333 mg of the pure *Z*-alkenol as a yellow oil (39%): TLC (hexanes/EtOAc, 80:20): R_f = 0.25; ¹H NMR (400 MHz, CDCl₃) δ 6.01 (td, *J* = 11, 7.4 Hz, 1H), 5.67 (td, *J* = 11, 1.2 Hz, 1H), 3.75 (t, 6.4 Hz, 2H), 2.63 (dq, *J* = 6.4, 1.2 Hz, 2H), 1.34 (br, 1H), 1.09 (s, 21H); ¹³C NMR (100 MHz, CDCl₃) δ 140.4, 112.2, 103.3, 95.9, 61.9, 33.9, 18.6, 11.3.

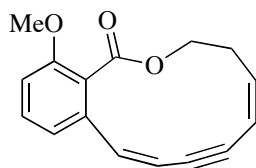


(Z)-6-(Triisopropylsilyl)hex-3-en-5-ynyl 2-((E)-2-iodovinyl)-6-methoxybenzoate (143). The enyne **142** (34.0 mg, 0.135 mmol) was azeotroped with toluene under

reduced pressure, then diluted with anhydrous THF (0.340 mL) and cooled to 0 °C. NaHMDS (0.135 mL, 0.135 mmol, 1M in THF) was added dropwise and the mixture stirred at 0 °C for one h. A THF solution (0.200 mL) of the vinyl iodide **108** (47.0 mg, 0.142 mmol) was added dropwise to the anion solution, with continued stirring for four h at 0 °C. Me₂SO₄ (0.051 mL, 0.540 mmol) was added to quench the resultant phenolate anion and the reaction was warmed to room temperature. After three h of stirring, the reaction was quenched with water and extracted with EtOAc (3x). The combined organic extracts were washed with brine, dried over MgSO₄ and purified via flash column chromatography (hexanes/EtOAc, 95:5 – 90:10) to provide 52.0 mg of the desired compound as a pale yellow oil (72%), along with a small amount of the alcohol (3.00 mg) (79% based on recovered starting material): TLC (hexane/EtOAc, 80:20): R_f = 0.55; ¹H NMR (400 MHz, CDCl₃) δ 7.42 (d, *J* = 15 Hz, 1H), 7.32 (t, *J* = 8.0 Hz, 1H), 6.99 (d, *J* = 8.0 Hz, 1H), 6.87 (d, *J* = 8.0 Hz, 1H), 6.86 (d, *J* = 15 Hz, 1H), 6.05 (td, *J* = 11, 7.0 Hz, 1H), 5.70 (dd, *J* = 11, 1.2 Hz, 1H), 4.43 (t, *J* = 7.2 Hz, 2H), 3.82 (s, 3H), 2.83-2.78 (m, 2H), 1.07 (s, 21H); ¹³C NMR (100 MHz, CDCl₃) δ 167.4, 156.6, 141.7, 139.4, 136.4, 130.6, 117.9, 112.4, 110.8, 103.1, 80.2, 64.3, 56.0, 29.8, 18.6, 11.3.

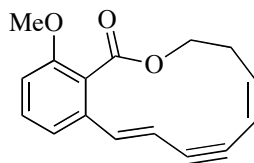


(Z)-Hex-3-en-5-ynyl 2-((E)-2-Iodovinyl)-6-methoxybenzoate (144). The enyne **143** (86.0 mg, 0.160 mmol), as a mixture of olefin isomers, was dissolved in anhydrous THF (1.60 mL) and cooled to 0 °C. TBAF (0.168 mL mL, 0.168 mmol, 1M in THF) was added dropwise. After 15 min, the reaction was quenched with the addition of silica gel, then the THF was removed by rotary evaporation and the crude mixture subjected to purification via flash column chromatography (hexanes/Et₂O, 100:0 – 80:20) to collect 58.0 mg of a 4:3 *Z:E* mixture of olefin isomers, as determined by ¹H NMR, as a yellow oil (95%): TLC (hexanes/Et₂O, 70:30): R_f = 0.20 for *Z*-enyne, 0.23 for *E*-enyne; IR (thin film) ν_{\max} = 3293, 2917, 1727, 1602, 1591, 1571, 1471, 1270, 1117, 1068 cm⁻¹; ¹H NMR (400 MHz, CDCl₃) δ 7.42 (d, *J* = 15 Hz, 1H), 7.32 (t, *J* = 8.0 Hz, 1H), 6.99 (d, *J* = 8.0 Hz, 1H), 6.87 (d, *J* = 8.0 Hz, 1H), 6.86 (d, *J* = 15 Hz, 1H), 6.11 (td, *J* = 11, 7.0 Hz, 1H), 5.70 (m, 1H), 4.44 (t, *J* = 6.4 Hz, 2H), 3.83 (s, 3H), 3.14 (d, *J* = 2.0 Hz, 1H), 2.80 (dq, *J* = 14, 1.2 Hz, 2H); ¹³C NMR (100 MHz, CDCl₃) δ 167.3, 156.6, 141.7, 140.6, 136.5, 130.7, 121.8, 117.8, 110.9, 110.8, 82.5, 80.3, 79.8, 64.1, 56.0, 29.7.



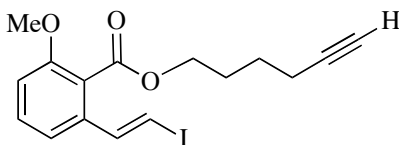
(5Z,9Z)-14-Methoxy-3,4-dihydro-1-oxabenzocyclododeca-5,9-dien-7-ynone (145).

CuI (5.0 mg, 0.026 mmol), PPh₃ (14 mg, 0.053 mmol) and K₂CO₃ (22 mg, 0.16 mmol) were suspended in anhydrous DMSO (20 mL). This suspension was heated at 120 °C for 30 min. The cycle precursor **144** (40 mg, 0.105 mmol) was dissolved in DMSO (15 mL) and added dropwise over one h. The reaction was stirred for an additional 1.5 h at 120 °C, then cooled to room temperature. To the cooled reaction mixture was added Et₂O and water. The aqueous layer was extracted with Et₂O (2x), the combined organic layers were washed with brine and dried over MgSO₄. The crude material was purified by flash column chromatography (hexanes/EtOAc, 100:0 – 85:15) to yield 10 mg of the Z,Z-dienyne cycle as a yellow oil and 12 mg of the starting material (37%, 53% based on recovered starting material): TLC (hexane/EtOAc, 80:20): R_f = 0.25; ¹H NMR (400 MHz, CDCl₃) δ 7.33 (t, *J* = 8.0 Hz, 1H), 6.87 (d, *J* = 8.0 Hz, 1H), 6.82-6.79 (m, 2H), 6.11 (td, *J* = 11, 6.8 Hz, 1H), 5.88 (d, *J* = 12 Hz, 1H), 5.66 (t, *J* = 11 Hz, 1H), 3.82 (s, 3H), *methylene protons not detected*; ¹³C NMR (100 MHz, CDCl₃) δ 168.3, 157.9, 139.6, 137.9, 136.5, 132.1, 130.6, 128.6, 122.6, 112.4, 111.4, 92.9, 89.4, 64.2, 56.3, 29.7; HRMS (ESI⁺), *m/z* calcd for C₁₆H₁₇O₃: 277.0835 (M+Na); found, 277.0832.



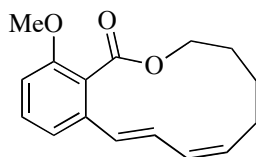
(5Z,9E)-14-Methoxy-3,4-dihydro-1-oxabenzocyclododeca-5,9-dien-7-ynone (146).

Following the procedure for the preparation of compound **145**, a fast workup and column allowed the isolation and spectroscopic identification of the title *E,Z*-enyne cycle **146**. TLC (hexane/EtOAc, 80:20): $R_f = 0.25$; IR (thin film) $\nu_{\max} = \text{cm}^{-1}$; ^1H NMR (400 MHz, CDCl_3) δ 7.76 (d, $J = 16$ Hz, 1H), 7.40 (t, $J = 8.0$ Hz, 1H), 7.23 (d, $J = 8.0$ Hz, 1H), 6.97 (d, $J = 8.0$ Hz, 1H), 6.30 (d, $J = 16$ Hz, 1H), 5.68-5.57 (m, 2H), 3.87 (s, 3H), *methylene protons not detected*.



(E)-Hex-5-ynyl 2-(2-iodovinyl)-6-methoxybenzoate (156). 5-Hexyn-1-ol (**155**) (50.0 mg, 0.510 mmol) was dissolved in anhydrous THF (1.40 mL) and cooled to 0 °C. NaHMDS (0.540 mL, 0.540 mmol, 1M in THF) was added dropwise and the mixture stirred at 0 °C for one h. A THF solution (0.640 mL) of the vinyl iodide **108** (163 mg, 0.490 mmol) was added dropwise to the anion solution, with continued stirring for two h at 0 °C. Me_2SO_4 (0.193 mL, 2.04 mmol) was added to quench the resultant phenolate anion and the reaction was warmed to room temperature. After three h of stirring, the reaction was quenched with water and extracted with EtOAc (3x). The combined organic extracts were washed with brine, dried over MgSO_4 and

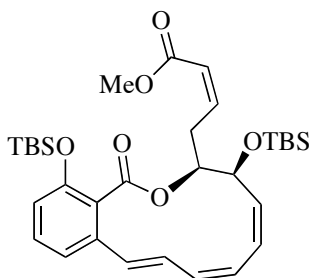
purified via flash column chromatography (hexanes/EtOAc, 95:5 – 88:12) to provide 152 mg of the desired compound as a colorless oil (85%): TLC (hexane/EtOAc, 80:20): $R_f = 0.35$; $^1\text{H NMR}$ (400 MHz, CDCl_3) δ 7.41 (d, $J = 15$ Hz, 1H), 7.32 (t, $J = 8.0$ Hz, 1H), 7.00 (d, $J = 7.9$ Hz, 1H), 6.88 (d, $J = 8.3$ Hz, 1H), 6.86 (d, $J = 15$ Hz, 1H), 4.39 (t, $J = 6.3$ Hz, 2H), 3.84 (s, 3H), 2.28 (dt, $J = 6.0, 2.7$ Hz, 2H), 1.97 (t, $J = 2.7$ Hz, 1H), 1.92-1.85 (m, 2H), 1.74-1.66 (m, 2H); $^{13}\text{C NMR}$ (100 MHz, CDCl_3) δ 167.4, 156.5, 141.7, 136.4, 130.5, 117.9, 110.7, 83.9, 80.2, 68.8, 65.0, 56.0, 27.7, 24.9, 18.1; HRMS (ESI^+), m/z calcd for $\text{C}_{16}\text{H}_{18}\text{O}_3$: 385.0301 (M+H); found, 385.0287.



(7Z,9E)-14-Methoxy-3,4,5,6-tetrahydro-1H-benzo[c][1]oxacyclododecin-1-one

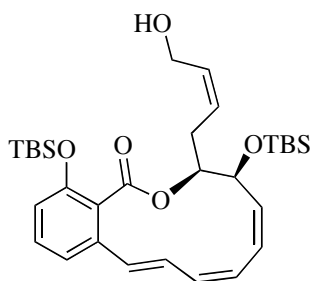
(157). $\text{Cu}(\text{OAc})_2$ (6.4 mg, 0.035 mmol), PPh_3 (28 mg, 0.106 mmol), K_2CO_3 (22 mg, 0.159 mmol) and HCO_2Na (29 mg, 0.424 mmol) were suspended in anhydrous DMF (11 mL). This suspension was heated at 110 °C for 30 min, during which time the solution turned from colorless to gold. The cycle precursor **156** (39 mg, 0.102 mmol) was dissolved in DMF (10 mL) and added dropwise over one h. The reaction was stirred for an additional two h at 110 °C, then cooled to room temperature. To the cooled reaction mixture was added Et_2O and saturated NH_4Cl solution. This mixture was stirred for two h, whereupon a white precipitate formed. The aqueous layer was

extracted with Et₂O (2x), the combined organic layers were washed with brine and dried over MgSO₄. The crude material was purified by flash column chromatography (hexanes/EtOAc, 95:5 – 90:10) to yield 10 mg of the diene cycle as a yellow oil (38%): TLC (hexane/EtOAc, 80:20): R_f = 0.30; ¹H NMR (400 MHz, CDCl₃) δ 7.29 (t, *J* = 8.0 Hz, 1H), 6.91 (d, *J* = 8.0 Hz, 1H), 6.86 (m, 3H), 6.53 (d, *J* = 16 Hz, 1H), 6.15 (t, *J* = 9.6 Hz, 1H), 5.65 (td, *J* = 11, 7.4 Hz, 1H), 4.51 (t, *J* = 5.0 Hz, 1H), 3.85 (s, 3H), 2.36 (q, *J* = 7.3 Hz, 2H), 1.83 (qu, *J* = 5.0 Hz, 1H), 1.71 (qu, *J* = 6.5 Hz, 1H); ¹³C NMR (100 MHz, CDCl₃) δ 168.6, 156.7, 137.7, 132.8, 130.9, 130.3, 130.1, 128.5, 128.3, 120.5, 109.7, 66.0, 56.0, 27.3, 26.2, 26.0; HRMS (ESI⁺), *m/z* calcd for C₁₆H₁₉O₃: 259.1334 (M+H); found, 259.1332.



(Z)-Methyl 4-((3S,4S,5Z,7Z,9E)-4,14-Bis(*tert*-butyldimethylsilyloxy)-1-oxo-3,4-dihydro-1*H*-benzo[*c*][1]oxacyclododecin-3-yl)but-2-enoate (170). A flask containing Pd(PPh₃)₄ (71 mg, 0.661 mmol) was flushed with CO (1 atm). To this flask was added DIPEA (0.044 mL, 0.245 mmol) and anhydrous MeOH (4.90 mL) at room temperature and the flask was flushed with CO again. A THF solution of vinyl iodide **67** (160 mg, 0.245 mmol in 1.23 mL THF) was added and the reaction stirred under one atm of CO for 45 min. The reaction mixture was filtered through a pad of

Celite and the Celite layer was eluted with Et₂O until the eluent was colorless. The crude material was purified by flash column chromatography (hexanes/Et₂O, 100:0 – 95:5) to collect 122 mg of the desired ester as a yellow oil (85%): TLC (hexanes/Et₂O, 80:20): R_f = 0.80; [α]_D²⁵ = -148 (c = 0.600, CHCl₃); IR (thin film) ν_{max} = 2972, 2861, 1732, 1648, 1561, 1152, 1056, 963 cm⁻¹; ¹H NMR (400 MHz, CDCl₃) δ 7.17 (t, *J* = 8.0 Hz, 1H), 7.06 (ddd, *J* = 16, 10, 0.5 Hz, 1H), 6.79 (d, *J* = 7.4 Hz, 1H), 6.75 (d, *J* = 8.1 Hz, 1H), 6.64 (d, *J* = 16 Hz, 1H), 6.46 (ddd, *J* = 12, 7.7, 5.6 Hz, 1H), 6.34 (t, *J* = 11 Hz, 1H), 5.97 (dd, *J* = 12, 4.1 Hz, 1H), 5.89-5.85 (m, 2H), 5.82 (t, *J* = 12 Hz, 1H), 5.24 (td, *J* = 9.1, 4.0 Hz, 1H), 4.64 (dd, *J* = 10, 3.2 Hz, 1H), 3.74 (s, 3H), 3.63-3.55 (m, 1H), 3.09-3.00 (m, 1H), 0.98 (s, 9H), 0.88 (s, 9H), 0.22 (s, 3H), 0.20 (s, 3H), 0.09 (s, 3H), 0.01 (s, 3H); ¹³C NMR (100 MHz, CDCl₃) δ 168.4, 166.6, 152.3, 146.3, 138.0, 132.4, 130.8, 130.6, 129.7, 129.3, 128.5, 128.0, 126.4, 121.2, 120.4, 117.8, 78.9, 66.5, 51.1, 29.7, 27.9, 25.8, 25.7, 18.4, 17.9, -4.1, -4.5, -5.0; HRMS (ESI), *m/z* calcd for C₃₂H₄₈NaO₆Si₂: 607.2887 (M+Na); found, 607.2861.

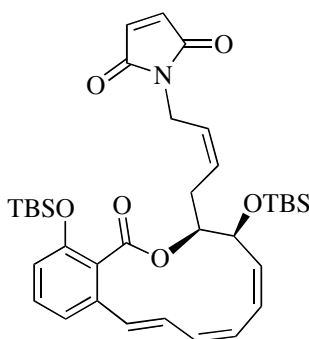


(3S,4S,5Z,7Z,9E)-4,14-Bis(*tert*-butyldimethylsilyloxy)-3-

((*Z*)-4-hydroxybut-2-enyl)-3,4-dihydro-1*H*-benzo[*c*][1]oxacyclododecin-1-one

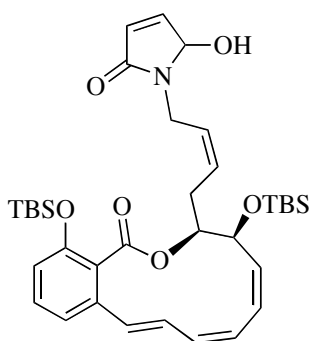
(166). Ester **170** (9.5 mg, 0.016 mmol) was dissolved in anhydrous CH₂Cl₂ (0.160 mL) and cooled to -78 °C. To this cooled solution was added DIBAL (0.037 mL, 0.037 mmol, 1M solution in CH₂Cl₂) dropwise (**Note: very slow addition of DIBAL is required to prevent side reactions*). After 1.5 h of reacting, the cooling bath was removed, the reaction quenched with EtOAc and Rochelle's salt solution was added. The mixture was warmed to room temperature and stirred for two h, or until both aqueous and organic layers were clear. The aqueous layer was extracted with EtOAc (3x), and the organic extracts combined, washed with brine and dried over MgSO₄. Purification via flash column chromatography (hexanes/EtOAc, 95:5 – 85:15) yielded 8 mg of pure allylic alcohol **166** as a colorless oil (90%): TLC (hexanes/EtOAc, 80:20): R_f = 0.30; [α]_D²⁵ = -94.5 (*c* = 1.32, CHCl₃); IR (thin film) ν_{max} = 3430 (br), 2959, 1729, 1256, 745 cm⁻¹; ¹H NMR (400 MHz, CDCl₃) δ 7.17 (t, *J* = 8.0 Hz, 1H), 7.05 (dd, *J* = 16, 11 Hz, 1H), 6.80 (d, *J* = 7.6 Hz, 1H), 6.76 (d, *J* = 8.2 Hz, 1H), 6.63 (d, *J* = 16 Hz, 1H), 6.34 (t, *J* = 11 Hz, 1H), 5.97 (dd, *J* = 12, 4.0 Hz, 1H), 5.87 (dd, *J* = 11, 4.0 Hz, 1H), 5.81-5.71 (m, 3H), 5.08 (br d, *J* = 10 Hz, 1H), 4.63 (dd, *J* = 10, 2.8

Hz, 1H), 4.32-4.28 (m, 1H), 4.16-4.10 (m, 1H), 2.79-2.74 (m, 1H), 2.63-2.56 (m, 1H), 1.63 (br, 1H), 0.99 (s, 9H), 0.86 (s, 9H), 0.19 (s, 3H), 0.17 (s, 3H), 0.10 (s, 3H), 0.01 (s, 3H); ^{13}C NMR (100 MHz, CDCl_3) δ 168.4, 152.0, 138.8, 132.2, 131.3, 130.7, 130.6, 129.7, 129.3, 128.7, 128.5, 127.9, 126.7, 121.6, 118.5, 79.6, 66.4, 58.5, 25.9, 18.4, 17.9, -4.0, -4.4, -4.5, -4.9; HRMS (ESI), m/z calcd for $\text{C}_{31}\text{H}_{48}\text{NaO}_5\text{Si}_2$: 579.2938 (M+Na); found, 579.2909.



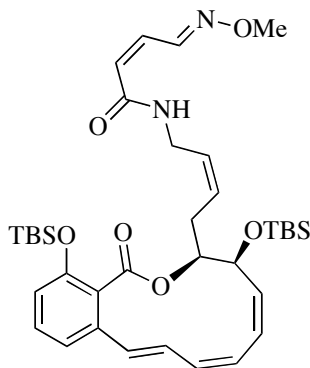
1-((Z)-4-((3S,4S,5Z,7Z,9E)-4,14-Bis(*tert*-butyldimethylsilyloxy)-1-oxo-3,4-dihydro-1H-benzo[*c*][1]oxacyclododecin-3-yl)but-2-enyl)-1H-pyrrole-2,5-dione (175). Allylic alcohol **166** (27 mg, 0.048 mmol), maleimide (**107**) (5 mg, 0.053 mmol) and PPh_3 (23 mg, 0.086 mmol) were dissolved in anhydrous THF (0.480 mL) and cooled to 0 °C. A solution of DEAD (0.039 mL, 0.086 mmol, 40% w/w solution in toluene) was added dropwise, watching the initial yellow color dissipate before an additional drop was added. The reaction was stirred for 15 min, then the volatiles were removed by rotary evaporation. Purification of the crude material by flash column chromatography (hexanes/ CH_2Cl_2 , 80:20 – 30:70, then hexanes/EtOAc, 80:20) yielded 19 mg of the desired allylic maleimide derivative **175** and two mg of

the allylic alcohol **166** (62%, 67% based on recovered starting material): TLC (hexanes/EtOAc, 80:20): $R_f = 0.35$; $[\alpha]_D^{25} = -111$ ($c = 0.310$, CHCl_3); IR (thin film) $\nu_{\text{max}} = 1729, 1155 \text{ cm}^{-1}$; $^1\text{H NMR}$ (400 MHz, CDCl_3) δ 7.16 (t, $J = 8.0$ Hz, 1H), 7.06 (dd, $J = 16, 11$ Hz, 1H), 6.79 (d, $J = 7.7$ Hz, 1H), 6.74 (d, $J = 8.0$ Hz, 1H), 6.63 (d, $J = 16$ Hz, 1H), 6.59 (s, 2H), 6.34 (t, $J = 11$ Hz, 1H), 6.00 (dd, $J = 12, 4.0$ Hz, 1H), 5.87 (dd, $J = 11, 4.1$ Hz, 1H), 5.85 (t, $J = 12$ Hz, 1H), 5.81-5.76 (m, 1H), 5.56-5.50 (m, 1H), 5.14 (td, $J = 10, 3.0$ Hz, 1H), 4.63 (dd, $J = 10, 3.0$ Hz, 1H), 4.24 (dd, $J = 15, 7.1$ Hz, 1H), 4.13 (dd, $J = 15, 7.1$ Hz, 1H), 2.97-2.91 (m, 1H), 2.76-2.68 (m, 1H), 0.97 (s, 9H), 0.89 (s, 9H), 0.19 (s, 3H), 0.18 (s, 3H), 0.11 (s, 3H), 0.02 (s, 3H); $^{13}\text{C NMR}$ (100 MHz, CDCl_3) δ 170.2, 168.4, 152.4, 137.8, 134.0, 132.2, 130.8, 130.7, 130.7, 129.7, 129.2, 128.3, 128.0, 126.6, 125.2, 121.2, 118.1, 79.6, 66.6, 34.5, 25.8, 25.8, 18.4, 17.9, -4.1, -4.2, -4.5, -4.9; HRMS (ESI), m/z calcd for $\text{C}_{35}\text{H}_{50}\text{NO}_6\text{Si}_2$: 636.3177 (M+H); found, 636.3169.



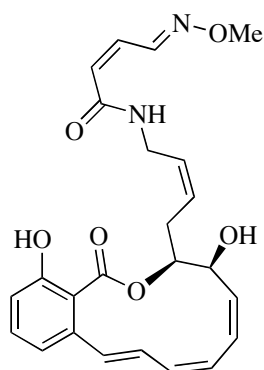
1-((Z)-4-((3S,4S,5Z,7Z,9E)-4,14-Bis(*tert*-butyldimethylsilyloxy)-1-oxo-3,4-dihydro-1*H*-benzo[*c*][1]oxacyclododecin-3-yl)but-2-enyl)-5-hydroxy-1*H*-pyrrol-2(5*H*)-one (178). Allyl maleimide **175** (15 mg, 0.0236 mmol) and $\text{CeCl}_3 \cdot 7\text{H}_2\text{O}$ (6

mg, 0.0236 mmol) were suspended in MeOH (0.100 mL) and cooled to 0 °C. NaBH₄ (0.9 mg, 0.0236 mmol) was added in one portion and the reaction stirred for 30 min. The reaction was diluted with MeOH (5 mL) and the volatiles removed by rotary evaporation. This process was repeated two more times, then the crude material was purified by flash column chromatography (hexanes/EtOAc, 90:10 – 50:50) to yield 13 mg of a dark yellow oil (86%), determined by ¹H NMR and LC/MS to be a 55:45 ratio of diastereomers. These diastereomers were not separated and the mixture used in the subsequent step: TLC (hexanes/EtOAc, 70:30): R_f = 0.20; [α]_D²⁵ = -61 (c = 0.25, CHCl₃); IR (thin film) ν_{max} = 3337 (br), 1732, 1690, 1596, 1455, 1253, 1168, 701 cm⁻¹; HRMS (ESI), *m/z* calcd for C₃₅H₅₂NO₆Si₂: 638.3333 (M+H); found, 638.3342.



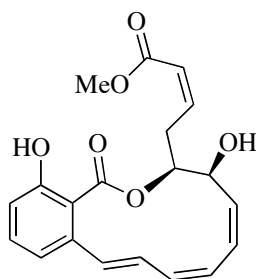
(2Z)-N-((Z)-4-((3S,4S,5Z,7Z,9E)-4,14-Bis(*tert*-butyldimethylsilyloxy)-1-oxo-3,4-dihydro-1H-benzo[*c*][1]oxacyclododecin-3-yl)but-2-enyl)-4-(methoxyimino)but-2-enamide (179). Hydroxy-pyrrolone **178** (13 mg, 0.020 mmol), NaHCO₃ (17 mg, 0.203 mmol), and MeONH₃Cl (17 mg, 0.203 mmol) were suspended in MeOH (0.200 mL) in a sealed vial. This suspension was heated to 75 °C for 12 h. Upon cooling,

the solvent was removed by rotary evaporation and the crude material purified by flash column chromatography (hexanes/EtOAc, 90:10 – 50:50) to yield 4.5 mg of the desired oxime amide **179** as a colorless oil (a 3:1 ratio of *E*:*Z* oxime ether stereoisomers by ¹H NMR) and 5 mg of the starting material (34%, 54% based on recovered starting material): TLC (hexanes/EtOAc, 70:30): R_f = 0.65; IR (thin film) ν_{\max} = 3308 (br), 1733, 1674, 1569, 1539, 1049, 700 cm⁻¹; ¹H NMR (400 MHz, CDCl₃) δ 8.96 (dd, *J* = 10, 0.8 Hz, 1H), 7.23-7.18 (m, 1H), 7.02 (dd, *J* = 16, 11 Hz, 1H), 6.85 (dd, *J* = 7.7, 3.6 Hz, 1H), 6.77 (d, *J* = 8.5 Hz, 1H), 6.63 (d, *J* = 16 Hz, 1H), 6.34 (t, *J* = 11 Hz, 1H), 6.21 (dd, *J* = 12, 10 Hz, 1H), 5.98 (dd, *J* = 12, 4.1 Hz, 1H), 5.88 (dd, *J* = 11, 4.2 Hz, 1H), 5.84 (br, 1H), 5.79-5.72 (m, 1H), 5.75 (t, *J* = 11 Hz, 1H), 5.71-5.64 (m, 1H), 5.46 (dt, *J* = 11, 0.8 Hz, 1H), 5.12-5.08 (m, 1H), 4.63 (dd, *J* = 10, 3.0 Hz, 1H), 4.09-3.99 (m, 1H), 3.93-3.85 (m, 1H), 3.91 (s, 3H), 2.71-2.68 (m, 2H), 0.98 (s, 9H), 0.89 (s, 9H), 0.17 (s, 3H), 0.15 (s, 3H), 0.10 (s, 3H), 0.01 (s, 3H); Minor *Z*-oxime ether isomer peaks: 8.42 (dd, *J* = 9.6, 0.9 Hz, 1H), 3.94 (s, 3H); ¹³C NMR (100 MHz, CDCl₃) δ 168.2, 164.7, 151.9, 147.8, 138.2, 133.2, 132.2, 131.3, 130.7, 130.5, 129.5, 128.7, 128.1, 127.5, 125.5, 122.1, 118.7, 79.5, 66.3, 62.1, 35.9, 25.9, 25.7, 18.4, 17.9, -4.0, -4.4, -4.5, -4.9; HRMS (ESI), *m/z* calcd for C₃₆H₅₅N₂O₆Si₂: 667.3599 (M+H); found, 667.3607.

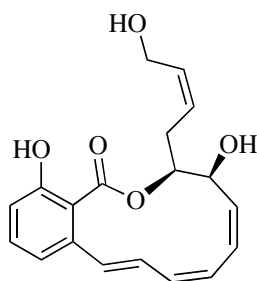


(2Z)-N-((Z)-4-((3S,4S,5Z,7Z,9E)-4,14-Dihydroxy-1-oxo-3,4-dihydro-1H-benzo[c][1]oxacyclododecin-3-yl)but-2-enyl)-4-(methoxyimino)but-2-enamide

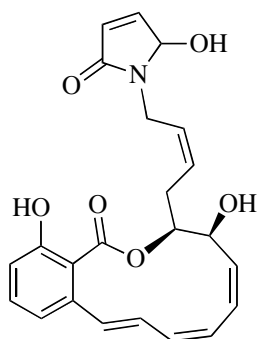
(165). To a THF solution (0.009 mL) of bis-TBS oxime ether **179** (6 mg, 0.009 mmol) at room temperature was added 0.055 mL of 5M HF/Py. solution. The reaction was stirred for 24 h, then quenched with pH 7 buffer. The aqueous layer was extracted with EtOAc (3x), the organic extracts washed with brine and dried over MgSO₄. Purification of the crude material by flash column chromatography (hexanes/EtOAc, 80:20 – 40:60) gave 3.5 mg of a tan solid (89%): TLC (hexanes/EtOAc, 50:50): R_f = 0.10; ¹H NMR (400 MHz, CDCl₃) δ 10.48 (br, 1H), 8.99 (dd, *J* = 10, 0.6 Hz, 1H), 7.32 (br, 1H), 6.90 (d, *J* = 7.9 Hz, 1H), 6.78-6.76 (m, 3H), 6.40 (t, *J* = 11 Hz, 2H), 6.30 (br, 1H), 6.08 (d, *J* = 13 Hz, 1H), 5.93 (br, 1H), 5.79 (br, 1H), 5.75 (d, *J* = 7.5 Hz, 1H), 5.65-5.61 (m, 1H), 5.58 (br, 1H), 5.47 (br, 1H), 4.40 (br, 1H), 3.93 (s, 3H), 3.87 (br, 1H), 3.02 (br, 1H), 2.67 (br, 1H), 2.51 (br, 1H), 1.29 (br, 1H); HRMS (ESI), *m/z* calcd for C₂₄H₂₇N₂O₆: 439.1869 (M+H); found, 439.1863; UPLC-MS analysis established 95.4% purity prior to biological testing.



(Z)-Methyl 4-((3S,4S,5Z,7Z,9E)-4,14-Dihydroxy-1-oxo-3,4-dihydro-1H-benzo[c][1]oxacyclododecin-3-yl)but-2-enoate (180). To a THF solution (0.220 mL) of bis-TBS ester **170** (13 mg, 0.022 mmol) at room temperature was added 0.135 mL of 5M HF/Py. solution. The reaction was stirred for 24 h, then quenched with pH 7 buffer. The aqueous layer was extracted with EtOAc (3x), the organic extracts washed with brine and dried over MgSO₄. Purification of the crude material by flash column chromatography (hexanes/EtOAc, 80:20 – 50:50) gave 7 mg of a colorless oil (89%): TLC (hexanes/EtOAc, 60:40): R_f = 0.10; ¹H NMR (400 MHz, CDCl₃) δ 10.30 (br, 1H), 7.30 (t, *J* = 8.0 Hz, 1H), 6.88 (d, *J* = 8.2 Hz, 1H), 6.77-6.71 (br m, 3H), 6.38 (br, 1H), 6.22 (br, 1H), 6.07 (br d, *J* = 12 Hz, 1H), 5.87 (d, *J* = 11 Hz, 1H), 5.81 (dd, *J* = 12, 4.9 Hz, 1H), 5.59 (br, 1H), 4.42 (br, 1H), 3.68 (s, 3H), 3.26 (br, 1H), 3.10-3.04 (m, 1H), 2.88 (br, 1H), 1.28 (br, 1H); HRMS (ESI), *m/z* calcd for C₂₀H₂₁O₆: 357.1338 (M+H); found, 357.1323; UPLC-MS analysis revealed 94.6% purity prior to biological testing.



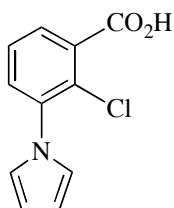
(3*S*,4*S*,5*Z*,7*Z*,9*E*)-4,14-Dihydroxy-3-((*Z*)-4-hydroxybut-2-enyl)-3,4-dihydro-1*H*-benzo[*c*][1]oxacyclododecin-1-one (181). To a THF solution (0.230 mL) of bis-TBS *Z*-allylic alcohol **166** (13 mg, 0.023 mmol) at room temperature was added 0.143 mL of 5M HF/Pyr. solution. The reaction was stirred for 24 h, then quenched with pH 7 buffer. The aqueous layer was extracted with EtOAc (3x), the organic extracts washed with brine and dried over MgSO₄. Purification of the crude material by flash column chromatography (hexanes/EtOAc, 50:50 – 30:70) gave 6 mg of a white solid (80%): TLC (hexanes/EtOAc, 40:60): R_f = 0.15; ¹H NMR (400 MHz, *d*₆-DMSO) δ 9.34 (s, 1H), 7.16 (t, *J* = 7.9 Hz, 1H), 6.92 (dd, *J* = 16, 12 Hz, 1H), 6.75 (d, *J* = 8.0 Hz, 1H), 6.70 (s, 1H), 6.68 (t, *J* = 8.4 Hz, 1H), 6.35 (t, *J* = 11 Hz, 1H), 5.96 (ddd, *J* = 17, 11, 4.2 Hz, 2H), 5.79 (t, *J* = 11 Hz, 1H), 5.61-5.49 (m, 2H), 5.31 (d, *J* = 4.6 Hz, 1H), 5.04 (td, *J* = 12, 2.0 Hz, 1H), 4.58 (t, *J* = 5.2 Hz, 1H), 4.36 (td, *J* = 10, 4.0 Hz, 1H), 4.10-3.98 (m, 2H), 2.73 (m, 1H), 2.39-2.31 (m, 1H), 1.27 (br, 1H); ¹³C NMR (100 MHz, *d*₆-DMSO) δ 168.2, 153.8, 137.4, 132.5, 132.1, 130.7, 129.8, 129.6, 129.5, 128.5, 128.4, 125.8, 121.8, 118.6, 114.1, 79.0, 64.5, 57.0, 24.9; HRMS (ESI), *m/z* calcd for C₁₉H₂₁O₅: 329.1389 (M+H); found, 329.1393; UPLC-MS analysis revealed 82.1% purity prior to biological testing.



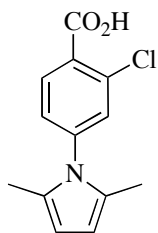
1-((Z)-4-((3S,4S,5Z,7Z,9E)-4,14-Dihydroxy-1-oxo-3,4-dihydro-1H-benzo[c][1]oxacyclododecin-3-yl)but-2-enyl)-5-hydroxy-1H-pyrrol-2(5H)-one (183). To a THF solution (0.141 mL) of bis-TBS hydroxy-pyrrole **178** (9 mg, 0.0141 mmol) at room temperature was added 0.086 mL of 5M HF/Py. solution. The reaction was stirred for 24 h, then quenched with pH 7 buffer. The aqueous layer was extracted with EtOAc (3x), the organic extracts washed with brine and dried over MgSO₄. Purification of the crude material by flash column chromatography (hexanes/EtOAc, 70:30 – 0:100) gave 4 mg of a tan solid (69%): TLC (hexanes/EtOAc, 40:60): R_f = 0.04; ¹H NMR (400 MHz, d₆-DMSO) δ 9.93 (d, *J* = 12 Hz, 1H), 7.16 (t, *J* = 7.9 Hz, 1H), 7.01 (d, *J* = 6.0 Hz, 1H), 6.98-6.90 (m, 1H), 6.76 (dd, *J* = 8.0, 5.0 Hz, 1H), 6.70 (s, 1H), 6.68 (t, *J* = 7.0 Hz, 1H), 6.36 (t, *J* = 11 Hz, 1H), 6.19 (dd, *J* = 9.1, 6.5 Hz, 1H), 6.09 (dd, *J* = 7.8, 6.0 Hz, 1H), 5.97 (ddd, *J* = 15, 11, 4.0 Hz, 2H), 5.81 (t, *J* = 11 Hz, 1H), 5.67-5.61 (m, 1H), 5.51-5.45 (m, 1H), 5.36-5.32 (m, 2H), 5.08 (td, *J* = 9.3, 5.0 Hz, 1H), 4.38 (td, *J* = 10, 3.8 Hz, 1H), 4.12-4.07 (m, 1H), 3.81 (dd, *J* = 15, 7.8 Hz, 1H), 2.86-2.78 (m, 1H), 2.58-2.50 (m, 1H); ¹³C NMR (100 MHz, d₆-DMSO) δ 168.4, 168.2, 153.9, 147.6, 137.4, 132.1, 130.7, 129.9,

129.6, 129.5, 128.6, 128.5, 128.4, 127.1, 121.8, 118.7, 114.2, 82.0, 81.9, 64.6, 35.4, 24.7, 20.8; HRMS (ESI), m/z calcd for $C_{23}H_{24}NO_6$: 410.1604 (M+H); found, 410.1591; UPLC-MS analysis revealed 85.5% purity prior to biological testing.

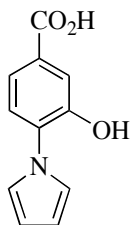
4.3.2 Chapter 2



2-Chloro-3-(1*H*-pyrrol-1-yl)benzoic Acid (242). 3-Amino-2-chloro-benzoic acid **241** (50 mg, 0.291 mmol) was dissolved in HOAc (0.090 mL). To this solution was added 2,5-dimethoxytetrahydrofuran (**229**) (40 mg, 0.040 mL, 0.306 mmol) and the mixture heated to reflux for two h. The solution was then cooled to room temperature and the volatiles removed under reduced pressure. The resultant material was dissolved in Et₂O, filtered through filter paper, and purified by flash column chromatography (hexanes/EtOAc, 50:50 – 40:60) to yield 9 mg of a white solid (14%): TLC (hexanes/EtOAc, 25:75): R_f = 0.60; ¹H NMR (400 MHz, *d*₆-DMSO) δ 13.66 (br, 1H), 7.66 (br d, J = 6.7 Hz, 1H), 7.50-7.47 (m, 2H), 6.99 (t, J = 2.2 Hz, 2H), 6.25 (t, J = 2.2 Hz, 2H); HRMS (ESI), m/z calcd for $C_{11}H_7ClNO_2$: 220.0171 (M-H); found, 220.0166.

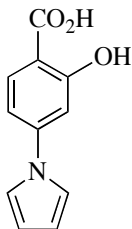


2-Chloro-4-(2,5-dimethyl-1H-pyrrol-1-yl)benzoic Acid (245). 4-Amino-2-chlorobenzoic acid (**243**) (100 mg, 0.583 mmol) was dissolved in HOAc (0.175 mL). To this solution was added 2,5-hexanedione (**244**) (70 mg, 0.072 mL, 0.612 mmol) and the mixture heated to reflux for two h. The solution was then cooled to room temperature and the volatiles removed under reduced pressure. The resultant material was dissolved in Et₂O, filtered through filter paper, and purified by flash column chromatography (hexanes/EtOAc, 50:50 – 40:60) to yield 4 mg of a white solid (3%): TLC (hexanes/EtOAc, 25:75): R_f = 0.50; ¹H NMR (400 MHz, *d*₆-DMSO) δ 13.58 (br, 1H), 7.89 (d, *J* = 8.2 Hz, 1H), 7.52 (d, *J* = 2.0 Hz, 1H), 7.34 (dd, *J* = 8.2, 2.0 Hz, 1H), 5.84 (s, 2H), 2.00 (s, 6H); ¹³C NMR (100 MHz, *d*₆-DMSO) δ 166.3, 141.3, 132.1, 131.4, 129.7, 127.7, 126.8, 106.8, 12.8; HRMS (ESI), *m/z* calcd for C₁₃H₁₁ClNO₂: 248.0484 (M-H); found, 248.0488.



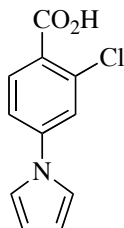
3-Hydroxy-4-(1H-pyrrol-1-yl)benzoic Acid (247). 4-Amino-3-hydroxy-benzoic acid (**246**) (100 mg, 0.653 mmol) was dissolved in HOAc (0.200 mL). To this

solution was added 2,5-dimethoxytetrahydrofuran (**229**) (91 mg, 0.089 mL, 0.686 mmol) and the mixture heated to reflux for two h. The solution was then cooled to room temperature and the volatiles removed under reduced pressure. The resultant material was dissolved in Et₂O, filtered through filter paper, and purified by flash column chromatography (hexanes/EtOAc, 50:50 – 40:60) to yield 10 mg of a brown solid (8%): TLC (hexanes/EtOAc, 25:75): R_f = 0.45; ¹H NMR (400 MHz, *d*₆-DMSO) δ 12.88 (br, 1H), 10.37 (br, 1H), 7.61 (d, *J* = 1.8 Hz, 1H), 7.44 (d, *J* = 1.8 Hz, 1H), 7.4 (s, 1H), 7.36 (dt, *J* = 7.6, 1.2 Hz, 1H), 7.21 (t, *J* = 2.2 Hz, 2H), 6.21 (t, *J* = 2.2 Hz, 2H).

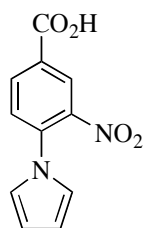


2-Hydroxy-4-(1*H*-pyrrol-1-yl)benzoic Acid (249). 4-Amino-2-hydroxy-benzoic acid (**248**) (100 mg, 0.653 mmol) was dissolved in HOAc (0.200 mL). To this solution was added 2,5-dimethoxytetrahydrofuran (**229**) (91 mg, 0.089 mL, 0.686 mmol) and the mixture heated to reflux for two h. The solution was then cooled to room temperature and the volatiles removed under reduced pressure. The resultant material was dissolved in Et₂O, filtered through filter paper, and purified by flash column chromatography (hexanes/EtOAc, 50:50 – 40:60) to yield 89 mg of a white solid (67%): TLC (hexanes/EtOAc, 25:75): R_f = 0.60; ¹H NMR (400 MHz, *d*₆-DMSO) δ 13.85 (br, 1H), 11.56 (br, 1H), 7.83 (d, *J* = 8.5 Hz, 1H), 7.50 (t, *J* = 2.2 Hz,

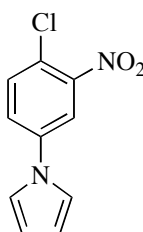
2H), 7.21 (d, $J = 2.2$ Hz, 1H), 7.18 (dd, $J = 8.5, 2.2$ Hz, 1H), 6.30 (t, $J = 2.2$ Hz, 2H); ^{13}C NMR (100 MHz, d_6 -DMSO) δ 171.6, 162.6, 145.2, 131.9, 119.1, 111.5, 109.7, 109.4, 106.2; HRMS (ESI), m/z calcd for $\text{C}_{11}\text{H}_8\text{NO}_3$: 202.0510 (M-H); found, 202.0506.



2-Chloro-4-(1H-pyrrol-1-yl)benzoic Acid (251). 4-Amino-2-chloro-benzoic acid (**250**) (100 mg, 0.583 mmol) was dissolved in HOAc (0.175 mL). To this solution was added 2,5-dimethoxytetrahydrofuran (**229**) (81 mg, 0.079 mL, 0.612 mmol) and the mixture heated to reflux for two h. The solution was then cooled to room temperature and the volatiles removed under reduced pressure. The resultant material was dissolved in Et_2O , filtered through filter paper, and purified by flash column chromatography (hexanes/EtOAc, 50:50 – 40:60) to yield 12 mg of a white solid (9%): TLC (hexanes/EtOAc, 25:75): $R_f = 0.60$; ^1H NMR (400 MHz, d_6 -DMSO) δ 13.31 (br, 1H), 7.89 (d, $J = 8.6$ Hz, 1H), 7.84 (d, $J = 2.2$ Hz, 1H), 7.67 (dd, $J = 8.6, 2.2$ Hz, 1H), 7.55 (t, $J = 2.2$ Hz, 2H), 6.32 (t, $J = 2.2$ Hz, 2H); ^{13}C NMR (100 MHz, d_6 -DMSO) δ 165.9, 142.5, 133.7, 132.7, 120.3, 119.2, 116.9, 111.6; HRMS (ESI), m/z calcd for $\text{C}_{11}\text{H}_7\text{ClNO}_2$: 220.0171 (M-H); found, 220.0168.

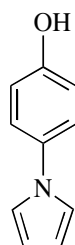


3-Nitro-4-(1H-pyrrol-1-yl)benzoic Acid (253). 4-Amino-3-nitro-benzoic acid (**252**) (100 mg, 0.549 mmol) was dissolved in HOAc (0.165 mL). To this solution was added 2,5-dimethoxytetrahydrofuran (**229**) (76 mg, 0.075 mL, 0.575 mmol) and the mixture heated to reflux for two h. The solution was then cooled to room temperature and the volatiles removed under reduced pressure. The resultant material was dissolved in Et₂O, filtered through filter paper, and purified by flash column chromatography (hexanes/EtOAc, 50:50 – 20:80) to yield 3 mg of a gold solid (2%): TLC (hexanes/EtOAc, 25:75): R_f = 0.20; ¹H NMR (500 MHz, *d*₆-DMSO) δ 13.79 (br, 1H), 8.50 (d, *J* = 2.2 Hz, 1H), 8.31 (dd, *J* = 8.4, 2.2 Hz, 1H), 7.83 (d, *J* = 8.4 Hz, 1H), 7.05 (t, *J* = 2.0 Hz, 2H), 6.39 (t, *J* = 2.0 Hz, 2H); ¹³C NMR (125 MHz, CDCl₃) δ 165.0, 143.8, 135.7, 134.1, 128.7, 128.0, 121.3, 111.5.



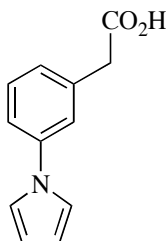
1-(4-Chloro-3-nitrophenyl)-1H-pyrrole (238). 4-Chloro-3-nitroaniline (**254**) (100 mg, 0.579 mmol) was dissolved in HOAc (0.174 mL). To this solution was added 2,5-dimethoxytetrahydrofuran (**229**) (80 mg, 0.079 mL, 0.608 mmol) and the mixture

heated to reflux for two h. The solution was then cooled to room temperature and the volatiles removed under reduced pressure. The resultant material was dissolved in Et₂O, filtered through filter paper, and purified by flash column chromatography (hexanes/EtOAc, 50:50 – 20:80) to yield 39 mg of a yellow solid (30%): TLC (hexanes/EtOAc, 25:75): R_f = 0.65; ¹H NMR (400 MHz, *d*₆-DMSO) δ 8.33 (d, 1H, *J* = 2.7 Hz), 7.95 (dd, *J* = 8.9, 2.7 Hz, 1H), 7.81 (d, *J* = 8.9 Hz, 1H), 7.53 (t, *J* = 2.3 Hz, 2H), 6.33 (t, *J* = 2.3 Hz, 2H); ¹³C NMR (100 MHz, CDCl₃) δ 148.5, 139.3, 132.5, 123.3, 120.0, 119.3, 115.2, 111.7.

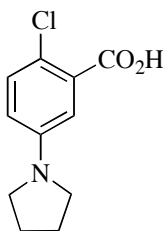


4-(1*H*-Pyrrol-1-yl)phenol (256). 4-Amino-phenol (**255**) (100 mg, 0.916 mmol) was dissolved in HOAc (0.300 mL). To this solution was added 2,5-dimethoxytetrahydrofuran (**229**) (127 mg, 0.125 mL, 0.962 mmol) and the mixture heated to reflux for two h. The solution was then cooled to room temperature and the volatiles removed under reduced pressure. The resultant material was dissolved in Et₂O, filtered through filter paper, and purified by flash column chromatography (hexanes/EtOAc, 50:50 – 40:60) to yield 70 mg of a white solid (48%): TLC (hexanes/EtOAc, 25:75): R_f = 0.85; ¹H NMR (400 MHz, *d*₆-DMSO) δ 9.48 (s, 1H), 7.32 (d, *J* = 8.8 Hz, 2H), 7.16 (t, *J* = 2.0 Hz, 2H), 6.83 (d, *J* = 8.8 Hz, 2H), 6.19 (t, *J* =

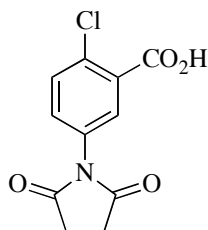
2.0 Hz, 2H); ^{13}C NMR (100 MHz, CDCl_3) δ 155.2, 132.3, 121.2, 119.1, 115.9, 109.6; LRMS (ES^+), m/z calcd for $\text{C}_{10}\text{H}_{10}\text{NO}$: 160.1 (M+H); found, 160.1.



2-(3-(1H-Pyrrol-1-yl)phenyl)acetic Acid (258). 3-Aminophenylacetic acid (**257**) (100 mg, 0.662 mmol) was dissolved in HOAc (0.200 mL). To this solution was added 2,5-dimethoxytetrahydrofuran (**229**) (92 mg, 0.090 mL, 0.695 mmol) and the mixture heated to reflux for two h. The solution was then cooled to room temperature and the volatiles removed under reduced pressure. The resultant material was dissolved in Et_2O , filtered through filter paper, and purified by flash column chromatography (hexanes/EtOAc, 50:50 – 40:60) to yield 27 mg of a pale yellow solid (20%): TLC (hexanes/EtOAc, 25:75): $R_f = 0.60$; ^1H NMR (400 MHz, d_6 -DMSO) δ 12.40 (br, 1H), 7.47-7.43 (m, 2H), 7.38 (t, $J = 7.6$ Hz, 1H), 7.33 (t, $J = 2.2$ Hz, 2H), 7.13 (d, $J = 7.5$ Hz, 1H), 6.26 (t, $J = 2.2$ Hz, 2H), 3.64 (s, 2H); ^{13}C NMR (100 MHz, CDCl_3) δ 172.5, 139.8, 136.7, 129.5, 126.4, 120.5, 118.9, 117.6, 110.4, 40.4; HRMS (ESI), m/z calcd for $\text{C}_{12}\text{H}_{10}\text{NO}_2$: 200.0717 (M-H); found, 200.0710.

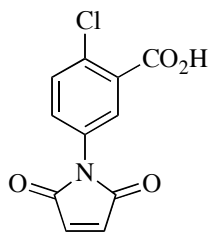


2-Chloro-5-(pyrrolidin-1-yl)benzoic Acid (261). 5-Amino-2-chlorobenzoic acid (**259**) (100 mg, 0.583 mmol) was dissolved in HOAc (0.200 mL). To this solution was added 1,4-dibromobutane (**260**) (139 mg, 0.076 mL, 0.641 mmol) and the mixture heated to 90 °C for 12 h. The solution was then cooled to room temperature and the volatiles removed under reduced pressure. The resultant material was dissolved in Et₂O, filtered through filter paper, and purified by flash column chromatography (hexanes/EtOAc, 60:40) to yield 16 mg of a yellow solid (12%): TLC (hexanes/EtOAc, 25:75): R_f = 0.50; ¹H NMR (400 MHz, *d*₆-DMSO) δ 13.14 (br, 1H), 7.24 (d, *J* = 8.8 Hz, 1H), 6.82 (d, *J* = 3.0 Hz, 1H), 6.64 (dd, *J* = 8.8, 3.0 Hz, 1H), 3.22 (t, *J* = 6.5 Hz, 4H), 1.95 (t, *J* = 6.5 Hz, 4H); ¹³C NMR (100 MHz, *d*₆-DMSO) δ 167.4, 146.1, 131.7, 130.7, 116.6, 115.1, 112.7, 47.4, 25.0; HRMS (ES⁺), *m/z* calcd for C₁₁H₁₃ClNO₂: 226.0635 (M+H); found, 226.0638.



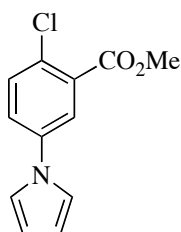
2-Chloro-5-(2,5-dioxopyrrolidin-1-yl)benzoic Acid (263). 5-Amino-2-chlorobenzoic acid (**259**) (100 mg, 0.583 mmol) was dissolved in HOAc (0.175 mL).

To this solution was added succinic anhydride (**262**) (61 mg, 0.612 mmol) and the mixture heated to reflux for two h. The solution was then cooled to room temperature and the volatiles removed under reduced pressure. The resultant material was dissolved in Et₂O, filtered through filter paper, and purified by flash column chromatography (hexanes/EtOAc, 60:40) to yield 59 mg of a yellow solid (40%): TLC (hexanes/EtOAc, 25:75): R_f = 0.50; ¹H NMR (400 MHz, *d*₆-DMSO) δ 13.50 (br, 1H), 7.76 (d, *J* = 2.5 Hz, 1H), 7.68 (d, *J* = 8.6 Hz, 1H), 7.45 (dd, *J* = 8.6, 2.5 Hz, 1H), 2.78 (s, 4H); ¹³C NMR (100 MHz, *d*₆-DMSO) δ 176.6, 165.9, 131.7, 131.6, 131.2, 131.2, 131.0, 129.4, 28.5; HRMS (ESI), *m/z* calcd for C₁₁H₇ClNO₄: 252.0069 (M-H); found, 252.0056.

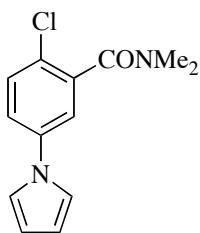


2-Chloro-5-(2,5-dioxo-2,5-dihydro-1H-pyrrol-1-yl)benzoic Acid (265). 5-Amino-2-chlorobenzoic acid (**259**) (500 mg, 2.914 mmol) was dissolved in HOAc (2.90 mL). To this solution was added maleic anhydride (**264**) (286 mg, 2.914 mmol) and the mixture heated to reflux for two h. The solution was then cooled to room temperature, upon which time a yellow precipitate formed. The precipitate was filtered and washed with water, dried under reduced pressure, and recrystallized from EtOH to yield 339 mg of a bright yellow solid (46%): TLC (hexanes/EtOAc, 25:75): R_f = 0.60; ¹H NMR (400 MHz, *d*₆-DMSO) δ 13.62, (br, 1H), 7.81 (d, *J* = 2.4 Hz, 1H),

7.68 (d, $J = 8.6$ Hz, 1H), 7.53 (dd, $J = 8.4, 2.5$ Hz, 1H), 7.21 (s, 2H); ^{13}C NMR (100 MHz, d_6 -DMSO) δ 169.5, 166.0, 134.8, 131.8, 131.2, 130.6, 130.4, 128.6; HRMS (ESI), m/z calcd for $\text{C}_{11}\text{H}_5\text{ClNO}_4$: 249.9913 (M-H); found, 249.9912.

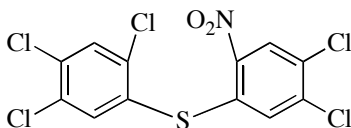


Methyl 2-Chloro-5-(1H-pyrrol-1-yl)benzoate (239). 2-Chloro-5-(1H-pyrrol-1-yl)benzoic acid (**226**) (10 mg, 0.045 mmol) was dissolved in anhydrous MeOH (0.090 mL) at room temperature. A solution of TMSCH_2N_2 (0.113 mL, 0.226 mmol, 2.0M in Et_2O) was added dropwise and a yellow color developed in the reaction medium. After five min of stirring, the reaction was quenched with three drops of HOAc and the volatiles were removed under reduced pressure. The resultant material was purified by flash column chromatography (hexanes/EtOAc, 70:30) to yield 10 mg of a brown oil (94%): TLC (hexanes/EtOAc, 70:30): $R_f = 0.75$; ^1H NMR (400 MHz, CDCl_3) δ 7.68 (d, $J = 2.7$ Hz, 1H), 7.31 (d, $J = 8.6$ Hz, 1H), 7.26 (dd, $J = 8.6, 2.7$ Hz, 1H), 6.90 (t, $J = 2.2$ Hz, 2H), 6.20 (t, $J = 2.2$ Hz, 2H), 3.79 (s, 3H); ^{13}C NMR (100 MHz, CDCl_3) δ 165.6, 139.3, 132.3, 131.0, 130.4, 124.1, 122.9, 110.3, 111.5, 52.8; HRMS (ES^+), m/z calcd for $\text{C}_{12}\text{H}_{11}\text{ClNO}_2$: 236.0478 (M+H); found, 236.0478.

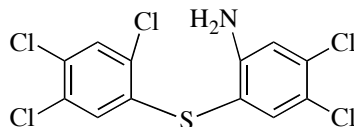


2-Chloro-*N,N*-dimethyl-5-(1*H*-pyrrol-1-yl)benzamide (240). 2-Chloro-5-(1*H*-pyrrol-1-yl)benzoic acid (**226**) (30 mg, 0.135 mmol) and Me₂NH₂Cl (12 mg, 0.149 mmol) were dissolved in anhydrous DMF (0.200 mL) at 0 °C. EDCI (40 mg, 0.203 mmol) was added in one portion and the reaction stirred for 16 h, allowing to warm to room temperature. The reaction was the diluted with Et₂O and quenched with cold 10% HCl solution. The organic layer was separated from the aqueous layer and the organic layer washed with water (3x), brine (1x) and dried over Na₂SO₄ to yield 10 mg of a white solid (24%): TLC (hexanes/EtOAc, 25:75): R_f = 0.65; ¹H NMR (400 MHz, CDCl₃) δ 7.44 (dd, *J* = 8.3, 0.6 Hz, 1H), 7.37-7.33 (m, 2H), 7.06 (t, *J* = 2.2 Hz, 2H), 6.37 (t, *J* = 2.2 Hz, 2H), 3.17 (s, 3H), 2.92 (s, 3H); ¹³C NMR (100 MHz, CDCl₃) δ 167.8, 140.0, 137.7, 130.9, 127.1, 121.8, 119.6, 119.3, 111.4, 38.3, 34.9; HRMS (ES⁺), *m/z* calcd for C₁₃H₁₄ClN₂O: 249.0795 (M+H); found, 249.0794.

4.3.3 Chapter 3

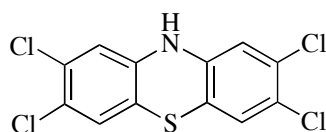


(4,5-Dichloro-2-nitrophenyl)(2,4,5-trichlorophenyl)sulfane (277). 2,4,5-Trichlorothiophenol (**275**) (20.7 g, 97.0 mmol), 1,2-dichloro-4-fluoro-5-nitrobenzene (**276**) (22.4 g, 107 mmol), K_2CO_3 (67.0 g, 485 mmol), $CaCO_3$ (7.31 g, 73.0 mmol) and two weight equivalents of activated 3Å mol. sieves were stirred and heated in refluxing CH_2Cl_2 (500 mL) for 21 h. Upon cooling to room temperature, a yellow precipitate formed that was filtered and washed with CH_2Cl_2 to yield 37.1 g of a yellow solid (97%): TLC (hexanes/EtOAc, 95:5): $R_f = 0.70$; 1H NMR (400 MHz, $CDCl_3$) δ 8.38 (s, 1H), 7.80 (s, 1H), 7.72 (s, 1H), 6.76 (s, 1H); ^{13}C NMR (100 MHz, $CDCl_3$) δ 139.8, 138.8, 138.6, 136.8, 135.9, 132.9, 132.6, 131.3, 130.5, 129.1, 128.6, 127.8; GC/MS : $t_R = 43:08$ min, 401 (10% ($C_{12}H_4Cl_5NO_2S^+$)), 354 (2% ($C_{12}H_3Cl_5S^+$)), 337 (3% ($C_{12}H_4Cl_5NO_2S^+$)), 302 (75% ($C_{12}H_4Cl_4NO_2S^+ - 64$)), 276 (3% ($C_{12}H_3Cl_3NO_2S^+ - 64$)), 250 (13% ($C_{12}H_4Cl_2S^+$)), 176 (12% ($C_{12}S^+$)); melting point 162-164 °C.



4,5-Dichloro-2-(2,4,5-trichlorophenylthio)aniline (278). To a refluxing solution of nitrobenzene **277** (44.4 g, 110 mmol) in HOAc (375 mL), acetone (1.5 L), and distilled water (375 mL) were added Fe filings (80 g total) in four portions over two

h. The reaction was refluxed for 30 additional min, then cooled. Upon cooling to room temperature, the solution pH was adjusted to 8 with 1N NaOH solution. The solution was then filtered through a pad of Celite and the rinsed with 1N NaOH solution, water, acetone and Et₂O until the solvent became colorless. The resulting eluent was then extracted with Et₂O, dried over MgSO₄ and concentrated under reduced pressure. The crude material was washed with hexanes and the hexanes were decanted, yielding 35.3 g of the desired aniline product **278** as a bright yellow solid (86%): TLC (hexanes/EtOAc, 95:5): R_f = 0.35; ¹H NMR (400 MHz, CDCl₃) δ 7.50 (s, 1H), 7.45 (s, 1H), 6.93 (s, 1H), 6.65 (s, 1H), 4.33 (s, 2H); ¹³C NMR (100 MHz, CDCl₃) δ 148.4, 138.4, 136.5, 135.3, 132.2, 131.0, 130.4, 130.0, 127.3, 121.6, 116.8, 111.4; GC/MS: t_R = 44:13 min, 371 (57% (C₁₂H₆Cl₅NS⁺)), 335 (44% (C₁₂H₅Cl₄NS⁺)), 301 (60% (C₁₂H₆Cl₃NS⁺)), 266 (10% (C₁₂H₆Cl₂NS⁺)), 230 (4% (C₁₂H₅CINS⁺)), 192 (17% (C₁₂H₂NS⁺)); melting point 190-192 °C.

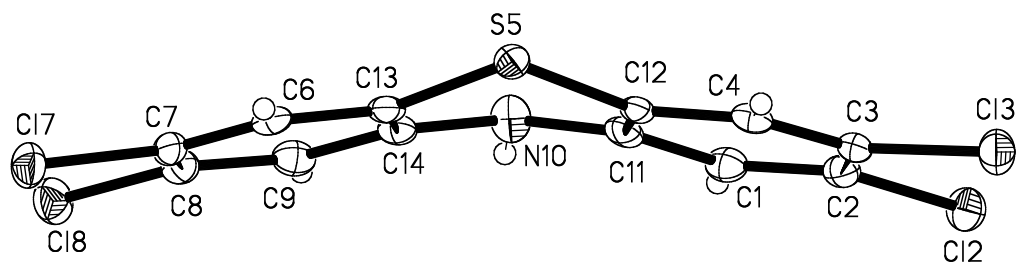
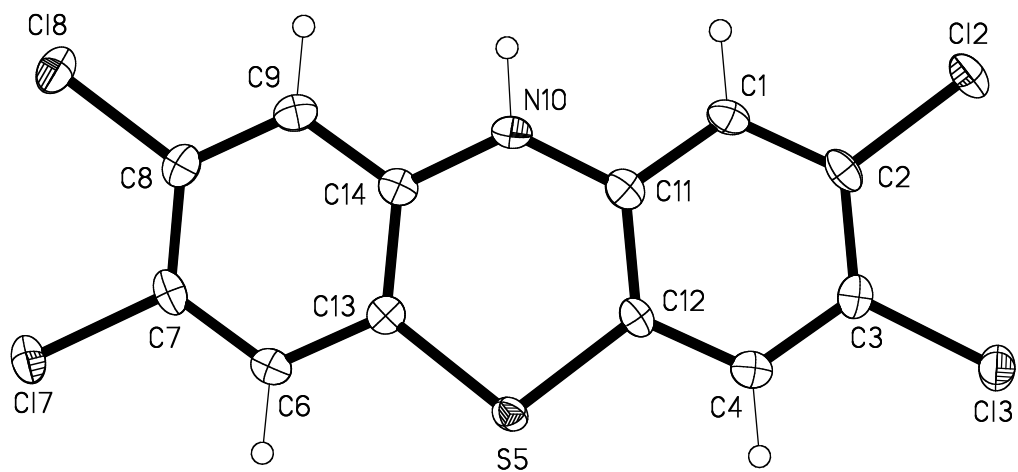
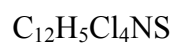


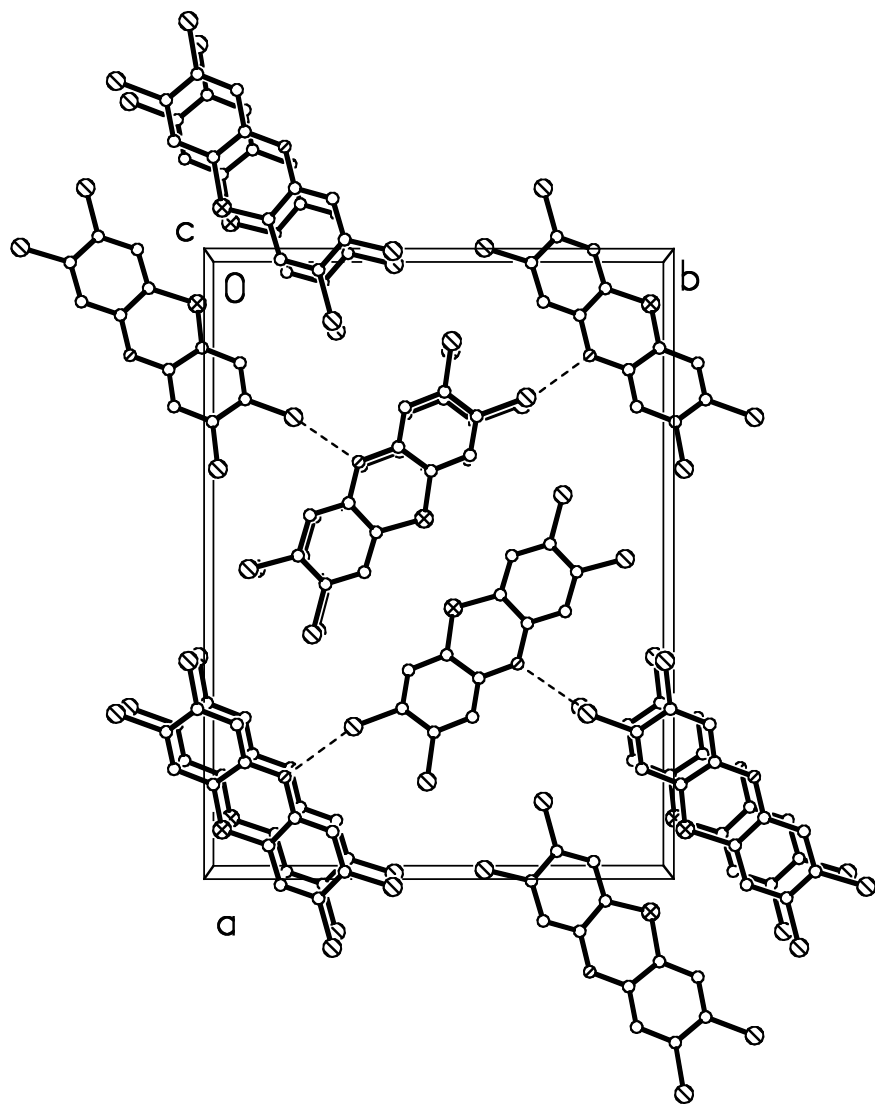
2,3,7,8-Tetrachloro-10H-phenothiazine (274). *Microwave conditions:* A solution containing Pd(OAc)₂ (4.65 mg, 0.0207 mmol) and 2-(dicyclohexyl-phosphano)-biphenyl (14.5 mg, 0.0414 mmol) in anhydrous DMF (4.65 mL) was prepared and added to aniline **278** (75.0 mg, 0.207 mmol) and NaO^tBu (27.0 mg, 0.282 mmol) in a microwave reaction vessel. The contents were flushed with argon for five min, capped, and exposed to microwave irradiation at 200 °C for two min. After the

reaction was complete, the DMF was removed by pouring the reaction solution into a separatory funnel containing aqueous sodium hydrosulfite (40 mL), the aqueous layer extracted with hexanes:EtOAc (50:50), concentrated under reduced pressure, and purified by flash chromatography hexanes:*t*-butyl methyl ether (90:10). The resultant product was then recrystallized from CHCl₃ to yield 26 mg of an off-white solid (37%).

Conventional heating: A solution containing Pd(OAc)₂ (4.65 mg, 0.0207 mmol) and 2-(dicyclohexylphosphano)-biphenyl (14.5 mg, 0.0414 mmol) in anhydrous DMF (4.65 mL) was prepared and added to aniline **278** (75.0 mg, 0.207 mmol) and sodium tert-butoxide (27.0 mg, 0.282 mmol) under an argon atmosphere. The reaction was stirred and heated at 150 °C for 1 h. After the reaction was complete, the reaction was cooled and diluted with a saturated solution of Na₂SO₃ then extracted with hexanes:EtOAc (50:50), concentrated under reduced pressure, and purified by flash chromatography as above. The solid was re-crystallized from CHCl₃ to yield 25 mg of the off-white solid (35 %): TLC (hexanes/EtOAc, 95:5): R_f = 0.45; ¹H NMR (400 MHz, CDCl₃) δ 7.01 (s, 2H), 6.63 (s, 1H), 5.83 (s, 1H); ¹³C NMR (100 MHz, CDCl₃) δ 139.7, 131.1, 127.4, 125.9, 117.6, 115.7; GC/MS: t_R = 49:34 min, 335 (73% (C₁₂H₅Cl₄NS⁺)), 300 (62% (C₁₂H₅Cl₃NS⁺)), 264 (11% (C₁₂H₄Cl₂NS⁺)), 230 (9% (C₁₂H₅CINS⁺)), 194 (4% (C₁₂H₄NS⁺)), 168 (12% ([CHCINS]²⁺)), 132 (14% (CHCINS²⁺)); melting point 224-226 °C.

Crystal Structure Report for Compound 274





Comment

The dihedral angle between the two 6-membered carbon rings was $18.50(9)^\circ$. The displacement ellipsoids were drawn at the 50% probability level.

Experimental

A pink needle-shaped crystal of dimensions 0.41 x 0.10 x 0.08 mm was selected for structural analysis. Intensity data for this compound were collected using a Bruker APEX ccd area detector¹ mounted on a Bruker D8 goniometer using with graphite-monochromated Mo Ka radiation ($\lambda = 0.71073 \text{ \AA}$). The sample was cooled to 100 K.² The intensity data were measured as a series of ω oscillation frames each of 0.25° for 15 sec / frame. The detector was operated in 512 x 512 mode and was positioned 5.054 cm from the sample. Coverage of unique data was 99.9% complete to 25.99 degrees in q . Cell parameters were determined from a non-linear least squares fit of 5247 peaks in the range $2.36 < q < 26.00^\circ$. A total of 6689 data were measured in the range $1.96 < q < 25.99^\circ$. The data were corrected for absorption by the semi-empirical method² giving minimum and maximum transmission factors of 0.6567 and 0.9158. The data were merged to form a set of 2155 independent data with $R(\text{int}) = 0.0233$.

The orthorhombic space group $Pna2_1$ was determined by systematic absences and statistical tests and verified by subsequent refinement. The structure was solved by direct methods and refined by full-matrix least-squares methods on F^2 .³ Hydrogen atom positions were initially determined by geometry and refined by a

riding model. Non-hydrogen atoms were refined with anisotropic displacement parameters. Hydrogen atom displacement parameters were set to 1.2 (1.5 for methyl) times the displacement parameters of the bonded atoms. A total of 163 parameters were refined against 1 space group restraint and 2155 data to give $wR(F^2) = 0.0764$ and $S = 1.065$ for weights of $w = 1/[s^2 (F^2) + (0.0600 P)^2]$, where $P = [F_o^2 + 2F_c^2] / 3$. The final $R(F)$ was 0.0284 for the 2122 observed, $[F > 4s(F)]$, data. The largest shift/s.u. was 0.001 in the final refinement cycle. The final difference map had maxima and minima of 0.521 and -0.225 e/Å³, respectively. The absolute structure was determined by refinement of the Flack parameter.⁴ The polar axis restraint was taken from Flack and Schwarzenbach.⁵

References

- (1) (a) Data Collection: SMART Software Reference Manual (1994). Bruker-AXS, 6300 Enterprise Dr., Madison, WI 53719-1173, USA. (b) Data Reduction: SAINT Software Reference Manual (1995). Bruker-AXS, 6300 Enterprise Dr., Madison, WI 53719-1173, USA.
- (2) G. M. Sheldrick (2000). SADABS. Program for Empirical Absorption Correction of Area Detector Data. University of Göttingen, Germany.
- (3) (a) G. M. Sheldrick (1994). SHELXTL Version 5 Reference Manual. Bruker-AXS, 6300 Enterprise Dr., Madison, WI 53719-1173, USA. (b) *International Tables for Crystallography, Vol C*, Tables 6.1.1.4, 4.2.6.8, and 4.2.4.2, Kluwer: Boston (1995).

(4) H. D. Flack, *Acta Cryst.* *A39*, 876-881 (1983).

(5) H. D. Flack and D. Schwarzenbach, *Acta Cryst.* *A44*, 499-506 (1988).

Table A. Crystal data and structure refinement for 03065a

Identification code	03065a
Empirical formula	C ₁₂ H ₅ Cl ₄ N S
Formula weight	337.03
Crystal system	Orthorhombic
Space group	<i>Pna</i> 2 ₁
Unit cell dimensions	$a = 20.7356(18) \text{ \AA}$ $a = 90^\circ$ $b = 15.4686(13) \text{ \AA}$ $b = 90^\circ$ $c = 3.7921(3) \text{ \AA}$ $g = 90^\circ$
Volume	1216.32(18) \AA^3
Z, Z'	4, 1
Density (calculated)	1.840 Mg/m ³
Wavelength	0.71073 \AA
Temperature	100(2) K
<i>F</i> (000)	672
Absorption coefficient	1.120 mm ⁻¹
Absorption correction	Semi-empirical from equivalents
Max. and min. transmission	0.9158 and 0.6567
Theta range for data collection	1.96 to 25.99°
Reflections collected	6689
Independent reflections	2155 [R(int) = 0.0233]
Data / restraints / parameters	2155 / 1 / 163

$wR(F^2 \text{ all data})$	$wR2 = 0.0764$
$R(F \text{ obsd data})$	$R1 = 0.0284$
Goodness-of-fit on F^2	1.065
Observed data [$I > 2s(I)$]	2122
Absolute structure parameter	0.01(7)
Largest and mean shift / s.u.	0.001 and 0.000
Largest diff. peak and hole	0.521 and -0.225 e/Å ³

Pertinent Equations

$$wR2 = [S [w(F_o^2 - F_c^2)^2] / S [w(F_o^2)^2]]^{1/2}$$

$$R1 = S ||F_o| - |F_c|| / S |F_o|$$

Table B. Atomic coordinates and equivalent isotropic displacement parameters for 03065a. $U(\text{eq})$ is defined as one third of the trace of the orthogonalized U_{ij} tensor.

	x	y	z	$U(\text{eq})$
C(1)	0.57689(11)	0.77389(15)	0.5877(7)	0.0177(5)
C(2)	0.51286(11)	0.79932(14)	0.5582(7)	0.0176(5)
Cl(2)	0.49186(3)	0.90198(4)	0.69331(19)	0.02254(16)
C(3)	0.46771(10)	0.74260(16)	0.4228(7)	0.0166(5)
Cl(3)	0.38742(2)	0.77147(4)	0.37295(18)	0.02273(16)
C(4)	0.48659(10)	0.66019(15)	0.3198(7)	0.0165(5)
S(5)	0.57261(2)	0.53227(4)	0.17962(18)	0.01547(15)
C(6)	0.67314(10)	0.43390(15)	0.4049(7)	0.0156(5)
C(7)	0.73396(10)	0.42031(15)	0.5383(7)	0.0175(5)
Cl(7)	0.76302(3)	0.31494(4)	0.56922(17)	0.02295(17)
C(8)	0.77122(10)	0.48909(16)	0.6544(7)	0.0185(5)
Cl(8)	0.84820(3)	0.47391(4)	0.8203(2)	0.02428(17)
C(9)	0.74672(10)	0.57235(16)	0.6416(7)	0.0186(5)
N(10)	0.66198(8)	0.67132(13)	0.4891(7)	0.0202(5)
C(11)	0.59645(11)	0.69274(15)	0.4762(7)	0.0167(5)
C(12)	0.55039(9)	0.63482(14)	0.3440(6)	0.0142(4)
C(13)	0.64829(10)	0.51734(14)	0.3841(7)	0.0150(5)

C(14) 0.68528(10) 0.58688(15) 0.5071(7) 0.0157(5)

Table C. Bond lengths [\AA] and angles [$^\circ$] for 03065a

C(1)-C(11)	1.385(3)	C(6)-H(6)	0.9500
C(1)-C(2)	1.389(3)	C(7)-C(8)	1.386(3)
C(1)-H(1)	0.9500	C(7)-Cl(7)	1.742(2)
C(2)-C(3)	1.382(3)	C(8)-C(9)	1.385(3)
C(2)-Cl(2)	1.725(2)	C(8)-Cl(8)	1.732(2)
C(3)-C(4)	1.390(3)	C(9)-C(14)	1.391(3)
C(3)-Cl(3)	1.734(2)	C(9)-H(9)	0.9500
C(4)-C(12)	1.383(3)	N(10)-C(14)	1.394(3)
C(4)-H(4)	0.9500	N(10)-C(11)	1.400(3)
S(5)-C(12)	1.765(2)	N(10)-H(10)	0.9499
S(5)-C(13)	1.766(2)	C(11)-C(12)	1.402(3)
C(6)-C(7)	1.375(3)	C(13)-C(14)	1.401(3)
C(6)-C(13)	1.392(3)		
		C(1)-C(2)-Cl(2)	
C(11)-C(1)-C(2)	120.8(2)	118.56(18)	
C(11)-C(1)-H(1)	119.6		
C(2)-C(1)-H(1)	119.6	C(2)-C(3)-C(4)	119.7(2)
C(3)-C(2)-C(1)	119.8(2)	C(2)-C(3)-Cl(3)	121.83(18)
C(3)-C(2)-Cl(2)		C(4)-C(3)-Cl(3)	118.43(18)
121.60(18)		C(12)-C(4)-C(3)	120.7(2)

C(12)-C(4)-H(4)	119.6	C(8)-C(9)-H(9)	120.0
C(3)-C(4)-H(4)	119.6	C(14)-C(9)-H(9)	120.0
C(12)-S(5)-C(13)		C(14)-N(10)-C(11)	
101.22(11)		124.05(19)	
C(7)-C(6)-C(13)	120.1(2)	C(14)-N(10)-H(10)	109.1
C(7)-C(6)-H(6)	119.9	C(11)-N(10)-H(10)	116.0
C(13)-C(6)-H(6)	119.9	C(1)-C(11)-N(10)	119.2(2)
C(6)-C(7)-C(8)	120.7(2)	C(1)-C(11)-C(12)	119.3(2)
C(6)-C(7)-Cl(7)		N(10)-C(11)-C(12)	121.5(2)
119.02(19)		C(4)-C(12)-C(11)	119.6(2)
C(8)-C(7)-Cl(7)		C(4)-C(12)-S(5)	118.76(17)
120.26(17)		C(11)-C(12)-S(5)	121.51(16)
C(9)-C(8)-C(7)	119.9(2)	C(6)-C(13)-C(14)	119.4(2)
C(9)-C(8)-Cl(8)		C(6)-C(13)-S(5)	118.38(17)
118.46(18)		C(14)-C(13)-S(5)	122.16(17)
C(7)-C(8)-Cl(8)		C(9)-C(14)-N(10)	119.1(2)
121.66(18)		C(9)-C(14)-C(13)	120.0(2)
C(8)-C(9)-C(14)	119.9(2)	N(10)-C(14)-C(13)	120.9(2)

Table D. Anisotropic displacement parameters ($\text{\AA}^2 \times 10^3$) for 03065a. The

anisotropic displacement factor exponent takes the form:

$$-2 p^2 [h^2 a^{*2} U_{11} + \dots + 2 h k a^* b^* U_{12}]$$

	U ₁₁	U ₂₂	U ₃₃	U ₂₃	U ₁₃	U ₁₂
C(1)	23(1)	16(1)	14(1)	-2(1)	-1(1)	-3(1)
C(2)	28(1)	11(1)	14(1)	2(1)	3(1)	3(1)
Cl(2)	31(1)	14(1)	23(1)	-2(1)	1(1)	4(1)
C(3)	18(1)	20(1)	12(1)	4(1)	2(1)	3(1)
Cl(3)	20(1)	22(1)	25(1)	0(1)	-1(1)	5(1)
C(4)	21(1)	17(1)	12(1)	4(1)	0(1)	-3(1)
S(5)	19(1)	14(1)	14(1)	-3(1)	-1(1)	1(1)
C(6)	19(1)	16(1)	11(1)	-1(1)	5(1)	-3(1)
C(7)	23(1)	14(1)	16(1)	2(1)	5(1)	5(1)
Cl(7)	24(1)	18(1)	27(1)	2(1)	3(1)	7(1)
C(8)	16(1)	24(1)	16(1)	2(1)	2(1)	1(1)
Cl(8)	17(1)	29(1)	28(1)	4(1)	-1(1)	2(1)
C(9)	19(1)	21(1)	16(1)	1(1)	0(1)	-4(1)
N(10)	18(1)	15(1)	27(1)	-2(1)	-2(1)	-4(1)
C(11)	23(1)	15(1)	13(1)	5(1)	1(1)	0(1)

C(12)	21(1)	12(1)	10(1)	3(1)	2(1)	2(1)
C(13)	17(1)	18(1)	10(1)	2(1)	2(1)	-1(1)
C(14)	19(1)	16(1)	12(1)	2(1)	2(1)	-2(1)

Table E. Hydrogen coordinates and isotropic displacement parameters for 03065a.

	x	y	z	U(eq)
H(1)	0.6076	0.8126	0.6854	0.021
H(4)	0.4553	0.6208	0.2317	0.020
H(6)	0.6480	0.3862	0.3267	0.019
H(9)	0.7719	0.6195	0.7246	0.022
H(10)	0.6883	0.7077	0.6305	0.024

Table F. Torsion angles [°] for 03065a.

C(11)-C(1)-C(2)-C(3)	1.3(4)	C(3)-C(4)-C(12)-C(11)	0.4(4)
C(11)-C(1)-C(2)-Cl(2)	-178.7(2)	C(3)-C(4)-C(12)-S(5)	-175.44(19)
C(1)-C(2)-C(3)-C(4)	0.6(4)	C(1)-C(11)-C(12)-C(4)	1.4(4)
Cl(2)-C(2)-C(3)-C(4)	-179.46(19)	N(10)-C(11)-C(12)-C(4)	-176.8(2)
C(1)-C(2)-C(3)-Cl(3)	-178.9(2)	C(1)-C(11)-C(12)-S(5)	177.2(2)
Cl(2)-C(2)-C(3)-Cl(3)	1.1(3)	N(10)-C(11)-C(12)-S(5)	-1.0(3)
C(2)-C(3)-C(4)-C(12)	-1.4(4)	C(13)-S(5)-C(12)-C(4)	-163.1(2)
Cl(3)-C(3)-C(4)-C(12)	178.0(2)	C(13)-S(5)-C(12)-C(11)	21.1(2)
C(13)-C(6)-C(7)-C(8)	0.2(4)	C(7)-C(6)-C(13)-C(14)	-1.3(4)
C(13)-C(6)-C(7)-Cl(7)	178.69(19)	C(7)-C(6)-C(13)-S(5)	175.2(2)
C(6)-C(7)-C(8)-C(9)	1.1(4)	C(12)-S(5)-C(13)-C(6)	161.3(2)
Cl(7)-C(7)-C(8)-C(9)	-177.5(2)	C(12)-S(5)-C(13)-C(14)	-22.3(2)
C(6)-C(7)-C(8)-Cl(8)	-179.5(2)	C(8)-C(9)-C(14)-N(10)	-178.6(2)
Cl(7)-C(7)-C(8)-Cl(8)	2.0(3)	C(8)-C(9)-C(14)-C(13)	-0.1(4)
C(7)-C(8)-C(9)-C(14)	-1.1(4)	C(11)-N(10)-C(14)-C(9)	-157.4(3)
Cl(8)-C(8)-C(9)-C(14)	179.5(2)	C(11)-N(10)-C(14)-C(13)	24.2(4)
C(2)-C(1)-C(11)-N(10)	176.0(2)	C(6)-C(13)-C(14)-C(9)	1.3(4)
C(2)-C(1)-C(11)-C(12)	-2.3(4)	S(5)-C(13)-C(14)-C(9)	-175.0(2)
C(14)-N(10)-C(11)-C(1)	156.3(3)	C(6)-C(13)-C(14)-N(10)	179.8(2)
C(14)-N(10)-C(11)-C(12)	-25.5(4)	S(5)-C(13)-C(14)-N(10)	3.4(3)

Table G. Hydrogen bonds for 03065a [\AA and $^\circ$].

D-H...A	d(D-H)	d(H...A)	d(D...A)	$\angle(\text{DHA})$
N(10)-H(10)...Cl(7)#1	0.95	2.56	3.492(2)	168.0

Symmetry transformations used to generate equivalent atoms:

#1 $-x+3/2, y+1/2, z+1/2$

4.4 References

- (1) Li, J. W. H.; Vederas, J. C. Drug Discovery and Natural Products: End of an Era or an Endless Frontier? *Science* **2009**, *325*, 161-165.
- (2) Butler, M. S. Natural Products to Drugs: Natural Product Derived Compounds in Clinical Trials. *Nat. Prod. Rep.* **2005**, *22*, 162-195.
- (3) Lipinski, C. A.; Lombardo, F.; Dominy, B. W.; Feeney, P. J. Experimental and Computational Approaches to Estimate Solubility and Permeability in Drug Discovery and Development Settings. *Adv. Drug Del. Rev.* **2001**, *46*, 3-26.
- (4) Yet, L. Chemistry and Biology of Salicylihalamide A and Related Compounds. *Chem. Rev.* **2003**, *103*, 4283-4306.
- (5) Erickson, K. L.; Beutler, J. A.; Cardellina, J. H.; Boyd, M. R. Salicylihalamides A and B, Novel Cytotoxic Macrolides from the Marine Sponge *Haliclona* Sp. *J. Org. Chem.* **1997**, *62*, 8188-8192.
- (6) Erickson, K. L.; Beutler, J. A.; Cardellina, J. H.; Boyd, M. R. Salicylihalamides A and B, Novel Cytotoxic Macrolides from the Marine Sponge *Haliclona* Sp. *J. Org. Chem.* **2001**, *66*, 1532-1532.
- (7) Dekker, K. A.; Aiello, R. J.; Haria, H.; Inagaki, T.; Sakakibara, T.; Suzuki, Y.; Thompson, J. F.; Yamauchi, Y.; Kojima, N. Novel Lactone Compounds from *Mortierella Verticillata* That Induce the Human Low Density Lipoprotein Receptor Gene: Fermentation, Isolation, Structural Elucidation and Biological Activities. *J. Antibiot.* **1998**, *51*, 14-20.

- (8) Harrold, M. In *Foye's Principles of Medicinal Chemistry*; Williams, D. A., Lemke, T. L., Eds.; Lippincott, Williams & Wilkins: Baltimore, MD, 2002, p 580-603.
- (9) Galinis, D. L.; McKee, T. C.; Pannell, L. K.; Cardellina, J. H.; Boyd, M. R. Lobatamides A and B, Novel Cytotoxic Macrolides from the Tunicate *Aplidium Lobatum*. *J. Org. Chem.* **1997**, *62*, 8968-8969.
- (10) McKee, T. C.; Galinis, D. L.; Pannell, L. K.; Cardellina, J. H.; Laakso, J.; Ireland, C. M.; Murray, L.; Capon, R. J.; Boyd, M. R. The Lobatamides, Novel Cytotoxic Macrolides from Southwestern Pacific Tunicates. *J. Org. Chem.* **1998**, *63*, 7805-7810.
- (11) Suzumura, K.-i.; Takahashi, I.; Matsumoto, H.; Nagai, K.; Setiawan, B.; Rantiatmodjo, R. M.; Suzuki, K.-i.; Nagano, N. Structural Elucidation of Ym-75518, a Novel Antifungal Antibiotic Isolated from *Pseudomonas* Sp. Q38009. *Tetrahedron Lett.* **1997**, *38*, 7573-7576.
- (12) Boyd, M. R.; Paull, K. D. Some Practical Considerations and Applications of the National Cancer Institute in Vitro Anticancer Drug Discovery Screen. *Drug Dev. Res.* **1995**, *34*, 91-109.
- (13) Kunze, B.; Jansen, R.; Sasse, F.; Höfle, G.; Reichenbach, H. Apicularens A and B, New Cytostatic Macrolides from *Chondromyces* Species (Myxobacteria): Production, Physico-Chemical and Biological Properties. *J. Antibiot.* **1998**, *51*, 1075-1080.

- (14) Jansen, R.; Kunze, B.; Reichenbach, H.; Höfle, G. Antibiotics from Gliding Bacteria, LXXXVI Apicularen A and B, Cytotoxic 10-Membered Lactones with a Novel Mechanism of Action from *Chondromyces* Species (Myxobacteria): Isolation, Structure Elucidation, and Biosynthesis. *Eur. J. Org. Chem.* **2000**, 913-919.
- (15) Hayakawa, Y.; Tomikawa, T.; Shin-Ya, K.; Arao, N.; Nagai, K.; Suzuki, K.-I. Oximidine III, a New Antitumor Antibiotic against Transformed Cells from *Pseudomonas* Sp. I. Taxonomy, Fermentation, Isolation, Physico-Chemical Properties and Biological Activity. *J. Antibiot.* **2003**, *56*, 899-904.
- (16) Hayakawa, Y.; Tomikawa, T.; Shin-Ya, K.; Arao, N.; Nagai, K.; Suzuki, K.-I.; Furihata, K. Oximidine III, a New Antitumor Antibiotic against Transformed Cells from *Pseudomonas* pp. II. Structure Elucidation. *J. Antibiot.* **2003**, *56*, 905-908.
- (17) Kim, J. W.; Shin-ya, K.; Furihata, K.; Hayakawa, Y.; Seto, H. Oximidines I and II: Novel Antitumor Macrolides from *Pseudomonas* sp. *J. Org. Chem.* **1999**, *64*, 153-155.
- (18) Frame, M. C. Src in Cancer: Deregulation and Consequences for Cell Behaviour. *Biochim. Biophys. Acta (BBA) - Reviews on Cancer* **2002**, *1602*, 114-130.
- (19) Downward, J. Targeting Ras Signalling Pathways in Cancer Therapy. *Nat. Rev. Cancer* **2003**, *3*, 11-22.
- (20) Frisch, S. M.; Mymryk, J. S. Adenovirus-5 E1A: Paradox and Paradigm. *Nat. Rev. Mol. Cell. Biol.* **2002**, *3*, 441-452.
- (21) Boyd, M. R.; Farina, C.; Belfiore, P.; Gagliardi, S.; Kim, J. W.; Hayakawa, Y.; Beutler, J. A.; McKee, T. C.; Bowman, B. J.; Bowman, E. J. Discovery of a Novel

Antitumor Benzolactone Enamide Class That Selectively Inhibits Mammalian Vacuolar-Type(H^+)-Atpases. *J. Pharmacol. Exp. Ther.* **2001**, *297*, 114-120.

(22) Hong, J.; Yokomakura, A.; Nakano, Y.; Ishihara, K.; Kaneda, M.; Onodera, M.; Nakahama, K.-I.; Morita, I.; Niikura, K.; Ahn, J.-W.; Zee, O.; Ohuchi, K. Inhibition of Vacuolar-Type (H^+)-Atpase by the Cytostatic Macrolide Apicularen A and Its Role in Apicularen A-Induced Apoptosis in Raw 264.7 Cells. *FEBS Lett.* **2006**, *580*, 2723-2730.

(23) Werner, G.; Hagenmaier, H.; Drautz, H.; Baumbartner, E.; Zähler, H. Metabolic Products of Microorganisms. 224'. Bafilomycins, a New Group of Macrolide Antibiotics - Production, Isolation, Chemical Structure and Biological Activity. *J. Antibiot.* **1984**, *37*, 110-117.

(24) Bowman, E. J.; Siebers, A.; Altendorf, K. Bafilomycins: A Class of Inhibitors of Membrane Atpases from Microorganisms, Animal Cells, and Plant Cells. *Proc. Natl. Acad. Sci. U. S. A.* **1988**, *85*, 7972-7976.

(25) Droese, S.; Bindseil, K. U.; Bowman, E. J.; Siebers, A.; Zeeck, A.; Altendorf, K. Inhibitory Effect of Modified Bafilomycins and Concanamycins on P- and V-Type Adenosinetriphosphatases. *Biochemistry* **2002**, *32*, 3902-3906.

(26) Kinashi, H.; Someno, K.; Sakaguchi, K. Isolation and Characterization of Concanamycins A, B, and C. *J. Antibiot.* **1984**, *38*, 1333-1343.

(27) Huss, M.; Ingenhorst, G.; König, S.; Gassel, M.; Drose, S.; Zeeck, A.; Altendorf, K.; Wiczorek, H. Concanamycin a, the Specific Inhibitor of V-ATPases, Binds to the V_0 Subunit C. *J. Biol. Chem.* **2002**, *277*, 40544-40548.

- (28) Woo, J.-T.; Shinohara, C.; Sakai, K.; Saumi, K.; Endo, A. Isolation, Characterization and Biological Activities of Concanamycins as Inhibitors of Lysosomal Acidification. *J. Antibiot.* **1992**, *45*, 1108-1116.
- (29) Lafourcade, C. L.; Sobo, K.; Kieffer-Jaquinod, S.; Garin, J. R.; van der Goot, F. G. Regulation of the V-ATPase Along the Endocytic Pathway Occurs through Reversible Subunit Association and Membrane Localization. *PLoS ONE.* **2008**, *3*, e2758.
- (30) Nishi, T.; Forgac, M. The Vacuolar (H⁺)-ATPases - Nature's Most Versatile Proton Pumps. *Nat. Rev. Mol. Cell Biol.* **2002**, *3*, 94-103.
- (31) Forgac, M. Vacuolar ATPases: Rotary Proton Pumps in Physiology and Pathophysiology. *Nat. Rev. Mol. Cell Biol.* **2007**, *8*, 917-929.
- (32) Martinez-Zaguilan, R.; Lynch, R. M.; Martinez, G. M.; Gillies, R. J. Vacuolar-Type (H⁺)-ATPases Are Functionally Expressed in Plasma Membranes of Human Tumor Cells. *Am. J. Physiol. Cell Physiol.* **1993**, *265*, C1015-C1029.
- (33) Wieczorek, H.; Brown, D.; Grinstein, S.; Ehrenfeld, J.; Harvey, W. R. Animal Plasma Membrane Energization by Proton-Motive V-ATPases. *BioEssays* **1999**, *21*, 637-648.
- (34) Farina, C.; Gagliardi, S. Selective Inhibitors of the Osteoclast Vacuolar Proton ATPase as Novel Bone Antiresorptive Agents. *Drug Discov. Today* **1999**, *4*, 163-172.
- (35) Hinton, A.; Bond, S.; Forgac, M. V-ATPase Functions in Normal and Disease Processes. *Pflügers Arch.* **2009**, *457*, 589-598.

- (36) Nelson, D. L.; Cox, M. M. *Lehninger Principles of Biochemistry*; 3rd Ed.; Worth Publishers: New York, NY, 2000.
- (37) Imai-Senga, Y.; Sun-Wada, G.-H.; Wada, Y.; Futai, M. A Human Gene, ATP6E1, Encoding a Testis-Specific Isoform of (H⁺)-ATPase Subunit E. *Gene* **2002**, *289*, 7-12.
- (38) Sennoune, S. R.; Bakunts, K.; Martinez, G. M.; Chua-Tuan, J. L.; Kebir, Y.; Attaya, M. N.; Martinez-Zaguilan, R. Vacuolar (H⁺)-ATPase in Human Breast Cancer Cells with Distinct Metastatic Potential: Distribution and Functional Activity. *Am. J. Physiol.* **2004**, *286*, C1443-1452.
- (39) Hanahan, D.; Weinberg, R. A. The Hallmarks of Cancer. *Cell* **2000**, *100*, 57-70.
- (40) Su, Y.; Zhou, A.; Al-Lamki, R. S.; Karet, F. E. The A-Subunit of the V-Type (H⁺)-Atpase Interacts with Phosphofructokinase-1 in Humans. *J. Biol. Chem.* **2003**, *278*, 20013-20018.
- (41) Fais, S.; De Milito, A.; You, H.; Qin, W. Targeting Vacuolar (H⁺)-ATPases as a New Strategy against Cancer. *Cancer Res.* **2007**, *67*, 10627-10630.
- (42) Sennoune, S.; Luo, D.; Martinez-Zaguilán, R. Plasmalemmal Vacuolar-Type (H⁺)-ATPase in Cancer Biology. *Cell Biochem. Biophys.* **2004**, *40*, 185-206.
- (43) Supino, R.; Petrangolini, G.; Pratesi, G.; Tortoreto, M.; Favini, E.; Bo, L. D.; Casalini, P.; Radaelli, E.; Croce, A. C.; Bottiroli, G.; Misiano, P.; Farina, C.; Zunino, F. Antimetastatic Effect of a Small-Molecule Vacuolar (H⁺)-Atpase Inhibitor in *in vitro* and *in vivo* Preclinical Studies. *J. Pharmacol. Exp. Ther.* **2008**, *324*, 15-22.

- (44) Rojas, J. D.; Sennoune, S. R.; Maiti, D.; Bakunts, K.; Reuveni, M.; Sanka, S. C.; Martinez, G. M.; Seftor, E. A.; Meininger, C. J.; G. Wu; Wesson, D. E.; Hendrix, M. J. C.; R. M.-Z. Vacuolar-Type (H^+)-ATPases at the Plasma Membrane Regulate pH and Cell Migration in Microvascular Endothelial Cells. *Am. J. Physiol. Heart Circ. Physiol.* **2006**, *291*, H1147-H1157.
- (45) Sennoune, S. R.; Martinez-Zaguilan, R. Plasmalemmal Vacuolar (H^+)-ATPases in Angiogenesis, Diabetes, and Cancer. *J. Bioenerg. Biomembr.* **2007**, *39*, 427-433.
- (46) Laurencot, C. M.; Andrews, P. A.; Kennedy, K. A. Inhibitors of Intracellular pH Regulation Induce cisplatin Resistance in EMT6 Mouse Mammary Tumor Cells. *Oncol. Res.* **1995**, *7*, 363-369.
- (47) Gatenby, R. A.; Gillies, R. J. Why Do Cancers Have High Aerobic Glycolysis? *Nat Rev Cancer.* **2004**, *4*, 891-899.
- (48) Nishihara, T.; Akifusa, S.; Koseki, T.; Kato, S.; Muro, M.; Hanada, N. Specific Inhibitors of Vacuolar Type (H^+)-ATPases Induce Apoptotic Cell Death. *Biochem. Biophys. Res. Commun.* **1995**, *212*, 255-262.
- (49) Aiko, K.; Tsujisawa, T.; Koseki, T.; Hashimoto, S.; Morimoto, Y.; Amagasa, T.; Nishihara, T. Involvement of Cytochrome C and Caspases in Apoptotic Cell Death of Human Submandibular Gland Ductal Cells Induced by Concanamycin A. *Cell. Signal.* **2002**, *14*, 717-722.
- (50) De Milito, A.; Iessi, E.; Logozzi, M.; Lozupone, F.; Spada, M.; Marino, M. L.; Federici, C.; Perdicchio, M.; Matarrese, P.; Lugini, L.; Nilsson, A.; Fais, S. Proton

Pump Inhibitors Induce Apoptosis of Human B-Cell Tumors through a Caspase-Independent Mechanism Involving Reactive Oxygen Species. *Cancer Res.* **2007**, *67*, 5408-5417.

(51) Torigoe, T.; Izumi, H.; Ishiguchi, H.; Uramoto, H.; Murakami, T.; Ise, T.; Yoshida, Y.; Tanabe, M.; Nomoto, M.; Itoh, H.; Kohno, K. Enhanced Expression of the Human Vacuolar (H⁺)-ATPase C Subunit Gene (ATP6I) in Response to Anticancer Agents. *J. Biol. Chem.* **2002**, *277*, 36534-36543.

(52) Whitehurst, A. W.; Bodemann, B. O.; Cardenas, J.; Ferguson, D.; Girard, L.; Peyton, M.; Minna, J. D.; Michnoff, C.; Hao, W.; Roth, M. G.; Xie, X.-J.; White, M. A. Synthetic Lethal Screen Identification of Chemosensitizer Loci in Cancer Cells. *Nature* **2007**, *446*, 815-819.

(53) Boya, P.; Gonzalez-Polo, R.-A.; Casares, N.; Perfettini, J.-L.; Dessen, P.; Larochette, N.; Metivier, D.; Meley, D.; Souquere, S.; Yoshimori, T.; Pierron, G.; Codogno, P.; Kroemer, G. Inhibition of Macroautophagy Triggers Apoptosis. *Mol. Cell. Biol.* **2005**, *25*, 1025-1040.

(54) Mathew, R.; Karantza-Wadsworth, V.; White, E. Role of Autophagy in Cancer. *Nat. Rev. Cancer* **2007**, *7*, 961-967.

(55) Kondo, Y.; Kanzawa, T.; Sawaya, R.; Kondo, S. The Role of Autophagy in Cancer Development and Response to Therapy. *Nat. Rev. Cancer* **2005**, *5*, 726-734.

(56) Bursch, W.; Ellinger, A.; Kienzl, H.; Torok, L.; Pandey, S.; Sikorska, M.; Walker, R.; Hermann, R. S. Active Cell Death Induced by the Anti-Estrogens

Tamoxifen and ICI 164 384 in Human Mammary Carcinoma Cells (MCF-7) in Culture: The Role of Autophagy. *Carcinogenesis* **1996**, *17*, 1595-1607.

(57) Kanzawa, T.; Germano, I. M.; Komata, T.; Ito, H.; Kondo, Y.; Kondo, S. Role of Autophagy in Temozolomide-Induced Cytotoxicity for Malignant Glioma Cells. *Cell Death Differ.* **2004**, *11*, 448-457.

(58) Paglin, S.; Hollister, T.; Delohery, T.; Hackett, N.; McMahon, M.; Sphicas, E.; Domingo, D.; Yahalom, J. A Novel Response of Cancer Cells to Radiation Involves Autophagy and Formation of Acidic Vesicles. *Cancer Res.* **2001**, *61*, 439-444.

(59) Huss, M.; Wieczorek, H. Inhibitors of V-ATPases: Old and New Players. *J. Exp. Biol.* **2009**, *212*, 341-346.

(60) Beutler, J. A.; McKee, T. C. Novel Marine and Microbial Natural Product Inhibitors of Vacuolar ATPase. *Curr. Med. Chem.* **2003**, *10*, 787-796.

(61) Bowman, B. J.; Bowman, E. J. Mutations in Subunit C of the Vacuolar ATPase Confer Resistance to Bafilomycin and Identify a Conserved Antibiotic Binding Site. *J. Biol. Chem.* **2002**, *277*, 3965-3972.

(62) Bender, T.; Huss, M.; Wieczorek, H.; Grond, S.; Zezschwitz, P. V. Convenient Synthesis of a [1-¹⁴C]Diazirinybenzoic Acid as a Photoaffinity Label for Binding Studies of V-ATPase Inhibitors. *Eur. J. Org. Chem.* **2007**, 3870-3878.

(63) Gagliardi, S.; Rees, M.; Farina, C. Chemistry and Structure Activity Relationships of Bafilomycin A(1), a Potent and Selective Inhibitor of the Vacuolar (H⁺)-Atpase. *Curr. Med. Chem.* **1999**, *6*, 1197-1212.

- (64) Bowman, E. J.; Gustafson, K. R.; Bowman, B. J.; Boyd, M. R. Identification of a New Chondropsin Class of Antitumor Compound That Selectively Inhibits V-ATPases. *J. Biol. Chem.* **2003**, *278*, 44147-44152.
- (65) Sasse, F.; Steinmetz, H.; Höfle, G.; Reichenbach, H. Archazolids, New Cytotoxic Macrolactones from *Archangium Gephyra* (Myxobacteria) Production, Isolation, Physico-Chemical and Biological Properties. *J. Antibiot.* **2003**, *56*, 520-525.
- (66) Huss, M.; Sasse, F.; Kunze, B.; Jansen, R.; Steinmetz, H.; Ingenhorst, G.; Zeeck, A.; Wieczorek, H. Archazolid and Apicularen: Novel Specific V-ATPase Inhibitors. *BMC Biochem.* **2005**, *6*.
- (67) Menche, D.; Hassfeld, J.; Steinmetz, H.; Huss, M.; Wieczorek, H.; Sasse, F. Archazolid-7-O- β -D-Glucopyranoside – Isolation, Structural Elucidation and Solution Conformation of a Novel V-ATPase Inhibitor from the Myxobacterium *Cystobacter Violaceus*. *Eur. J. Org. Chem.* **2007**, 1196-1202.
- (68) Menche, D.; Hassfeld, J.; Steinmetz, H.; Huss, M.; Wieczorek, H.; Sasse, F. The First Hydroxylated Archazolid from the Myxobacterium *Cystobacter Violaceus*: Isolation, Structural Elucidation and V-ATPase Inhibition. *J. Antibiot.* **2007**, *60*, 328-331.
- (69) Menche, D.; Hassfeld, J.; Sasse, F.; Huss, M.; Wieczorek, H. Design, Synthesis, and Biological Evaluation of Novel Analogues of Archazolid: A Highly Potent Simplified V-ATPase Inhibitor. *Bioorg. Med. Chem. Lett.* **2007**, *17*, 1732-1735.

- (70) Nozawa, K.; Tsuda, M.; Ishiyama, H.; Sasaki, T.; Tsuruo, T.; Kobayashi, J. I. Absolute Stereochemistry and Antitumor Activity of Iejimalides. *Biorg. Med. Chem.* **2006**, *14*, 1063-1067.
- (71) Kazami, S.; Muroi, M.; Kawatani, M.; Kubota, T.; Usui, T.; Kobayashi, J. i.; Osada, H. Iejimalides Show Anti-Osteoclast Activity *Via* V-ATPase Inhibition. *Biosci., Biotechnol., Biochem.* **2006**, *70*, 1364-1370.
- (72) Diyabalanage, T.; Amsler, C. D.; McClintock, J. B.; Baker, B. J. Palmerolide A, a Cytotoxic Macrolide from the Antarctic Tunicate *Synoicum Adareanum*. *J. Am. Chem. Soc.* **2006**, *128*, 5630-5631.
- (73) Niikura, K.; Takeshita, N.; Chida, N. A Novel Inhibitor of Vacuolar ATPase, FR202126, Prevents Alveolar Bone Destruction in Experimental Periodontitis in Rats. *J. Toxicol. Sci.* **2005**, *30*, 297-304.
- (74) Gagliardi, S.; Nadler, G.; Consolandi, E.; Parini, C.; Morvan, M.; Legave, M.-N.; Belfiore, P.; Zocchetti, A.; Clarke, G. D.; James, I.; Nambi, P.; Gowen, M.; Farina, C. 5-(5,6-Dichloro-2-Indolyl)-2-Methoxy-2,4-Pentadienamides: Novel and Selective Inhibitors of the Vacuolar (H⁺)-Atpase of Osteoclasts with Bone Antiresorptive Activity. *J. Med. Chem.* **1998**, *41*, 1568-1573.
- (75) Nadler, G.; Morvan, M.; Delimoge, I.; Belfiore, P.; Zocchetti, A.; James, I.; Zembryki, D.; Lee-Rycazewski, E.; Parini, C.; Consolandi, E.; Gagliardi, S.; Farina, C. (2Z,4E)-5-(5,6-Dichloro-2-Indolyl)-2-Methoxy-N-(1,2,2,6,6-Pentamethyl-piperidin-4-Yl)-2,4-Pentadienamide, a Novel, Potent and Selective Inhibitor of the Osteoclast V-ATPase. *Bioorg. Med. Chem. Lett.* **1998**, *8*, 3621-3626.

- (76) Petrangolini, G.; Supino, R.; Pratesi, G.; Bo, L. D.; Tortoreto, M.; Croce, A. C.; Misiano, P.; Belfiore, P.; Farina, C.; Zunino, F. Effect of a Novel Vacuolar-H⁺-ATPase Inhibitor on Cell and Tumor Response to Camptothecins. *J. Pharmacol. Exp. Ther.* **2006**, *318*, 939-946.
- (77) Xie, X.-S.; Padron, D.; Liao, X.; Wang, J.; Roth, M. G.; De Brabander, J. K. Salicylihalamide A Inhibits the V₀ Sector of the V-ATPase through a Mechanism Distinct from Bafilomycin A1. *J. Biol. Chem.* **2004**, *279*, 19755-19763.
- (78) Speckamp, W. N.; Hiemstra, H. Intramolecular Reactions of N-Acyliminium Intermediates. *Tetrahedron* **1985**, *41*, 4367-4416.
- (79) Wu, Y.; Seguil, O. R.; De Brabander, J. K. Synthesis and Initial Structure-Activity Relationships of Modified Salicylihalamides. *Org. Lett.* **2000**, *2*, 4241-4244.
- (80) Wu, Y.; Liao, X.; Wang, R.; Xie, X. S.; De Brabander, J. K. Total Synthesis and Initial Structure-Function Analysis of the Potent V-ATPase Inhibitors Salicylihalamide A and Related Compounds. *J. Am. Chem. Soc.* **2002**, *124*, 3245-3253.
- (81) Wu, Y.; Esser, L.; Brabander, J. K. D. Revision of the Absolute Configuration of Salicylihalamide A through Asymmetric Total Synthesis. *Angew. Chem. Int. Ed.* **2000**, *39*, 4308-4310.
- (82) Smith, A. B.; Zheng, J. Total Synthesis of (-)-Salicylihalamide A and Related Congeners. *Tetrahedron* **2002**, *58*, 6455-6471.

- (83) Lebreton, S.; Xie, X.-S.; Ferguson, D.; Brabander, J. K. D. Ring-Closing Metathesis: A Powerful Tool for the Synthesis of Simplified Salicylilalamide-Based V-ATPase Inhibitors. *Tetrahedron* **2004**, *60*, 9635-9647.
- (84) Tang, S.; Erickson, K. L. Synthesis and Cytotoxicity of a Salicylilalamide A Analogue. *J. Nat. Prod.* **2008**, *71*, 898-901.
- (85) Sugimoto, Y.; Konoki, K.; Murata, M.; Matsushita, M.; Kanazawa, H.; Oishi, T. Design, Synthesis, and Biological Evaluation of Fluorinated Analogues of Salicylilalamide. *J. Med. Chem.* **2008**, *52*, 798-806.
- (86) Shen, R.; Lin, C. T.; Bowman, E. J.; Bowman, B. J.; Porco, J. A. Lobatamide C: Total Synthesis, Stereochemical Assignment, Preparation of Simplified Analogues, and V-ATPase Inhibition Studies. *J. Am. Chem. Soc.* **2003**, *125*, 7889-7901.
- (87) Shen, R.; Lin, C. T.; Bowman, E. J.; Bowman, B. J.; Porco, J. A. Synthesis and V-ATPase Inhibition of Simplified Lobatamide Analogues. *Org. Lett.* **2002**, *4*, 3103-3106.
- (88) Shen, R.; Inoue, T.; Forgac, M.; Porco, J. A. Synthesis of Photoactive Acyclic Analogues of the Lobatamides. *J. Org. Chem.* **2005**, *70*, 3686-3692.
- (89) Dorman, G.; Prestwich, G. D. Benzophenone Photophores in Biochemistry. *Biochemistry* **2002**, *33*, 5661-5673.
- (90) Bhattacharjee, A.; Seguil, O. R.; DeBrabander, J. K. Total Synthesis and Biological Evaluation of Apicularen A and Synthetic Analogs. *Tetrahedron Lett.* **2001**, *42*, 1217-1220.

- (91) Petri, A. F.; Sasse, F.; Maier, M. E. Synthesis and Biological Evaluation of Apicularen A Analogues. *Eur. J. Org. Chem.* **2005**, 1865-1875.
- (92) Nicolaou, K. C.; Kim, D. W.; Baati, R.; O'Brate, A.; Giannakakou, P. Total Synthesis and Biological Evaluation of (-)-Apicularen A and Analogues Thereof. *Chem. Eur. J.* **2003**, *9*, 6177-6191.
- (93) Jundt, L.; Steinmetz, H.; Luger, P.; Weber, M.; Kunze, B.; Reichenbach, H.; Höfle, G. Isolation and Structure Elucidation of Cruentarens A and B - Novel Members of the Benzolactone Class of ATPase Inhibitors from the Myxobacterium *Byssovorax Cruenta*. *Eur. J. Org. Chem.* **2006**, 5036-5044.
- (94) Kunze, B.; Steinmetz, H.; Hofle, G.; Huss, M.; Wieczorek, H.; Reichenbach, H. Cruentaren, a New Antifungal Salicylate-Type Macrolide from *Byssovorax Cruenta* (Myxobacteria) with Inhibitory Effect on Mitochondrial ATPase Activity. *J. Antibiot.* **2006**, *59*, 664-668.
- (95) Kunze, B.; Sasse, F.; Wieczorek, H.; Huss, M. Cruentaren A, a Highly Cytotoxic Benzolactone from Myxobacteria Is a Novel Selective Inhibitor of Mitochondrial F₁-Atpases *FEBS Lett.* **2007**, *581*, 2523-2527.
- (96) Vintonyak, V. V.; Cal, M. Synthesis and Biological Evaluation of Cruentaren A Analogues *Chem. Eur. J.* **2008**, *14*, 3709-3720.
- (97) Wang, X.; Bowman, E. J.; Bowman, B. J.; John A. Porco, J. Total Synthesis of the Salicylate Enamide Macrolide Oximidine III: Application of Relay Ring-Closing Metathesis. *Angew. Chem. Int. Ed.* **2004**, *43*, 3601-3605.

- (98) Wessjohann, L. A.; Ruijter, E. In *Natural Product Synthesis I*; Mulzer, J. H., Ed.; Springer-Verlag Berlin Heidelberg: Germany, **2005**, p 137-184.
- (99) Ziegler, K. *Methoden Der Organischen Chemie*; Georg Thieme Verlag: Stuttgart, 1955; Vol. 2.
- (100) Ruggli, P. Über Ringe Mit Dreifacher Bindung. Über das Optimum der Gliederzahl. *Justus Liebigs Ann. Chem.* **1913**, *399*, 174-182.
- (101) Illuminati, G.; Mandolini, L. Ring Closure Reactions of Bifunctional Chain Molecules. *Acc. Chem. Res.* **2002**, *14*, 95-102.
- (102) Parenty, A.; Moreau, X.; Campagne, J. M. Macrolactonizations in the Total Synthesis of Natural Products. *Chem. Rev.* **2006**, *106*, 911-939.
- (103) Scheufler, F.; Maier, M. E. Synthesis of a Model System for the Macrocyclic Subunit of the Oximidines. *Synlett* **2001**, *2001*, 1221-1224.
- (104) Inanaga, J.; Hirata, K.; Saeki, H.; Katsuki, T.; Yamaguchi, M. A Rapid Esterification by Means of Mixed Anhydride and Its Application to Large-Ring Lactonization. *Bull. Chem. Soc. Jpn.* **1979**, *52*, 1989-1993.
- (105) Casadei, M. A.; Galli, C.; Mandolini, L. Ring-Closure Reactions. 22. Kinetics of Cyclization of Diethyl (ω -Bromoalkyl)Malonates in the Range of 4- to 21-Membered Rings. Role of Ring Strain. *J. Am. Chem. Soc.* **2002**, *106*, 1051-1056.
- (106) Coleman, R.; Garg, R. Stereocontrolled Synthesis of the Diene and Triene Macrolactones of Oximidines I and II: Organometallic Coupling Versus Standard Macrolactonization. *Org. Lett.* **2001**, *3*, 3487-3490.

- (107) Okuro, K.; Furuune, M.; Enna, M.; Miura, M.; Nomura, M. Synthesis of Aryl- and Vinylacetylene Derivatives by Copper-Catalyzed Reaction of Aryl and Vinyl Iodides with Terminal Alkynes. *J. Org. Chem.* **1993**, *58*, 4716-4721.
- (108) Yoshimura, F.; Kawata, S.; Hirama, M. Synthetic Study of Kedarcidin Chromophore: Atropselective Construction of the Ansamacrolide. *Tetrahedron Lett.* **1999**, *40*, 8281-8285.
- (109) Sonogashira, K.; Tohda, Y.; Hagihara, N. A Convenient Synthesis of Acetylenes: Catalytic Substitutions of Acetylenic Hydrogen with Bromoalkenes, Iodoarenes and Bromopyridines. *Tetrahedron Lett.* **1975**, *16*, 4467-4470.
- (110) Harvey, J. E.; Raw, S. A.; Taylor, R. J. K. The First Synthesis of the Epoxide-Containing Macrolactone Nucleus of Oximidine I. *Tetrahedron Lett.* **2003**, *44*, 7209-7212.
- (111) Esquivel, B.; Dominguez, R. M.; Hernández-Ortega, S.; Toscano, R. A.; Rodríguez-Hahn, L. Salvigenane and Isosalvipuberulan Diterpenoids from *Salvia Leucantha*. *Tetrahedron* **1994**, *50*, 11593-11600.
- (112) Labrecque, D.; Charron, S.; Rej, R.; Blais, C.; Lamothe, S. Enantioselective Total Synthesis of Salicylihalamides A and B. *Tetrahedron Lett.* **2001**, *42*, 2645-2648.
- (113) Herb, C.; Bayer, A.; Maier, M. E. Total Synthesis of Salicylihalamides A and B. *Chem. Eur. J.* **2004**, *10*, 5649-5660.
- (114) Fürstner, A.; Dierkes, T.; Thiel, O. R.; Blanda, G. Total Synthesis of (-)-Salicylihalamide. *Chem. Eur. J.* **2001**, *7*, 5286-5298.

- (115) Coleman, R. S.; Liu, P.-H. Divergent and Stereocontrolled Synthesis of the Enamide Side Chains of Oximidines I/II/III, Salicylihalamides A/B, Lobatamides A/D, and CJ-12,950. *Org. Lett.* **2004**, *6*, 577-580.
- (116) Kuramochi, K.; Watanabe, H.; Kitahara, T. Synthetic Study on Oximidines: A Concise Synthesis of (*Z*)-Enamides. *Synlett* **2000**, *2000*, 397-399.
- (117) Raw, S. A.; Taylor, R. J. K. Approaches to Oximidines, Lobatamides and Related Natural Products: The Coupling Reactions of 3-Iodoacrolein *O*-Methyl Oximes. *Tetrahedron Lett.* **2000**, *41*, 10357-10361.
- (118) Wang, X.; Porco, J. A. Total Synthesis of the Salicylate Enamide Macrolide Oximidine II. *J. Am. Chem. Soc.* **2003**, *125*, 6040-6041.
- (119) Allred, G. D.; Liebeskind, L. S. Copper-Mediated Cross-Coupling of Organostannanes with Organic Iodides at or Below Room Temperature. *J. Am. Chem. Soc.* **1996**, *118*, 2748-2749.
- (120) Shen, R.; Porco, J. A. Synthesis of Enamides Related to the Salicylate Antitumor Macrolides Using Copper-Mediated Vinylic Substitution. *Org. Lett.* **2000**, *2*, 1333-1336.
- (121) Bhattacharjee, A.; De Brabander, J. K. Synthesis of Side Chain Truncated Apicularen A. *Tetrahedron Lett.* **2000**, *41*, 8069-8073.
- (122) Brown, H. C.; Jadhav, P. K.; Bhat, K. S. Chiral Synthesis Via Organoboranes. 13. A Highly Diastereoselective and Enantioselective Addition of [(*Z*)- ω -Alkoxyallyl]Diisopinocampheylboranes to Aldehydes. *J. Am. Chem. Soc.* **2002**, *110*, 1535-1538.

- (123) Fürstner, A.; Konetzki, I. Synthesis of 2-Hydroxy-6-[[[(16*R*)- β -D-Mannopyranosyloxy]Heptadecyl]Benzoic Acid, a Fungal Metabolite with GABA_A Ion Channel Receptor Inhibiting Properties. *Tetrahedron*. **1996**, *52*, 15071-15078.
- (124) Haack, T.; Haack, K.; Diederich, W. E.; Blackman, B.; Roy, S.; Pusuluri, S.; Georg, G. I. Formal Total Syntheses of the (-)-Salicylihalamides A and B from D-Glucose and L-Rhamnose. *J. Org. Chem.* **2005**, *70*, 7592-7604.
- (125) Yang, K.; Blackman, B.; Diederich, W.; Flaherty, P. T.; Mossman, C. J.; Roy, S.; Ahn, Y. M.; Georg, G. I. Formal Total Synthesis of (+)-Salicylihalamides A and B: A Combined Chiral Pool and RCM Strategy. *J. Org. Chem.* **2003**, *68*, 10030-10039.
- (126) Stork, G.; Zhao, K. A Stereoselective Synthesis of (*Z*)-1-Iodo-1-Alkenes. *Tetrahedron Lett.* **1989**, *30*, 2173-2174.
- (127) Seyferth, D.; Heeren, J. K.; Singh, G.; Grim, S.; Hughes, W. B. Studies in Phosphinemethylene Chemistry XIII. Routes to Triphenylphosphine-Halomethylenes and Dihalomethylenes. *J. Organomet. Chem.* **1966**, *5*, 267-274.
- (128) Haack, T.; Kurtkaya, S.; Snyder, J. P.; Georg, G. I. Studies toward the Synthesis of Oximidines I and II. *Org. Lett.* **2003**, *5*, 5019-5022.
- (129) Takai, K.; Nitta, K.; Utimoto, K. Simple and Selective Method for Aldehydes (RCHO) \Rightarrow (*E*)-Haloalkenes (RCH=CHX) Conversion by Means of a Haloform-Chromous Chloride System. *J. Am. Chem. Soc.* **1986**, *108*, 7408-7410.

- (130) Kim, J. Y.; Shin, J. E. N.; Chun, K. H. An Effective Synthesis of 4-*O*-*Tert*-Butyldimethylsilyl-2,3-*O*-Isopropylidene-*L*-Threose and Erythrose: Useful Chiral Building Blocks in Synthesis. *Bull. Korean Chem. Soc.* **1996**, *17*, 478-480.
- (131) Dess, D. B.; Martin, J. C. Readily Accessible 12-I-5 Oxidant for the Conversion of Primary and Secondary Alcohols to Aldehydes and Ketones. *J. Org. Chem.* **2002**, *48*, 4155-4156.
- (132) Ireland, R. E.; Liu, L. An Improved Procedure for the Preparation of the Dess-Martin Periodinane. *J. Org. Chem.* **2002**, *58*, 2899-2899.
- (133) Kabbara, J.; Hoffmann, C.; Schinzer, D. Stephens-Castro-Coupling of Halogenated Vinylic and Allylic Silanes with (Homo-)Propargylic Compounds. *Synthesis* **1995**, *1995*, 299-302.
- (134) Ohe, F. v. d.; Bruckner, R. Stereoselective Synthesis of Freelingyne and Related [ω]-Alkylidenebutenolides Via Vinylogous Mukaiyama Aldol Additions. *New J. Chem.* **2000**, *24*, 659-669.
- (135) Barone, V.; Peralta, J. E.; Contreras, R. H.; Snyder, J. P. DFT Calculation of NMR J_{FF} Spin-Spin Coupling Constants in Fluorinated Pyridines. *J. Phys. Chem. A.* **2002**, *106*, 5607-5612.
- (136) Ramsey, N. F. Electron Coupled Interactions between Nuclear Spins in Molecules. *Phys. Rev.* **1953**, *91*, 303.
- (137) Bauer, M.; Maier, M. E. Synthesis of the Core Structure of Salicylihalamide A by Intramolecular Suzuki Reaction. *Org. Lett.* **2002**, *4*, 2205-2208.

- (138) Holloway, G. A.; Hugel, H. M.; Rizzacasa, M. A. Formal Total Synthesis of Salicylhalamides A and B. *J. Org. Chem.* **2003**, *68*, 2200-2204.
- (139) Molander, G. A.; Rivero, M. R. Suzuki Cross-Coupling Reactions of Potassium Alkenyltrifluoroborates. *Org. Lett.* **2001**, *4*, 107-109.
- (140) Molander, G. A.; Dehmel, F. Formal Total Synthesis of Oximidine II Via a Suzuki-Type Cross-Coupling Macrocyclization Employing Potassium Organotrifluoroborates. *J. Am. Chem. Soc.* **2004**, *126*, 10313-10318.
- (141) Pawlak, J.; Nakanishi, K.; Iwashita, T.; Borowski, E. Stereochemical Studies of Polyols from the Polyene Macrolide Lienomycin. *J. Org. Chem.* **2002**, *52*, 2896-2901.
- (142) Frantz, D. E.; Fassler, R.; Tomooka, C. S.; Carreira, E. M. The Discovery of Novel Reactivity in the Development of C-Alkyne Bond-Forming Reactions: In Situ Generation of Zinc Acetylides with ZnII/R₃N. *Acc. Chem. Res.* **2000**, *33*, 373-381.
- (143) Hadfield, A.; Schweitzer, H.; Trova, M. P.; Green, K. Practical, Large-Scale Synthesis of 2,2-Dimethyl-5-Hydroxy-4-Oxo-Benzo-1,4-Dioxin. *Synth. Commun.* **1994**, *24*, 1025-1028.
- (144) Corey, E. J.; Rucker, C. Useful Synthetic Reagents Derived from 1-Triisopropylsilylpropyne and 1,3-Bis-(Triisopropylsilyl)Propyne. Direct, Stereoselective Synthesis of Either *Z* or *E* Enynes. *Tetrahedron Lett.* **1982**, *23*, 719-722.
- (145) Jeffery, T. On the Efficiency of Tetraalkylammonium Salts in Heck Type Reactions. *Tetrahedron* **1996**, *52*, 10113-10130.

- (146) Karabelas, K.; Hallberg, A. Synthesis of 1-Trimethylsilyl 1,3-Dienes by the Palladium-Catalyzed Reaction of Trimethylvinylsilane with Vinyl Iodides/Silver Nitrate or Vinyl Triflates. *J. Org. Chem.* **1988**, *53*, 4909-4914.
- (147) Stamos, D. P.; Taylor, A. G.; Kishi, Y. A Mild Preparation of Vinyl iodides from Vinylsilanes. *Tetrahedron Lett.* **1996**, *37*, 8647-8650.
- (148) McDougal, P. G.; Rico, J. G.; Oh, Y.-I.; Condon, B. D. A Convenient Procedure for the Monosilylation of Symmetric 1,*n*-Diols *J. Org. Chem.* **1986**, *51*, 3388-3390.
- (149) Nacro, K.; Baltas, M.; Gorrichon, L. Attempt to Rationalize the Diastereoselectivity in the Addition of Ester Enolate to Optically Active A,B-Epoxyaldehydes. *Tetrahedron* **1999**, *55*, 14013-14030.
- (150) Xu, D.; Park, C. Y.; Sharpless, K. B. Study of the Regio- and Enantioselectivity of the Reactions of Osmium Tetroxide with Allylic Alcohols and Allylic Sulfonamides. *Tetrahedron Lett.* **1994**, *35*, 2495-2498.
- (151) Fernandes, R. A.; Kumar, P. A Stereoselective Synthesis of Dihydrosphingosine. *Eur. J. Org. Chem.* **2000**, 3447-3449.
- (152) Sharpless, K. B.; Amberg, W.; Bennani, Y. L.; Crispino, G. A.; Hartung, J.; Jeong, K. S.; Kwong, H. L.; Morikawa, K.; Wang, Z. M. The Osmium-Catalyzed Asymmetric Dihydroxylation: A New Ligand Class and a Process Improvement. *J. Org. Chem.* **2002**, *57*, 2768-2771.
- (153) Wuts, P. G. M.; Greene, T. W. In *Greene's Protective Groups in Organic Synthesis (Fourth Edition)* 2006, p 16-366.

- (154) Tsunoda, T.; Suzuki, M.; Noyori, R. A Facile Procedure for Acetalization under Aprotic Conditions. *Tetrahedron Lett.* **1980**, *21*, 1357-1358.
- (155) Breuilles, P.; Oddon, G.; Uguen, D. Toward a Total Synthesis of an Aglycone of Spiramycin; a Chiron Approach to the C-1/C-4 and the C-13/C-15 Fragments. *Tetrahedron Lett.* **1997**, *38*, 6607-6610.
- (156) Ishiwata, A.; Sakamoto, S.; Noda, T.; Hirama, M. Synthetic Study of Pinnatoxin A: Intramolecular Diels-Alder Approach to the AG-Ring. *Synlett* **1999**, 692-694.
- (157) Claridge, T. D. W.; Davies, S. G.; Lee, J. A.; Nicholson, R. L.; Roberts, P. M.; Russell, A. J.; Smith, A. D.; Toms, S. M. Highly (*E*)-Selective Wadsworth-Emmons Reactions Promoted by Methylmagnesium Bromide. *Org. Lett.* **2008**, *10*, 5437-5440.
- (158) Ghosh, A. K.; Kim, J.-H. An Enantioselective Synthesis of the C1-C9 Segment of Antitumor Macrolide Peloruside A. *Tetrahedron Lett.* **2003**, *44*, 3967-3969.
- (159) Saito, S.; Kuroda, A.; Tanaka, K.; Kimura, R. A Novel Reducing System for Acetal Cleavage: $\text{BH}_3 \cdot \text{S}(\text{CH}_3)_2 \cdot \text{BF}_3 \cdot \text{O}(\text{C}_2\text{H}_5)_2$ Combination. *Synlett* **1996**, *1996*, 231-233.
- (160) Akiyama, K.; Yamamoto, S.; Fujimoto, H.; Ishibashi, M. Total Synthesis of TT-1 (Rasfonin), an α -Pyrone-Containing Natural Product from a Fungus *Trichurus Terrophilus*. *Tetrahedron* **2005**, *61*, 1827-1833.
- (161) Surivet, J.-P.; Vatele, J.-M. First Total Synthesis of (-)-8-Epi-9-Deoxygoniopyrpyrone *Tetrahedron Lett.* **1998**, *39*, 9681-9682.

- (162) Chandrasekhar, S.; Reddy, Y. R.; Reddy, C. R. Regioselective Reductive Ring Opening of Cyclic 1,2- and 1,3-Benzylidene Acetals. *Chem. Lett.* **1998**, *27*, 1273-1274.
- (163) Gateau-Olesker, A.; Cl  ophax, J.; G  ero, S. D. Chiral Synthesis of 3,4-Disubstituted 2-Azetidinones from (*R,R*)-(+)-Tartaric Acid. *Tetrahedron Lett.* **1986**, *27*, 41-44.
- (164) Heapy, A. M.; Wagner, T. W.; Brimble, M. M. Synthesis of the FG Fragment of the Pectenotoxins. *Synlett* **2007**, *15*, 2359-2362.
- (165) Ager, D. J. The Peterson Reaction. *Synthesis* **1984**, 384-398.
- (166) Kira, K.; Isobe, M. Acetylene Cobalt Complex and Vinylsilane Strategy in the Synthesis of Ciguatoxin (D)EF Analog. *Tetrahedron Lett.* **2000**, *41*, 5951-5955.
- (167) Denmark, S. E.; Yang, S.-M. Intramolecular Silicon-Assisted Cross-Coupling: Total Synthesis of (+)-Brasilenyne. *J. Am. Chem. Soc.* **2002**, *1241*, 15195-15197.
- (168) Overman, L. E.; Lesuisse, D.; Hashimoto, M. Synthetic Applications of N-Acylamino-1,3-Dienes. 10. Importance of Allylic Interactions and Stereoelectronic Effects in Dictating the Steric Course of the Reaction of Iminium Ions with Nucleophiles. An Efficient Total Synthesis of (\pm)-Gephyrotoxin. *J. Am. Chem. Soc.* **2002**, *105*, 5373-5379.
- (169) Palaz  n, J. M.; Mart  n, V. S. Enantioselective Total Synthesis of 6(*R*),7(*R*)-3-*cis*-9-*cis*-12-*cis*,6-Acetoxy-7-Chloropentadeca-3,9,12-Trien-1-Yne and Its 3-*trans*-Isomer. *Tetrahedron Lett.* **1988**, *29*, 681-684.

- (170) Sheldrake, H. M.; Jamieson, C.; Burton, J. W. The Changing Faces of Halogenated Marine Natural Products : Total Synthesis of the Reported Structures of Elatényne and an Enyne from *Laurencia Majuscula*. *Angew. Chem. Int. Ed.* **2006**, *45*, 7199-7202.
- (171) Yamakado, Y.; Ishiguro, M.; Ikeda, N.; Yamamoto, H. Stereoselective Carbonyl Olefination Via Organosilicon Compounds. *J. Am. Chem. Soc.* **1981**, *103*, 5568-5570.
- (172) Barder, T. E.; Walker, S. D.; Martinelli, J. R.; Buchwald, S. L. Catalysts for Suzuki-Miyaura Coupling Processes: Scope and Studies of the Effect of Ligand Structure. *J. Am. Chem. Soc.* **2005**, *127*, 4685-4696.
- (173) Bates, C. G.; Saejueng, P.; Venkataraman, D. Copper-Catalyzed Synthesis of 1,3-Enynes. *Org. Lett.* **2004**, *6*, 1441-1444.
- (174) Cunico, R. F.; Bedell, L. The Triisopropylsilyl Group as a Hydroxyl-Protecting Function. *J. Org. Chem.* **1980**, *45*, 4797-4798.
- (175) Okukado, N.; VanHorn, D. E.; Klima, W. L.; Negishi, E.-I. A Highly Stereo-, Regio-, and Chemoselective Synthesis of Conjugated Dienes by the Palladium-Catalyzed Reaction of (*E*)-1-Alkenylzirconium Derivatives with Alkenyl Halides. *Tetrahedron Lett.* **1978**, *12*, 1027-1030.
- (176) Negishi, E.-I.; Takahashi, T.; Baba, S.; Horn, D. E. V.; Okukado, N. Palladium- or Nickel-Catalyzed Reactions of Alkenylmetals with Unsaturated Organic Halides as a Selective Route to Arylated Alkenes and Conjugated Dienes: Scope, Limitations and Mechanism. *J. Am. Chem. Soc.* **1987**, *109*, 2393-2401.

- (177) Negishi, E.-I. Palladium- or Nickel-Catalyzed Cross Coupling. A New Selective Method for Carbon-Carbon Bond Formation. *Acc. Chem. Res.* **1982**, *15*, 340-348.
- (178) Mahoney, W. S.; Brestensky, D. M.; Stryker, J. M. Selective Hydride-Mediated Conjugate Reduction of α,β -Unsaturated Carbonyl Compounds Using $[(\text{Ph}_3\text{P})\text{CuH}]_6$. *J. Am. Chem. Soc.* **1988**, *110*, 291-292.
- (179) Daeuble, J. F.; McGettigan, C.; Stryker, J. M. Selective Reduction of Alkynes to *Cis*-Alkenes by Hydrometallation Using $[(\text{Ph}_3\text{P})\text{CuH}]_6$. *Tetrahedron Lett.* **1990**, *31*, 2397-2400.
- (180) Boland, W.; Schroer, N.; Sieler, C.; Feigel, M. 96. Stereospecific Syntheses and Spectroscopic Properties of Isomeric 2,4,6,8-Undecatetraenes. New Hydrocarbons from the Marine Brown Alga *Gijfordia Mitchellae*. *Helv. Chim. Acta.* **1987**, *70*, 1025-1040.
- (181) Kauffman, G. B.; Fang, L. Y.; Viswanathan, N.; Townsend, G. In *Inorg. Synth.*; Smith, L. H., Jr., Ed.; John Wiley & Sons: New York, NY, 1983, p 101-103.
- (182) Brestensky, D. M.; Huseland, D. E.; McGettigan, C.; Stryker, J. M. Simplified, "One-Pot" Procedure for the Synthesis of $[(\text{Ph}_3\text{P})\text{CuH}]_6$, a Stable Copper Hydride for Conjugate Reductions. *Tetrahedron Lett.* **1988**, *29*, 3749-3752.
- (183) Zawisza, A. M.; Muzart, J. Pd-Catalyzed Reduction of Aryl Halides Using Dimethylformamide as the Hydride Source. *Tetrahedron Lett.* **2007**, *48*, 6738-6742.
- (184) Wassmundt, F. W.; Kiesman, W. F. Efficient Catalysis of Hydrodediazoniations in Dimethylformamide. *J. Org. Chem.* **2002**, *60*, 1713-1719.

- (185) Marx, G. S. Reduction of Diazonium Fluoroborates in Dimethylformamide, Catalyzed by Rhodium Complexes. *J. Org. Chem.* **2002**, *36*, 1725-1726.
- (186) Dilts, J. A.; Shriver, D. F. A Cryoscopic Study of Copper (I) Hydride-Phosphine Complexes *J. Am. Chem. Soc.* **1969**, *91*, 4088-4091.
- (187) Deutsch, C.; Krause, N.; Lipshutz, B. H. CuH-Catalyzed Reactions. *Chem. Rev.* **2008**, *108*, 2916-2927.
- (188) Mahoney, W. S.; Stryker, J. M. Hydride-Mediated Homogeneous Catalysis. Catalytic Reduction of α,β -Unsaturated Ketones Using $[(\text{Ph}_3\text{P})\text{CuH}]_6$ and H_2 . *J. Am. Chem. Soc.* **1989**, *111*, 8818-8823.
- (189) Lipshutz, B. H. Rediscovering Organocopper Chemistry through Copper Hydride. It's All About the Ligand. *Synlett* **2009**, *4*, 0509-0524.
- (190) Lee, D.-W.; Yun, J. Direct Synthesis of Stryker's Reagent from a Cu(II) Salt. *Tetrahedron Lett.* **2005**, *46*, 2037-2039.
- (191) Mankad, N. P.; Laitar, D. S.; Sadighi, J. P. Synthesis, Structure, and Alkyne Reactivity of a Dimeric (Carbene)Copper(I) Hydride. *Organometallics* **2004**, *23*, 3369-3371.
- (192) Rao, S. A.; Periasamy, M. Hydrocupration of Alkynes: A Simple Synthesis of (*E,E*)-1,3-Dienes. *J. Chem. Soc., Chem. Commun.* **1987**, 495-496.
- (193) Lee, A. S.-Y.; Hu, Y.-J.; Chu, S.-F. A Simple and Highly Efficient Deprotecting Method for Methoxymethyl and Methoxyethoxymethyl Ethers and Methoxyethoxymethyl Esters. *Tetrahedron* **2001**, *57*, 2121-2126.

- (194) Jiang, L.; Job, G. E.; Klapars, A.; Buchwald, S. L. Copper-Catalyzed Coupling of Amides and Carbamates with Vinyl Halides. *Org. Lett.* **2003**, *5*, 3667-3669.
- (195) Vintonyak, V. V.; Maier, M. E. Synthesis of the Core Structure of Cruentaren A. *Org. Lett.* **2007**, *9*, 655-658.
- (196) Walker, M. A. The Mitsunobu Reaction: A Novel Method for the Synthesis of Bifunctional Maleimide Linkers. *Tetrahedron Lett.* **1994**, *35*, 665-668.
- (197) Walker, M. A. A High Yielding Synthesis of *N*-Alkyl Maleimides Using a Novel Modification of the Mitsunobu Reaction. *J. Org. Chem.* **1995**, *60*, 5352-5355.
- (198) Boerjesson, L.; Csoeregh, I.; Welch, C. J. Synthesis and Conformational Analysis of 2,9-Disubstituted 1-Oxaquinolizidines. *J. Org. Chem.* **1995**, *60*, 2989-2999.
- (199) Bergeron, R. J.; McManis, J. S.; Perumal, P. T.; Algee, S. E. The Total Synthesis of Alcaligin. *J. Org. Chem.* **1991**, *56*, 5560-5563.
- (200) Hoye, T. R.; Hu, M. Macrolactonization Via TI(IV)-Mediated Epoxy-Acid Coupling: A Total Synthesis of (-)-Dactylolide [and Zampanolide]. *J. Am. Chem. Soc.* **2003**, *125*, 9576-9577.
- (201) Bayer, A.; Maier, M. E. Synthesis of Enamides from Aldehydes and Amides. *Tetrahedron* **2004**, *60*, 6665-6667.
- (202) Koppel, I.; Koppel, J.; Degerbeck, F.; Grehn, L.; Ragnarsson, U. Acidity of Imidodicarbonates and Tosylcarbamates in Dimethyl Sulfoxide. Correlation with Yields in the Mitsunobu Reaction. *J. Org. Chem.* **1991**, *56*, 7172-7174.

- (203) Tsunoda, T.; Yamamiya, Y.; Itô, S. 1,1'-(Azodicarbonyl)Dipiperidine-Tributylphosphine, a New Reagent System for Mitsunobu Reaction. *Tetrahedron Lett.* **1993**, *34*, 1639-1642.
- (204) Saegusa, T.; Kobayashi, S.; Ito, Y. Radical Reaction of Isocyanide with Thiol. *J. Org. Chem.* **1970**, *35*, 2118-2121.
- (205) <http://www.textbookofbacteriology.net/resantimicrobial.html>. Todar, K. Todar's Online Textbook of Bacteriology.
- (206) Mitscher, L. A. In *Foye's Principles of Medicinal Chemistry*; 5th ed.; Williams, D. A., Lemke, T. L., Eds.; Lippincott Williams & Wilkins: Baltimore, MD, 2002, p 819-864.
- (207) Ham, B. "Chemistry versus the Superbugs!" *Chemistry* Autumn 2005, **2005**, 25-29.
- (208) Heijenoort, J. v. Recent Advances in the Formation of the Bacterial Peptidoglycan Monomer Unit. *Nat. Prod. Rep.* **2001**, *18*, 503-519.
- (209) Meroueh, S. O.; Bencze, K. Z.; Heseck, D.; Lee, M.; Fisher, J. F.; Stemmler, T. L.; Mobashery, S. Three-Dimensional Structure of the Bacterial Cell Wall Peptidoglycan. *Proc. Natl. Acad. Sci. U. S. A.* **2006**, *103*, 4404-4409.
- (210) Marquardt, J. L.; Siegele, D. A.; Kolter, R.; Walsh, C. T. Cloning and Sequencing of Escherichia Coli Murz and Purification of Its Product, a UDP-N-Acetylglucosamine Enolpyruvyl Transferase. *J. Bacteriol.* **1992**, *174*, 5748-5752.

- (211) Brown, E. D.; Vivas, E. I.; Walsh, C. T.; Kolter, R. MurA (MurZ), the Enzyme That Catalyzes the First Committed Step in Peptidoglycan Biosynthesis, Is Essential in *Escherichia Coli*. *J. Bacteriol.* **1995**, *177*, 4194-4197.
- (212) Priestman, M. A., The University of Kansas, 2005.
- (213) Schönbrunn, E.; Svergun, D. I.; Amrhein, N.; Koch, M. H. J. Studies on the Conformational Changes in the Bacterial Cell Wall Biosynthetic Enzyme UDP-*N*-Acetylglucosamine Enolpyruvyltransferase (MurA). *Eur. J. Biochem.* **1998**, *253*, 406-412.
- (214) Schönbrunn, E.; Eschenburg, S.; Krekel, F.; Luger, K.; Amrhein, N. Role of the Loop Containing Residue 115 in the Induced-Fit Mechanism of the Bacterial Cell Wall Biosynthetic Enzyme MurA. *Biochemistry* **2000**, *39*, 2164-2173.
- (215) Skarzynski, T.; Mistry, A.; Wonacott, A.; Hutchinson, S. E.; Kelly, V. A.; Duncan, K. Structure of UDP-*N*-Acetylglucosamine Enolpyruvyl Transferase, an Enzyme Essential for the Synthesis of Bacterial Peptidoglycan, Complexed with Substrate UDP-*N*-Acetylglucosamine and the Drug Fosfomycin. *Structure* **1996**, *4*, 1465-1474.
- (216) Eschenburg, S.; Priestman, M.; Schönbrunn, E. Evidence That the Fosfomycin Target Cys115 in UDP-*N*-Acetylglucosamine Enolpyruvyl Transferase (MurA) Is Essential for Product Release. *J. Biol. Chem.* **2005**, *280*, 3757-3763.
- (217) Eschenburg, S.; Kabsch, W.; Healy, M. L.; Schönbrunn, E. A New View of the Mechanisms of UDP-*N*-Acetylglucosamine Enolpyruvyl Transferase (MurA) and 5-Enolpyruvylshikimate-3-Phosphate Synthase (AroA) Derived from X-Ray

Structures of Their Tetrahedral Reaction Intermediate States. *J. Biol. Chem.* **2003**, 278, 49215-49222.

(218) An, M.; Maitra, U.; Neidlein, U.; Bartlett, P. A. 5-Enolpyruvylshikimate 3-Phosphate Synthase: Chemical Synthesis of the Tetrahedral Intermediate and Assignment of the Stereochemical Course of the Enzymatic Reaction. *J. Am. Chem. Soc.* **2003**, 125, 12759-12767.

(219) Bentley, R. The Shikimate Pathway - a Metabolic Tree with Many Branches. *Crit. Rev. Biochem. Mol. Biol.* **1990**, 25, 307-384.

(220) Kishore, G. M.; Shah, D. M. Amino Acid Biosynthesis Inhibitors as Herbicides. *Annu. Rev. Biochem.* **1988**, 57, 627-663.

(221) Hendlin, D.; Stapley, E. O.; Jackson, M.; Wallick, H.; Miller, A. K.; Wolf, F. J.; Miller, T. W.; Chalet, L.; Kahan, F. M.; Foltz, E. L.; Woodruff, H. B.; Mata, J. M.; Hernandez, S.; Mochales, S. Phosphonomycin, a New Antibiotic Produced by Strains of *Streptomyces*. *Science* **1969**, 166, 122-123.

(222) Kahan, F. M.; Kahan, J. S.; Cassidy, P. J.; Kropp, H. The Mechanism of Action of Fosfomycin (Phosphonomycin). *Ann. N. Y. Acad. Sci.* **1974**, 235, 364-386.

(223) Baum, E. Z.; Montenegro, D. A.; Licata, L.; Turchi, I.; Webb, G. C.; Foleno, B. D.; Bush, K. Identification and Characterization of New Inhibitors of the *Escherichia Coli* MurA Enzyme. *Antimicrob. Agents Chemother.* **2001**, 45, 3182-3188.

- (224) Nilsson, A. I.; Berg, O. G.; Aspevall, O.; Kahlmeter, G.; Andersson, D. I. Biological Costs and Mechanisms of Fosfomycin Resistance in *Escherichia Coli*. *Antimicrob. Agents Chemother.* **2003**, *47*, 2850-2858.
- (225) Kadner, R. J.; Winkler, H. H. Isolation and Characterization of Mutations Affecting the Transport of Hexose Phosphates in *Escherichia Coli*. *J. Bacteriol.* **1973**, *113*, 895-900.
- (226) Venkateswaran, P. S.; Wu, H. C. Isolation and Characterization of a Phosphononmycin-Resistant Mutant of *Escherichia Coli* K-12. *J. Bacteriol.* **1972**, *110*, 935-944.
- (227) Garcia-Lobo, J. M.; Ortiz, J. M. TN2921, a Transposon Encoding Fosfomycin Resistance. *J. Bacteriol.* **1982**, *151*, 477-479.
- (228) Arca, P.; Hardisson, C.; Suarez, J. E. Purification of a Glutathione S-Transferase That Mediates Fosfomycin Resistance in Bacteria. *Antimicrob. Agents Chemother.* **1990**, *34*, 844-848.
- (229) Arca, P.; Rico, M.; Brana, A. F.; Villar, C. J.; Hardisson, C.; Suarez, J. E. Formation of an Adduct between Fosfomycin and Glutathione: A New Mechanism of Antibiotic Resistance in Bacteria. *Antimicrob. Agents Chemother.* **1988**, *32*, 1552-1556.
- (230) Smet, K. A. D.; Kempell, K. E.; Gallagher, A.; Duncan, K.; Young, D. B. Alteration of a Single Amino Acid Residue Reverses Fosfomycin Resistance of Recombinant MurA from *Mycobacterium Tuberculosis*. *Microbiology* **1999**, *145*, 3177-3184.

- (231) Kim, D. H.; Lees, W. J.; Kempell, K. E.; Lane, W. S.; Duncan, K.; Walsh, C. T. Characterization of Cys115 to Asp Substitution in the *Escherichia Coli* Cell Wall Biosynthetic Enzyme UDP-GlcNAc Enolpyruvyl Transferase (MurA) That Confers Resistance to Inactivation by the Antibiotic Fosfomycin. *Biochemistry* **1996**, *35*, 4923-4928.
- (232) Barbosa, M. D.; Yang, G.; Fang, J.; Kurilla, M. G.; Pompliano, P. L. Development of a Whole-Cell Assay for Peptidoglycan Biosynthesis Inhibitors. *Antimicrob. Agents Chemother.* **2002**, *46*, 943-946.
- (233) Dai, H. J.; Parker, C. N.; Bao, J. J. Characterization and Inhibition Study of Mura Enzyme by Capillary Electrophoresis. *J. Chromatogr. B* **2001**, *799*, 123-132.
- (234) Devito, J. A.; Mills, J. A.; Liu, V. G.; Agarwal, A.; Sizemore, C. F.; Yao, Z.; Stoughton, D. M.; Cappiello, M. G.; Barbosa, M. D.; Foster, L. A.; Pompliano, D. L. An Array of Target-Specific Screening Strains for Antibacterial Discovery. *Nat. Biotechnol.* **2002**, *20*, 478-483.
- (235) Steinbach, A.; Scheidig, A. J.; Klein, C. D. The Unusual Binding Mode of Cnicin to the Antibacterial Target Enzyme MurA Revealed by X-Ray Crystallography. *J. Med. Chem.* **2008**, *51*, 5143-5147.
- (236) Bachelier, A.; Mayer, R.; Klein, C. D. Sesquiterpene Lactones Are Potent and Irreversible Inhibitors of the Antibacterial Target Enzyme MurA. *Bioorg. Med. Chem. Lett.* **2006**, *16*, 5605-5609.

- (237) Lanzetta, P. A.; Alvarez, L. J.; Reinach, P. S.; Candi, O. A. An Improved Assay for Nanomole Amounts of Inorganic Phosphate. *Anal. Biochem.* **1979**, *100*, 95-97.
- (238) Knorr, L. Einwirkung des Diethylbernsteinsäure-Esters auf Ammoniak und Primäre Amin Basen. *Chem. Ber.* **1885**, *18*, 299-311.
- (239) Paal, C. Synthese von Thiophen- und Pyrrolderivaten. *Chem. Ber.* **1888**, *18*, 367-371.
- (240) Clauson-Kaas, N.; Tyle, Z. Preparation of *Cis* and *Trans* 2,5-Dimethoxy-2-(Acetamidomethyl)-2,5-Dihydrofuran, of *Cis* and *Trans* 2,5-Dimethoxy-2-(Acetamidomethyl)-Tetrahydrofuran and of 1-Phenyl-2-(Acetamidomethyl)-Pyrrole. *Acta Chem. Scand.* **1952**, *6*, 667-670.
- (241) Fogassy, K.; Kovács, K.; Keserű, G. R. M.; Töke, L. S.; Faigl, F. Solvent and Ligand Effects on Selective Mono- and Dilithiation of 1-(Chlorophenyl)Pyrroles and 1-(Methoxyphenyl)Pyrroles. *J. Chem. Soc., Perkin Trans. 1* **2001**, 1039–1043
- (242) Pan, Y.; Lu, H.; Fang, Y.; Fang, X.; Chen, L.; Qian, J.; Wang, J.; Li, C. Synthesis of Pyrroles Via Copper-Catalyzed Coupling of Amines with Bromoenones. *Synthesis* **2007**, *2007*, 1242-1246.
- (243) Corbet, J.-P.; Mignani, G. Selected Patented Cross-Coupling Reaction Technologies. *Chem. Rev.* **2006**, *106*, 2651-2710.
- (244) Ley, S. V.; Thomas, A. W. Modern Synthetic Methods for Copper-Mediated C(Aryl)–O, C(Aryl)–N, and C(Aryl)–S Bond Formation. *Angew. Chem. Int. Ed.* **2003**, *42*, 5400-5449.

- (245) Ullmann, F. Ueber eine neue Bildungsweise von Diphenylaminderivaten. *Chem. Ber.* **1903**, *36*, 2382-2384.
- (246) Iram, G. Ueber Phenylierungen bei Gegenwart von Kupfer als Katalysator. *Chem. Ber.* **1906**, *39*, 1691-1692.
- (247) Antilla, J. C.; Baskin, J. M.; Barder, T. E.; Buchwald, S. L. Copper-Diamine-Catalyzed *N*-Arylation of Pyrroles, Pyrazoles, Indazoles, Imidazoles, and Triazoles *J. Org. Chem.* **2004** *69*, 5578-5587.
- (248) Jiang, L.; Buchwald, S. L. In *Metal-Catalyzed Cross-Coupling Reactions*; Meijere, A. D., Diederich, F., Eds.; Wiley-VCH: Weinheim, Germany, 2004; Vol. 1, p 699.
- (249) Hartwig, J. F.; Kawatsura, M.; Hauck, S. I.; Shaughnessy, K. H.; Alcazar-Roman, L. M. Room-Temperature Palladium-Catalyzed Amination of Aryl Bromides and Chlorides and Extended Scope of Aromatic C-N Bond Formation with a Commercial Ligand. *J. Org. Chem.* **1999**, *64*, 5575-5580.
- (250) Mann, G.; Hartwig, J. F.; Driver, M. S.; Fernandez-Rivas, C. Palladium-Catalyzed C-(Sp²) Bond Formation: *N*-Arylation of Aromatic and Unsaturated Nitrogen and the Reductive Elimination Chemistry of Palladium Azolyl and Methyleneamido Complexes. *J. Am. Chem. Soc.* **1998**, *120*, 827-828.
- (251) Wolfe, J. P.; Wagaw, S.; Marcoux, J.-F.; Buchwald, S. L. Rational Development of Practical Catalysts for Aromatic Carbon-Nitrogen Bond Formation. *Acc. Chem. Res.* **1998**, *31*, 805-818.

- (252) Yu, S.; Saenz, J.; Srirangam, J. K. Facile Synthesis of *N*-Aryl Pyrroles Via Cu(II)-Mediated Cross Coupling of Electron Deficient Pyrroles and Arylboronic Acids. *J. Org. Chem.* **2002**, *67*, 1699-1702.
- (253) Quach, T. D.; Batey, R. A. Ligand- and Base-Free Copper(II)-Catalyzed C–N Bond Formation: Cross-Coupling Reactions of Organoboron Compounds with Aliphatic Amines and Anilines. *Org. Lett.* **2003**, *5*, 4397-4400.
- (254) Sugihara, H.; Matsumoto, N.; Hamuro, Y.; Kawamatsu, Y. Oral Hypoglycemic Agents: 1-(2-Carboxyphenyl)Pyrroles. *Arzneim.-Forsch.* **1974**, *24*, 1560-1563.
- (255) Fang, Y.; Leysen, D.; Ottenhijm, H. C. J. A Facile Synthesis of *N*-Substituted Pyrroles. *Synth. Commun.* **1995**, *25*, 1857-1861.
- (256) Dolphin, D. Porphyrinogens and Porphodimethenes, Intermediates in the Synthesis of *Meso*-Tetraphenylporphins from Pyrroles and Benzaldehyde. *J. Heterocycl. Chem.* **1970**, *7*, 275-283.
- (257) Bernhard, N.; Wolfgang, S. Simple Method for the Esterification of Carboxylic Acids. *Angew. Chem. Int. Ed. in Eng.* **1978**, *17*, 522-524.
- (258) Trujillo-Ferrara, J.; Santillan, R.; Beltrán, H. I.; Farfán, N.; Höpfl, H. ¹H and ¹³C NMR Spectra for a Series of Arylmaleamic Acids, Arylmaleimides, Arylsuccinamic Acids and Arylsuccinimides. *Magn. Reson. Chem.* **1999**, *37*, 682-686.

- (259) Beddell, C. R.; Goodford, P. J.; Norrington, F. E.; Wilkinson, S.; Wootton, R. Compounds Designed to Fit a Site of Known Structure in Human Haemoglobin. *Br. J. Pharmacol.* **1976**, *37*, 201-209.
- (260) Congreve, M.; Murray, C. W.; Blundell, T. L. Keynote Review: Structural Biology and Drug Discovery. *Drug Discov. Today* **2005**, *10*, 895-907.
- (261) Varghese, J. N. Development of Neuraminidase Inhibitors as Anti-Influenza Virus Drugs. *Drug Dev. Res.* **1999**, *46*, 176-196.
- (262) Erlanson, D. A.; McDowell, R. S.; O'Brien, T. Fragment-Based Drug Discovery. *J. Med. Chem.* **2004**, *47*, 3463-3482.
- (263) Rees, D. C.; Congreve, M.; Murray, C. W.; Carr, R. Fragment-Based Lead Discovery. *Nat. Rev. Drug Discov.* **2004**, *3*, 660-672.
- (264) Hajduk, P. J. Fragment-Based Drug Design: How Big Is Too Big? *J. Med. Chem.* **2006**, *49*, 6972-6976.
- (265) Abad-Zapatero, C.; Metz, J. T. Ligand Efficiency Indices as Guideposts for Drug Discovery. *Drug Discov. Today* **2005**, *10*, 464-469.
- (266) Hopkins, A. L.; Groom, C. R.; Alex, A. Ligand Efficiency: A Useful Metric for Lead Selection. *Drug Discov. Today* **2004**, *9*, 430-431.
- (267) Murray, C. W.; Rees, D. C. The Rise of Fragment-Based Drug Discovery. *Nat. Chem.* **2009**, *1*, 187-192.
- (268) Klein, C. D.; Bachelier, A. Molecular Modeling and Bioinformatical Analysis of the Antibacterial Target Enzyme MurA from a Drug Design Perspective. *J. Comput. Aided Mol. Des.* **2006**, *20*, 621-628.

- (269) Sybyl 7.1, T.T Associates, St. Louis, MO, 2007.
- (270) Gasteiger, J.; Marsili, M. Iterative Partial Equalization of Orbital Electronegativity: A Rapid Access to Atomic Charges. *Tetrahedron* **1980**, *36*, 3219–3228.
- (271) Morris, G. M.; Goodsell, D. S.; Halliday, R. S.; Huey, R.; Hart, W. E.; Belew, R. K.; Olson, A. J. Automated Docking Using a Lamarckian Genetic Algorithm and Empirical Binding Free Energy Function. *J. Comput. Chem.* **1998**, *19*, 1639–1662.
- (272) IResearch Library, ChemNavigator, Inc., San Diego, CA, 2006.
- (273) Unity 4.4.3, The Tripos Associates, St. Louis, MO, 2007.
- (274) Concord 7.1, The Tripos Associates, St. Louis, MO, 2007.
- (275) Schönbrunn, E.; Eschenburg, S.; Luger, K.; Kabsch, W.; Amrhein, N. Structural Basis for the Interaction of the Fluorescence Probe 8-Anilino-1-Naphthalene Sulfonate (ANS) with the Antibiotic Target MurA. *Proc. Natl. Acad. Sci. U. S. A.* **2000**, *97*, 6345-6349.
- (276) Eschenburg, S.; Priestman, M. A.; Abdul-Latif, F. A.; Delachaume, C.; Fassy, F.; Schönbrunn, E. A Novel Inhibitor That Suspends the Induced Fit Mechanism of UDP-N-Acetylglucosamine Enolpyruvyl Transferase (MurA). *J. Biol. Chem.* **2005**, *280*, 14070-14075.
- (277) Eschenburg, S.; Schönbrunn, E. Comparative X-Ray Analysis of the Un-Liganded Fosfomycin-Target MurA. *Proteins: Structure, Function, and Genetics* **2000**, *40*, 290-298.

- (278) http://en.wikipedia.org/wiki/Polychlorinated_dibenzodioxins.
- (279) Schechter, A.; Cramer, P.; Boggess, K.; Stanley, J.; Pöschke, O.; Olson, J.; Silver, A.; Schmitz, M. Intake of Dioxins and Related Compounds from Food in the U.S. Population. *J. Toxicol. Environ. Health, A: Curr. Iss.* **2001**, *63*, 1-18.
- (280) Geyer, H. J.; Schramm, K.-W.; Anton Feicht, E.; Behechti, A.; Steinberg, C.; Brüggemann, R.; Poiger, H.; Henkelmann, B.; Kettrup, A. Half-Lives of Tetra-, Penta-, Hexa-, Hepta-, and Octachlorodibenzo-*p*-Dioxin in Rats, Monkeys, and Humans—A Critical Review. *Chemosphere* **2002**, *48*, 631-644.
- (281) *Goodman & Gilman's the Pharmacological Basis of Therapeutics 10th Edition*; The McGraw-Hill Companies: New York, NY, 2001.
- (282) Geyer, H. J.; Scheunert, I.; Rapp, K.; Kettrup, A.; Korte, F.; Greim, H.; Rozman, K. Correlation between Acute Toxicity of 2,3,7,8-Tetrachlorodibenzo-*p*-Dioxin (TCDD) and Total Body Fat Content in Mammals. *Toxicology* **1990**, *65*, 97-107.
- (283) Seefeld, M. D.; Keeseey, R. E.; Peterson, R. E. Body Weight Regulation in Rats Treated with 2,3,7,8-Tetrachlorodibenzo-*p*-Dioxin. *Toxicol. Appl. Pharmacol.* **1984**, *76*, 526-536.
- (284) Kociba, R. J.; Keyes, D. G.; Beyer, J. E.; Carreon, R. M.; Wade, C. E.; Dittenber, D. A.; Kalnins, R. P.; Frauson, L. E.; Park, C. N.; Barnard, S. D.; Hummel, R. A.; Humiston, C. G. Results of a Two-Year Chronic Toxicity and Oncogenicity Study of 2,3,7,8-Tetrachlorodibenzo-*p*-Dioxin in Rats. *Toxicol. Appl. Pharmacol.* **1978**, *46*, 279-303.

- (285) Kociba, R. J.; Keeler, P. A.; Park, C. N.; Gehring, P. J. 2,3,7,8-Tetrachlorodibenzo-*p*-Dioxin (TCDD): Results of a 13-Week Oral Toxicity Study in Rats. *Toxicol. Appl. Pharmacol.* **1976**, *35*, 553-574.
- (286) Peterson, R. E.; Theobald, H. M.; Kimmel, G. L. Developmental and Reproductive Toxicity of Dioxins and Related Compounds: Cross-Species Comparisons. *Crit. Rev. Toxicol.* **1993**, *23*, 283-335.
- (287) Croutch, C. R.; Lebofsky, M.; Schramm, K.-W.; Terranova, P. F.; Rozman, K. K. 2,3,7,8-Tetrachlorodibenzo-*p*-Dioxin (TCDD) and 1,2,3,4,7,8-Hexachlorodibenzo-*p*-Dioxin (HXCDD) Alter Body Weight by Decreasing Insulin-Like Growth Factor I (IGF-I) Signaling. *Toxicol. Sci.* **2005**, *85*, 560-571.
- (288) Arking, R. Aging: A Biological Perspective. *Am. Sci.* **2003**, *91*, 508-515.
- (289) Li, X. L.; Johnson, D. C.; Rozman, K. K. Reproductive Effects of 2,3,7,8-Tetrachlorodibenzo-*p*-Dioxin (TCDD) in Female Rats: Ovulation, Hormonal Regulation, and Possible Mechanism(s). *Toxicol. Appl. Pharmacol.* **1995**, *133*, 321-327.
- (290) Rozman, K. K.; Doull, J. Scientific Foundations of Hormesis. Part 2. Maturation, Strengths, Limitations, and Possible Applications in Toxicology, Pharmacology, and Epidemiology. *Crit. Rev. Toxicol.* **2003**, *33*, 451-462.
- (291) Thunberg, T. In *Biologic Mechanisms of Dioxin Action*; Poland, A., Kimbrough, R. D., Eds.; Cold Spring Harbor Laboratory: Cold Spring Harbor, NY, 1984, 333-344.

- (292) McKinney, J. D.; Fawkes, J.; Jordan, S.; Chae, K.; Oatley, S.; Coleman, R. E.; Briner, W. 2,3,7,8-Tetrachlorodibenzo-*p*-Dioxin (TCDD) as a Potent and Persistent Thyroxine Agonist: A Mechanistic Model for Toxicity Based on Molecular Reactivity. *Environ. Health Perspect.* **1985**, *61*, 453.
- (293) Poland, A.; Knutson, J. C. 2,3,7,8-Tetrachlorodibenzo-*p*-Dioxin and Related Halogenated Aromatic Hydrocarbons: Examination of the Mechanism of Toxicity. *Annu. Rev. Pharmacol. Toxicol.* **1982**, *22*, 517-554.
- (294) Fried, K. W.; Bazzi, R.; Lopez, W. L.; Corsten, C.; Schramm, K.-W.; Bell, D. R.; Rozman, K. K. Relationship between Aryl Hydrocarbon Receptor-Affinity and the Induction of Erod Activity by 2,3,7,8-Tetrachlorinated Phenothiazine and Derivatives. *Toxicol. Appl. Pharmacol.* **2007**, *224*, 147-155.
- (295) Rozman, K. K. Search for the Mechanism of Toxicity of Dioxins. *Exp. Toxicol. Pathol.* **1992**, *44*, 473-480.
- (296) Roth, W.; Voorman, R.; Aust, S. D. Activity of Thyroid Hormone-Inducible Enzymes Following Treatment with 2,3,7,8-Tetrachlorodibenzo-*p*-Dioxin. *Toxicol. Appl. Pharmacol.* **1988**, *92*, 65-74.
- (297) Pohjanvirta, R.; Junoven, R.; Karenlampi, S.; Raunio, H.; Tuomisto, J. Hepatic Ah-Receptor Levels and the Effect of 2,3,7,8-Tetrachlorodibenzo-*p*-Dioxin (TCDD) on Hepatic Microsomal Monooxygenase Activities in a TCDD-Susceptible and -Resistant Rat Strain. *Toxicol. Appl. Pharmacol.* **1988**, *92*, 131-140.
- (298) Yoko, N.; Keiji, W.; Yoshiaki, F.-K.; Takatoshi, I.; Kaoru, K.; Fumio, I. Dibenz[*O*]Pyrene-Induced Genotoxic and Carcinogenic Responses Are Dramatically

Suppressed in Aryl Hydrocarbon Receptor-Deficient Mice. *Int. J. Cancer.* **2004**, *112*, 179-183.

(299) Tsutomu, S.; Yoshiaki, F.-K. Metabolic Activation of Polycyclic Aromatic Hydrocarbons to Carcinogens by Cytochromes P450 1A1 and 1B1. *Cancer Sci.* **2004**, *95*, 1-6.

(300) Nebert, D. W.; Dalton, T. P.; Okey, A. B.; Gonzalez, F. J. Role of Aryl Hydrocarbon Receptor-Mediated Induction of the Cyp1 Enzymes in Environmental Toxicity and Cancer. *J. Biol. Chem.* **2004**, *279*, 23847-23850.

(301) Rozman, K. K.; Lebofsky, M.; Pinson, D. M. Chronic Toxicity and Carcinogenicity of 1,2,3,4,6,7,8-Heptachlorodibenzo-*p*-Dioxin Displays a Distinct Dose/Time Toxicity Threshold ($c \times t = k$) and a Life-Prolonging Sub-Threshold Effect. *Food Chem. Toxicol.* **2005**, *43*, 729-740.

(302) Liu, H.; Biegel, L.; Narasimhan, T. R.; Rowlands, C.; Safe, S. Inhibition of Insulin-Like Growth Factor-I Responses in MCF-7 CESS1 by 2,3,7,8-Tetrachlorodibenzo-*p*-Dioxin and Related Compounds. *Mol. Cell. Endocrinol.* **1992**, *87*, 19-28.

(303) Gao, X.; Son, D. S.; Terranova, P. F.; Rozman, K. K. Toxic Equivalency Factors of Polychlorinated Dibenzo-*p*-Dioxins in an Ovulation Model: Validation of the Toxic Equivalency Concept for One Aspect of Endocrine Disruption. *Toxicol. Appl. Pharmacol.* **1999**, *157*, 107-116.

(304) Thorp, W. T. S.; Henning, W. L.; Shigley, J. F. Phenothiazine as an Anthelmintic for Breeding Ewes. *J. Anim. Sci.* **1945**, *4*, 133-140.

- (305) Klein, C. L.; Conrad, J. M., III Structure of a New Crystallographic Form of Chlorpromazine Hydrochloride Hemihydrate. *Acta Crystallogr. Sect. C: Cryst. Struct. Commun.* **1986**, *42*, 1083-1085.
- (306) Boer, F. P.; van Remoortere, F. P.; North, P. P.; Neuman, M. A. The Crystal and Molecular Structure of 2,3,7,8-Tetrachlorodibenzo-*p*-Dioxin. *Acta Crystallogr. Sect. B: Struct. Sci.* **1972**, *28*, 1023-1029.
- (307) Bodea, C.; Silberg, I. Recent Advances in the Chemistry of Phenothiazines. *Adv. Heterocycl. Chem.* **1968**, *9*, 321-371.
- (308) Saraf, S.; Al-Omran, F.; Al-Saleh, B. Recent Advances in the Synthesis of Phenothiazines. *Heterocycles* **1987**, *26*, 239-273.
- (309) Nodiff, E. A.; Craig, P. N. Synthesis of Phenothiazines. V. Some Halogen-Containing Phenothiazines. *J. Org. Chem.* **1961**, *26*, 824-828.
- (310) Joseph, K. S.; Aija, Z.; Albert, A. M. The Synthesis of 6,9-Dioxo-, 6,9- and 7,9-Dihydroxyehlorpromazines, Possible Metabolites of Chlorpromazinem. *J. Heterocycl. Chem.* **1979**, *16*, 1227-1232.
- (311) Ojha, K. G.; Jain, S. K.; Gupta, R. R. Studies on 1-Nitro-7-Ethoxy Phenothiazines. *Synth. Comm.* **1979**, *9*, 457 - 463.
- (312) Grotta, H. M.; T. F. Page, J.; Riggle, C. J.; Manian, A. A. Some Hydroxylated Derivatives of Chlorpromazine. *J. Heterocycl. Chem.* **1967**, *4*, 611-618.
- (313) Li, D.-X.; Yue, Q.-I.; Chen, L. Synthesis of N-Ethylphenothiazine and Its Derivatives. *Journal of Shaviji University, China* **1988**, *3*, 66-71.

- (314) Fried, K. W., Master's Thesis. Ludwig-Maximilians-Universität München, 2000.
- (315) Béchamp, A. J. Ueber Die Einwirkung der Eisenoxydulsalze auf Nitronaphthalin und Nitrobenzol. *Justus Liebigs Ann. Chem.* **1854**, 92, 401-403.
- (316) Wu, Y.-J.; He, H.; L'Heureux, A. Copper-Catalyzed Coupling of (*S*)-1-(3-Bromophenyl)-Ethylamine and N-H Containing Heteroarenes Using Microwave Heating. *Tetrahedron Lett.* **2003**, 44, 4217-4218.
- (317) Wolfe, J. P.; Tomori, H.; Sadighi, J. P.; Yin, J.; Buchwald, S. L. Simple, Efficient Catalyst System for the Palladium-Catalyzed Amination of Aryl Chlorides, Bromides, and Triflates. *J. Org. Chem.* **2000**, 65, 1158-1174.
- (318) Maes, B. U.; Loones, K. T. J.; Lemeire, G. L. F.; Dommissie, R. A. The First Rapid Palladium-Catalyzed Aminations of (Azahetero)Aryl Chlorides under Temperature-Controlled Microwave Heating. *Synlett* **2003**, 1822-1825.
- (319) Wolfe, J. P.; Singer, R. A.; Yang, B. H.; Buchwald, S. L. Highly Active Palladium Catalysts for Suzuki Coupling Reactions. *J. Am. Chem. Soc.* **1999**, 121, 9550-9561.
- (320) Reuber, M. D. D. A Transplantable Bile-secreting Hepatocellular Carcinoma in the Rat. *J. Natl. Cancer Inst.* **1961**, 26, 891-897.
- (321) Pitot, H. C.; Peraino, C.; Marse, P. A.; Potter, V. R. Hepatoma in Tissue Culture Compared with Adapting Liver *in Vivo*. *J. Nat. Cancer Inst. Monogr.* **1964**, 13, 229-245.

- (322) Riddick, D. S.; Huang, Y.; Harper, P. A.; Okey, A. B. 2,3,7,8-Tetrachloro-*p*-Dioxin Versus 3-Methylcholanthrene: Comparative Studies of Ah Receptor Binding, Transformation, and Induction of Cyp1A1. *J. Biol. Chem.* **1994**, 12118-12128.
- (323) Mahju, M. A.; Maickel, R. P. Accumulation of Phenothiazine Tranquilizers in Rat Brain and Plasma after Repeated Dosage. *Biochem. Pharmacol.* **1969**, 18, 2701-2710.
- (324) Fried, K. W.; Schneider, C. M.; Schramm, K.-W.; Datta, A.; Chahbane, N.; Corsten, C.; Powell, D. R.; Lenoir, D.; Kettrup, A.; Terranova, P.; Georg, G. I.; Rozman, K. K. From Dioxin to Drug Lead - the Development of 2,3,7,8-Tetrachlorophenothiazine. *ChemMedChem.* **2007**, 2, 890-897.
- (325) Doods, K.; GSF - Forschungszentrum für Umwelt und Gesundheit, Institut für Ökologische Chemie, Ökotoxikologie Gruppe: Neuherber, Germany, 2003.
- (326) Donato, M. T.; Gomezlechon, M. J.; Castell, J. V. A Microassay for Measuring Cytochrome P450IA1 and Cytochrome P450IIB1 Activities in Intact Human and Rat Hepatocytes Cultured on 96-Well Plates. *Anal. Biochem.* **1993**, 213, 29-33.
- (327) Boos, K.-S.; Grimm, C.-H. High-Performance Liquid Chromatography Integrated Solid-Phase Extraction in Bioanalysis Using Restricted Access Precolumn Packings. *TrAC, Trends Anal. Chem.* **1999**, 18, 175-180.
- (328) Boos, K.-S.; Rudolphi, A.; Vielhauer, S.; Walfort, A.; Lubda, D.; Eisenbeiss, F. Alkyl-Diol Silica (ADS): Restricted Access Precolumn Packings for Direct

Injection and Coupled-Column Chromatography of Biofluids. *Fresenius J. Anal. Chem.* **1995**, 352, 684-690.